Seismic signature and physics of intense sediment transport in mountain rivers : insights from laboratory experiments and field observations

Marco Piantini

THÈSE

Pour obtenir le grade de

DOCTEUR DE L'UNIVERSITÉ GRENOBLE ALPES

École doctorale : STEP - Sciences de la Terre de l'Environnement et des Planètes
Spécialité : Sciences de la Terre et de l'Environnement
Unité de recherche : Institut des Géosciences de l'Environnement

Signature sismique et physique du transport sédimentaire intense dans les rivières de montagne : investigations avec expériences de laboratoire et observations de terrain

Seismic signature and physics of intense sediment transport in mountain rivers: insights from laboratory experiments and field observations

Présentée par :

Marco PIANTINI

Direction de thèse :

Alain RECKING Chercheur, Université Grenoble Alpes	Directeur de thèse
Florent GIMBERT CHARGE DE RECHERCHE, Université Grenoble Alpes	Co-encadrant de thèse

Rapporteurs :

Matteo BERTI
PROFESSEUR, Alma Mater Studiorum-Università di Bologna
Olivier POULIQUEN
DIRECTEUR DE RECHERCHE, CNRS délégation Provence et Corse

Thèse soutenue publiquement le **20 mars 2023**, devant le jury composé de :

Alain RECKING CHARGE DE RECHERCHE HDR, INRAE Clermont-Auvergne-Rhône-Alpes	Directeur de thèse
Matteo BERTI PROFESSEUR, Alma Mater Studiorum-Università di Bologna	Rapporteur
Olivier POULIQUEN DIRECTEUR DE RECHERCHE, CNRS délégation Provence et Corse	Président
Anne MANGENEY PROFESSEUR DES UNIVERSITES, Université Paris Cité	Examinatrice
Kristen COOK CHARGE DE RECHERCHE, IRD - ISTerre	Examinatrice
Cédric LEGOUT MAITRE DE CONFERENCES HDR, Université Grenoble Alpes	Examinateur

Invités :

Florent Gimbert
CHARGE DE RECHERCHE, IGE
Velio Coviello
CHARGE DE RECHERCHE, CNR - IRPI

To my family

To my friends

To people suffering

And to those who take care of them

Acknowledgements

19/06/2023

I think that these are at the same time the easiest and most difficult lines of the manuscript to write. The easiest, because I feel extremely grateful for the time I spent at IGE, at INRAE, in Grenoble, and the words "thank you" come out spontaneously from my mouth. This is not sentimentalism, but reality. These lines are also the most difficult, though. How can I remember everyone? I have been lucky enough to meet many wonderful people (in and out of the lab) that have helped me to enjoy this journey, even when spending only some hours together. Besides these words, I hope I have demonstrated my gratitude to all these people in person.

This manuscript is the fruit of the research I have been able to carry out, therefore I cannot help but thank my supervisors first, Alain Recking and Florent Gimbert.

Alain gave me the key of the laboratory of hydraulics at IRSTEA (later on become INRAE) in October 2018, for the traineeship of my master thesis that paved the way for my PhD. Already at that time I was impressed by his experience in fluvial geomorphology and hydraulics, but in particular by his trust in students' works: Alain tells you the goal to reach, but it is up to you to build your path. Thank you Alain for the freedom you gave me during these years of experiments and investigations, and for inspiring me while talking about rivers when a sentence was sometimes sufficient to clarify days of overthinking. Thank you for motivating me during my moments of scientific hesitations and for your exhortations (tough at the moment but, looking back, needed). I have also appreciated the patience you had in managing a master in procrastination like me: I know what it means to adapt to different way of working. You helped me leave my comfort zone and if I know something more about the world of research and mountain rivers is because of the expertise you shared with me.

Florent was my main supervisor during the PhD, and he was the first to introduce me to the fantastic world of environmental seismology. I have been always amazed by his capacity to merge different disciplines and approaches (geophysics, glacier dynamics, fluvial processes, physical modelling, experiments, …) and his passion in doing research. Thank you Florent for your contagious enthusiasm, your willingness to discuss, your availability in explaining me how to use seismic methods and interpret seismic signals (over and over), but also your suggestions on how to write a paper, make a poster, or give a talk. I really felt like you sincerely cared about my professional growth. I cannot count the times I knocked at your door saying "Florent, est-ce que t'as une minute?", and then this minute became half an hour. I have extremely appreciated the fact that our scientific discussions were not lessons of a professor to the student, but rather a dynamic exchange of ideas: how fruitful the discussions were when we disagreed! Last but not least, thank you for the time spent in talking about society, culture, for laughing together at my (not always funny) jokes, and sharing personal feelings when sad events hit our lab. I couldn't have asked for a better supervision, in terms of science and human relationships.

I have spent a large amount of time in the laboratory of hydraulics at INRAE doing experiments. It is my pleasure but also "moral duty" to thank Hervé Bellot. Hervé, your presence has been crucial for my experiments, from my traineeship to my PhD. Despite the enormous amount of engagements and your busy schedule, you were always available for me. Thank you for your practical help in the lab, installing instruments, building stuff, or assisting me during the experiments. I have particularly enjoyed our discussions, and you inspired me also by a scientific point of view thanks to your interest in the interpretation of the observations. Thank you for your energy and laughter.

On the same line, I cannot help but thank the technical support I have had during these years. The INRAE can benefit from the super team composed of Christian Eymond-Gris, Alexis Buffet, and Firmin Fontaine. I cannot imagine the lab without them. In particular, thank you Christian for the time you spent with me for reparations and installations on the flume. Thank you for your evergreen availability and huge expertise. I loved spending some time at the "atelier" talking about life, music, and of course… bikes! Thank you for your kindness. Thank you Alexis for your availability, always with the smile despite the amount of work to do. I would also like to thank Frédéric Ousset and our unforgettable Xavier Ravanat, whose support has been crucial to start the experiments of my PhD.

I would also like to thank Maarten Bakker, with whom I have spent more than 3 years at both INRAE and IGE. Thank you Maarten for your help for interpreting seismic observations and for sharing with me your methods: your experience and friendship meant a lot to me. Sincere thanks to Guillaume Piton, whose PhD manuscript inspired me a lot during my experiments. Thank you Guillaume for your help in collecting data for the analysis on the Storm Alex.

Finally, by a scientific point of view I would like to thank the Committee that has followed me during the PhD: Eric Larose, Francesco Comiti, Philippe Frey, and Philippe Roux. You trained me for the defense with your questions and comments, and gave me interesting suggestions. I would like to thank the jury of my defense: Olivier Pouliquen, Matteo Berti, Anne Mangeney, Kristen Cook, and Cédric Legout. It has been an honour for me to share my research with you and benefit from your expertise. Thank you for your time, your questions, constructive criticism, and suggestions. I would like to thank Velio Coviello, invited participant to my defense. Velio has suddenly passed away less than two weeks after my defense during an accident in the mountains, and I should have worked with him in the postdoc I'm currently doing at CNR-IRPI in Padova (Italy). Thank you Velio for what you did in the field of seismic monitoring of debris flows, but in particular thank you for your smile, your energy and the "free spirit" I have been able to feel when we discussed and met. I will try to do something good also for you.

If I take a step back, this PhD would not have been possible without the support of the IGE and INRAE laboratories. I would like to thank the two labs for providing a beautiful working environment and state-of-the-art tools to do research. Many thanks to the direction of the labs, administration, IT, the cleaning service, the security staff (for their patience when I happened to be in the lab finishing experiments beyond the allowed hours!), and all the people involved. Thanks also to the communication services for spreading our research and organising events for all of us. I believe that sometimes with some arrogance we (who directly do research) think that all these people work for us, when in fact we are all on the same level and work together.

Many thanks to the CryoDyn, ETNA, and LESSEM teams at IGE and INRAE. It has been a real pleasure to spend these years with such special people and friends. I am terribly afraid of forgetting someone (I have always been paranoid), which is why I will not mention any particular names. A huge thank you to my office mates, PhD students, permanents, postdocs and interns. I have grown so much thanks to you. Thank you for your presence. Coffee breaks, quizzes, political and cultural discussions, weekend together, beers, raclettes, hikes, laughter, and tears. Last year, we tragically lost a dear friend and colleague of the CryoDyn team, Jérémie Mouginot. It is still hard, especially for those who were close to him, but from those weeks of heavy sadness I will never forget the union of the group. We were all one, no one was alone. Thank you to everyone for the hugs, the emotions, the words of comfort we shared. And thank you Jérémie for your kindness, your smile, your irony, and your presence in the lab. As your daughter asked us, we will never forget you.

If I have truly enjoyed this journey, it is also thanks to my life "grenoblois" out of the lab. I have spent wonderful years at "Maison Perreau" with my roommates. Thank you for the time we spent together (Covid-19 lockdown included!), our dinners and weekends. Thank you to all the friends from all over the world that I have met during these years. Special thanks go to the voluntary

association “Grain de Sel Hors-les-Murs”, which I have discovered during my PhD. Sometimes, when we are busy, we forget what is most important. I want to sincerely thank all the people I met, volunteers and people in need, for showing me what humility, simplicity and brotherly help is all about. All these elements should be present in the world of research too. If our society survives, it is thanks to this type of association that operates discreetly in the areas forgotten by the State. Thank you to the parish of St Joseph, a catholic community of young believers in Grenoble. From the outside (and sadly also according to someone inside), religion means rules to follow, certainty, and conviction in something which is totally disconnected from the ground. In fact, I deeply believe that if lived correctly, faith is a continuous training in facing doubts and reality. Thank you for being an example of authentic faith based on love and compassion, which is as far away as possible from judgement and bigotry and those who use religion for political ends.

Finally, thank you to my Italian friends who have always supported me over these years, with our calls and reunions every time I came back home for the holidays. A big, big thank you to my parents, who have always showed me enthusiasm (more than mine) and pure joy for my adventure despite being far from the scientific and academic world. Thank you to mamma e babbo, and to my extra-large family, for having always taught me that “we” is better than “I”, both in joy and in sorrow, and that yes, “love is strong as death”.

I think very few will read this manuscript (especially the acknowledgements...), but let me leave a humble advice for supervisors and students: be yourself, do not hide your weaknesses, your shortcomings, your difficulties, even personal ones. Be kind and patient, students with your supervisors, and supervisors with your students. And be happy and smiling, publishing papers can wait until next week… ☺

Summary

Mountain rivers can be the place of very intense sediment transport which has the potential to strongly shape the landscape and impact the safety of inhabited areas. However, our understanding on the physics of the processes is limited by a lack of field observations, which is linked to the unpredictable and destructive nature of such events. The use of passive seismology has been proposed as an alternative to classical monitoring techniques. Fluvial processes exert force fluctuations on the riverbed, and these forces generate ground vibrations that can be detected continuously and remotely by seismometers. Although seismic signals contain unique information about their source, the potential of using seismic observations to investigate intense sediment transport has been explored only partially.

In this PhD we investigate the physics of intense sediment transport in mountain rivers through a multidisciplinary approach involving seismic methods. We moved on two different but parallel tracks, that is, laboratory experiments and field observations, in order to explore the processes at different spatial scales and across a wide range of river settings.

In the laboratory, we focused our analysis on steep low-order mountain rivers, which are episodically subject to massive sediment pulses from the destabilization of upstream sediment deposits. We observed that, more than by the hydraulic forcing, deposit destabilization and pulse propagation along the channel are driven by significant grain-to-grain interactions in which the action of fine particles play a central role. The seismic observations collected during the experiments showed non-trivial relationships between the basal force fluctuations generated by the body of the sediment pulses and several flow properties. However, most complexities are suppressed by the unique negative relationship exhibited by force fluctuations and solid concentration. We advance that solid concentration best describes force fluctuations as being a proxy for particle agitation, and we propose to interpret this link within the framework of the local $\mu(I)$ rheology of dense granular flows.

In the field, we investigated the dynamics of flood events that occurred in the Séveraisse River (Écrins Massif) and in the Vésubie and Roya catchments (Maritime Alps), the latter of which was particularly extreme and devastating. On the Séveraisse River, we localized active areas of sediment transport at high resolution by means of a dense seismic array, and we inferred high sediment transport rates and morphological changes based on frequency-based scaling relationships between water discharge measurements and seismic power. On the Vésubie and Roya catchments, the seismic observations captured the general evolution of the extreme flood as depicted by the rainfall-runoff simulations, but they also unravelled intense sediment transport resulting from landscape perturbations that couldn't be explained solely by the hydraulics.

Finally, with this PhD we have shown that intense sediment transport in mountain rivers is characterized by a strong interplay between hydraulic forcing, sediment supply conditions, and interactions within the granular phase. In this complex scenario, we have demonstrated that seismic methods constitute a valid tool to resolve a diversity of processes that is difficult to explore through classical theories and monitoring techniques.

Résumé

Les rivières de montagne peuvent expérimenter phénomènes de transport sédimentaire très intense qui ont le potentiel de façonner fortement le paysage tout en constituant un aléa pour les zones habitées. Cependant, notre compréhension de la physique de ces processus est limitée par un manque d'observations de terrain, ce qui est lié à la nature imprévisible et destructrice de ces événements. L'utilisation de la sismologie passive a été proposée comme une alternative aux techniques de suivi classiques. Les processus fluviaux exercent des fluctuations de force sur le lit de la rivière, et ces forces génèrent des vibrations dans le sol qui peuvent être détectées en continu et à distance par des sismomètres. Bien que les signaux sismiques contiennent des informations uniques sur leur source, le potentiel de l'utilisation des observations sismiques pour étudier le transport sédimentaire intense n'a été que partiellement exploré.

Dans cette thèse, nous étudions la physique du transport sédimentaire intense dans les rivières de montagne par une approche multidisciplinaire impliquant des méthodes sismiques. Nous avons suivi deux voies différentes mais parallèles, au laboratoire et sur le terrain, afin d'explorer les processus à différentes échelles spatiales et dans un large éventail de contextes fluviaux.

Au laboratoire, nous avons focalisé notre analyse sur les rivières de montagne à forte pente, qui sont susceptible de recevoir des bouffées sédimentaires provenant de la déstabilisation des dépôts sédimentaire en tête de bassin versant. Nous avons observé que, plus que par le forçage hydraulique, la déstabilisation des dépôts et la propagation des bouffées étaient dictées par de fortes interactions granulaires, au cours desquelles les particules fines jouent un rôle central. Les observations sismiques ont montré des relations non triviales entre les fluctuations de force basale générées par le corps des bouffées sédimentaires et plusieurs propriétés de l'écoulement. Cependant, au-delà de ces complexités, une relation négative unique a été obtenue entre les fluctuations de force et la concentration solide. Cette concentration apparait être un bon proxy de l'agitation des particules, comme le suggère la rhéologie locale $\mu(I)$ des écoulements granulaires denses.
Sur le terrain, nous avons étudié la dynamique d'événements de crue qui se sont produits sur la Séveraisse (Massif des Écrins) et dans les bassins versants de la Vésubie et de la Roya (Alpes maritimes), ce dernier événement ayant été particulièrement extrême et dévastateur. Sur la Séveraisse, nous avons localisé des zones actives de transport sédimentaire à haute résolution avec un réseau sismique dense, et nous avons déduit des flux élevés de transport sédimentaire et des changements morphologiques en nous basant sur les relations à différentes bandes de fréquence entre les mesures de débit d'eau et la puissance sismique. Sur les bassins versants de la Vésubie et de la Roya, nous avons montré que les observations sismiques capturaient l'évolution générale de la crue telle qu'elle est décrite par les simulations pluie-débit, mais qu'elles permettaient également de mettre en évidence un transport sédimentaire intense résultant de perturbations du lit et des versants, qui ne pouvait être expliqué uniquement par l'hydraulique.

Avec cette thèse nous avons montré que le transport sédimentaire intense dans les rivières de montagne est caractérisé par une synergie entre le forçage hydraulique, les conditions d'alimentation sédimentaire, et les interactions au sein de la phase granulaire. Dans ce scénario complexe, nous avons démontré que les méthodes sismiques constituent un outil unique pour résoudre une diversité de processus qui est difficile à explorer dans le cadre des théories et techniques de suivi classiques.

Key words: Mountain rivers, intense sediment transport, passive seismology
Mots clés: Rivières de montagne, transport sédimentaire intense, sismologie passive

Chapter 1: Introduction

1.1 Humans and rivers

In the fortunate part of the world where the access to education is guaranteed by law, almost every child has attended a history lesson regarding the vicissitudes of an old region of Western Asia considered as one of the cradles of human civilization: Mesopotamia. This toponym comes from the ancient Greek and literally means "land between rivers". Indeed, this area is located between the Tigris and Euphrates rivers in the northern part of the so-called Fertile Crescent, which nowadays spans portions of several modern States of the Middle East. The presence of both rivers was of great importance for the prosperity of the populations that settled there over the centuries (among them, we most probably remember the Sumerians, Assyrians and Babylonians), it drove the development of agriculture and inspired innovative technologies of water storage (Morozova, 2005). Similarly, we should have heard about the key role played by the Nile River in the fortune of ancient Egyptians (Figure 1.1). The Nile not only constituted a mean of transporting materials for the expert architects of ancient Egypt, but also brought nutrient-rich sediments to lands and water to inhabitants, encouraging the development of agricultural skills and innovative techniques for benefitting from floods. We cannot fail to mention the watery origins of Rome and the Roman Empire: rivers flowed at the core of Romans' life through irrigating farms and transporting people and goods, and they were also a mean for the Empire to map boundaries and control the territory (Campbell, 2012).

Figure 1.1 : The Nile mosaic of Palestrina. The Nile mosaic of Palestrina is a floor mosaic that was part of a grotto in Palestrina, a town of Ancient Rome in central Italy. It dates to c. 100 BCE and it depicts life around the Nile during a flood, in its passage from the Blue Nile to the Mediterranean Sea. This artwork manifests the interest that Roman artists started showing in ancient Egyptian exoticism, but is also one of the most important examples of "Nilotic landscape" portraying the central role played by the Nile River for ancient civilizations. Retrieved from (https://www.worldhistory.org).

However, rivers constituted a double-edged sword since all these ancient civilizations were highly vulnerable to environmental stresses. Although the inhabitants of Mesopotamia benefited from the floods of the Tigris and Euphrates rivers, it could happen that the drainage basin reacted in a dramatic manner to the heavy rains of mountain regions. As a result, large valleys previously crossed by streams could suddenly find themselves high and dry, whereas entire villages could be submerged by angry waters. These river dynamics have long been acknowledged as protagonists in the development of Mesopotamian civilizations (Schumm, 1977), even to the point of being a potential cause of decline for some of them (Adams, 1981). The Nile river was an unquestionable source of prosperity for ancient Egypt, but the political history of its region followed cycles of crisis that appear to coincide with negative Nile behaviors such as alternating extreme lack of water and catastrophic floods (Butzer, 1984). In front of these dramatic events, we can imagine that river activity started concerning humans. Why and how do rivers move? Can we anticipate flood events? The Roman Empire was not sheltered from the wildness of rivers. Lawyers and land surveyors at the time recognized the need to find a balance between the benefits and the dangers related to living in the proximity of water courses (Campbell, 2012). In this regard, unique information can be retrieved from ancient documents about the administrative consequences of river floods:

"There is **more than one type of alluvial activity** through which rivers inflict loss on landholders. For example, the river Padus (Po), leaving its bed, bursts through the middle of someone's farm and makes an island between its old and new course. In this case the question concerns who should own the soil that it deposited, since the nearest landholder is suffering no small loss, as a river which is public property is flowing through his land"

(Land Disputes T42.18-25, Agennius Urbicus. The English text is provided by Campbell (2012))

And again:

"The dispute concerns the soil that a river deposits, and complex questions are thereby produced, namely, whether it should belong to the person on the opposite bank whose land has been augmented on the retreat of the river water, or whether the man who lost some of his land should cross over and take possession of that soil that the river deposited. But against this is raised a very subtle point, namely, that **the soil that one man lost does not immediately cross over to the other bank but is removed and washed away**. On the other hand, the neighbour receives a very different type of soil, because, while the former lost soil that was perhaps cultivated and fertile, the latter was left with a residue of **sand**, **stones and mud** washed up by the flood water"

(Papyrus from Oxyrhynchus (*P. Oxy.* III.486, lines 14–16, A.D. 131). The English text is provided by Campbell (2012))

Through the simple descriptions of the writers, legal matters set/put aside, we can appreciate a certain awareness of the complexity of river processes related to sediment transport. It was already acknowledged that rivers transport a wide range of sediments of all sizes through different "alluvial activities", and that especially during flood events we do not necessarily know where the material comes from and how far it will be transported before deposition. Hundreds and hundreds of years later, many scientists would have tried to solve the puzzle of sediment transport. We will see in the following that many investigations are still work in progress.

1.2 Theories of sediment transport

1.2.1 Sediment transport style and threshold for motion

From the fragments of ancient history proposed in the previous paragraph we understand that rivers cannot be considered passive spectators or static boundaries in a map, but rather living entities that move, expands, retire, and redistribute mass across the Earth's surface. Fluvial systems have indeed the power to shape the landscape as they mobilize most of the global fluxes of sediments, from uplands to basin outlet, acting like "jerky conveyor belts" (Ferguson, 1981). Historically, the total sediment load of a river has been classified by its mode of transport. We distinguish between suspended load, which consists in the fine material carried within the water column by turbulence (e.g. silt, clay, and fine sand), and bedload, including the coarser material that rolls, slides, and saltates in direct contact with the riverbed (Gilbert, 1914). If we further consider the sediment load carried in solution from chemical weathering, this is defined as dissolved load (Figure 1.2).

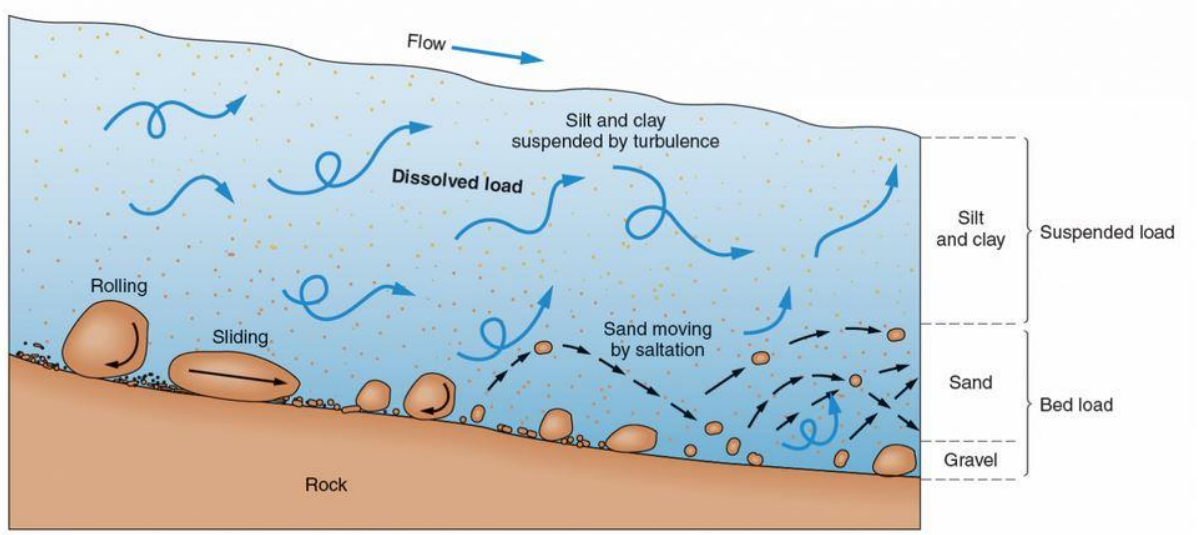

Figure 1.2 : Conceptual representation of the sediment load transported by a river. The transport of the coarsest particles is defined as bedload and consists in the material that rolls, slides, and saltates over the riverbed. The fine particles that are carried by turbulence and flow downstream within the water column constitute the suspended load. Finally, the material that is carried in solution mostly in the form of ions is called dissolved load. Retrieved from (https://worldrivers.net).

At the turn of the late 19th and early 20th century scientists recognized the need to quantify bedload transport, that is, understand incipient motion conditions and estimate the amount of sediments moved under certain flow conditions. Bedload transport predictions are indeed of primary importance not only to describe fluvial morphology (Schumm, 1977), but also to restore river habitat (Buffington et al., 2004), and manage natural risks for humans (Badoux et al., 2014).

At the particle scale, the pioneering framework for incipient motion conditions was built by Shields (1936), who formalized previous intuitions of du Boys (1879). Shields carried out an extensive experimental work to investigate bedload transport and proposed that sediment mobility could be seen as a threshold process in which particles start moving when the dimensionless shear stress

induced by the water flow (i.e. the Shields stress τ^*) exceed a critical value, which is defined as the critical Shields stress τ_{cr}^*:

$$\tau^* = \frac{\tau}{g(\rho_s - \rho_w)D} > \tau_{cr}^* \quad (1)$$

where $\tau = \rho {u_*}^2$ is bed shear stress approximated under the assumption of uniform flow, ρ_w is water density, $u^* = \sqrt{ghS}$ is the bed shear stress velocity, g is acceleration due to gravity, h is flow stage, S is channel slope, ρ_s is sediment density, D is particle diameter. Shields showed that the critical stress varied with the particle Reynolds number ($Re^* = \frac{u^* D}{\nu}$, where ν is water dynamic viscosity) but it reaches an approximately constant asymptotic value when $Re^* > 1000$, i.e. for rough and turbulent flows. After this fundamental contribution, Shields' theory has been developed and revisited over the years. Although Shields proposed a unique critical Shields parameter, different values for particle mobility were found (Meyer-Peter and Mueller, 1948; Parker et al., 2003). In a review on the subject, Buffington and Montgomery (1997) advanced that, along with methodological bias (e.g. definition and/or measurements techniques for the shear stress τ), multiple factors could influence the critical Shields stress. Several studies demonstrated that complexities arise in the case of mountain rivers, where the critical Shields stress has been shown to increase mainly because of large bed roughness relative to flow depth (Solari and Parker, 2000; Lamb et al., 2008; Recking, 2009; Prancevic and Lamb, 2015). Due to their shallow water flows, particle shape and exposure become important factors to consider (Ashida and Bayazit, 1973; Armanini and Gregoretti, 2005), while the presence of poorly sorted sediment mixtures enhances the influence of hiding and protrusion effects between particles of different size (Wilcock and Southard, 1988; Wilcock et al., 2001).

1.2.2 The equilibrium concept

In parallel, and at a bigger scale, du Boys (1879) and Gilbert (1914) laid the foundation of bedload transport predictions through describing the tendency (or not) of rivers to transport sediments. In particular, Gilbert (1914) defined the river transport capacity as "the maximum load a stream can carry", which was proposed to be a function of various factors such as channel slope, water discharge, and particle size. A river section at transport capacity is said to be at equilibrium because it conveys as much material as it can. If one of the variables mentioned above changes, the equilibrium is disrupted and a river can switch to under or over capacity conditions: in the first case, it will erode material from its bed, in the second one it will deposit some. Some decades after, Lane (1955) gave a quantitative expression to this definition, stating that rivers adjust their slope in order to balance sediment flux and water discharge (Figure 1.3).

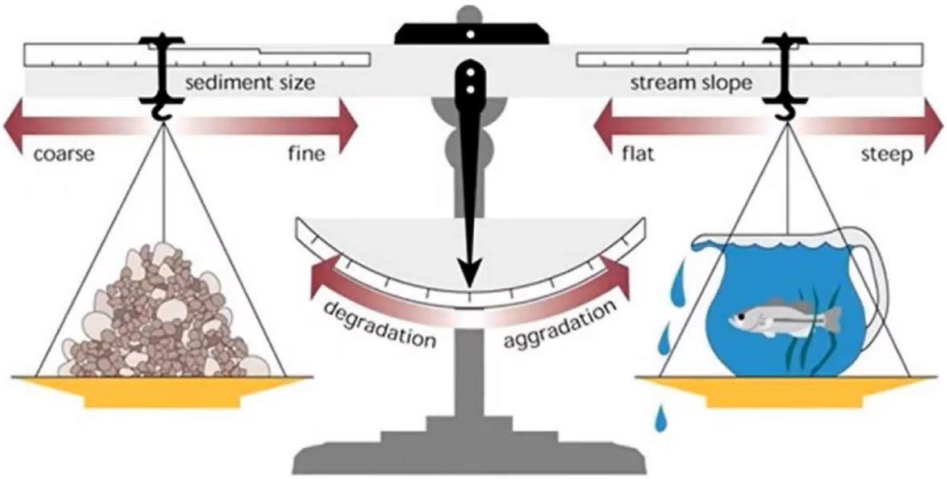

Figure 1.3 : The Lane's balance. This schematic model shows the different relationships that exist between the variables controlling the equilibrium state of a river. A riverbed degrades or aggrades depending on the sediment load and size (left side of the balance), and on the water discharge and channel slope (right side of the balance). Retrieved from Stein et al. (2012).

One of the best known theory on river systems, that is their quest for equilibrium (Lane, 1955), has also been one of the most debated. Lane himself recognized that neither in very short or long time periods natural rivers can be considered to be in equilibrium. Years later this intuition has been confirmed by a large number of laboratory experiments and field observations showing that natural rivers experience strong fluctuations, from instantaneous to seasonal time scales and under similar mean flow conditions (Gomez et al., 1989; Hoey, 1992; Ancey and Heyman, 2014). Due to this evidence, the idea that rivers adapt to boundary conditions to reach an equilibrium state has been also criticized conceptually. For instance, Phillips (2010) states that the real job of a river is to transport water, while erosion and deposition are merely a by-product of hydrological processes. According to this view, equilibrium (i.e. slope adjustments) is a potential outcome that emerges from, and not a goal of, river processes. Although this difference may be seen as "philosophical", the author argues that this change of perspective should influence interpretations and predictions. However, even within this paradigm, one question remains: why does bedload transport fluctuate?

Some authors explain this "noisy dynamics" (Ancey, 2020) by the intrinsic stochastic nature of sediment transport. For instance, the probabilistic framework of the Einstein's model (1950) inspired the theory of collective entrainment, for which bursts of bedload transport are due to clusters of sediments mobilized by inter-particle collisions around the threshold of motion (Ancey et al., 2008; Heyman et al., 2013; Lee and Jerolmack, 2018). Other works have proposed extrinsic sources of fluctuations, such as particular bed topography (Ferguson, 2003), or sediment supply conditions (Recking, 2014; Piton and Recking, 2017). In particular, the latter can be a predominant factor in mountain rivers where the transported sediments are not always supplied by the bed, which is composed of rarely mobile and erodible elements (e.g. big boulders, steps or bedrock), but rather provided by episodic inputs of material coming from outside. For these rivers, the sediment transport activity highly depends on the connection (or not) with external sediment sources such as hillslopes, eroded cliffs or glaciers (Recking, 2012; Piton and Recking, 2017; Comiti et al., 2019; Liébault et al., 2022). The presence of cyclic bedload fluctuations occurring under steady flow conditions (Hubbell, 1987) has suggested the presence of processes controlling their

periodicity. In this case, among physical processes such as bedforms migration (Gomez et al., 1989) and water flow hysteresis (Ryan et al., 2005), nowadays grain sorting is a process largely recognized as a trigger of bedload fluctuations in gravel-bed rivers (Iseya and Ikeda, 1987; Frey and Church, 2009; Recking et al., 2009; Bacchi et al., 2014).

1.2.3 Bedload transport predictions

Under the hypothesis of steady-state relationships between sediment supply and transport capacity, one can attempt to estimate bedload fluxes. Einstein (1950) approached bedload transport as a probability problem and proposed a dimensionless parameter called "intensity of bedload" defined as:

$$\Phi = \frac{q_v}{\sqrt{\left(\frac{\rho_s}{\rho_w} - 1\right) g D^3}} \tag{2}$$

where q_v is the volumetric sediment flux per unit width to predict. Most equations for predicting q_v are based on the Einstein's parameter and have been derived by fitting laboratory data or field measurements. They express Φ as a function of multiple variables such as river slope and width, water discharge, sediment size, and Shields stress (Meyer-Peter and Mueller, 1948; Schoklitsch, 1962; Ackers and White, 1973; Bagnold, 1980; Van Rijn, 1984; Abrahams and Gao, 2006).

Thanks to a growing number of laboratory experiments and field observations, existing bedload equations have been tested. It has been shown that most equations can lead to under or over predictions with errors attaining several orders of magnitude. Overall, errors are higher when dealing with mountain rivers where bedload fluxes are usually overestimated (Rickenmann, 2001; Bathurst, 2007; Chiari and Rickenmann, 2011; Schneider et al., 2016). The divergence between predictions and field observations has been mainly related to biases concerning the theories. First, equations are usually built on data coming from 1-D narrow flume experiments, which could be not representative of the wide range of natural riverbed morphologies potentially impacting sediment transport processes (Francalanci et al., 2012; Recking et al., 2016). Second, as seen above, at steep slopes there is also high uncertainty about the most suitable critical Shields parameter to consider, and this is reflected in predictions since the parameter is often used as input parameter to retrieve bedload fluxes. Furthermore, equations are obtained with reference to a single particle diameter which is usually representative of the fine fraction (D_{50}, i.e. the 50th percentile particle diameter), while the poorly sorted sediment mixture commonly found in natural rivers might require a calculation size-by-size (Wilcock and Crowe, 2003) or the choice of a characteristic particle diameter representative of the coarsest fraction (D_{84}) (Recking, 2010).

1.3 Dealing with granular complexities

1.3.1 A granular phenomenon

Despite many advances in observational and experimental methods, it is still challenging to study sediment transport and this is highlighted by the difficulty of predicting particle mobility and bedload fluxes. For this reason, over the years several explanations have been discussed to interpret the discrepancies between predictions and observations, and modifications have been proposed. However, by looking more closely, these modifications are of second order because they challenge the basis on which models are built only partially, that is, considering sediment transport as a process driven solely by hydromorphic factors. Particles are mobile when a critical shear stress, water discharge, or stream power is exceeded, and the amount of sediments moved by the flow is strictly linked to this surplus. In this regard, I find it interesting to highlight the results of Recking et al. (2012), who showed that equations for bedload predictions are most efficient when compared to long-term field measurements, such as sediment volumes collected at the inter-annual or annual time scale. The fact that equations work better for estimating long-term river sediment budgets rather than capturing bedload fluctuations or instantaneous values of bedload transport could be due to hydraulic conditions being adequate for explaining the evolution of a river over relatively large time scale, but they may be not sufficient to describe the physics of sediment transport at small spatial and temporal scale. Although the hydraulic forcing undoubtedly plays a key role in the sediment transport physics, the processes occurring within the granular phase (i.e. grain-to-grain interactions) should not be overlooked according to relatively recent studies (Frey and Church, 2009, 2011; Houssais et al., 2015). This school of thought has probably its roots in the theories of collective entrainment (Ancey et al., 2008), which started drawing the attention to the fact that, while flowing along a river, a particle is not the maker of its own fortune, which also depends on the behavior of the neighbour particles transported with it or constituting the bed. This aspect is particularly exacerbated during intense sediment transport, when the interactions between particles are significant.

For these reasons, it has been proposed that bedload transport should be investigated as a "granular phenomenon" (Frey and Church, 2011), that is, through the laws describing granular flows. Granular flows are often classified (Forterre and Pouliquen, 2008) into three different regimes (Figure 1.4): a gaseous regime in which the flow is dilute and rapid and particles interact mainly by binary collisions (Goldhirsch, 2003); an intermediate regime in which the granular flow is dense but still flows like a liquid, with particles interacting both through collisions and frictional contacts (GDR MiDi, 2004); a dense quasi-static regime in which the deformations are very slow and particles interact mainly by frictional contacts (Campbell, 2002). Bedload transport is thought to experience all these states, from quasi-static within the bed to gaseous in the upper bedload layer (Maurin et al., 2016).

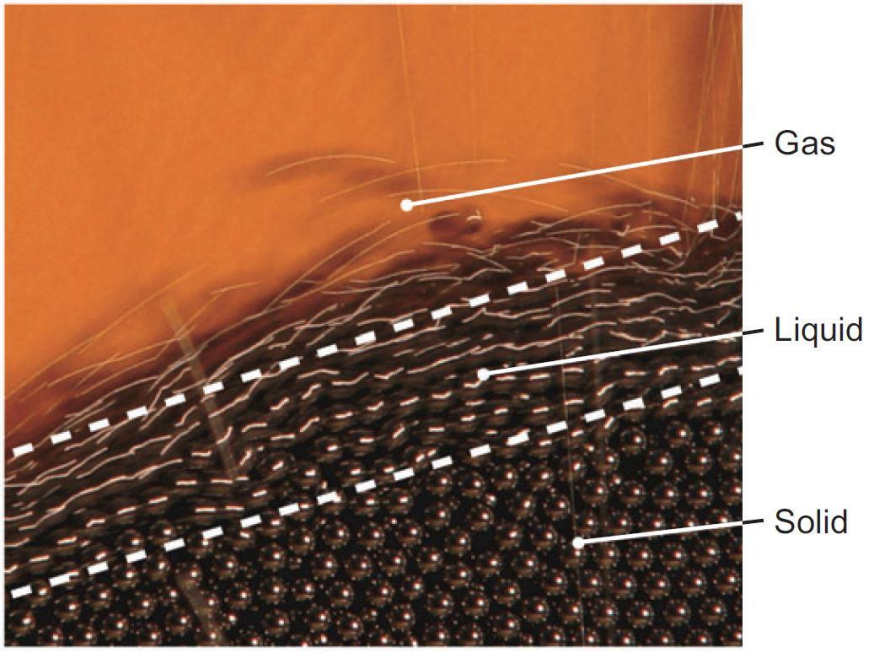

Figure 1.4 : Granular flow of spherical beads. This photo illustrates three different regions that develops through pouring beads on a pile. We can observe the different flow regimes: a solid region at the bottom with no movement or very slow deformations (quasi-static), a liquid region with dense layers of beads, and a gaseous region with beads bouncing downslope. Retrieved from Forterre & Pouliquen (2008).

The dilute and rapid regime has mainly been described using the kinetic theory of granular gases (Campbell, 1990; Goldhirsch, 2003). Alternatively, dense granular flows (liquid regime) have been described through the local $\mu(I)$ rheology, which is based on the dimensional analysis of granular systems in a sheared configuration (GDR MiDi, 2004; da Cruz et al., 2005; Forterre and Pouliquen, 2008). The unique dimensionless number controlling the system is the so-called inertial number I:

$$I = \frac{\dot{\gamma} D}{\sqrt{\frac{P}{\rho_s}}} \tag{3}$$

This number compares the microscopic time scale of particles rearrangement due to a confining pressure P and the macroscopic time scale linked to deformation due to shear rate $\dot{\gamma}$. Small values of I correspond to a quasi-static regime where macroscopic deformation is slow compared to microscopic rearrangement, while large values of I are associated with rapid flows. The dimensional analysis tells us that to switch from a regime to another, one can either increase the shear rate or decrease the pressure. Although the original theory refers to dry granular flows, the $\mu(I)$ local rheology has also been extended to account for the presence of interstitial fluids (Courrech du Pont et al., 2003; Cassar et al., 2005).

Following the same granular argument, the interactions between particles can be described in terms of network of contact forces, also known as force chains (Furbish et al., 2008). Contact forces are vectors of momentum transport, which are considered to affect the rheological behavior of granular flows (Macaulay and Rognon, 2020). Force chains carry significant implications for

granular processes, such as producing shear forces necessary for particle entrainment (Estep and Dufek, 2012), reducing the resistance to mass failure (Booth et al., 2014), or localising basal forces many time greater than the weight of single particles (Furbish et al., 2008). However, these processes have been rarely considered in the study of sediment transport in rivers.

1.3.2 The occurrence of grain sorting

The importance of studying the interactions between grains is emphasized in the case of a poorly sorted sediment mixture, in which significant grain sorting processes occur. This phenomenon has been observed in debris flows (Iverson, 1997), described for dry granular flows (Gray, 2018), and has also important implications for bedload transport in rivers (Frey and Church, 2009). We can distinguish two distinct sorting processes: if the sediment mixture is at rest, fine particles can percolate spontaneously in the voids between the bigger particles, but when the sediment mixture is mobile (e.g. subject to shear stress) the percolation mechanisms are enhanced by kinetic sieving and squeeze expulsion (Savage and Lun, 1988). The study of grain sorting has drawn the attention of geomorphologists and hydraulic engineers since the beginning of the XX century (Gilbert, 1914; Iseya and Ikeda, 1987; Recking et al., 2009; Bacchi et al., 2014). Through this wide range of flume experiments and field observations it has been shown that a riverbed subject to constant feeding conditions can experience cyclic states of (i) surface armouring and low bedload transport rates, associated with the percolation of fine particles in the subsurface, and (ii) armour breakings and bedload bursts, associated with the release of fine particles from the subsurface. The introduction of fine particles is thought to enhance the transport efficiency of the coarser material through reducing bed roughness (Bacchi et al., 2014; Dudill et al., 2018), or forming a lubrication layer (Chassagne et al., 2020) as observed in the case of granular avalanches (Linares-Guerrero et al., 2007). As mountain rivers are typically composed of poorly sorted sediment mixture, it becomes crucial to take into account these mechanisms to understand the complexity of sediment transport in such environments.

1.4 Mountain rivers: a place for intense sediment transport events

In the previous paragraphs we have seen that mountain rivers are not always efficient machines for transporting sediments. Bed roughness can strongly dissipate the flow energy, hiding effects caused by the presence of big boulders affect particle mobility, and deficits in sediment availability from the bed reduce transport rates. However, under particular conditions mountain rivers can leave their quiescent state to experience very intense sediment transport events. How can this happen?

Mountain catchments usually exhibit high degrees of hydrological and landscape connectivity (Wohl, 2010). The high degree of hydrological connectivity is related to the capability of water to move very rapidly throughout the landscape. Thanks to the steepness of the reliefs (Figure 1.5) rainfall, rain-on-snow, and snowmelt easily turn into surface runoff, potentially leading to high in-channel water discharge able to rework riverbed topography, even dramatically in the case of flood events. Landscape connectivity is also high in the sense that various landforms (e.g. hillslopes, cliffs, moraines, glaciers) are close to rivers. These landforms constitute sediment production zones because they are the place of mass wasting processes such as rockfalls, slope failure or gully erosions (Figure 1.5) The material can be stored for a variable amount of time in slope or terraces, which act like buffers for the sediment cascade (Harvey, 2001; Fryirs, 2013; Heckmann and Schwanghart, 2013). However, when destabilized by rainfall and/or surface runoff, these deposits become a quasi-unlimited source of sediments for the coupled channels, which are therefore prone to receive sudden bed-external material. In addition to this kind of sediment supply that mainly interests headwater streams, large amount of material can also be conveyed by landslides generated from the rainfall-induced failure of the hillslopes. In forested catchments, these instabilities can supply large amount of wood to rivers, a factor that enhances the morphological impact of floods (Comiti et al., 2008; Lucía et al., 2015). These two ingredients (i.e. hydrological and landscape connectivity) cooperate in triggering very intense sediment transport events, for which the theoretical frameworks of suspended and bedload transport valid for lowland rivers become incomplete. The physics of these events is diverse and depend on the morphology and location of the river within the catchment.

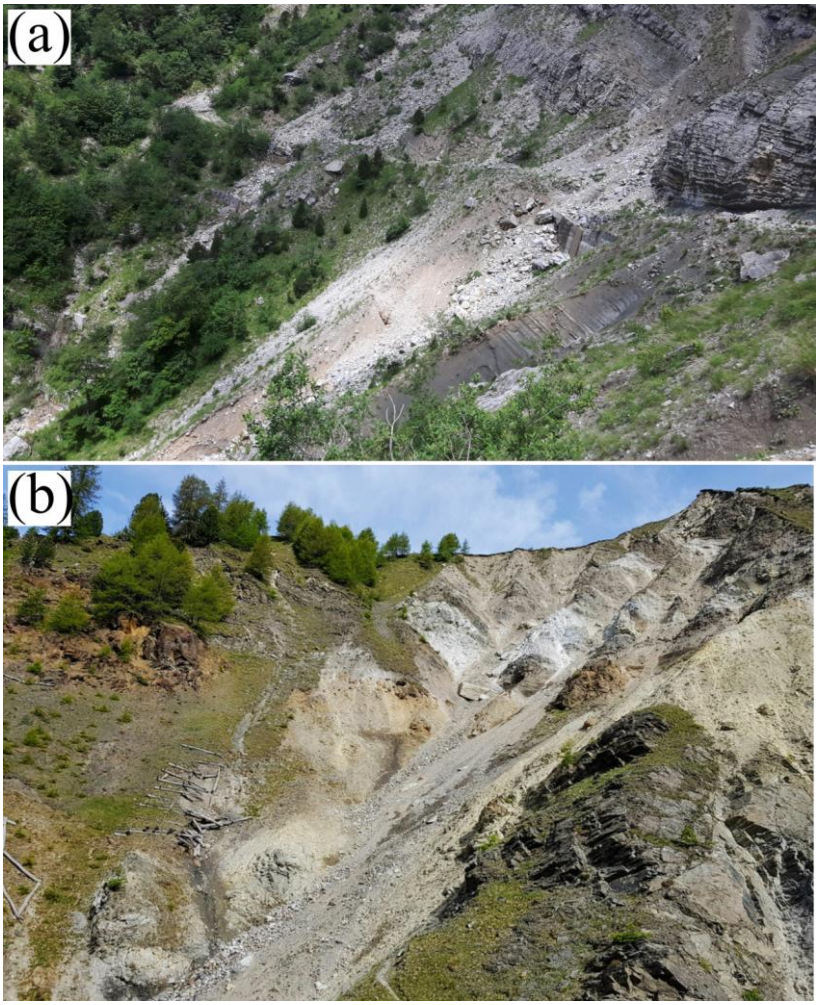

Figure 1.5 : The upper part of the mountain catchments of the (a) Roize River (France) and (b) Gadria Creek (Italy). We can observe large amount of material generated by mass wasting processes that accumulates both on steep reliefs and areas of decreased slope. The steepness and the confinement of the hillslopes promote the formation of significant runoff in case of strong hydrological events. Photo in (b) is courtesy of Velio Coviello.

1.4.1 Sediment-laden flows from bed-external sediment inputs

In the upper part of mountain catchments, steep and confined low-order rivers[1] are really close to sediment production zones. In this configuration, intense sediment transport events are thought to be mainly generated by abrupt bed-external sediment inputs (Figure 1.6).

On very steep slopes, debris flows can develop. Debris flows are gravity-driven flows exhibiting a significant solid concentration (often greater than 50%) where both the solid and fluid phase influence the motion (Iverson, 1997). These events usually initiate on deposits characterized by $S > 30 - 35$ % (Prancevic et al., 2014; Palucis et al., 2018), but can also propagate in downstream channels having $S \sim 10 - 15$ % thanks to the high initial momentum (Bertrand et al., 2013). Debris

[1] The order of a river is a positive whole number indicating the degree of branching of a river system. In most theories, streams located in the upper part of the catchment are characterized by a low order.

flows are characterized by a poorly sorted sediment mixture (ranging from clay to boulders), significant flow velocity and thickness, long runout distance and high impact forces (Iverson, 1997; Jakob et al., 2005; Berti et al., 2020). Debris flows are typically constituted by a coarse front carrying the largest clasts, sometimes collected along the path, which is followed by a finer-grained flow body and a more dilute tail (Iverson, 1997; Hungr, 2000) (Figure 1.6c). Another common feature of debris flows is their surging behavior, which has been mainly associated with regressive instabilities due to temporary flow blockage along the channel, and progressive instabilities, associated with roll wave dynamics (Zanuttigh and Lamberti, 2007; Kean et al., 2013).

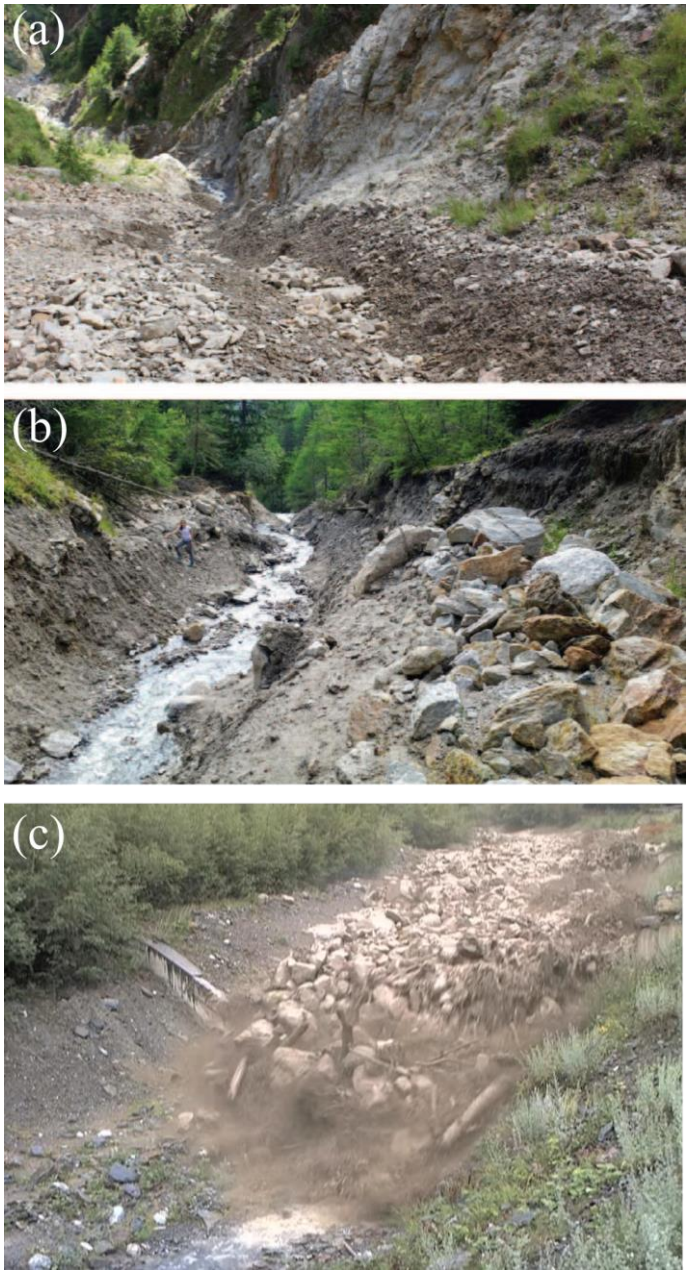

Figure 1.6 : The Gadria catchment (Eastern Italian Alps). (a) View on the main sediment source of the (b) downstream reach. (c) Debris flow generated by the destabilization of the upstream deposits propagating in the river. We can observe the large clasts and boulders carried by the debris flow front. Photos in (a) and (b) are retrieved from Coviello et al. (2021), photo in (c) is a snapshot from (https://www.youtube.com/watch?v=DXA7D82S4Ow).

The literature usually distinguishes two triggering mechanisms for debris flows: mobilization from landslide, when an increase of pore water pressure during intense rainfall events leads to the failure of the soil at a slip surface (Montgomery et al., 2009), and mobilization by surface runoff, for which sediment deposits destabilize at a critical water discharge (Coe et al., 2008). Compared to the former, the triggering mechanism of runoff-generated debris flows is still not clear (Kean et al., 2013). Given the difficulty to directly and quantitatively estimate surface runoff in the initiation zone, predictions on debris flow occurrence are mainly based on rainfall data. These thresholds tell us when a certain sediment transport event is potentially triggered, but the processes governing the destabilization of sediment deposits such as grain-to-grain bulking or en masse failure are still not completely understood (Coe et al., 2008). In the last years extensive monitoring networks have been developed to monitor the initiation zones of debris flows (Gregoretti et al., 2016; Comiti et al., 2014), but the understanding of particle-scale processes is rarely achieved in the field (Imaizumi et al., 2006). In this context, laboratory experiments could shed some light as they ensure controlled boundary conditions and enable the monitoring of several quantities at a time. However, only a few experimental works exist on the subject (Gregoretti, 2000; Prancevic et al., 2014; Palucis et al., 2018), and all of them use a nearly uniform grain size distribution, which is in contrast with the wide and often bimodal grain size distribution of mountain rivers (Casagli et al., 2003; Sklar et al., 2017).

Exogenous sediment inputs do not necessarily take the form of debris flows. Sediment pulse is the term which is typically used to define a large sediment flux propagating downstream, translating as a coherent wave and/or dispersing in place (Sutherland et al., 2002; Brummer and Montgomery, 2003). Previous studies have investigated the evolution of sediment pulses in gravel-bed rivers characterized by slope of ~ 1 %, wherein the riverbed has been shown to actively interact with the injected material (Lisle et al., 1997; Sutherland et al., 2002; Cui et al., 2003; Cui and Parker, 2005; Sklar et al., 2009). However, low-order rivers are generally armoured and constituted of rarely mobile boulders. In this configuration, sediment pulses are expected to move downstream with limited exchange of material with the local bed, which is usually composed by a grain size distribution that can be much different from the transported sediments (Piton and Recking, 2017). There are no experimental studies that investigate sediment pulse dynamics in such a configuration, and the few post-event field observations do not provide information about their spatial and temporal dynamics.

1.4.2 Debris floods and riverbed disruptions

In lower parts of mountain catchments, rivers are characterized by a wide range of morphologies. Their bed is not necessarily confined and heavily armoured as for low-order streams, but present alluvial sections such as plane-bed or braided reaches (Piton and Recking, 2017) which can be strongly reworked by high in-channel water discharges. During these events, sediment transport is intense because it is associated with strong geomorphological changes like channel widening and avulsions, deep incisions and bank erosion (Scorpio et al., 2022) (Figure 1.7).

Church & Jacop (2020) propose the term debris flood to describe "a flood during which the entire bed, possibly barring the very largest clasts, mobilizes for at least a few minutes and over a length scale of at least 10 times the channel width". This definition gathers a number of processes occurring in mountain rivers usually characterized by lower slope compared to debris flow-prone channels. While the motion of debris flows is mainly dictated by gravity, and the liquid and solid fraction are so thoroughly mixed that they appear to behave as a unique phase, debris floods are considered to be distinctive two-phase flows mainly driven by the tractive force of water, with a solid concentration that is still significant but usually < 50 % (Hungr et al., 2014).

The triggering dynamics of debris floods is still poorly understood, and mainly rely on video recordings or post-event investigations of the remaining sediment deposits (Manville and White, 2003; Church and Jakob, 2020). Similar to debris flows, debris floods can propagate in surges and are considered to be triggered by shear stresses induced by the water flow, which in this case is thought to dramatically exceed the critical Shields stress for motion (Church and Jakob, 2020). Debris floods arise from the mobilization of large portion of bed material as a result of extreme shear stress and additional momentum transfer through grain-to-grain collisions, but the local bed is not necessarily destabilized as these events can develop in upstream sections. Finally, debris floods can also result from the progressive dilution of debris flows in slower-flowing streams or increased water discharge (Church and Jakob, 2020).

Figure 1.7 : The impact of extreme floods. In October 2020, the Maritime Alps were hit by the Storm Alex that caused dramatic floods in several mountain catchments. The event was associated with very high water discharges and intense sediment transport that disrupted large parts of the fluvial landscape. (a) Bank erosion and deposition of material on roads. (b) Large bank collapse next to the Saint-Martin-Vésubie village and strong impact on river morphology. Photo credits: Florent Adamo/Cerema.

Most studies on debris floods in mountain rivers document pre- and post- states, aiming at quantifying the geomorphological impacts of such events within the channel and, more in general, in the landscape (Borga et al., 2014; Nelson and Dubé, 2016; Surian et al., 2016; Scorpio et al., 2018, 2022). By contrast, less is known about their intra-event physics (Brenna et al., 2021). This is mainly due to the lack of real-time measurements and observations (Borga et al., 2014), which is also due to the fact that floods often damage the instrumentation of the gauged sections for water discharge measurements. The picture gets worse for sediment transport processes, which are a difficult puzzle to solve although understanding how and when sediment moves is crucial to predict channel evolution and interpret morphological changes (Brenna et al., 2021). These knowledge gaps highlight the need for an alternative way to monitor rivers to better understand their dynamics.

1.5 Measuring bedload transport in mountain rivers

1.5.1 In-situ measurements

One difficulty in studying bedload transport in mountain streams is our limitation in monitoring such environment. Bedload transport measurements have been traditionally done directly by hand using samplers to collect and measure the amount of material transported over a given interval (Bunte et al., 2004). However, obtaining an accurate estimation of bedload by this approach is expensive and lacks temporal resolution. Automatic bedload sampling methods by means of bedload traps, have been developed for continuous surveys (Lenzi et al., 1999; Rickenmann et al., 2012), but these methods are technically challenging: they require access to the channel bed, either through the installation of sampling devices or through deployment during periods of bedload transport, and sampling duration is limited by the volume of bedload each sampler can hold.

Thanks to recent progress in both hardware technology and methodology, in the last decades several surrogate methods for monitoring bedload have been developed (Gray et al., 2010). These novel technologies can be divided in active or passive sensors. Active sensors are based on the emission of a signal and the recording of the response. Among them we distinguish Doppler current profilers (Figure 1.8a), able to estimate apparent bed velocities and infer bedload transport rates (Rennie, 2004); radars, emitting and receiving electromagnetic waves scattered by transported particles; smart tracers (Figure 1.8b), which enable particle tracking in river system through using microsensors (Gray et al., 2010). By contrast, passive sensors record signals that are generated naturally. For instance, Japanese pipes, recording the acoustic waves generated by particles colliding with the instrument (Mizuyama et al., 2010); geophone plates, which are installed on the riverbed and detect the sound produced by particles impacting a steel plate (Rickenmann et al., 2014); and hydrophones (Figure 1.8c), which measure the sound generated by particles hitting the riverbed and propagates in the water column (Geay et al., 2017).

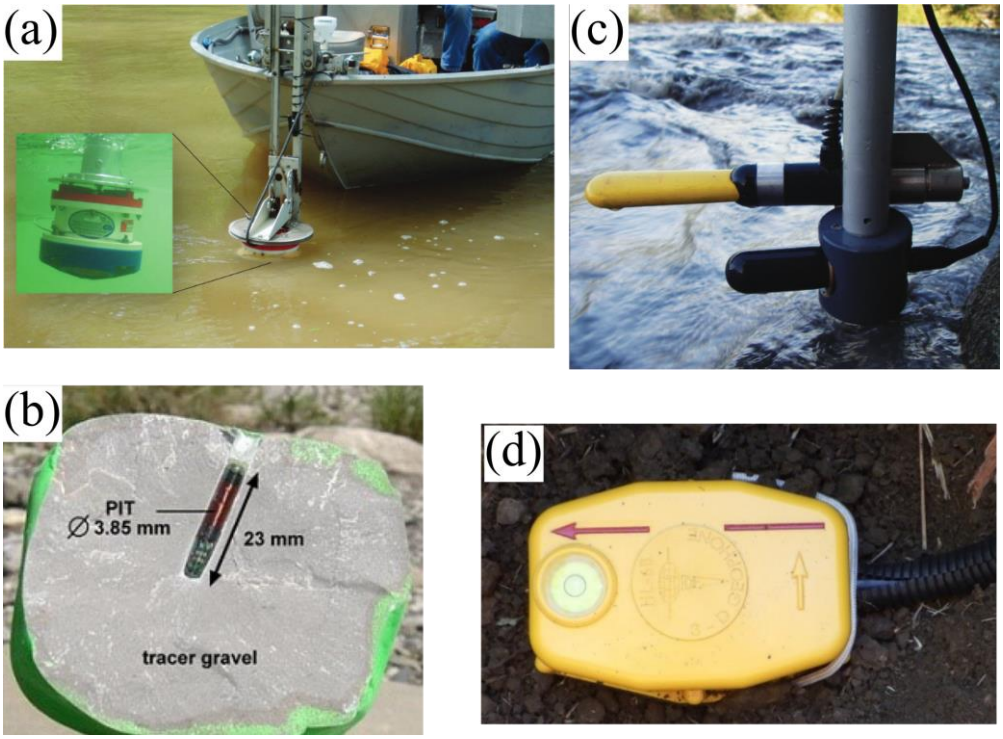

Figure 1.8 : Examples of surrogate monitoring methods. (a) Deployment of an acoustic Doppler current profiler from a boat. (b) Tracer gravel having a glass-encapsulated transponder (PIT tag). (c) Hydrophone on the channel bank before immersion for measurements. (d) Seismometer installed on the ground close to a river. Photos in (a) and (c) are retrieved from Gray et al. (2010), photo in (b) is retrieved from Liebault et al. (2012), and photo in (d) is retrieved from Chapuis et al. (2022).

Although these surrogate monitoring methods constitute a significant improvement compared to direct bedload sampling, they still require access to the channel bed. This severely limits the range of rivers and discharges in which bedload transport can be measured, especially for mountain rivers and in the case of intense sediment transport that is unpredictable, destructive, and often occur in remote areas (Mao et al., 2009).

1.5.2 Seismology as an alternative method

In order to acquire field observations and overcome practical limitations of direct measurements and existing surrogate techniques, seismic methods have been proposed to provide a novel and indirect measure of bedload transport. Seismic monitoring has several advantages compared to other methods. It is continuous, i.e. seismometers ensure the measure of ground vibrations for long period of time (depending on their capacity and battery); remote, i.e. seismometers can be placed at distance from the target, preventing them from being damaged by the processes; non-invasive, i.e. seismometers do not interfere with the state of the processes (Figure 1.8d).

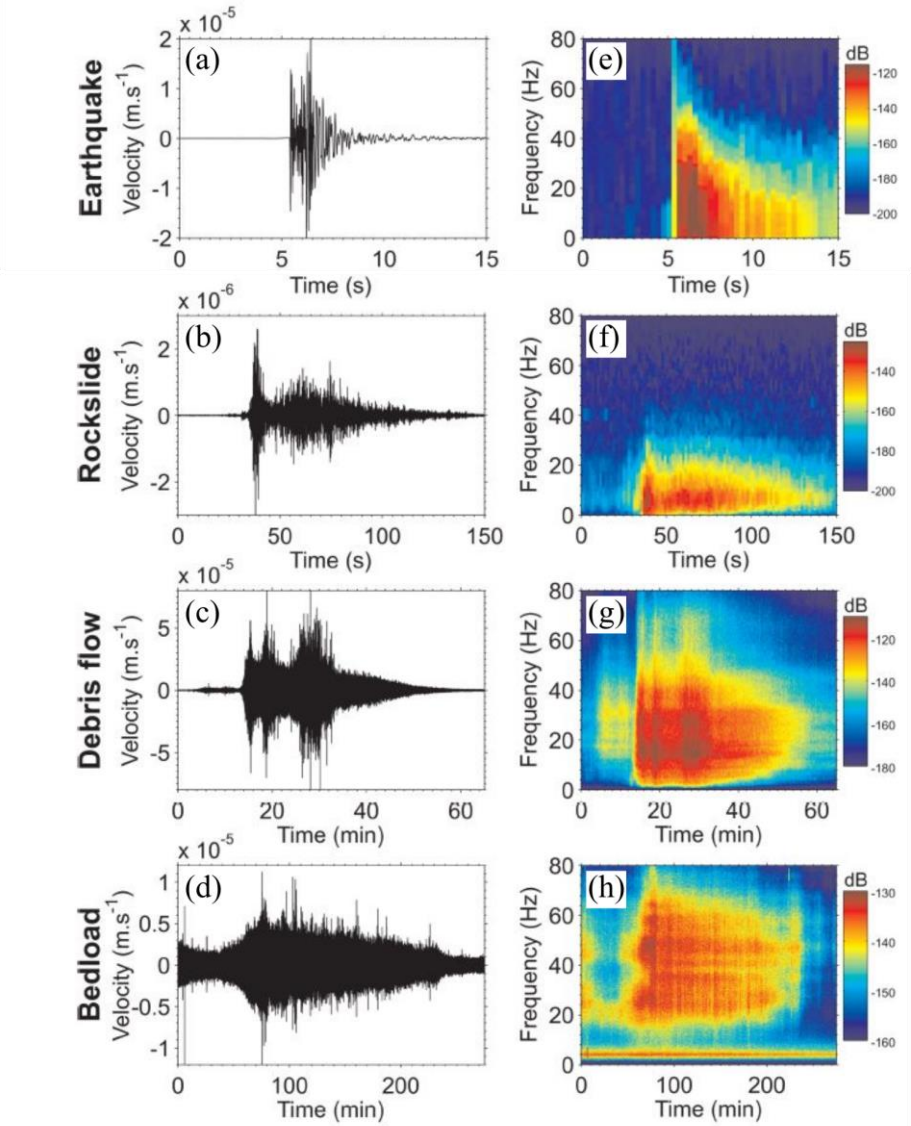

Figure 1.9 : Seismic signals generated by different natural processes: earthquake in (a) and (e), rockslide in (b) and (f), debris flow in (c) and (g), and bedload in (d) and (h). On the left, the seismic signals are shown as values of ground velocity over time, while on the right they are converted in power spectral density (PSD) through the fast Fourier transform (FFT). The seismic power is shown in decibels and as a function of time and frequency, with different colors corresponding to different level of power. Retrieved and adapted from Burtin et al. (2016).

A seismometer installed on the ground records signals from more than just earthquakes. A wide range of processes acting at or close to the Earth's surface, when transferring force fluctuations to the ground, can generate elastic waves that propagate in the surrounding medium (Figure 1.9 (Figure 8). The existence of ambient seismic signals due to natural processes was recognized more than one century ago by scientists designing the instrumentation for earthquake detection, but it was frequently interpreted as something polluting the seismograms, therefore to identify and discard (Frantti, 1963). It is from the second half of the XX century that the sensitivity of seismometers to the signal emitted by natural surface processes started timidly to be seen as an opportunity (for a review see (Larose et al., 2015; Cook and Dietze, 2022). Since then, ambient seismic signals have been used to monitor ocean storms (Gilmore, 1947), snow avalanches

(Kishimura and Izumi, 1997), glacial processes (Ekström et al., 2003), landslides (Kanamori and Given, 1982), and, last but not least, fluvial processes (Govi et al., 1993; Basile et al., 1996), and debris flows (Arattano and Moia, 1999; Marchi et al., 2002). But specifically, what does a seismometer record?

1.5.3 On the nature of the seismic signal

The displacement of mass at the Earth's surface generates elastic seismic waves that propagate from the source location to the surrounding medium until they are detected by a receiver, usually a seismometer. Seismic signals are usually registered as voltage fluctuations and, when digitized by the data logger, as counts. Through using the sensitivity of the sensor and data logger, they can be converted back to ground velocity. The velocity time series $u(t)$ of vertical ground motion can be expressed as:

$$u(t) = A\, e^{i\omega t} \tag{4}$$

where t is time, A is the signal amplitude, i the unit imaginary number, and the product ωt is the signal phase, with the angular frequency $\omega = 2\pi f$, where f is the signal frequency. The resulting time-series constitutes the seismogram (Figure 1.9a, b, c, and d).

The most common tool to characterize a seismic signal is an analysis in the time-frequency domain. The continuous seismic signal is commonly divided into short segments, on which a window function is applied and a fast Fourier transform (FFT) is performed to obtain a series of spectra, or power spectral density (PSD) estimates. These are compiled in time to give the equivalent of a spectrogram, showing the distribution of seismic power in time and frequency (Figure 1.9e, f, g, and h). Several methods exist in the literature to reduce the variance of the spectrum that generally arises from the simple use of the FFT. Among them, we cite the Welch's averaging method, in which a time-series is split into multiple overlapping segments and the PSD is computed on each individual segment. Then, an average PSD over all the segments is determined. Spectrograms are often shown in units of decibels (dB), which is a logarithmic unit, with 1 dB = 10log10 ($m^2s^{-2}Hz^{-1}$) (Figure 1.9).

Each variable of equation (3) carries different information on the processes that generate it. The amplitude illustrates the magnitude of the event that generates the seismic signal, and can be also used to investigate amplification or attenuation properties of the medium in which the signal propagates. The phase contains temporal information of the seismic signal, and the analysis of phase delays between multiple seismometers can be used to locate the source of the seismic signal.

Following its emission at the source location, the radiated seismic signal dissipates its energy (i.e. the amplitude decays) while propagating in the medium. This is due to two major mechanisms: anelastic attenuation and geometrical spreading. Anelastic attenuation is linked to shearing processes within the medium through which the seismic wave travels. Geometrical spreading implies that as the wave front moves out from the source location, the released energy is spread over an increasing area, and therefore the amplitude decreases with distance. This means that by studying amplitude decay one can also obtain information about the location of the source. In

order to quantify the dissipation of a seismic signal, it is crucial to know its frequency. Indeed, low frequency seismic signals are less sensitive to attenuation effects compared to high frequency seismic signals. This means that events generating seismic signals at low frequencies can be recorded at high distances from the source, while those generating high frequency seismic signals can be lost far away from the source. In practice, this behavior imposes a trade-off in the installation of a seismic network.

1.6 The river-induced seismic signals: a review

1.6.1 Observations

1.6.1.1 Water flow turbulence and bedload transport

Govi et al. (1993) and Basile et al. (1996) were the first to show that fluvial processes generate high-frequency (> 1 Hz) ground vibrations, and that the seismic signal could be used to monitor rivers. Govi et al. (1993) showed that the average ground velocity detected next to a stream of the Gallina valley in northwest Italy approximated quite well the hydrograph of a flood occurred in the same stream, and they also noted the presence of microseismic impulse peaks during the rising and falling limb of the flood which they linked to the transport of coarse sediments. Through their simple analysis, the authors were able to identify two important sources of river-induced ground vibrations, that is, water flow and sediment transport. Some years later, at a Conference of Hydraulics in Turin, Basile et al. (1996) showed the results of their laboratory experiments carried out in a steep channel (5 %) to investigate the relationship between bedload fluxes and ground vibrations. The main finding was the predominant role played by particle diameter and sediment flux in the generation of ground vibrations.

In the first part of the XX century several studies confirmed these findings by suggesting that a consistent portion of river-induced ground vibrations could come from particles impacting the riverbed (Burtin et al., 2008; Hsu et al., 2011; Roth et al., 2014). This was inferred by the presence of hysteresis behaviors in the relationship between water discharge or flow stage and seismic power: instead of a unique relationship between these two quantities, different levels of ground vibrations associated with similar water flow conditions on the rising and falling limbs of floods or over the year were highlighted (e.g. Figure 1.10). The authors attributed this behavior to different degrees of bedload activity during the monitoring period (Burtin et al., 2008; Hsu et al., 2011; Schmandt et al., 2013; Roth et al., 2014; Chao et al., 2015). Supplementary evidence of the role played by bedload in generating ground vibrations was provided by the direct comparison of the seismic power with sediment samples (Burtin et al., 2011), and geophone plate measurements (Roth et al., 2016).

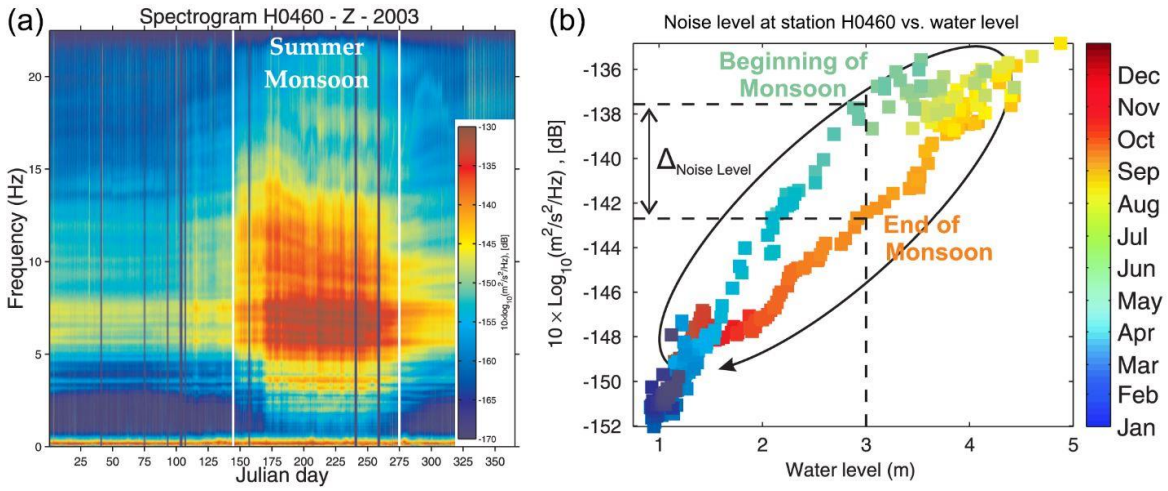

Figure 1.10 : Seismic observations on the Trisuli River (Nepal). (a) Ground vibrations recorded over the year and shown in the spectrogram in terms of seismic power as a function of time and frequency. We can observe high levels of seismic power during the monsoon in summer. (b) Daily average seismic power in the 3-15 Hz frequency band as a function of the water level measured in the Trisuli River. Retrieved from Burtin et al. (2016).

Progress in the comprehension of river-induced ground vibrations was made through the observation that the hysteresis between water discharge or flow stage and seismic power was less significant at low frequencies (< 10 Hz) than at high frequencies ($> 10 - 15$ Hz) (Schmandt et al., 2013; Gimbert et al., 2014). This led the authors to advance that water flow and bedload transport generate ground vibrations in different frequency bands.

While the findings presented above have been mainly obtained through using single seismic sensor, bedload transport has been also studied under the lens of multiple seismic sensors installed in the proximity of rivers. Analysis of the spatial distribution of seismic amplitudes (Schmandt et al., 2017), or of the phase delays between the sensors (Burtin et al., 2010; Chao et al., 2015), allowed to identify river sections subject to high bedload fluxes. The capability to localize sources of ground vibrations has grown particularly in the last decade through the use of network of seismic sensors, the so-called dense seismic arrays. This method has been used to investigate the spatiotemporal dynamics of natural processes such as hydrothermal activity (Legaz et al., 2009), and subglacial water flows (Nanni et al., 2021), but it has not yet been tested in river settings.

1.6.1.2 The particular case of debris flows

Ground vibrations resulting from debris flows have received considerable attention for decades (Arattano and Moia, 1999; Marchi et al., 2002; Huang et al., 2007). The first studies took advantage of multiple seismic sensors installed along channels to estimate the velocity of debris flows, and by means of flow stage measurements they suggested that debris flow fronts were the dominating source of ground vibrations (Arattano and Moia, 1999; Marchi et al., 2002). Some years later, Huang et al. (2007) underlined the importance of knowing soil properties to interpret the seismic signal

generated by debris flows, and their analysis in the time-frequency domain linked the varying frequency content of the signal to different debris flow phases.

Due to the destructive nature of such events, seismic observations have been extensively used to develop early warning systems (Marchi et al., 2002; Coviello et al., 2015; Walter et al., 2017; Chmiel et al., 2021), but in the last decade several studies have attempted to investigate the seismic signal (or, equivalently, the amplitude of the force fluctuations generating it) to infer bulk flow properties. Field observations have been used to estimate debris flow entrainment (Kean et al., 2015), kinetic energy (Coviello et al., 2019), thickness and mass (McCoy et al., 2013; Zhang et al., 2021a), and velocity (Zhang et al., 2021b). In parallel, these links have been recently investigated through downscaled laboratory experiments in which, rather than the seismic signal, the basal force fluctuations have been more often investigated (Hsu et al., 2014; Arran et al., 2021; Allstadt et al., 2020; Haas et al., 2021; Bachelet et al., 2021). The different experimental setups are shown in Figure 1.11 and the corresponding experimental conditions are described in Table 1.1.

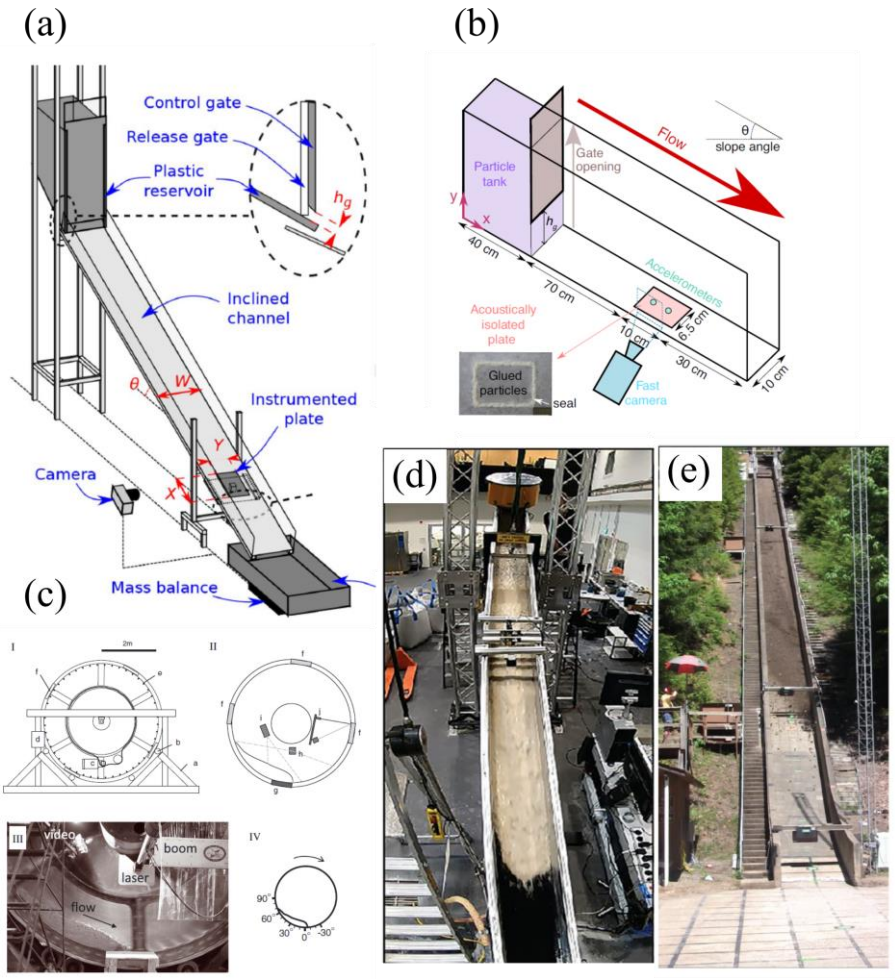

Figure 1.11 : Experimental investigations on the seismic signature of highly concentrated sediment flows. (a) and (b) Schematic representations of the experimental setup used by Arran et al. (2021) and Bachelet et al. (2021), respectively, in which dry spherical glass beads are released from an upstream reservoir to an inclined channel. (c) Photo and schematic representations of the apparatus used by Hsu et al. (2014), which consisted in a vertically rotating drum recirculating dry and wet flows of natural sediments. (d) Photo of the experimental setup used by Haas et al. (2021), in which wet natural sediments are released from a forced-action mixer to an inclined channel. (e) Photo of the experimental setup used by Allstadt et al. (2020), in

which wet natural sediments are released from a hopper to an inclined channel. The images are retrieved by the corresponding works.

Table 1.1 : Experimental configuration and boundary conditions of the existing experiments on the seismic signature of highly concentrated sediment flows.

	DEVICE	SEISMIC QUANTITY	SOLID INPUT	FLOW TYPE	SEDIMENT TYPE	GRAIN SIZE DISTRIBUTION
Hsu et al. (2014)	Vertical rotating drum	Basal force fluctuations	Rotating mass	Dry and wet Granular Flow	Natural sediments	Narrow, wide, bimodal
Arran et al. (2020)	Tilted channel	Basal force fluctuations	Upstream gate release	Dry Granular Flow	Spherical glass beads	Uniform
Allstadt et al. (2020)	Tilted channel	Basal force fluctuations and seismic signal	Upstream gate release	Wet Granular Flow	Natural sediments	Wide
Haas et al. (2021)	Tilted channel	Basal force fluctuations and seismic signal	Upstream gate release	Wet Granular Flow	Natural sediments	Wide multimodal distribution
Bachelet et al. (2021)	Tilted channel	Basal acoustic emissions	Upstream gate release	Dry Granular Flow	Spherical glass beads	Uniform

Existing laboratory and field observations reveal not straightforward relationships between flow properties and amplitude of force fluctuations. Coarse debris flows have been shown to generate stronger force fluctuations compared to finer ones (Haas et al., 2021; Hsu et al., 2014; Zhang et al., 2021a), but the presence of big particles does not necessarily correspond to high force fluctuations, likely depending on their position relative to the bed (Zhang et al., 2021a). Hsu et al. (2014) and Bachelet et al. (2021) suggest that the average downstream velocity scales with force fluctuations and acoustic emissions, respectively, whereas Allstadt et al. (2020) and Zhang et al. (2021b) observe a rather low correlation. Certain investigations show amplitude of force fluctuations that is positively correlated with flow thickness and mass (McCoy et al., 2013; Zhang et al., 2021a), others report poorer correlations when bulk density varies fast (Allstadt et al., 2020), or even negative correlations in the case of mud-saturated debris flows (Hsu et al., 2014).

Among all these studies, Allstadt et al. (2020) were the first to emphasize this complexity by investigating several flow properties altogether. Figure 1.12 from their experimental study shows the relationships between the flow properties and the normal fluctuating stresses generated by debris flows as a function of time. We can observe hysteresis behaviors between the mean normal and the fluctuating stresses (Figure 1.12a and e), and relationships that vary over time (Figure 1.12d, e, and h). The authors suggest the need to consider the interrelationships between flow properties in terms of "flow style", and conclude: "[…] we cannot say anything conclusive about the physical relationship between fluctuating stresses and any of the examined bulk characteristics other than that there are definitely systematic trends among many flow factors of interest. However, the relationships are complex and likely involve interrelated factors".

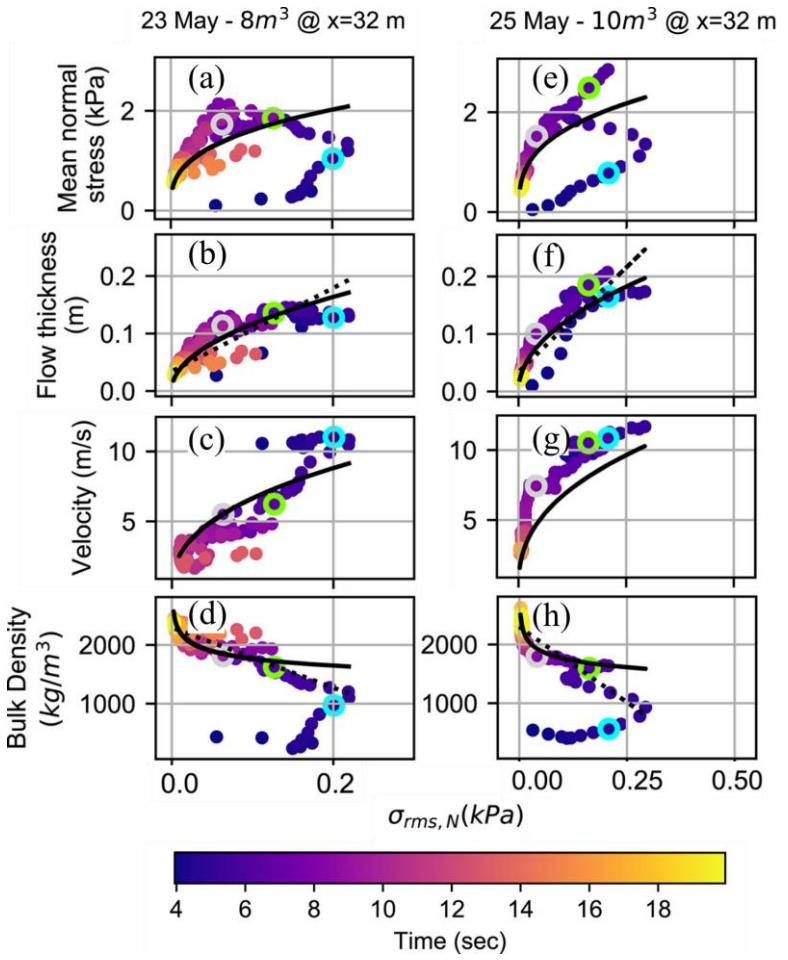

Figure 1.12 : Force fluctuations generated by debris flows. The two columns correspond to two experiments in which a different volume of sediments was released from the upstream hopper (see Figure 1.11e). Each panel shows the relationships between the debris flow properties (mean normal stress, flow thickness, velocity, and bulk density) and the generated normal fluctuating stresses. Retrieved and adapted from Allstadt et al. (2020).

In addition to the macroscopic flow properties presented above, Bachelet et al. (2021) investigated the seismic power generated by granular flows also at the grain scale. The instrumentation of their experimental setup allowed for accessing the shear rate and grain velocity fluctuations within the granular flow. They observed a positive relationship between seismic power and grain velocity fluctuations and, through applying the $\mu(I)$ theory, seismic power was also found to scale with the dry inertial number I_{dry}. This latter finding was confirmed by the experiments of Arran et al. (2021), who investigated the seismic signature of granular flows in the laboratory.

1.6.1.3 What about extreme floods?

Although the capability of seismic methods to monitor high-energy fluvial processes such as floods and debris flows has been acknowledged over the years (Hsu et al., 2011; Kean et al., 2015), their

potential for investigating the physics of extreme floods at high temporal and spatial resolution has only very recently been tested. Cook et al. (2018) used seismic observations to study the dynamics of a catastrophic GLOF (glacial lake outburst flood) that hit a mountain region of the Himalayas destroying infrastructures and buildings. An array of seismometers installed at the catchment scale provided crucial insights on the behavior of an event that lacked adequate real-time measurements. The records revealed the occurrence of two distinct peaks of seismic power which the authors associated to the passage of a fast water wave constituting the flood front, and of a slower but more energetic pulse of coarse material. Moreover, Cook et al. (2018) used seismic signals collected in different frequency ranges ($\Delta f = 2 - 5\ Hz$ and $\Delta f = 20 - 80\ Hz$) and distance from the river to obtain proxies for water flow stages and bedload fluxes, respectively. They showed that while the low frequency seismic power returned to pre-flood levels within some hours after the flood, the high frequency seismic power was characterized by higher levels for several days. This was interpreted as the persistence of high sediment transport rates activated by the event.

Similarly, Maurer et al. (2020) studied the dynamics of a GLOF occurred in the Himalayas in 1994 causing fatalities and exceptional damages in the region. Thanks to a seismic array deployed for different purposes, the authors were able to estimate the duration and the propagation velocity of the flood, and to track its evolution along the river.

These works show that seismic methods are ideally suited for investigating the physics of extreme flood events and their long-term impact on river activity. However, until now extensive seismic investigations of large-magnitude flood events are rare and limited to glacial lake outburst floods.

1.6.2 Modelling

1.6.2.1 Water flow turbulence and bedload transport

A significant step forward in the field of fluvial seismology was made through the definition of mechanistic models for the seismic signal generated by bedload transport (Tsai et al., 2012; Gimbert et al., 2019) and turbulent flow (Gimbert et al., 2014), with the aim to link river-induced ground vibrations to fluvial processes for quantitative purposes.

Tsai et al. (2012) built a physical framework to relate the force fluctuations exerted by particles impacting the riverbed with the seismic signal measured on the riverbank. The model considers not only the generation, but also the propagation of seismic waves in the medium. If we temporarily ignore the propagation of the seismic wave, under the hypothesis of random individual particle impacts, the seismic power P due to forces associated with instantaneous particle impacts on the riverbed (i.e. impact duration is shorter than the period of the seismic wave $1/f$) can be written as:

$$P = \frac{n}{t_i} I^2 \tag{5}$$

where $\frac{n}{t_i}$ is the total rate of particle impacts, n is the number of impacting particles, $\frac{1}{t_i}$ is the particle impact rate, and $I = mu_N\gamma$ is the basal impulse exerted by a particle of mass m impacting the bed with a bed-normal velocity u_N, γ is a factor that accounts for the elasticity of particle impact, where

$\gamma = 1$ corresponds to perfectly inelastic impact and $\gamma = 2$ to a perfectly elastic impact. The total rate of particle impacts can be written as a function of the bedload flux q_b and other parameters such as the vertically-averaged stream-wise particle velocity, the depth-averaged particle settling velocity, and the bedload layer height. By assuming spherical particles of diameter D such that $m \sim D^3$, Tsai et al. (2012) obtain that the seismic power due to bedload transport scales as $P \sim q_b {D_{94}}^3$, where D_{94} is the diameter associated with the 94th percentile of the considered grain size distribution. We can therefore observe that according to their model, seismic power scales linearly with the bedload flux and with the diameter characteristic of the coarsest fraction of the sediment mixture to the third power. If one is interested in estimating the bedload flux from seismic observations, an accurate grain size distribution is needed for performing model inversions.

Gimbert et al. (2014) built a physical model for seismic power associated with the force fluctuations exerted on the riverbed by the turbulent water column. Together with the influence of parameters such as the channel slope or bed roughness, the authors predict a significant scaling of the seismic power with the flow stage h as $P \sim h^{7/3}$, meaning that ground vibrations are strongly set by water flow stage. In a further development of the model for subglacial water flow, Gimbert et al. (2016) found that the seismic power scaled with the water discharge Q_w as $P \sim {Q_w}^{1.4}$. An important prediction of the model is that the turbulent flow generates seismic signals at lower frequencies compared to bedload transport, as suggested by field observations (see Section 1.6.1.1). As low frequency seismic signals are less sensitive to attenuation effects during propagation compared to high frequency seismic signals, for seismic sensors installed significantly far from to the river, water turbulence-induced seismic power is expected to dominate over bedload transport over a wide range of frequencies. By contrast, at relatively small distance bedload transport might constitute the dominating source of ground vibrations (Figure 1.13). Together with flow strength (i.e. water discharge or level), Gimbert et al. (2014) noted that channel slope and bed roughness also play a role in the turbulent processes generating seismic power, meaning that changes in these parameters can impact the seismic signature of rivers. Roth et al. (2017) took advantage of this finding to explain hysteresis behaviors between water discharge and seismic power that couldn't result from changes in sediment transport activity as proposed by previous works (see Section 1.6.1.1).

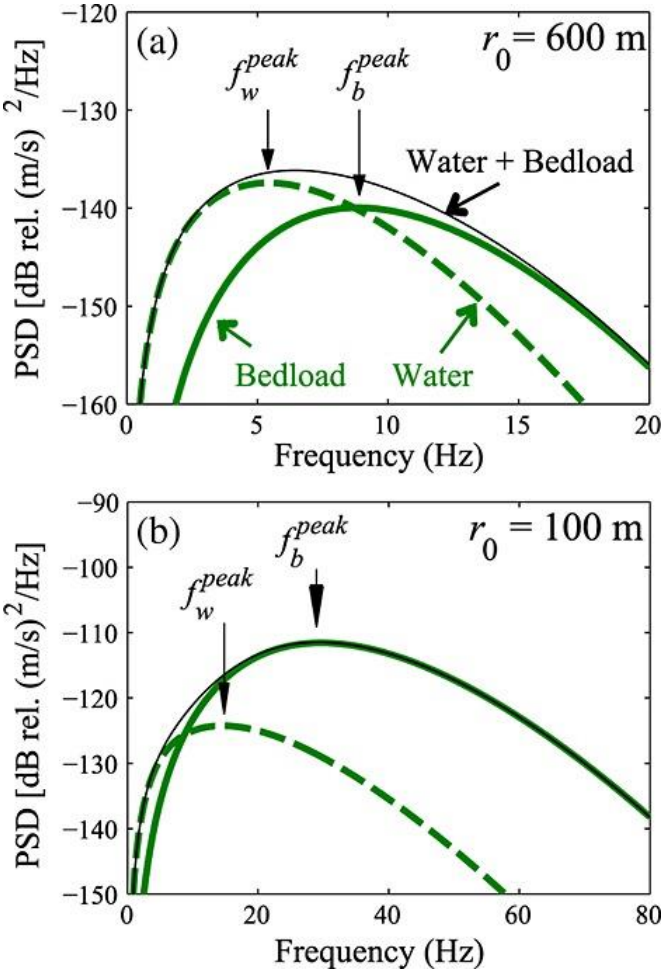

Figure 1.13 : Modelled seismic power for turbulent water flow (dashed green curve) and bedload (continuous green curve) through the models of Gimbert et al. (2014) and Tsai et al. (2012). The thin black curve indicates the sum of the two models. Seismic power is shown as a function of frequency for two different distances: (a) $r_0 = 600$ m and (b) $r_0 = 100$ m. Retrieved from Gimbert et al. (2014).

The general predictions of these models are consistent with field observations from a range of river settings (Schmandt et al., 2013; Bakker et al., 2020; Lagarde et al., 2021) and laboratory experiments (Gimbert et al., 2018). In particular, Bakker et al. (2020) observed that for the Séveraisse River (French Alps) the seismic power at 10 Hz scaled with water discharge with an exponent that is really close to that predicted by the turbulence model of Gimbert et al. (2016) (Figure 1.14a). At higher frequencies ($f = 30$ Hz and $f = 50$ Hz), we can observe a clear change in the scaling that occurs as the water discharge exceeds a value corresponding to the modelled threshold for full particle mobility ($Q_w = 11.9$ m³/s, vertical dashed line) (Figure 1.14b and c). According to the authors this demonstrates that at these frequencies (and this distance from the river) bedload transport dominates over water flow turbulence. This was confirmed by the observation that the exponent of 5.3 in the scaling relationship at 50 Hz matches the rating curve $q_b \sim {Q_w}^{5.3}$ linking water discharge (Q_w) and bedload flux (q_b) found by Misset et al. (2020) in the same study area. For $f = 50$ Hz, at lower discharges ($Q_w < 11.9$ m³/s) there exists a period with a steeper response (thin red line in Figure 1.14c). The latter followed a large flood occurring on August, which probably led to low rates of bedload transport that are not visible at lower frequencies. Moreover, Bakker et al. (2020) showed that the model of Tsai et al. (2012) was able to estimate bedload fluxes with an

uncertainty of less than one order of magnitude. The bedload model was also verified for relatively low sediment fluxes in the laboratory (Gimbert et al., 2019), but a validation is still missing for sediment transport at capacity.

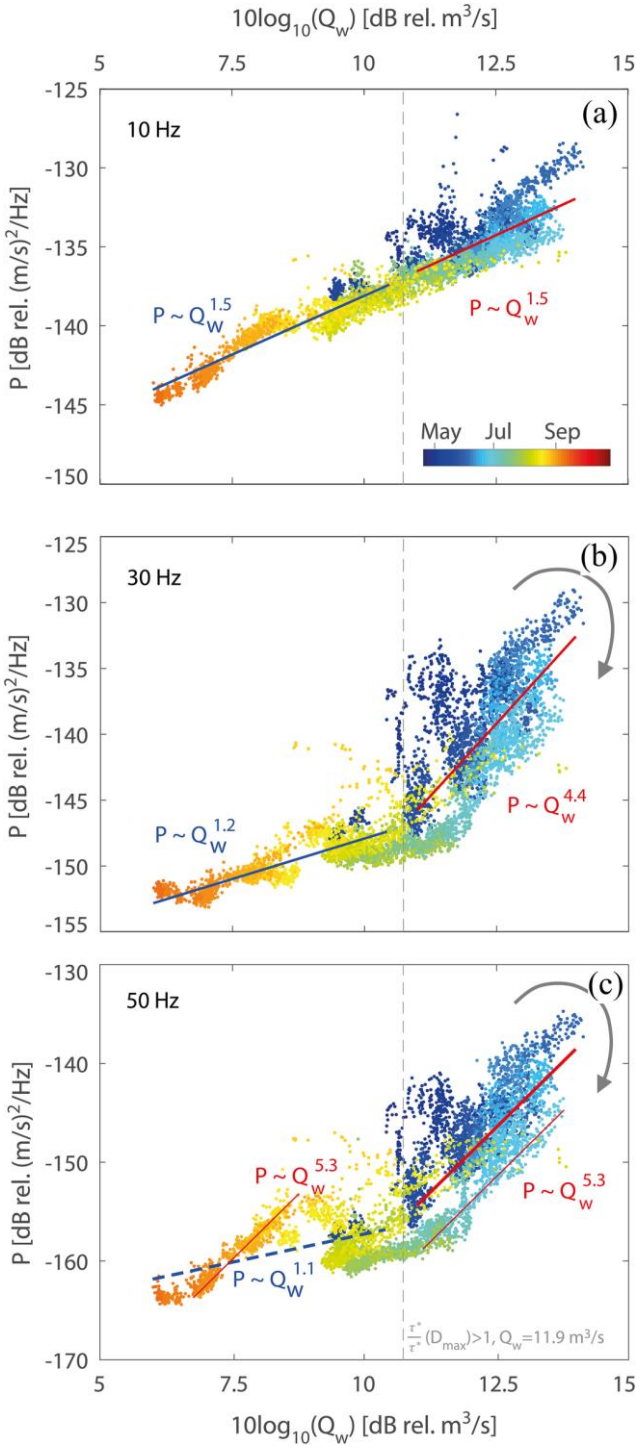

Figure 1.14 : Seismic observations on the Séveraisse River. Water discharge measurements (expressed in decibel in the bottom labels, and in m^3/s at the top) are shown against seismic power at different frequencies: (a) f = 10 Hz, (b) f = 30 Hz, and (c) f = 50 Hz. Least squares regressions are shown with lines of different color depending on the exponent of the power-law. The dashed line in (c) indicates poor fit. The vertical dashed line in the panels shows the modelled threshold for full particle mobility. Retrieved from Bakker et al. (2020).

1.6.2.2 Highly concentrated sediment flows

Recently, several mechanistic models for the generation of force fluctuations by highly concentrated sediment flows have also been proposed (Lai et al., 2018; Farin et al., 2019; Zhang et al., 2021a; Bachelet et al., 2021), with the aim to provide a framework for using seismic signals to obtain quantitative estimates of debris and granular flow properties. Most models are built on the framework proposed by Tsai et al. (2012) (equation 5), in which the estimation of seismic power relies on the definition of the total rate of impacts $\frac{n}{t_i}$ and the bed-normal particle impact velocity u_N. Based on the prediction of Tsai et al. (2012) that seismic power is mostly generated by the very coarse fraction of the sediment mixture, Lai et al. (2018) developed their model focussing on the debris flow front, as being usually composed of clasts and boulders. Under the hypothesis of a "washboard" flow style in which the front is pushed from behind by the rest of the flow, u_N is considered to be proportional to the downstream average velocity of the sediment flow $\bar{u}_x$. Following the same approach, clasts are assumed to impact the bed every time they encounter roughness elements, approximated to be characterized by a length scale similar to clast diameter, and the basal particles are therefore associated with an impact rate of $\frac{\bar{u}_x}{D}$. Integrating over the area A over which the clasts are distributed and assuming a solid concentration $\phi = 1$, the total rate of impacts can be written as $\frac{\bar{u}_x A}{D^3}$. As in Tsai et al. (2012) the particle mass is approximated as D^3, and the seismic power is found to scale as $P \sim {\bar{u}_x}^3 D^3$, showing a strong dependency on the downstream average velocity of the sediment flow and particle diameter.

Farin et al. (2019) followed the same approach, but in contrast with Lai et al. (2018) they modelled the seismic power generated by a debris flow as the sum of the contribution by all its components: the body, the snout, the lip, and the saltating front (Figure 1.15). In this review we present the modelling of the body and the snout, which were shown to dominate over the other components (Farin et al., 2019). Similar to Lai et al. (2018), force fluctuations are considered to be generated by impacts that are bed roughness-controlled, that is, particles impact the bed as they encounter bed roughness elements during their advection. However, Farin et al. (2019) estimate the number of particles per meter square of the bed for the body and snout as $\frac{\phi p(D)}{D^2}$, where $p(D)$ is the grain size distribution, so that the total rate of impacts becomes $\frac{\bar{u}_x}{D^3}\phi p(D)$. The authors further distinguish between thin ($D \sim h$) and thick ($D \ll h$) debris flows. In the case of thin flows, considered the most common case, the seismic power was found to scale as $P \sim {\bar{u}_x}^3 D^3 \phi p(D)$.

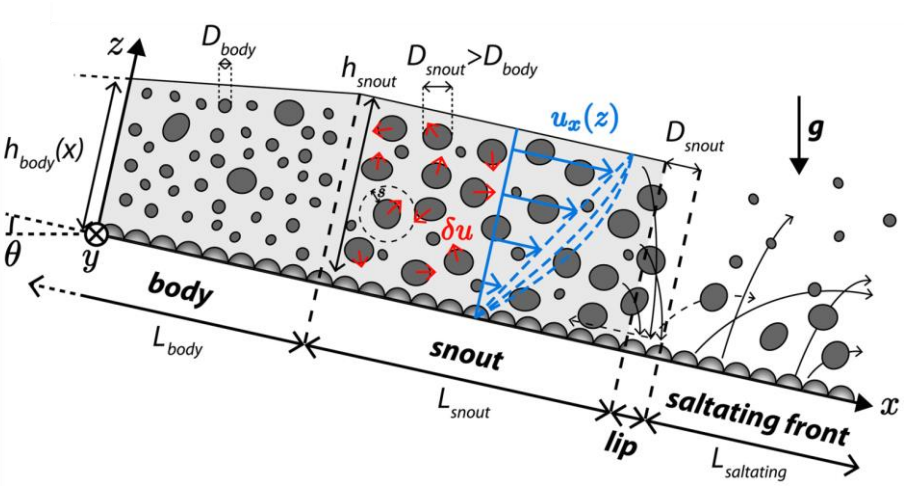

Figure 1.15 : Sketch of a debris flow. The model by Farin et al. (2019) follows this subdivision to define the different regions of a debris flow: the body, the snout, the snout's lip, and the saltating front. Each component is associated with different characteristics. In particular, the snout is thicker than the body and is characterized by particles of bigger size. Particles are associated with a certain average downstream $u_x(z)$ and fluctuating δu velocity. Retrieved from Farin et al. (2019).

The model of Zhang et al. (2021) for basal force fluctuations generated by debris flows was built on the basis of existing models (Tsai et al., 2012; Farin et al., 2019), but they introduced the concept of multi-particle force chains forming within the mass and acting on the channel bed. The authors hypothesize that dense particle concentration promotes the formation of force chains, which transmit collision forces towards the bed. In this case, the force generated by random single particles described by Tsai et al. (2012) must be multiplied by the number of particles in the force chains, which can be written as $N = (\frac{L_c}{D})^{\eta}$, where L_c is the length of the force chains considered proportional to the flow thickness, and $0 \leq \eta \leq 1$ is a dimensionless parameter reflecting the relative contribution of random single-particle impact and multi-particle force chains. Under these assumptions, and through expressing the downstream average velocity as a function of the flow thickness h, the basal force fluctuations become a main function of h and particle diameter D.

The model by Bachelet et al. (2021), built for describing the acoustic emissions (i.e. very high frequency seismic signals) of granular flows, approaches the problem by considering the interactions between different layers of particles within the depth of the flow, and hypothesize that the local impact rate is the rate at which a particle overrides another particle of the layer below at its relative downstream velocity. The particle impact velocity is therefore described by the particle velocity fluctuation in the corresponding layer. The final radiated elastic power strongly scales with particle velocity fluctuations.

Except for the model of Zhang et al. (2021), these theories have been only recently tested in the laboratory in the context of dry granular flows (Arran et al., 2021), and the model for thin debris flows by Farin et al. (2019) seems to be the most accurate in reproducing the experimental observations.

1.7 Research questions and outline

In the previous paragraphs we have seen that studying sediment transport, despite the progress and steps forward made over the last decades, is still characterized by several open questions. This is particularly true for the intense sediment transport that suddenly hits mountain rivers, for which external factors (e.g. steep slope, abrupt sediment supply, wide grain size distribution), internal dynamics (e.g. strong grain-to-grain interactions, grain sorting processes), and varying interaction with the riverbed (from little sediment exchange to significant morphological impacts) lead to a diversity of complex processes that is difficult to channel in the frameworks of classical theories.

We have also seen that passive seismology, thanks to its capability to overcome the unpredictable and destructive nature of intense sediment transport, constitute an alternative method to give new observational insights for such events. However, most seismic models still need a validation, and the potential of using seismic observations to explore the physics of intense sediment transport has been explored only partially.

The objective of this PhD is to shed some light on the physics of intense sediment transport in mountain rivers through a multidisciplinary approach involving seismic methods, which we apply in different river settings and at different spatial scales. In this PhD thesis we address two main thematic questions:

Question 1 – What are the triggering and propagation dynamics of intense sediment transport in low-order mountain rivers, and what is their seismic signature?

Question 2 – How can we best use seismic observations to investigate intense sediment transport at the field scale and over a range of river settings?

In order to answer **Question 1**, we have conducted downscaled laboratory experiments at the INRAE Research Centre of Grenoble. We dedicate three chapters of the manuscript to this study (chapter 2, 3, and 4). We have addressed **Question 2** through different field observations performed (i) in the Séveraisse river (Écrins Massif) during a campaign carried out in summer 2019, and (ii) in the Vésubie and Roya rivers (Maritime Alps), whose catchments were hit by an extreme flood event caused by the Storm Alex in October 2020. We dedicate two chapters to this study (chapter 5 and 6). Finally, chapter 7 is devoted to a summary of the results and future perspectives.

Chapter 2: Triggering and propagation of exogenous sediment pulses in mountain channels: insights from flume experiments with seismic monitoring

2.1 Preface

The adventure of this PhD did not really start at the beginning of my doctoral contract. It started one year before, while I was a master student in Environmental Engineering at the University of Florence (Italy). During the last year of my university studies, I expressed to professor Luca Solari, who transmitted me the interest in fluvial hydraulics, the desire to discover the world of research. Given my willingness to try something abroad, Luca mentioned me the opportunity to carry out my master thesis with his colleague Alain Recking from the INRAE Research Centre of Grenoble, in France. I loved the idea, Alain was motivated in having (another) Italian student working with him and so I left the Tuscan village of Montale to start an experience of 6 months in Grenoble.

The protagonist of the master thesis would have been sediment transport in mountain rivers, with a focus on the steep and confined streams that are located in the upper part of mountain catchments. These streams are known to experience sediment pulses coming from upstream sediment production zones, but little is known about their dynamics – Alain told me. How to investigate the subject? Laboratory experiments in a flume to build literally from scratch. Once the construction was finished and after weeks of tests, the flume was ready for the experiments and we started discussing about the instrumental equipment. That was when a researcher called Florent Gimbert from the IGE Research Centre (Grenoble) appeared on stage, expressing his interest in following the experiments. Why don't you install some seismometers on the channel – he said. You know, sediment transport generates seismic signals and these signals contain a lot of information about the source that generate them. I did not know anything about the topic, but I found it really fascinating. At that time, I could not imagine that this internship would have set the base for the beginning of a PhD thesis.

This chapter presents and summarizes the results of the laboratory experiments carried out during the first part of my PhD, in continuity with the preliminary findings of my master thesis. The chapter is constituted by a paper that is edited on the Earth Surface Dynamics (ESurf) journal: **Piantini, M.**[1,2], Gimbert, F.[1], Bellot, H.[2], and Recking, A.[2] (2021): Triggering and propagation of exogenous sediment pulses in mountain channels: insights from flume experiments with seismic monitoring, Earth Surf. Dynam., 9, 1423–1439, https://doi.org/10.5194/esurf-9-1423-2021

[1] University Grenoble Alpes, CNRS, IRD, Institute for Geosciences and Environmental Research (IGE), Grenoble, France

[2] University Grenoble Alpes, INRAE, CNRS, IRD, Grenoble INP, IGE, 38000 Grenoble, France

Préface

L'aventure de cette thèse n'a pas vraiment commencé au début de mon contrat doctoral. Tout a commencé un an auparavant, alors que j'étais étudiant en master d'Ingénierie Environnementale à l'Université de Florence (Italie). Pendant la dernière année de mes études universitaires, j'ai exprimé au professeur Luca Solari, qui m'a transmis l'intérêt pour l'hydraulique fluviale, le désir de découvrir le monde de la recherche. Vu ma volonté de tenter quelque chose à l'étranger, Luca m'a mentionné l'opportunité de réaliser ma thèse de master avec son collègue Alain Recking du centre de recherche INRAE de Grenoble, en France. J'ai adoré l'idée, Alain était motivé par le fait d'avoir un (autre) étudiant italien travaillant avec lui et j'ai donc quitté le village toscan de Montale pour commencer une expérience de 6 mois à Grenoble.

Le protagoniste de la thèse de master aurait été le transport sédimentaire dans les rivières de montagne, avec un accent sur les cours d'eau confinés qui sont situés en tête des bassins versants. Comment étudier ce sujet ? Des expériences de laboratoire dans un canal à construire littéralement à partir de zéro. Une fois la construction terminée et après des semaines de tests, le canal était prêt pour les expériences et nous avons commencé à discuter de l'équipement instrumental. C'est alors qu'un chercheur appelé Florent Gimbert, du centre de recherche IGE à Grenoble, est apparu sur scène. Pourquoi ne pas installer des sismomètres sur le canal - a-t-il dit. Vous savez, le transport sédimentaire génère des signaux sismiques et ces signaux contiennent beaucoup d'informations sur la source qui les génère. Je ne connaissais rien sur ce sujet, mais j'ai trouvé cela vraiment fascinant. À l'époque, je ne pouvais pas imaginer que ce stage aurait été la base d'un doctorat.

Ce chapitre présente et résume les résultats des expériences de laboratoire réalisées au cours de la première partie de mon doctorat, en continuité avec les résultats préliminaires de ma thèse de master. Le chapitre est constitué d'un article qui est édité sur la revue scientifique Earth Surface Dynamics (ESurf): **Piantini, M.**[1,2], Gimbert, F.[1], Bellot, H.[2], and Recking, A.[2] (2021): Triggering and propagation of exogenous sediment pulses in mountain channels: insights from flume experiments with seismic monitoring, Earth Surf. Dynam., 9, 1423–1439, https://doi.org/10.5194/esurf-9-1423-2021

[1] University Grenoble Alpes, CNRS, IRD, Institute for Geosciences and Environmental Research (IGE), Grenoble, France

[2] University Grenoble Alpes, INRAE, CNRS, IRD, Grenoble INP, IGE, 38000 Grenoble, France

2.2 Abstract

In the upper part of mountain river catchments, large amounts of loose debris produced by mass-wasting processes can accumulate at the base of slopes and cliffs. Sudden destabilizations of these deposits are thought to trigger energetic sediment pulses that may travel in downstream rivers with little exchange with the local bed. The dynamics of these exogenous sediment pulses remain poorly known because direct field observations are lacking, and the processes that control their formation and propagation have rarely been explored. Here we carry out flume experiments with the aims of investigating (i) the role of sediment accumulation zones in the generation of sediment pulses, (ii) their propagation dynamics in low-order mountain channels, and (iii) the capability of seismic methods to unravel their physical properties. We use an original setup wherein we supply water discharge and sediment flux to a low-slope storage zone acting like a natural sediment accumulation zone that is connected to a downstream 18 % steep channel equipped with geophones. We show that the ability of the self-formed deposit to generate sediment pulses is controlled by the fine fraction of the mixture. In particular, when coarse grains coexist with a high content of finer particles, the storage area experiences alternating phases of aggradation and erosion strongly impacted by grain sorting. The upstream processes also influence the composition of the sediment pulses, which are formed by a front made of the coarsest fraction of the sediment mixture, a body composed of a high concentration of sand corresponding to the peak of sediment flux, and a diluted tail that exhibits a wide grain size distribution. Seismic measurements reveal that the front dominates the overall seismic noise, but we observe a complex dependency between seismic power and sediment pulse transport characteristics, which questions the applicability of existing seismic theories in such a context. These findings challenge the classical approach for which the sediment budget of mountain catchments is merely reduced to an available volume, since not only hydrological but also granular conditions should be considered to predict the occurrence and propagation of such sediment pulses.

2.3 Introduction

Sediment transport processes play a key role in fluvial geomorphology (Schumm, 1977) and natural risk management (Badoux et al., 2014), since they exert a major control on the intensity with which rivers can impact the landscape and the safety of inhabited regions. This is particularly evident in mountain catchments, where catastrophic floods are exacerbated by a rapid hydrological response to rainfall (high hydrological connectivity; Wohl, 2010) and a large mobilization of sediments (Recking, 2014). Predicting when and how sediments move throughout mountain channels, however, remains challenging since onset of motion criteria and bedload transport laws have mostly been established for lowland rivers and have limited applicability to mountain environments (Schneider et al., 2016). Mountain rivers are characterized by a wide range of morphological units whose peculiarities cannot be neglected when studying sediment transport (Lee and Ferguson, 2002; Comiti et al., 2009; Zimmermann et al., 2010). For instance, several works have shown that large-scale bed roughness is expected to affect bed shear stress (Bathurst et al., 1983; Solari and Parker, 2000; Lamb et al., 2008; Recking, 2009; Prancevic and Lamb, 2015), and grain sorting processes have a stronger impact in term of producing bedload fluctuations compared to lowland streams (Recking et al., 2009; Bacchi et al., 2014). Moreover, the steepness of mountain channels

may help trigger debris flows, which are energetic transport processes whereby the solid volume fraction is so high (greater than 50%) that the solid phase influences the behaviour of the flow as much as the fluid phase (Iverson, 1997). The conditions of transition from bedload to debris flow remain debated, partly due to lacking field observations (Mao et al., 2009; Prancevic et al., 2014).

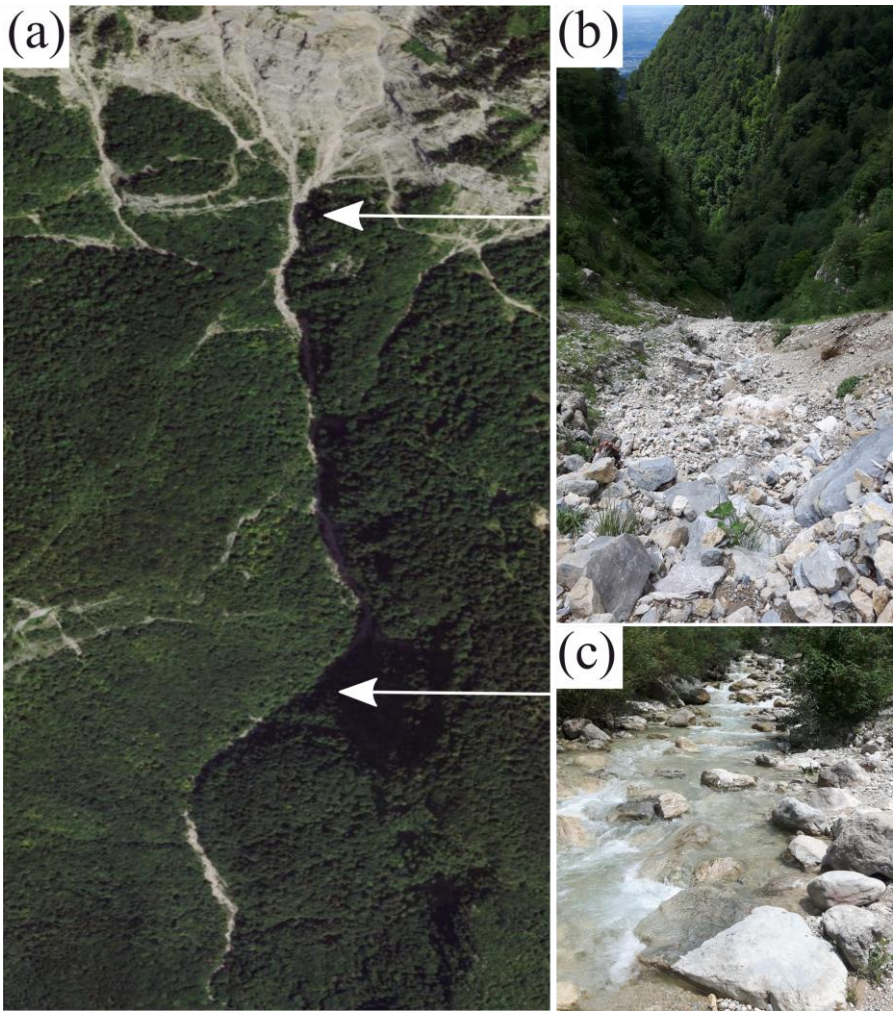

Figure 2.1 : (a) The Roize River, a typical mountain stream configuration with (b) a production zone with sediment deposits that are several metres thick and show evidence of large incisions and (c) a transfer zone consisting of a narrow steep step-pool morphology. Photo credit: (a) IGN France (https://www.geoportail.gouv.fr, last access: 16 July 2020).

For both fluvial and debris flows processes, in addition to the hydrological forcing, sediment supply conditions play an important role (Benda and Dunne, 1997; Bovis and Jakob, 1999; Recking, 2012) and their spatial and temporal variabilities add complexity to predictions. Mountain channels that are coupled to sediment production zones (high landscape connectivity; Wohl, 2010) are particularly prone to receiving episodic inputs of material coming from upstream sections of the catchment, where sediments produced by mass-wasting processes accumulate in the form of talus slope or along lowslope stretches as loose scree deposits. However, this storage is often temporary, since rainfall and runoff descending from upper slopes can destabilize these accumulation zones and trigger sediment transport towards downstream channels (Berti et al., 1999; Fontana and Marchi, 2003; Gregoretti and Fontana, 2008). This is, for example, the case in

the Roize River, France (Figure 2.1a). The upper part of the catchment is characterized by cliffs producing a large amount of debris that accumulates at the slope's toe (Figure 2.1b and (Lamand et al., 2017)), and as a result of hydrological and gravitational phenomena, sediments are occasionally released to the coupled reach (Figure 2.1c) where they are transported downstream to a reception zone (sediment trap). The dynamics of transport throughout the river reach have been shown to be strongly related to the activity of these headwater sediment sources (Piton and Recking, 2017). Thanks to exogenous inputs of sediments, such streams can suddenly switch from supply-limited to overcapacity conditions, as illustrated in (Figure 2.2 showing that the non-alluvial and inactive bed of the Ruisseau de la Gorge (French Alps) suddenly experienced a large transport event in 2015. As the transported sediments were much finer than the bed in place, an upstream and exogenous input of the material was suggested.

Figure 2.2 : Effect of a sediment pulse at a bridge section of the Ruisseau de la Gorge (France), a stream that was known by local engineers as having been inactive for decades. The transported material was much finer ($D_{50} = 96$ mm, $D_{84} = 169$ mm) than the bed in place ($D_{50} = 250$ mm, $D_{84} = 413$ mm).

Several works have shown that exogenous sediment inputs in a river usually take the form of *sediment pulses*, defined in the literature as disturbances in bed elevation that propagate downstream, translating as a coherent wave and/or dispersing in place (Sutherland et al., 2002; Brummer and Montgomery, 2006). Previous studies have investigated the evolution of these sediment pulses in gravel-bed rivers characterized by a maximum slope of 1%, wherein the streambed has been shown to actively interact with the injected material (Lisle et al., 1997; Sutherland et al., 2002; Cui et al., 2003; Cui and Parker, 2005; Sklar et al., 2009). However, low-order mountain rivers usually present geological controls such as rarely mobile boulders and bedrock outcrops, as well as much steeper slopes. In this context, sediment pulses are expected to be

transported downstream with a marginal morphological impact on the underlying bed, following the "travelling bedload" concept (Piton and Recking, 2017). To the best of our knowledge, there are no experimental studies that investigate sediment pulse propagation in such a configuration, and the few post-event field observations do not provide information about their spatial and temporal dynamics. Classical monitoring methods reveal scarce effectiveness for observing pulse-like events (Mao et al., 2009), and therefore sediment pulses are challenging to track due to their localized and potentially energetic nature. In this context, seismic methods represent a robust alternative for providing a non-invasive and continuous monitoring of torrential processes (Burtin et al., 2016) and catastrophic floods (Cook et al., 2018). As sediment transport generates ground vibrations, mechanistic models have been defined to understand the links between river processes and the generated seismic noise (Tsai et al., 2012; Gimbert et al., 2014; Lai et al., 2018; Farin et al., 2019). Applicability of seismic theories for bedload under a relatively low transport rate has been demonstrated in the laboratory (Gimbert et al., 2019) and in the field (Bakker et al., 2020). Seismic models for more concentrated sediment flows have also been tested in the laboratory in the context of dry granular flows (Arran et al., 2021) and in the field in the context of debris flows (Zhang et al., 2021). However, the extent to which existing theories apply to a variety of sediment transport flows including sediment pulses, which may lie between bedload transport and debris flows, remains to be investigated.

In this study we conduct laboratory experiments (i) to explore the role of sediment accumulation zones in the generation of sediment pulses, (ii) to investigate their propagation dynamics in low-order mountain channels, and (iii) to test the capability of seismic methods to infer the flow properties associated with such sediment transport events. We use an original setup wherein instead of feeding the flume section directly as usually done, we supply liquid and sediment flux to a low-slope storage zone connected to the upstream part of a 18% steep channel. Such an experimental configuration allows us to investigate if a self-formed deposit can generate sediment pulses and how these later propagate in the downstream channel. In Section 2.4 we present the experimental setup and the measurement protocol. Then in Section 2.5 we present our experimental results regarding both the storage area and the channel. Finally, in Section 2.6 and 2.7 we discuss the key results and describe the main implications for mountain stream morphodynamics.

2.4 Material and methods

2.4.1 Experimental setup and measurements

We use a 6 m long flume made of (i) a 1 m long and on average 0.5 m wide trapezoidal-shaped upstream storage area ($\sim$ 0% – 1%) and (ii) a 5m long and 0.1 m wide downstream steep (18% slope) channel (Figure 2.3).

Water discharge recirculation is ensured by a pump supplied by a reservoir placed at the flume outlet, whose level is kept constant through an overflow drain. The discharge value is measured with an electromagnetic flowmeter, and the flow rate is controlled numerically using a calibrated voltage– discharge relationship. We use a sediment feeding system composed of a hopper connected to a conveyor belt for the sediment flux. The sediment flux is controlled by the velocity of the conveyor belt, which is measured by a sensor fixed on one of its rotation axes. As for the

water supply we set a calibrated equation in order to regulate the sediment flux from the computer.

The topographic evolution of the storage area is monitored with a sensing camera (Microsoft Kinect) that allows us to reproduce a virtual 3-D model from the images through depth-sensing techniques: a light is firstly projected by an infrared sensor; then the reflected pattern is captured to recover the geometry of the object by computing the light's time of flight. The device is used to estimate the volume variation of the deposit and its longitudinal slope. We video record each experiment with two webcams placed at the inlet section and along the channel (Microsoft HD LifeCam Cinema). Three sections are equipped with a remote transducer ultrasonic sensor (Banner Q45UR Series) having a sampling frequency of 100Hz and a geophone (3-D Geophone PE-6/B) (Figure 2.3) to respectively measure the flow surface elevation and detect flow-induced seismic flume motion generated by particle impacts (Govi et al., 1993). The data from the geophones are recorded on a DATA-CUBE^3 logger with a sampling frequency of 800 Hz. In order to explore the properties of the seismic noise, we compute the power spectral density (PSD) of the signal recorded along the vertical by performing a fast Fourier transform with the Welch's averaging method (Welch, 1967). According to this method the time series is split into overlapping segments (here we chose an overlap of 50 %), and the final PSD results from the average of the PSDs of each segment. We focus on sediment-transport-related seismic noise by getting rid of other sources emitted by the experimental device (e.g. water pump, water flow in pipes and on the flume) through normalizing the raw signal by the seismic power occurring under similar experimental conditions but with no sediment transport (Supporting Information). We measure the sediment flux by sampling the outgoing sediments at the channel exit, and we compute the grain size distribution of the samples from sieve measurements. It is worth noting that sediment flux is measured by hand and is consequently not continuous in time, and the sampling frequency is adapted to flow conditions. As flow surface elevation and seismic noise are monitored at a different section than the outlet sediment flux, a time lag between measurements is present. In order to compute the expected temporal delay and to properly compare the measured data, we time-shift the outlet sediment flux by estimating the velocity of the flux with a cross-correlation between the three flow surface elevation time series. Such a time-shift procedure is appropriate for the seismic analysis thanks to significant signal amplification (+5 dB on average) occurring near the geophone in our experimental setting (Supporting Information).

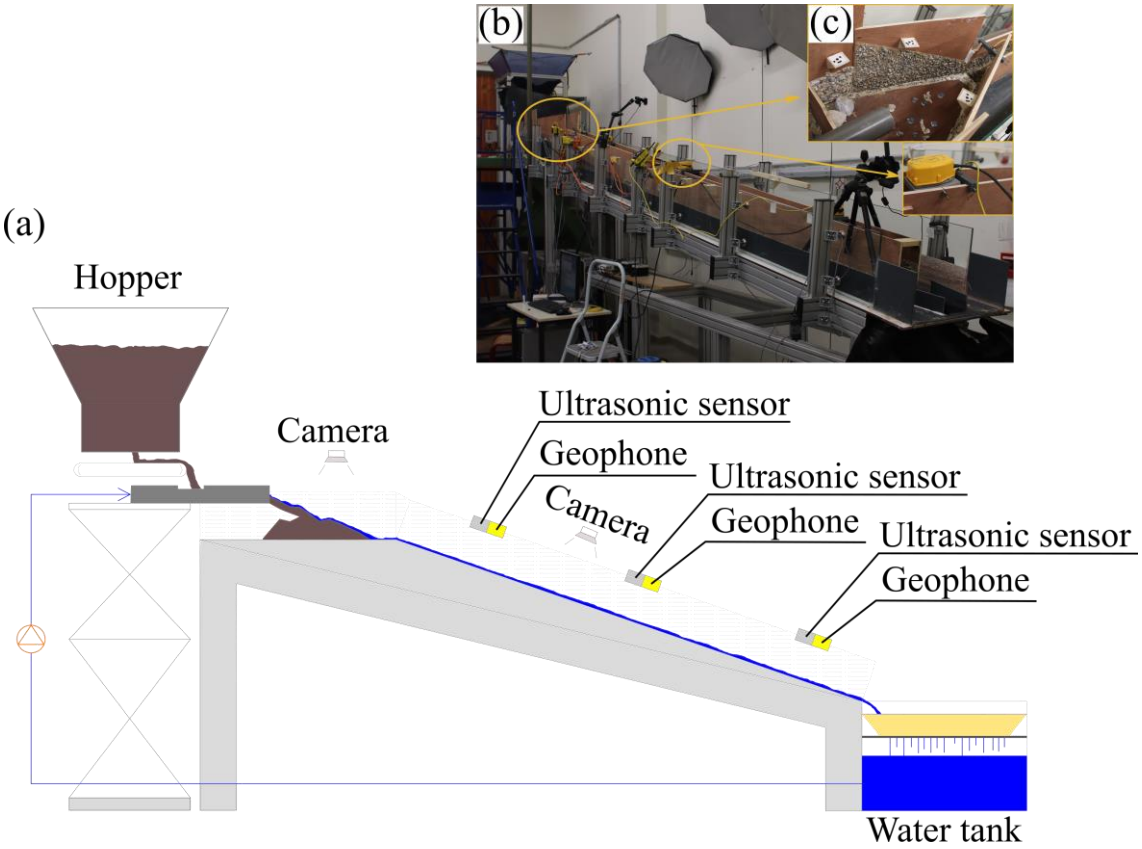

Figure 2.3 : (a) Scheme of the flume with the instrumental equipment. (b) A photo of the flume. (c) A zoom-in of (i) the upstream storage area and (ii) one of the three sections equipped with a geophone (yellow device) and an ultrasonic sensor (grey housing).

2.4.2 Experimental scaling and input conditions

Although this work does not aim at being the analogue of a particular natural prototype, we have built the flume and set the boundary conditions under several scaling considerations. While the dimensionless characteristics of the flume (e.g. slope and sediment transport concentration) can be directly compared to the field, the definition of a scaling parameter is required to estimate the scale reduction of other dimensional parameters of the flume. We follow the approach of Piton (2016) and define a geometrical scaling parameter λ as the ratio between a characteristic particle diameter of the natural and experimental river. We choose the $84th$ percentile grain diameter as a proxy for bed roughness, which exerts a major control on river hydraulics:

$$\lambda = \frac{D_{84,natural\ channel}}{D_{84,experimental\ channel}} \quad (6)$$

where $D_{84,natural\ channel}$ is the characteristic particle diameter of the natural channel and $D_{84,experimental\ channel}$ is that of our experimental setup.

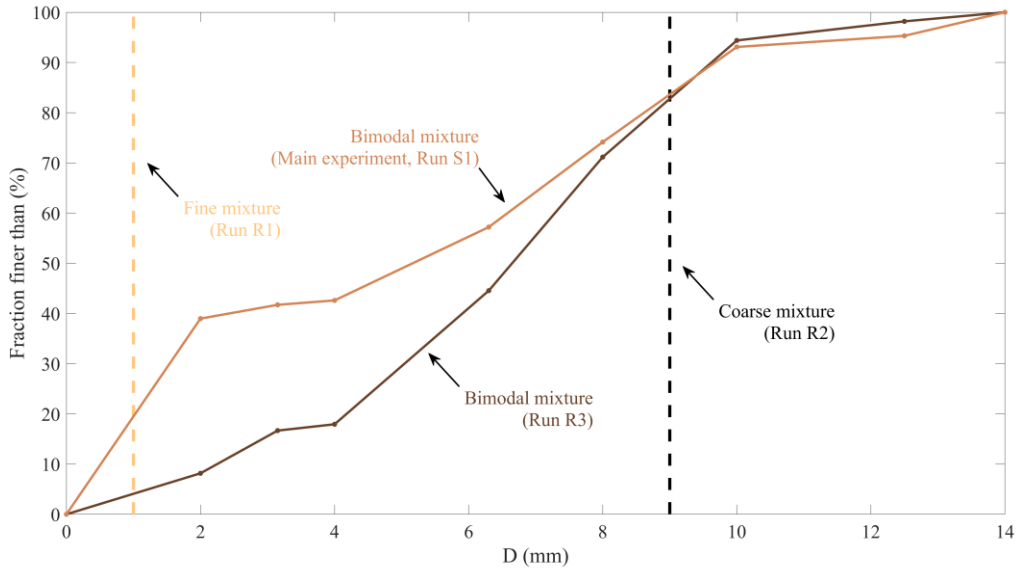

Figure 2.4 : Grain size distribution of the different sediment mixtures used in the experiments.

Mountain channels are typically characterized by a wide bimodal grain size distribution ranging from fine elements to large boulders provided by an external sediment supply (John Wolcott, 1988; Casagli et al., 2003; Sklar et al., 2017). This is why we choose a bimodal grain size distribution characterized by two modes corresponding to sand ($0.5\ mm < D < 2\ mm$) and cobbles ($4\ mm < D < 8\ mm$) (Table 2.1 and Figure 2.4) as input. The poorly sorted mixture is obtained with respect to grain size distribution utilized in previous experimental works on steep slope (Bacchi et al., 2014) and is characterized by $D_{50} = 5.16\ mm$ and $D_{84} = 9\ mm$. In order to reproduce the immobile natural roughness of confined bedrock torrents, we glue sediments to the bed and side walls of the flume.

Table 2.1 : Experimental conditions

Main Experiment	***Reference experiments***	***Supplementary experiment***
$Q_w = 0.45$ l/s $Q_s = 80$ g/s $C = 6.7\%$ $Fr = 1.66$ $Re = 2417$ $Re^* = 530$ $\frac{H}{D_{84}} = 0.70$ $\tau^* = 0.08$ $\tau^*_{cr} = 0.09$ $\tau^*/_{\tau^*_{cr}} = 0.89$ Duration = 0.5 h Bimodal mixture	Varying grain size distribution: 1. Run R1: Uniform fine mixture 2. Run R2: Uniform coarse mixture 3. Run R3: Bimodal mixture with a reduced fine fraction	Without storage area: 1. Run S1

Considering two well-documented steep mountain streams as reference natural channels, the Rio Cordon River (Italy) (Lenzi et al., 2004; Mao and Lenzi, 2007; Schneider et al., 2014) and the Erlenbach River (Switzerland) (Turowski et al., 2009; Schneider et al., 2014), we obtain $\lambda \approx 32$ computed as the average over those two reference streams ($\lambda = 41$ for the Rio Cordon and $\lambda = 23$ for the Erlenbach rivers).

Following the guidelines of Peakall et al. (1996), channel width and length, and depositional height are expected to scale linearly with λ, while the liquid discharge per unit channel is expected to scale as $\lambda^{1.5}$. Our experimental flume width is thus equivalent to a natural channel width of about 3.2 m, consistent with typical mountain stream widths (Table 2.2). The up-scaled channel length corresponds to 160 m, which can be considered as a natural channel reach. The dimensionless experimental slope of 18% falls within the range of steep mountain streams (Table 2.2).

Table 2.2 : Main characteristics of the Rio Cordon and Erlenbach rivers considered to scale the experimental conditions. The values of liquid discharge for the reference channels refer to a recurrence interval of 5 years (Schneider et al., 2014). The up-scaled experimental values are computed using $\lambda = 32$.

	Rio Cordon	***Erlenbach***	***Up-scaled experiments***
D_{84} (mm)	366	206	288
Slope (%)	13.6	15	18
Width (m)	5.3	3.5	3.2
Q_w (m²/s)	$\approx$ 1.14	$\approx$ 0.87	$\approx$ 0.80

Concerning the upstream storage area, its size is mainly dictated by technical constraints since we use a preexisting steel channel as support for the flume (Figure 2.3). Nevertheless, the chosen geometry leads to the formation of a maximum ≈ 0.15 m thick deposit, which would correspond to a deposit of about 5 m thick in a natural context, consistent with field observations in mountain upper catchments (Berti et al., 1999; Imaizumi et al., 2006). The basal slope in the storage area is arbitrarily set to $\sim 0 - 1\%$ in order to reduce the transport capacity and let the deposit develop. The influence of storage area's geometry on the observed processes will be discussed.

We chose the flow discharge with respect to standard similitude criteria. In particular we verify that channel's flow conditions are supercritical ($Fr > 1$), fully turbulent ($Re > 2000$) and hydraulically rough ($Re^* > 70$) by computing the Froude Fr, Reynolds Re, and Reynolds particle number Re^*, consistently with natural mountain streams (Peakall et al., 1996; Asano and Uchida, 2016). Estimating these parameters requires an estimate of the flow velocity which is computed following Rickenmann and Recking (2011). Finally, considering the above requirements and the flume setup, we prescribe water discharge per unit channel width of 0.0045 m²/s which is equivalent to about 0.80 m²/s in the field. From Schneider et al. (2014), this discharge value is associated with flood events having a recurrence interval of about 5 years for the Rio Cordon and the Erlenbach rivers. The feeding of the upstream storage area set in order to obtain a high sediment concentration ($C = 6.7\%$, computed as Q_s/Q_w). The main experiment is characterized by an in-channel transport stage τ^*/τ^*_{cr} close to 1, where τ^* is the mean Shields stress and τ^*_{cr} the critical Shields stress. We calculate the mean Shields stress as $\tau^* = \frac{\tau}{g(\rho_s - \rho_w)D_{84}}$, where bed shear stress is approximated under the assumption of uniform flow as $\tau = \rho_w u_*^2$, ρ_w is water density and $u_* = \sqrt{ghS}$ is the bed shear stress velocity, with h equal to water level, S being the channel slope, g is acceleration due to gravity, ρ_s is sediment density and D_{84} is the $84th$ percentile particle diameter. The critical shear stress is considered slope dependent and formulated following Recking et al. (2008) as $\tau^*_{cr} = 0.15\, S^{0,275}$. The overall experimental conditions are summarized in Table 2.1.

2.4.3 Additional experiments

In addition to the main experiment, we conduct additional experiments with different grain size distributions in order to explore the effect of grain size heterogeneity on the behaviour of the deposit. We test a bimodal distribution characterized by a reduced amount of sand (30% less in

weight, Run R3 in Table 2.1 and Figure 2.4), and two nearly uniform mixtures characterized by a mean diameter of 1 mm and 9 mm, respectively Run R1 and Run R2 in Table 2.1 and Figure 2.4. We also carry out a supplementary experiment (Supporting Information) that consists in feeding the 18% steep channel directly using the bimodal mixture of the main experiment. Input water discharge and sediment flux values are kept constant for each run.

2.5 Results

2.5.1 Dynamics of the deposit in the storage area

The temporal variation of the deposit's volume detected using the Kinect Camera measurements during the Main Experiment is shown with the brown curve on Figure 2.5, while the mechanisms involved in its evolution are investigated through looking at an associated video (movie S2.1) and selected images (Figure 2.5). During the first minutes (about 5 min), the flow is characterized by a limited transport capacity, which results in nearly total deposition with no sediments reaching the downstream channel. The water flow mainly bypasses the deposit on the sides, although some infiltration also occurs, as attested by subsurface flows coming out of the deposit toe. However, after a while (about 6 min) a large portion of the deposit is submerged, while its upper part experiences a thin but significant surface water flow (movie S2.1). Local failures efficiently move clusters of sediments at the front of the deposit and on the flanks, such that the deposit grows up in the vertical and horizontal direction until it approaches the connected steep channel. We observe that grains at the surface are preferentially coarse as a result of the downward percolation of finer particles (kinematic sieving, sensu Frey and Church, 2009). These bigger grains create an armour at the surface and also roll to the deposit's toe (yellow bordered particles in Figure 2.5c), both processes stabilizing the whole mass. At this stage, the volume reaches its maximum (point 1 in Figure 2.5a) with a slope of $\approx 53\%$ (brown curve in Figure 2.5b) when the armour suddenly breaks and a major *en masse* failure of the deposit is triggered. The armour breaking leads to the formation of a channelized flow that erodes the deposit and transports sediments over a smooth bed of sand, previously hidden in the subsurface (point 2 in Figure 2.5a and red bordered area in Figure 2.5d). After this first large destabilization that evacuates the eroded material towards the downstream main channel, the deposit reaches its lowest longitudinal slope ($\approx 25\%$) that results in a decreased transport capacity. However, some sediments are still prone to leave the storage area through a small incised channel, such that the total volume does not change significantly (plateau that nearly lasts 300 s after point 2 in Figure 2.5a). A new armoured surface starts developing with the formation of bars made of coarse particles, which makes a new aggradation phase possible as the water flow becomes shallow and unchannelized (the sheet flow described by Parker (1998)). The deposit reaches another peak in volume with a heavily armoured surface (point 3 in Figure 2.5a and e) before another destabilization occurs. We observe four alternating aggradation and erosion phases until the end of the run, interspersed with minor releases to the channel (see black arrows in Figure 2.5a). Aggradation and erosion phases fluctuate between an average deposit's slope of $\approx 48\%$ (range 45% - 53%) and 23% (range 22% - 25%), respectively. The last $1000\ s$ of the experiment are characterized by a generalized depletion of material due to the congestion of the storage area that is no longer able to retain sediments.

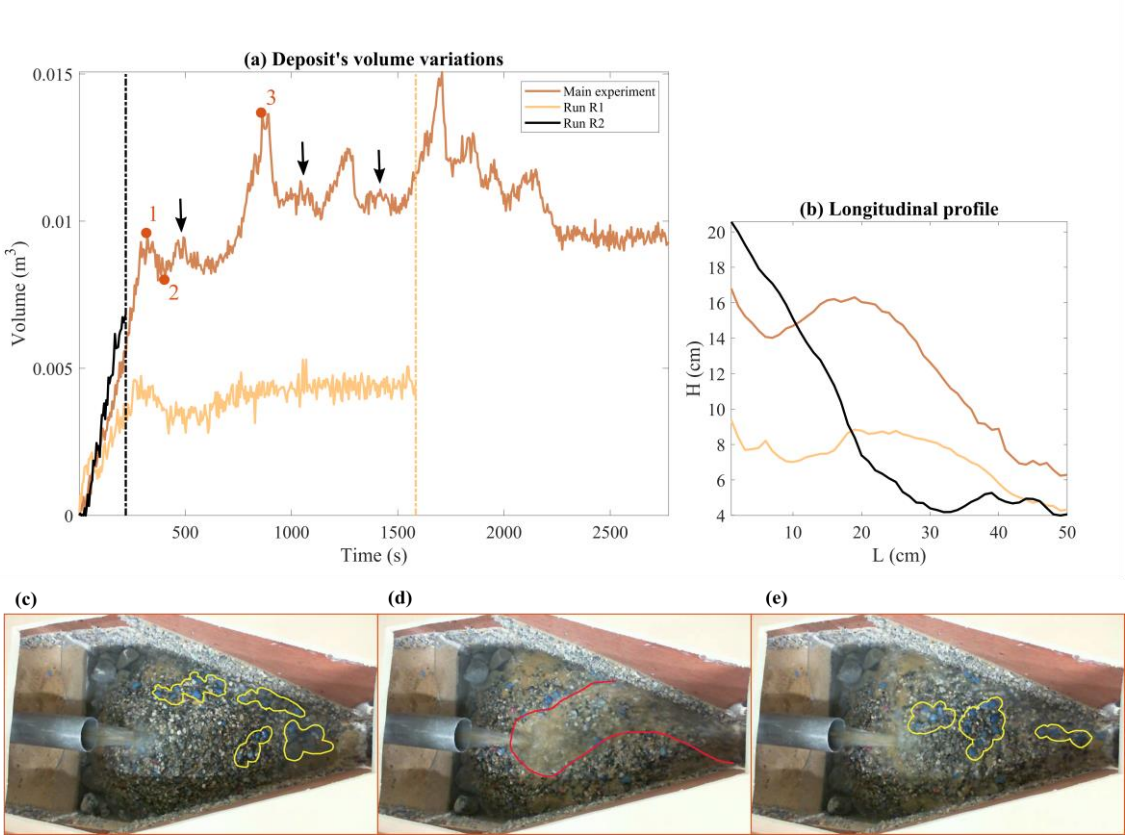

Figure 2.5 : (a) Results from the Kinect Camera for the three runs. The volume variation of the deposit is shown versus time. The two vertical dotted lines show the end of the runs with the uniform mixtures. The black arrows indicate the sediment releases occurring after the larger destabilizations and before the following aggradation phase described in the text. The orange dots and numbers refer to the images below: the frames of the video recording represent the steps of the cyclic behaviour experienced by the storage area, with (c) aggradation phase of the deposit and armouring at its maximum; (d) sediment pulse to the channel following the destabilization of the deposit with sand no more hidden but exposed to the flow; (e) new armouring phase. The yellow bordered particles form the surface armour, while the red bordered area shows the destabilized masse. (b) Comparison between the longitudinal profiles of the deposit for the three experiments when the aggradation phase is at its maximum. The profile is the result of the intersection between the deposit and a plane normal to the storage area's base and parallel to the channel.

Interestingly, we find that the alternating behaviour as described above no longer occurs when using uniform sediment mixtures. The experiment using the mixture of sand (Run R1) first exhibits an aggradation phase during the first 250 s (cream-coloured curve in Figure 2.5a) but sand quickly reaches the inlet section of the channel and the storage area starts to release sediments with a mean sediment flux of 156 g/s, before reaching an equilibrium with the inlet sediment flux (movie S2.2). The plateau in the cream-coloured curve of Figure 2.5 indicates that an equilibrium phase is achieved with no significant deposition or erosion. The experiment carried out with the coarse mixture (Run R2) leads to the formation of a steep pile in front of the injection tube. As the mobility of the grains is low, the deposit grows quickly in the vertical direction and reaches the height of the injection tube long before approaching the channel inlet. Other than for the interlocking effect of the particles, the video recording (movie S2.3) clearly shows that the high permeability of the

mixture causes the water to fully infiltrate, leading to nearly dry flow conditions at the surface (no water surface flow). We observe a similar behaviour in Run R3 using a bimodal mixture characterized by a low percentage of sand (around 10% by weight, Figure 2.4), whose video recording (movie S2.4) shows a strong stability of the deposit and no pulses are generated. The different mobility of the three mixtures presented here is materialized by the longitudinal profile computed for each experiment during the maximum extension of the deposit (Figure 2.5b). Sand easily reaches the inlet section of the channel and particles are washed away by the flow by preventing the deposit to grow in volume (cream-coloured curve in Figure 2.5b). The coarse material is on the other side of the spectrum as the stability of the mixture allows the deposit to reach a 66 % longitudinal gradient (burgundy curve in Figure 2.5b). In between these two conditions, the deposit made of the bimodal mixture is able to develop radially thanks to local destabilizations that spread material towards the channel (brown curve in Figure 2.5b).

Based on these observations, we hypothesize that, in our experiments, the ability of the deposit to experience alternating phases of storage and erosion with the generation of sediment pulses is controlled by the presence of sand and its downward percolation through the coarser grains. The processes potentially involved will be discussed.

2.5.2 Sediment pulse's propagation in the downstream channel

We investigate the propagation and physical characteristics of the sediment pulses with a specific experiment focused on the channel having the boundary conditions of the Main Experiment (see Table 2.1). We use the middle section's ultrasonic and geophone sensors, as well as the hand-made measurements of sediment flux and grain size distribution at the channel outlet. After the time shifting procedure (see Section 2.4.1), we find a clear correlation between flow surface elevation and sediment flux measurements (Figure 2.6): the passage of sediment pulses causes distinct peaks of about 60 s in the flow surface elevation time series (Figure 2.6a). The biggest peaks are associated with a sediment flux of about 340 g/s (Figure 2.6b), which is up to four times larger than the prescribed solid input of 80 g/s, and a sediment concentration that reaches 26.8% in volume. The magnitude of the sediment pulses is controlled by the dynamics of the upstream storage area, as confirmed by the supplementary experiment Run S1 in Supporting Information in which we feed the 18% steep channel directly with the same bimodal sediment mixture and observe no significant sediment flux fluctuations (movie S2.5). The second sediment flux peak around $t = 700$ s is smaller than the others, since its height is ~ 1 cm and its mean sediment flux is almost equal to the prescribed solid input ($Q_S = 84$ g/s). We find that this pulse is the result of a sediment release occurring just before the second cycle of aggradation/erosion in the upstream storage area.

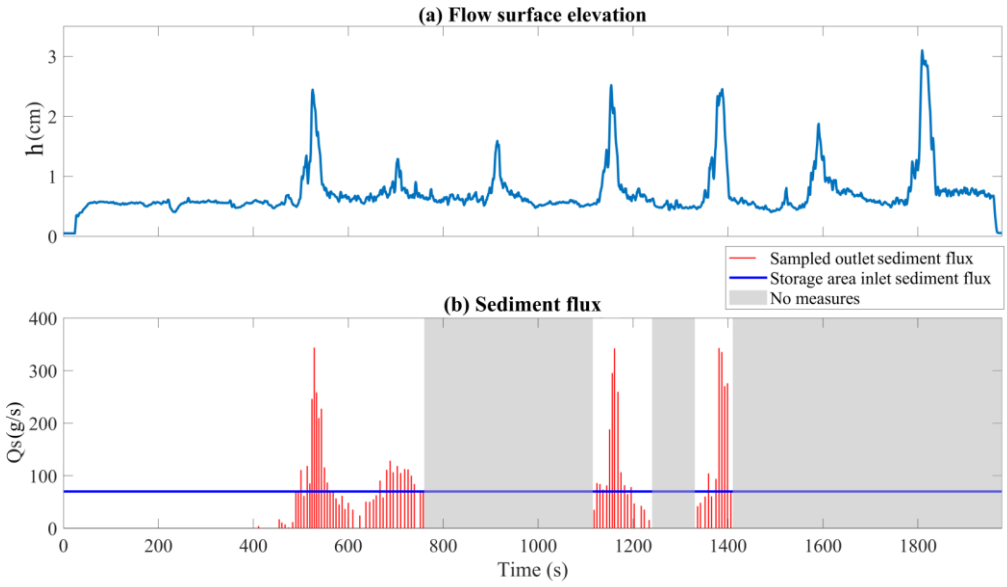

Figure 2.6 : In-channel measurement time series of flow surface elevation and sediment flux. Panel (a) shows flow surface elevation as measured in the middle section. Panel (b) shows outlet sediment flux (red bars) as compared with inlet sediment flux (blue horizontal line). It is worth recalling that these measurements refer to a different experiment from that presented in Figure 2.5.

The three sediment pulses that result from major destabilizations in the storage area are all characterized by the same composition (Figure 2.7a): a front made of the coarsest fraction of the sediment mixture, a body that exhibits a predominance of sand and a tail characterized by a wide grain size distribution (Figure 2.7b). This varying grain size distribution mainly results from the processes that occur in the storage area. The front made of the coarsest particles constituting the deposit surface ($D_{84} = 12.12$ mm in average from all front's samples) is inherited from the coarser grains being the first ones to be destabilized in the storage area. These coarser grains always precede the peak of sediment flux, and are materialized in the flow stage measurements by a small bump preceding the main pulse's peaks (Figure 2.6a). On the opposite, the sand, which is initially hidden below the surface in the storage area, only emerge and is transported towards the channel when the bulk mass is destabilized. This large destabilization constitutes the flow surface elevation peak, which exhibits finer grains ($D_{84} = 7.43$ mm) and the highest concentration of sand (33 % by weight). The falling limb of the sediment pulse is composed of a wider grain size distribution ($D_{84} = 7.85$ mm) with a high percentage of sand as well (40 % by weight), but with a decreased sediment flux as a result of the next aggradation phase starting to store sediments in the storage area. This peculiar composition is absent in the second sediment flux peak, where all the samples exhibit an average $D_{84} = 8.63$ mm with little inter-samples variations.

The video recorded one meter upstream of the middle section (movie S2.6) allows us to characterize the transport mechanics associated with each part of the pulse. The pulse's front exhibits typical bedload dynamics with grains saltating, rolling, and sliding on the bed (see the first 15 s in movie S2.6). The coarsest fraction occasionally gets stuck and forms small lateral clusters, consistent with transport for these large grain sizes occurring near the threshold of motion (see Methods). These bedforms are ephemeral since sudden impacts of grains can destroy their structure incorporating them in the main flow, causing the motion of the biggest elements

constituting the front to be quite intermittent. The pulse's body is conversely characterized by an enhanced mobility. Our instrumental equipment does not allow us to deeply investigate the nature of the interactions occurring in this dense granular flow (i.e. collisional or frictional, sensu (GDR MiDi, 2004)), but an important role in the transition between the dynamics of the front and that of the body seems to be played by the sand input, since the change in mobility arises when fine particles enter the channel (around $t = 0{:}\,0{:}\,22$ in movie S2.6). Although the grain size distribution is mainly imposed by the storage area, the pulse's body is also subject to in-channel grain sorting: fine sediments percolate to the subsurface while bigger grains are pushed upward and roll over them. Despite having the same size, we observe that the velocity of these elements is almost doubled compared to the particles constituting the front, and we advance that size segregation is the driving mechanism for this enhanced mobility. It is worth noting that as a result of this process, a portion of the coarse upper layer of the body can eventually move ahead and reach the already developed front before it reaches the outlet section. That is why the first samples exceeding a value of 200 g/s of each sediment pulse, despite being considered part of the pulse's body because of the high sediment flux, are characterized by a consistent portion of coarse grains. As the solid concentration decreases, the tail of the sediment pulse is no more congested and is characterized by a saltation dynamics ($t = 0{:}\,0{:}\,35$ in movie S2.6). As opposed to the front, which has comparable sediment flux values, the tail of the pulse is also composed of fine grains. As a consequence, thanks to an enhanced transport capacity (Wilcock et al., 2001; Curran and Wilcock, 2005), the coarsest fraction of the mixture moves relatively fast. This varying dynamics is missing for the second sediment flux peak, which exhibits a constant bedload dynamics (movie S2.6).

2.5.3 Pulse-induced seismic motion

The passage of the sediment pulses is associated with significant increases in seismic power over the whole frequency range, with the highest variations occurring above 200 Hz and being of about 30 dB (Figure 2.7c, e.g. $t = 500$ s to $t = 1000$ s and $t = 1100$ s to $t = 1450$ s). Comparing the outlet sediment flux samples and the spectrogram (Figure 2.7) we observe that seismic power varies considerably during the sediment pulse. Highest mean power always corresponds to the passage of the front, while the body and the tail are comparatively associated with much lower values (respectively -9 dB and -6 dB compared to the front). We verify that highest seismic power is indeed exclusively due to the passage of the pulse's front thanks to video recordings, on which we observe that (i) most of the channel is occupied by the front and the sediment pulse body is not yet present when the peak of seismic power is reached, and (ii) seismic power starts decreasing when front's particles get out of the channel. Similarly, the seismic signature of the second peak sediment flux is characterized by a high level of seismic power above 200 Hz, but as opposed to that of bigger sediment pulses, seismic power is proportional to the sediment flux, with higher seismic power in the $200 - 300$ Hz frequency range during the passage of higher sediment flux.

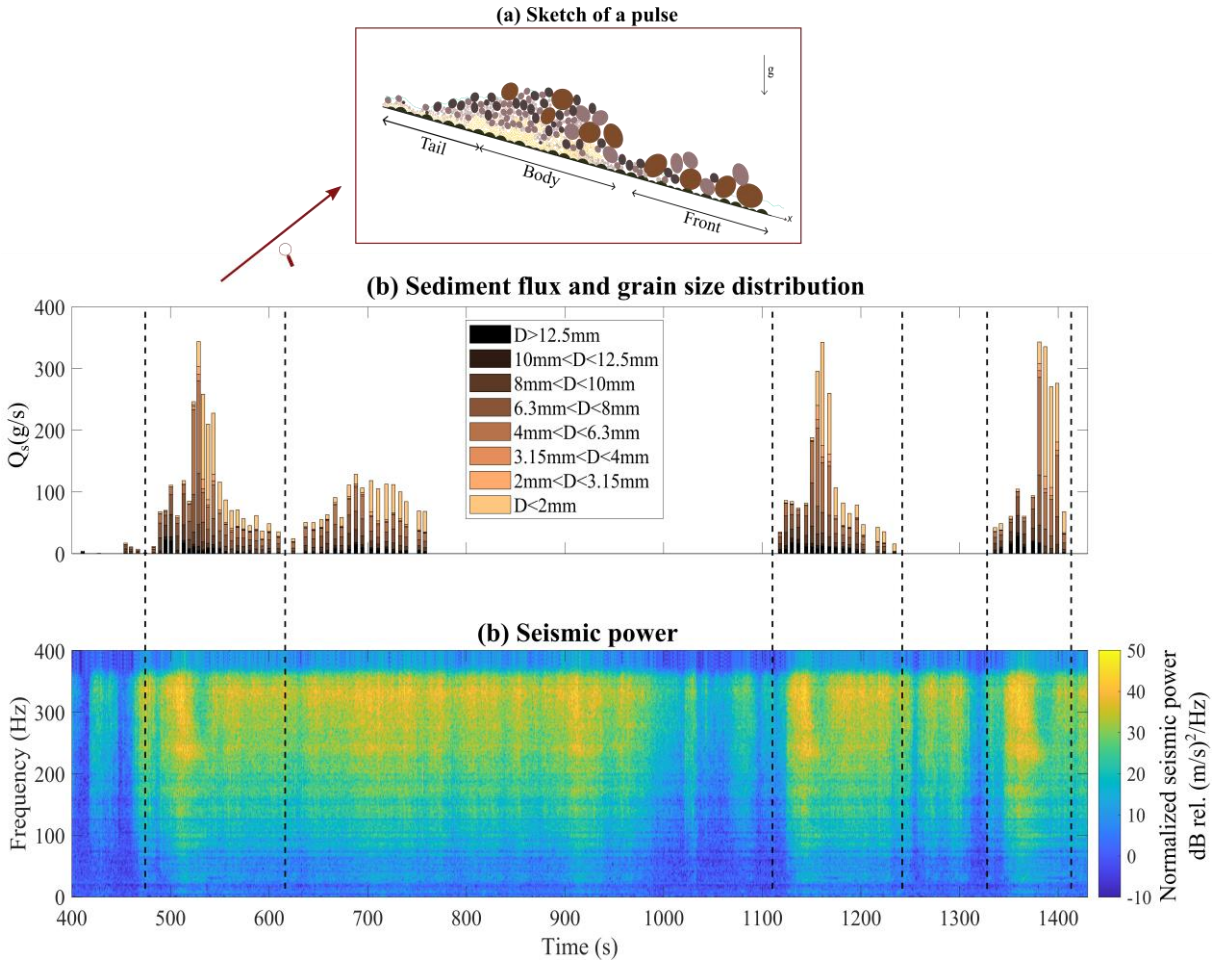

Figure 2.7 : (a) Sketch of the sediment pulse. Sediment pulses can be divided in three parts: a front, a body and a tail. (b) The four sampled pulses and the small sediment flux peak are presented with their grain size distribution. Each coloured bar refers to the particle diameter displayed in the legend, while the bar length is proportional to the percentage in weight of the related particle size. (c) Seismic power detected in the middle section of the flume. The seismic power is normalized with the mean seismic power computed under no sediment transport conditions, and it is shown as a function of time and frequency, where different colors refer to different level of power.

2.6 Discussion

2.6.1 The impact of the experimental conditions on the behavior of the upstream storage area

Here we discuss the extent to which the geometric specificities of the storage area (e.g. the size and the slope of the basin) as well as the boundary conditions (i.e. the input discharges) may have an impact on our observations. The size of the storage area controls the maximum volume of the deposit. A bigger size takes longer to fully fill before the deposit approaches the downstream channel and destabilizes, therefore longer periods of aggradation are expected. In such a case, the magnitude of the erosion phase (i.e. the eroded volume) might be bigger given the larger surface exposed to the flow. By contrast, a smaller storage area might mean more frequent but smaller destabilizations. Similar implications are expected through varying the basal slope of the storage

area, since higher slope would exert stronger stresses on particles due to gravity, likely leading to more frequent and smaller destabilizations, and vice versa. Different inputs of water discharge and sediment flux may also have an impact on the frequency and magnitude of destabilization cycles, the former by changing the stress on the surface particles, the latter by affecting the rate of aggradation. Thus, we believe that the frequency and magnitude of aggradation and erosion phases are mainly set by the geometry of the storage area and the boundary conditions. As a result, we avoid interpreting these aspects and concentrate our analysis on the processes associated with destabilization.

2.6.2 The control of the finest fraction on the en masse destabilization of sediment accumulation zones

This experimental setup has been designed to investigate if a self-formed deposit could generate sediment pulses for a downstream channel. We find that the bimodal deposit (Main experiment) exhibits a pulsating behaviour, i.e. self-induced alternating phases of storage and release of sediments under steady external forcing. In our experiments, the period of each cycle is likely dependent on deposit's surface slope variations, since the major destabilizations of the deposit always occur within a small range of longitudinal gradient ($48\ \% \pm 3\ \%$) and the following aggradation phases as well ($23\ \% \pm 1\ \%$). However, we suggest that the dynamics of these alternating phases is mainly controlled by the presence of a fine fraction (sand in our experiments) and its downward percolation.

While kinematic sieving stabilizes the deposit during the aggradation phase through building a coarse armour on the surface as observed in alluvial beds (Recking et al., 2009; Bacchi et al., 2014), the presence of sand in the subsurface not only triggers but also enhances *en masse* erosion. We link the triggering mechanism to a decrease in the deposit's hydraulic conductivity: when sand moves downward in the mixture, it fills the interstices between grains and obstruct the subsurface water flow; as water can hardly infiltrate, a surface flow develops and starts increasing shear stresses on the particles constituting the armour, which is consequently prone to instability when a certain slope is reached. The effect of fines on the hydraulic conductivity of a sediment deposit and its failure has been investigated by Hu et al. (2017, 2018) with flume experiments on the initiation of flow-like landslides. The authors show that the low hydraulic conductivity of mixtures rich in fines (called in the above-mentioned papers as "small particles" to underline their non-cohesive nature) promotes pore pressure's build-up and the consequent failure of the granular deposit. Similarly, fines' availability has been proposed as a factor able to lower the threshold of debris flow initiation from loose sediment deposit for increasing pore water pressure (Baer et al., 2017). Since our experimental equipment does not allow to estimate pore pressure, we cannot draw conclusions about its potential increase upon failure. However, the video recording makes us hypothesize that surface water flow exerts a major control on the destabilization process. We do not observe a well-defined slope rupture of the soil but rather the disintegration of deposit's armour that slides downstream under drag forces (e.g. $\mathrm{t} = 0{:}05{:}32$ or $\mathrm{t} = 0{:}08{:}25$ in movie S2.1). It is only at a later stage that the incision deepens due to the formation of a channelized flow (e.g. $\mathrm{t} = 0{:}06{:}45$).

Thus, we propose that large parts of deposit's armour fail *en masse* once the deposit is destabilized thanks to the percolated sand, that acts as a carpet over which the overlying grains slide. This

"granular lubrication" effect has been reported in previous works, where small particles are shown to increase the run-out length of granular avalanches (Linares-Guerrero et al., 2007; Phillips et al., 2006) and the mobility of granular column (Lai et al., 2017). Interestingly, Hu et al. (2017) wonder if the viscous interface between water and small particles could affect the flow-sliding: our observations on granular lubrication can be seen as additional evidence supporting their intuition. Changes in pore pressures occurring after soil's failure have also been shown to help debris flow mobilization through decreasing its frictional strength until liquefaction (Iverson, 1997; Iverson et al., 1997). Although this process could help destabilization in our experiments, we believe that its effect is not major since the armoured surface is made of coarse grains ensuring relatively efficient drainage conditions, and thus likely preventing large pore pressure build-ups. Iverson et al. (1997) point out that the transition from localized failure to wider and generalized sediment flow might also occur without contraction (i.e. without additional pore pressure variations) if the mass becomes agitated enough through developing granular temperature while moving downslope, which may also occur in our case.

The experiments using the uniform coarse material and the bimodal mixture characterized by a low fraction of sand (Run R2 and Run R3, respectively) support our hypotheses since for equal boundary conditions the deposit shows a much inhibited mobility without any releases to the channel. Run R2 is characterized by a high hydraulic conductivity, and the deposit behaves like a dry granular pile with small grain avalanches that barely spread over the storage area. Run R3 is characterized by the development of a limited surface water flow, and a single destabilization with an extremely confined run-out ($t = 0{:}\,03{:}\,45$ in movie S2.4) with no channelized flows eroding the mass.

Although the processes that drive the massive failure of sediment accumulation zones may be many, the presence of a fine fraction seems to be the common denominator. Therefore, we propose that the granulometric composition of deposits should be carefully taken into account to assess their propensity to abruptly evacuate material to downstream channels. We acknowledge that direct field measurements are often difficult to carry out in the upper part of mountain catchments, but geological maps and high-resolution topographic surveys (Loye et al., 2016) could be sufficient for a diagnostic analysis on grain size distribution, as the amount of small sized fraction mostly depends on the local lithology and type of mass wasting processes involved in sediment production (e.g. fragmentation in rock avalanches (Zhang and McSaveney, 2017) and landslides (Davies and McSaveney, 2009)).

2.6.3 The dynamics of sediment pulse's body as set by the sand input from the storage area

Our experiments show that the sediment pulses travel downstream with ephemeral interaction with the bed, since the channel is completely free of sediments after the passage of the pulse's tail. Here we would like to stress how the massive input of fine particles during the upstream erosion phase influences the dynamics of the pulse. While at the beginning the sediment pulse's front is characterized by intermittent dynamics and a reduced velocity, the motion of the biggest particles is dramatically enhanced with the body's arrival and passage. Over one century ago Gilbert (1914) demonstrated that the introduction of fine particles could enhance the transport efficiency of a mixture, and many works investigated this process experimentally (Wilcock et al., 2001; Curran and Wilcock, 2005), but only recent experimental studies underline the role played by grain sorting

(Recking et al., 2009; Bacchi et al., 2014; Dudill et al., 2018; Chassagne et al., 2020). Whereas Bacchi et al. (2014) and Dudill et al. (2018) show that fines enhance the mobility of big particles by smoothing the surface where they move, Chassagne et al. (2020) propose from numerical modelling that after percolation fines can create a "conveyor belt" transporting at higher velocity the overlying coarse grains. Although the authors showed that an exclusive "conveyor belt" contribution on the increased mobility of larger grains implies a net separation between the two main sizes, which is missing in our experiments since particles are quite mixed on the surface, from the video recording big particles appear to be passively transported downstream over a fast layer of small grains (blue pebbles over a yellowish carpet from $t = 0{:}\,0{:}\,25$ to $t = 0{:}\,0{:}\,32$ in movie S2.6). These observations lead us to suggest that the efficiency with which the pulse's body is digested by the channel without leaving any trace mainly depends on the capability of fine particles to carry coarser particles as a result of grain sorting, rather than hydrodynamics.

2.6.4 Similarities with debris flow events

Sediment pulses' dynamics exhibits remarkably similar characteristics to those of stony debris flows (Takahashi, 2014). A first similarity consists in the granulometric composition: a front made of boulders, a body characterized by a wide grain size distribution and a much more diluted tail (Iverson, 1997; Stock and Dietrich, 2006; Takahashi, 2014). To our knowledge this feature has been exclusively associated with processes occurring in the transportation zone such as in-channel size segregation (Iverson, 1997). Although we observe this latter process as well, our experimental work shows that a selective entrainment of grains also occurs in initiation zones, which can then have a significant role for influencing the textural composition of downstream propagating pulses. Given the difficulty of carrying out direct field observations in initiation zones (Berti et al., 1999; Imaizumi et al., 2006; McCoy et al., 2012; Loye et al., 2016), we suggest that this kind of experimental setup could be useful for investigating the mechanisms of both debris flow initiation and transportation.

Our findings also confirm the hypothesis of Kean (2013) for which the presence of a sediment accumulation zone can play a key role in the triggering of cyclic debris flow surges resulting from alternate aggradation and mass failure phases. In particular, the authors point out that the regressive instabilities (sensu Zanuttigh and Lamberti, 2007) of those debris flows that are generated by water runoff (i.e. runoff-induced debris flows) may develop thanks to the presence of local low-slope sections of the channel where sediments can temporally be stored and then suddenly released. Channel portions characterized by a local decrease in sediment transport capacity, referred to as "sediment capacitors", can turn steady or quasi-steady supply conditions into discrete debris flow pulses. In modelling this phenomenon, Kean et al. (2013) use a uniform grain size distribution but acknowledge that a wide grain size distribution might affect surge characteristics. Our experiments corroborate this consideration and further stress how the granulometric composition of deposits can exacerbate the debris flows' pulsating behavior.

2.6.5 Links between pulse's dynamics and seismic noise

We observe a complex seismic response to sediment pulses, characterized by a non-unique dependency of seismic power on sediment transport characteristics such as grain size and sediment flux. Highest seismic power is caused by the propagating front, consistent with the presence of larger grains causing more energetic impacts (Tsai et al., 2012). However, reduced seismic power is observed during the passage of the pulse body, although this latter is associated with the highest sediment flux, a parameter which is often aimed at being inverted from the seismic signal (Tsai et al., 2012; Bakker et al., 2020). Using the prediction of Tsai et al. (2012) that seismic power approximately scales as $D_{94}^3 q_s$, where D is the particle diameter and q_s is sediment flux, we find that the reduced seismic power of 9 dB between the front and the body of the pulse cannot be explained solely by changes in D and q_s, since D decreasing by about a factor of 0.7 ($D_{94} = 12.93$ mm for the front compared to $D_{94} = 9.32\ mm$ for the body) and q_s increasing by about a factor of 4 (from 80 g/s for the front up to 340 g/s for the body) would yield approximately constant seismic power. Since seismic records show a reduced sensitivity to the pulse's body, which in fact accounts for the largest fraction of the sediment flux, the capability of existing models of reliably inverting solid discharge from seismic power is questioned for this kind of transport processes.

Since our sediment pulses show similarities with debris flows (see previous Section), we find appropriate to compare our observations also with expectations from theories of debris flow-induced seismic noise. Conveniently, the limited channel length in our experimental setup allows us to study the seismic responses of the three different parts of the pulse (front, body, and tail) separately, since when one component of the pulse acts the other one is not yet on the channel or has already left it. On the contrary, in the field all parts of the pulse can potentially contribute to the overall measured seismic noise, such that the drop in seismic power observed in our experiments during the passage of the body could be "hidden" in the field by the seismic noise induced by a louder upstream tail and downstream front. Our observations are consistent with most field surveys and models, for which the front (sometimes referred to as snout) generates a stronger seismic power than the following flow as it carries the largest clasts (Arattano and Moia, 1999; Lai et al., 2018; Coviello et al., 2019; Farin et al., 2019; Allstadt et al., 2020). However, the relationship between seismic noise and flow thickness is contrasting. While some observations show correlation between flow thickness and fluctuating basal stresses (Allstadt et al., 2020) and some models reveal no or rare direct dependence (Lai et al., 2018; Farin et al., 2019), our experiments show a clear negative correlation since pulse's body is characterized by the peak of flow surface elevation (Figure 2.6). According to Cole et al. (2009) and Allstadt et al. (2020), this could be explained by body's high bulk density. Indeed, they observe a negative correlation between bulk density and seismic noise, and therefore propose that more agitated flows are "louder" than denser and plug-like flows. This interpretation would be also consistent with the increase of seismic noise associated to the pulse's tail, which is again much more diluted than the body.

Further work remains to be conducted in order to fully unravel the control of the pulse's internal dynamics on the generated seismic noise. In particular, it appears as essential to more quantitatively investigate the effect of grain sorting, which likely plays a crucial role through pushing upward the biggest particles, thus preventing them from directly impacting the bed and

reducing their contribution to seismic noise. This would be consistent with the field observations of Kean et al. (2015), who suggest that the presence of a sediment layer over the bedrock can strongly damp the seismic signal generated by a debris flow[2]. Detailed analysis of particle impact velocities, rates and applied forces across the different grain sizes and the different pulses components would help further addressing these aspects.

2.7 Conclusions

We carry out flume experiments characterized by an original setup where instead of feeding the flume section directly as usually done, we supply with liquid and solid discharge a low slope storage zone acting like a natural sediment accumulation zone and connected to a 18 % steep channel.

Under constant feeding conditions, when a bimodal grain size distribution with a high fraction of fine particles is used, the storage area is subject to alternating aggradation and erosion phases. The high morphological mobility of the deposit is due to several autogenic processes, but the presence of sand appears to play a key role. In particular, if during the aggradation phase grain sorting enhances the stability of the deposit in coarsening its surface thanks to the downward percolation of the fine particles, we propose that the infilling of the subsurface with fine material contributes to the destabilization of the deposit by two means: (i) it reduces the hydraulic conductivity of the deposit and causes the formation of a significant surface water flow that in turn increases the stresses over the armoured layer, (ii) it acts like a smooth carpet where the coarser grains slides *en masse*.

The erosion phases correspond to the generation of sediment pulses towards the downstream channel. The evolution of the sediment deposit affects not only the magnitude of the sediment pulses, but also their rheology and dynamics. When major destabilizations of the sediment deposit occur, each sediment pulse can be divided in three different components as follows: a front having a low sediment flux made of the coarsest fraction of the sediment mixture, inherited by the destabilization of deposit's surface; a body that corresponds to the peak of sediment flux, composed of a high concentration of sand coming from deposit's subsurface; a tail characterized by a low sediment flux and a wide grain size distribution, with sediments still transported while the next aggradation phase starts to develop in the storage area.

Pulses in sediment transport can be detected by seismic measurements. We find that the sediment pulse's front dominates the overall seismic noise. However, we report a complex link between seismic power and the different parts of the sediment pulse, which questions the validity of current models and theories to such transport dynamics. Further work is needed to unravel the role of the different pulse's geometrical and dynamical parameters on the generated seismic noise.

From a practical point of view, these results have strong implications in natural risk management. First, we show that the proximity of upstream sediment accumulation zones must be considered a potential source of sediment pulses for mountain rivers, regardless of bed sediments' availability. Second, since the grain size distribution is shown to have a direct influence on the mobility (i.e. stability) of debris deposits, we challenge the classical approach for which the *sediment budget* of

[2] During the defense of this PhD, the examiner Anne Mangeney correctly pointed out that this was also observed by Bachelet et al. (2018) in the laboratory.

mountain catchments is merely reduced to an available volume and hydrological conditions are considered the main factor controlling the activation of external sediment supply. Instead, the granular conditions of deposits that are coupled with mountain streams or stored in low slope portion of the channel should be considered for assessing the occurrence and dynamics of such dramatic transport events. Finally, our seismic findings challenge the application of current theoretical frameworks to invert bedload flux from the seismic noise associated with this kind of transport processes.

Acknowledgements

We acknowledge the support of the INRAE Research Centre of Grenoble for the laboratory and instrumental equipment. We thank Christian Eymond-Gris, Frédéric Ousset, and Xavier Ravanat for the technical support in the development of the flume. We thank Maarten Bakker for helping in the analysis of the seismic data. We thank Guillaume Piton for the constructive discussion on the experimental scaling of the flume. We thank the two anonymous reviewers for comments which helped improve the quality of the paper.

Financial support

This research has been supported by the Agence Nationale de la Recherche (grant no. 17-CE01-0008).

2.8 Supporting Information

Introduction

In Section S2.1 we present the method used for the normalization of the seismic power and its result. In Section S2.2 we discuss the reference experiment carried out without the storage area. Finally, in Section S2.3 we show the experiment for testing the spatial variability of seismic noise along the flume

S2.1: Normalization of the seismic power

In addition to sediment transport, several sources contribute to the seismic signal detected in the channel, such as the water pump, water flow and storage area's processes. In order to focus on the sediment transport-induced seismic noise and also remove flume resonance effects, we normalize the seismic power by subtracting (in the dB space) the mean seismic power corresponding to a 200 s long time window selected at the beginning of the experiment from the raw signal. Figure 2.8 shows the comparison between the raw and normalized seismic power. We can observe how the mentioned sources produce low frequency seismic noise and that flume resonance, materialized by horizontal bands in Figure 2.8a, is not as much visible in Figure 2.8b.

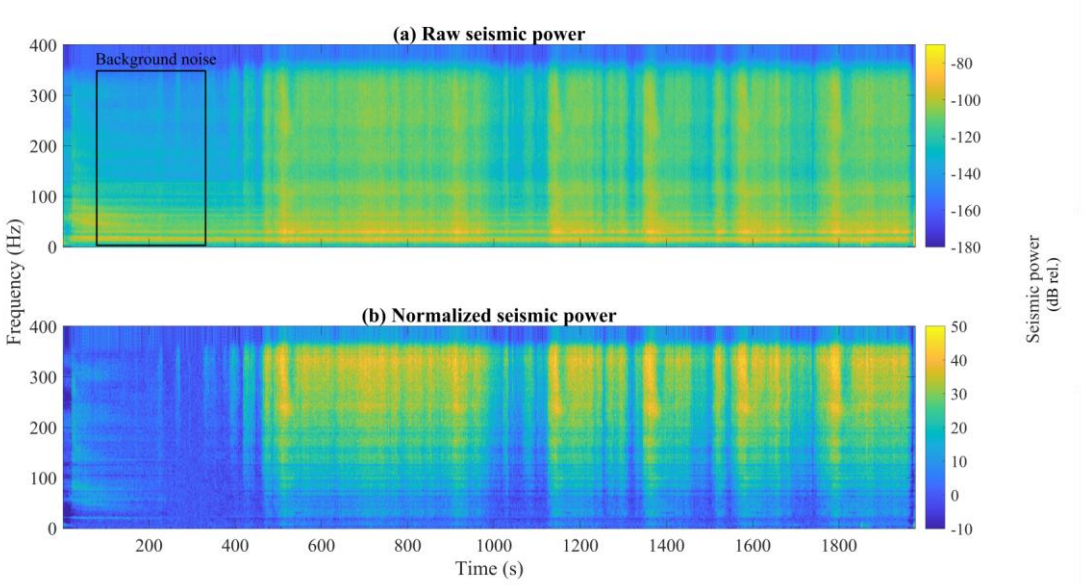

Figure 2.8 : Comparison between the raw spectrogram (panel (a)) and the normalized one (panel (b)). The seismic power is shown as a function of time and frequency, where different colors refer to different level of power.

S2.2: Supplementary experiment without the storage area

In order to test in-channel sediment storage potential and discriminate the processes controlled by upstream sediment accumulation zone, we carry out a supplementary experiment that consists in feeding the 18 % steep channel directly. We investigate the channel response in terms of flow surface elevation, seismic noise and outlet sediment flux (respectively, Figure 2.9a, b, and c). We observe minor fluctuations in the flow surface elevation and its instantaneous variation is likely due to the detection of moving particles (Figure 2.9a). Indeed, by means of the camera installed above the upper part of the channel we observe that the material is transported downstream with no bed aggradation. However, the coarsest fraction of the sediment mixture occasionally gets stuck close to the rough sidewalls. These particles act as local obstructions dissipating the energy otherwise available for sediment transport, leading to the formation of small lateral clusters. Nevertheless, these bedforms are transient since sudden impacts of grains can destroy their structure. Therefore, their influence is marginal and does not affect the flow. This is confirmed by the outlet sediment flux shown in Figure 2.9c: during the run, the transport rate exhibits only small fluctuations since more than 80 % of the samples have a variation lower than ± 20 % around a mean value equal to the inlet sediment flux ($Qs = 80$ g/s). We expect that the few peaks around 100 g/s are the result of the destabilisation of the ephemeral bedforms that develop along the channel. Observations remain identical even at higher sampling frequency (see the fourth and seventh groups of bars in panel c). The samples are characterized by a similar grain size distribution, with minor variations that likely depend on the input sediment flux being characterized by a varying grain size distribution. However, coarser grain size distribution could result from clusters' destabilizations. No significant changes over time are highlighted in the seismic power measurements (Figure 2.9b), confirming that the sediment flux remains almost constant during the experiment. Moreover, the impact of sediment clusters' mobilization is supposed to be very low compared to the magnitude of the continuous bedload transport experienced by the channel.

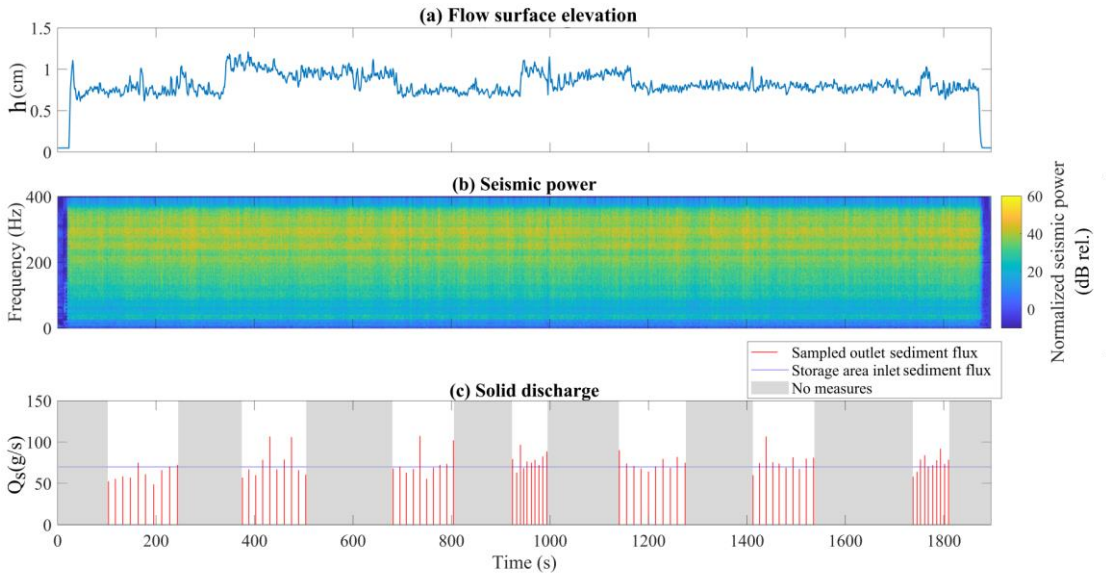

Figure 2.9 : Comparison between measures. (a) Flow surface elevation detected by the ultrasonic sensor placed in the middle section of the flume. (b) Seismic power detected in the middle section of the flume. The seismic power is shown in decibel and computed as a function of time and frequency, where different colors refer to different level of power. (c) Comparison between inlet sediment flux (blue line) with the sampled outlet sediment flux (red bars).

S2.3: Testing the spatial variability of the seismic noise

We carry out a specific test in order to investigate the potential spatial changes in the seismic response of the flume to a given force solicitation. We record the seismic noise generated by identical impacts of a pebble of known mass ($m = 66\ g$) dropped from a known height ($z = 10$ cm) in 18 different points along the channel. We observe that in the $100 - 350$ Hz frequency range of interest for sediment transport the seismic power varies within 10 dB, with the highest amplification effects being placed right near and upstream of the geophone used in our analysis (Figure 2.10). We can therefore consider the seismic noise recorded in the middle section as induced by in-channel processes occurring all over the flume with preferential sensitivity to a 1 m long segment centered on the geophone's location.

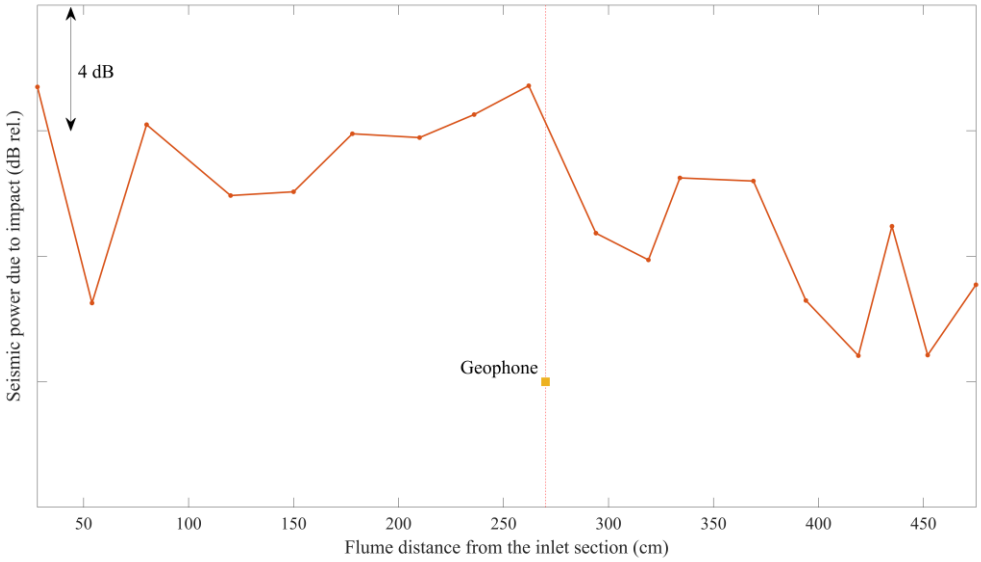

Figure 2.10 : Measured variations of seismic power along the flume. Each point results from the mean of the seismic power (in the $200 - 350$ Hz frequency range) due to three identical impact in prescribed locations. The yellow square represents the position of the geophone used in the analysis.

Additional Supporting Information (Files uploaded separately)

Movie S2.1: Storage area with bidomal mixture, https://doi.org/10.5446/51666

Movie S2.2: Storage area with fine mixture, https://doi.org/10.5446/51981

Movie S2.3: Storage area with coarse mixture, https://doi.org/10.5446/51982

Movie S2.4: Storage area with bidomal mixture (low fraction of sand), https://doi.org/10.5446/51984

Movie S2.5: Sediment flux during the supplementary experiment, https://doi.org/10.5446/51985

Movie S2.6: Sediment pulse during the main experiment, https://doi.org/10.5446/51986

Movie S2.7: Solid discharge peak during the main experiment, https://doi.org/10.5446/51987

Chapter 3: Solid concentration as a main proxy for basal force fluctuations generated by highly concentrated sediment flows

3.1 Preface

The laboratory experiments presented in the previous chapter allowed us to explore the triggering and propagation dynamics of sediment pulses in low-order mountain rivers by a geomorphological point of view, which was a component of the first scientific question of this PhD. However, the analysis of the seismic signal generated by the highly concentrated sediment flow opened a sort of Pandora's box. Why is the body of the sediment pulses characterized by a decrease of seismic power? Why are existing theories unable to explain this observation? We realized that the instrumental equipment was not adapted to answer these questions. This feeling is well described by an e-mail that I sent to my thesis directors at the beginning of the second year of my PhD, here translated in English:

"Today I'm doing experiments at IRSTEA (former name of the INRAE Research Centre, ed), I need to clarify my doubts about the seismic... I feel like we want to model processes (sediment pulses) that we haven't yet fully understood."

The experiments gave us interesting insights on the mechanisms occurring during the propagation, but at the same time they highlighted a complexity (e.g. grain sorting and grain-to-grain interactions) which was only partially captured by the instrumental equipment. This motivated us to improve the instrumentation and carry out a novel set of experiments with the aim to better understand the seismic signature of these sediment transport processes, which represented the second component of the first scientific question of this PhD.

This chapter presents and summarizes the results of the laboratory experiments carried out mostly during the second year of my PhD. The chapter is constituted by a paper that is edited on the Geophysical Research Letter (GRL) journal: **Piantini, M.**[1,2], Gimbert, F.[1], Korkolis, E.[1], Rousseau, R.[2], Bellot, H.[2], and Recking, A.[2] (2023): Solid concentration as a main proxy for basal force fluctuations generated by highly concentrated sediment flows. Geophysical Research Letters, 50, e2022GL100345. https://doi.org/10.1029/2022GL100345

[1] University Grenoble Alpes, CNRS, IRD, Institute for Geosciences and Environmental Research (IGE), Grenoble, France

[2] University Grenoble Alpes, INRAE, CNRS, IRD, Grenoble INP, IGE, 38000 Grenoble, France

Préface

Les expériences de laboratoire présentées dans le chapitre précédent nous ont permis d'explorer la dynamique d'activation et de propagation des bouffées sédimentaires dans les rivières de montagne d'un point de vue géomorphologique, ce qui était une composante de la première question scientifique de cette thèse. Cependant, l'analyse du signal sismique généré par ces bouffées sédimentaires une sorte de boîte de Pandore. Pourquoi le corps est-il caractérisé par une diminution de puissance sismique ? Pourquoi les théories existantes sont-elles incapables d'expliquer cette observation ? Nous avons réalisé que l'équipement instrumental n'était pas adapté pour répondre à ces questions. Ce sentiment est bien décrit par un mail que j'ai envoyé à mes directeurs de thèse au début de la deuxième année de mon doctorat :

« Aujourd'hui je manipe à IRSTEA, il faut que je m'enlève des doutes sur la sismique...j'ai l'impression que l'on veut modeler des processus (vagues sédimentaires) que nous n'avons pas encore bien compris »

Les expériences nous avaient donné des indications intéressantes sur les mécanismes se produisant lors de la propagation de ces bouffées, mais en même temps elles avaient mis en évidence une complexité (par exemple les interactions granulaires) qui n'était que partiellement captée par l'équipement instrumental. Cela nous a motivé à améliorer l'instrumentation et à réaliser des nouvelles expériences avec le but de mieux comprendre la signature sismique de ces processus, ce qui représentait la deuxième composante de la première question scientifique de cette thèse.

Ce chapitre présente et résume les résultats des expériences de laboratoire menées principalement au cours de la deuxième année de mon doctorat. Le chapitre est constitué d'un article qui est édité sur le journal Geophysical Research Letter (GRL) : **Piantini, M.**[1,2], Gimbert, F.[1], Korkolis, E.[1], Rousseau, R. [2], Bellot, H. [2], and Recking, A.[2] (2023): Solid concentration as a main proxy for basal force fluctuations generated by highly concentrated sediment flows. Geophysical Research Letters, 50, e2022GL100345. https://doi.org/10.1029/2022GL100345

[1] University Grenoble Alpes, CNRS, IRD, Institute for Geosciences and Environmental Research (IGE), Grenoble, France

[2] University Grenoble Alpes, INRAE, CNRS, IRD, Grenoble INP, IGE, 38000 Grenoble, France

3.2 Abstract

Sediment flows generate ground vibrations by exerting force fluctuations on the riverbed. Linking force fluctuations to properties of highly concentrated sediment flows, however, remains particularly challenging due to complexities arising from grain-to-grain interactions. Here we conduct downscaled flume experiments in which we specifically measure force fluctuations and local seismic vibrations together with flow properties of highly concentrated sediment flows at high spatial and temporal resolution. We observe hysteresis behaviors between force fluctuations amplitude and flow surface elevation and mass that occur during complex changes in internal flow dynamics. By contrast, force fluctuations amplitude exhibits a unique negative relationship with solid concentration. We suggest this is due to the rheology of dense granular flows, where solid concentration is a proxy for particle agitation. We therefore advance that solid concentration should be incorporated in seismic models of such sediment flows as a key parameter describing inter-particle collisions and impacts to the bed.

3.3 Introduction

Flowing through the landscape, rivers generate high-frequency ground vibrations (> 1 Hz) by exerting force fluctuations on their bed (Burtin et al., 2016; Larose et al., 2015). There is well-established evidence that seismic sensors detect ground vibrations from a wide variety of fluvial sediment transport events including very energetic ones (Arattano and Moia, 1999; Burtin et al., 2016; Cook et al., 2018, 2021), calling for seismology as an appealing way to remotely monitor sediment transport characteristics and processes.

Through experiments and field observations, numerous efforts have recently been dedicated to investigate the relationships between the amplitude of force fluctuations and the properties of various sediment flows, ranging from bedload to debris flows (Allstadt et al., 2020; Bakker et al., 2020; Cole et al., 2009; Coviello et al., 2018; Gimbert et al., 2019; Haas et al., 2021; Hsu et al., 2014; McCoy et al., 2013; Zhang et al., 2021b). In parallel, physically based mechanistic models have been developed to establish quantitative links between the flow properties and the generated seismic signal (Tsai et al., 2012; Gimbert et al., 2019; Bachelet et al., 2021; Farin et al., 2019; Lai et al., 2018; Zhang et al., 2021b). Models concerning bedload transport predict that sediment flux and transported grain sizes are major control parameters, mainly setting the rate and the amplitude of particle impacts against bed roughness elements. These theoretical expectations have been verified through experiments and field observations under relatively low bedload transport rates (Bakker et al., 2020; Gimbert et al., 2019; Lagarde et al., 2021).

However, more complexity arises with highly concentrated sediment flows, for which existing observations reveal not straightforward relationships between flow properties and amplitude of force fluctuations. Coarse granular and debris flows have been shown to generate stronger force fluctuations compared to finer ones (Haas et al., 2021; Hsu et al., 2014; Zhang et al., 2021b), but the presence of big particles does not necessarily correspond to high force fluctuations, likely depending on their position relative to the bed (Zhang et al., 2021b). Hsu et al. (2014) suggest that average sediment flow velocity exerts a primary control on force fluctuations, whereas Allstadt et al. (2020) and Zhang et al. (2021a) observe a rather low correlation. Certain investigations show amplitude of force fluctuations that is positively correlated with flow thickness and mass (McCoy

et al., 2013; Zhang et al., 2021b), others report poorer correlations when bulk density varies fast (Allstadt et al., 2020), or even negative correlations in the case of mud-saturated debris flows (Hsu et al., 2014). These contrasted results suggest that internal flow dynamics in addition to macro flow properties must be studied in order to better understand observations (Allstadt et al., 2020).

In this view, Piantini et al. (2021) designed laboratory experiments enabling strong changes in the internal flow dynamics of highly concentrated sediment flows, characterized by a wide bimodal grain size distribution enhancing grain sorting processes (Frey and Church, 2009; Iverson et al., 2010; Johnson et al., 2012) and rheological stratification, where the latter is meant as the occurrence of significant variations of flow rheology over depth (Armanini et al., 2005; GDR MiDi, 2004; Manville and White, 2003; Y. K. Sohn, 1997). They show that these complex processes strongly affect the generated seismic power. In particular, they observe a strong decrease in seismic power associated with the passage of the main body of the sediment flow, which they argue is in contradiction with expectations from theory. They evoke several physical mechanisms as potential drivers of this behavior, but limitations in the experimental instrumentation prevented them from identifying the specific physics controlling the seismic signature, and understanding whether such physics may be described as a function of certain bulk flow properties.

Here we investigate sediment flows similar to those in (Piantini et al., 2021) but with improved instrumentation composed of a combination of cameras, seismic and force sensors that allow us to track several in-stream flow properties and their seismic signature at high spatial and temporal resolution. Thanks to this novel set of experiments, we demonstrate that, despite complexities in internal flow dynamics, solid concentration is a good proxy for the amplitude of basal force fluctuations. We suggest that this finding can be explained by the link between solid concentration and particle agitation, which appears to control inter-particle collisions and impacts to the bed when solid concentration is sufficiently high.

3.4 Methods

3.4.1 Experimental setup and measurements

We carry out laboratory experiments in a flume composed of a 5-m long and 0.1-m wide straight steep channel (slope of 18%), connected in its upstream part to a 1-m long and on average 0.5-m wide storage area (slope of $0 - 1\%$) (Figure 3.1). The bed and sidewalls of the flume are covered with sediments fixed with silicone. Every run consists in feeding the upstream storage area with constant water discharge Q_l ($Q_l \in [0.48; 0.55\ l/s]$) and sediment flux Q_s ($Q_s \in [70; 100\ g/s]$) whose values are based on similitude criteria to reproduce typical supercritical and fully turbulent flood conditions in mountain rivers (Froude number $Fr \in [1.63; 1.66]$ and Reynolds number $Re \in [2417; 3525]$; see (Piantini et al., 2021) for overall scaling considerations). We use a bimodal grain size distribution typical of mountain rivers (John Wolcott, 1988; Sklar et al., 2017), with one mode corresponding to sand (0.5 mm $< D <$ 2 mm) and the other to cobbles (4 mm $< D <$ 8 mm), and with $D_{50} = 5$ mm and $D_{84} = 9$ mm.

Seismically relevant quantities are measured through seismic and force sensors. Four Glaser-type KRNBB-PC piezoelectric sensors, which we here refer to as seismic sensors, are mounted on the outside of one of the sidewalls of the channel, using mounting brackets and double-sided adhesive tape (Supporting Information). The sensors are connected via an AMP-12BB-J preamplifier to an

Elexis Spectrum digitizer with sampling frequency f_s set to 200 kHz. The mean basal force ($\bar{F}$) and force fluctuations are measured by coupling a 0.07-m wide and 0.1-m long rectangular steel plate onto the channel bed with two piezoelectric force sensors (model Kistler Typ 9601A21 connected to a Kistler 5073 charge amplifier) measuring the normal and downslope forces exerted by the flow on the plate (using $f_s = 30$ kHz). The plate is mechanically isolated from the rest of the flume to minimize its sensitivity to flume vibrations, and is covered by sediments fixed with silicone (Supporting Information).

We also monitor several in-stream flow properties simultaneously. We measure the flow surface elevation (h) in three different sections of the channel (Figure 3.1) by means of three ultrasonic sensors (Banner Q45UR Series, using $f_s = 100$ Hz). We sample and sieve the sediment flux (Q_s) by hand at the flume outlet with a frequency of about 1 sample / 5 sec. We estimate the in-stream solid concentration as:

$$\phi(t) = \frac{\rho(t) - \rho_w}{\rho_s - \rho_w} \tag{7}$$

where $\rho(t)$ is the bulk density, calculated as the ratio between the sediment flow mass and the relative volume, $\rho_s = 2618$ kg/m^3 is the sediment density, estimated experimentally for sediments at rest and assumed not to vary significantly during the experiment, and $\rho_w = 1000$ kg/m^3 is the density of water (see calculation in Supporting Information). We also estimate the macroscopic velocity of the sediment flows (U_x) and the downstream velocity of the biggest particles (u_x) by combining multiple sets of observations such as particle tracking in videos and time delays in flow surface elevation and seismic measurements (Supporting Information). Video recordings are made by means of multiple cameras: a Canon EOS 200D installed perpendicular to the channel bed and covering a stretch of 0.30 m close to the upstream seismic sensor SS1, an inclined webcam (Microsoft HD LifeCam Cinema) offering a wide view on the section with the force sensor FS, and a Canon EOS 100D camera providing a side view on a stretch of 0.10 m close to the downstream seismic sensor SS4 through a window made in the channel sidewall (Figure 3.1).

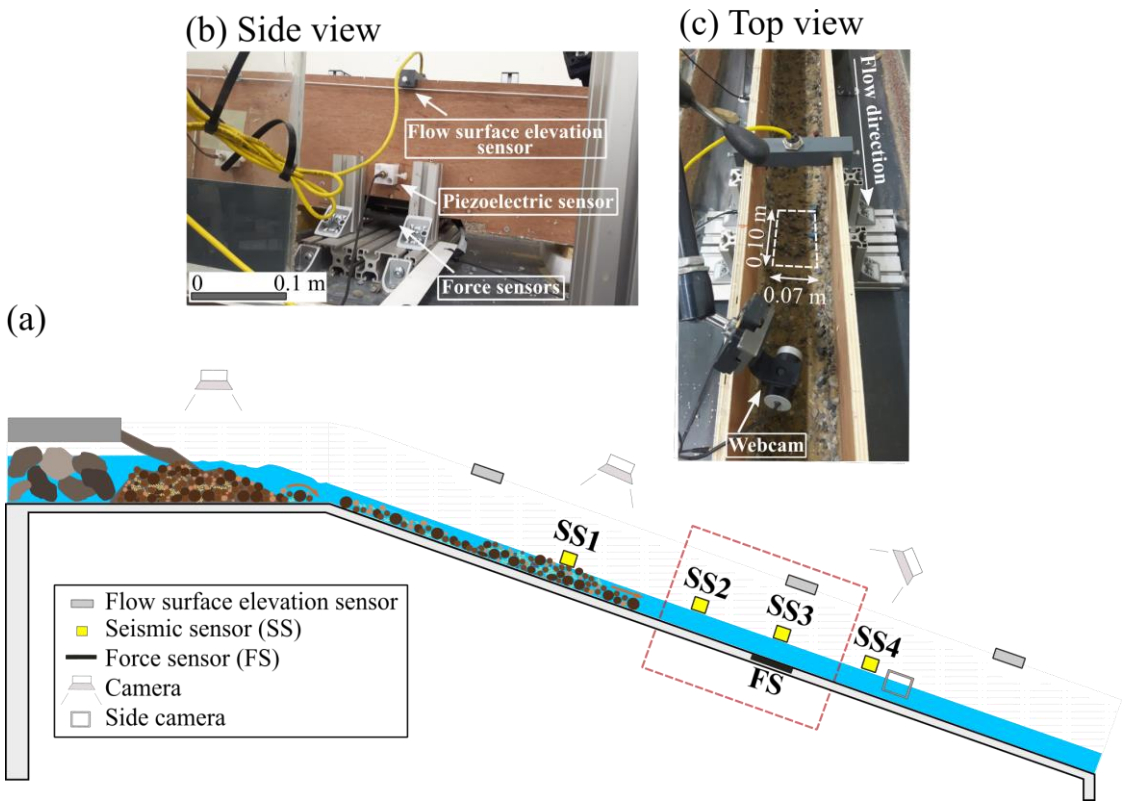

Figure 3.1 : (a) Sketch of the experimental flume. (b) Side view and (c) top view of a 0.6-m long stretch of the flume including the section equipped with a flow surface elevation sensor, a seismic sensor, and the force sensor. The red dashed square in panel (a) is shown in side view on panel (b). The white dashed square in (c) highlights the area occupied by the steel plate connected to the force sensor.

3.4.2 Analyzing seismic and force data

We analyze the seismic and normal force fluctuations time series through computing the power spectral density (PSD) using Welch's averaging method (Welch, 1967). Time series are split into 50 % overlapping segments of 0.5 s for the seismic signal and 1 s for the force signal. Before force power computation, we apply a band-bass Butterworth filter to the force signal in the frequency range $100 - 2500$ Hz to avoid dealing with strong plate resonances. We focus on this frequency range also because the contribution to seismic vibrations of impacts on the sidewall is particularly noticeable above 2500 Hz (Supporting Information), and that of water flow is significant below 100 Hz (Piantini et al., 2021). In the selected frequency range, seismic waves are strongly attenuated with distance, such that the most contributing sources are located within about 1 m around the sensors (Supporting Information). We compute the mean force by applying a low pass filter below frequency $f = 1.5$ Hz to the force signal. Force power and flow property time series are smoothed using a 5-s moving window for the results presented in Section 3.5.3.

3.4.3 Generation and propagation of the sediment flows

The sediment deposit that forms in the storage area is subject to alternating stages of aggradation and erosion, with every erosion generating sediment pulses that propagate in the downstream steep channel (Piantini et al., 2021). The self-triggered destabilizations of the upstream sediment deposit generate a downstream propagating pulse made of three distinct sediment transport phases exhibiting different dynamics and grain size compositions. Phase I ("Front bedload" in Figure 3.2d) is characterized by a constant and relatively low sediment flux (i.e. similar to that imposed by the boundary conditions to the storage area, $35 < Q_s < 100$ g/s) and a coarse grain size distribution (Figure 3.2i and m). Phase II ("Highly concentrated sediment flow" in Figure 3.2b and c) is characterized by a thick sediment flux ($Q_s > 150$ g/s and h_{max}~3 cm) exhibiting a wide grain size distribution made of a varying amount of fines ($D < 2$ mm) (Figure 3.2i and m, and Figure 3.3a and e). Phase III ("Tail bedload" in Figure 3.2a) is characterized by a low sediment flux similar to phase I ($35 < Q_s < 150$ g/s) although it exhibits a wider grain size distribution with a different content C of big grains ($C_{D>8\,mm}^{Phase\ I} = 58\%$ against $C_{D>8\,mm}^{Phase\ III} = 27\%$, see Figure 3.2i and m). We investigate four sediment pulses in total, two of them are presented in the main text (referred to here as Exp #1 and Exp #2) and the two others in Supporting Information.

3.5 Results

3.5.1 Local in-stream dynamics

Phase I is dilute, with ϕ ranging from 0.15 to 0.25, and exhibits typical bedload dynamics, i.e. grains saltate, roll, and slide in direct contact with the bed (see movie S3.1 and S3.2), with a mean downstream velocity $u_x \approx 0.27$ m/s (Figure 3.2e). Phase II spans a range of solid concentrations reaching up to $\phi = 0.6$, thus approaching the maximum solid concentration $\phi_{max} = 0.7$ associated with sediments at rest (Supporting Information), and exhibits a strong vertical rheological stratification. Surface particles are mainly driven by boundary shear stress (i.e. flowing water) and grain collisions, whereas deeper particles constitute a thick sediment flow and are mainly driven by frictional and enduring contact (see movie S3.1 and S3.2). These dynamics appear similar to that observed for sheetflows on steep slopes (Palucis et al., 2018) and for highly concentrated sediment flows (Armanini et al., 2005; Manville and White, 2003; Y. K. Sohn, 1997), where a flux of particles driven by shear stress overlays a denser sediment flow that moves *en masse*. A strong increase in fines content occurs during phase II (Figure 3.2i and m), and stands out significantly in the video recordings as clear water becomes brownish and "muddy" when the maximum fines content passes under the cameras (Figure 3.2b, and movie S3.1 and S3.2). These fines further enhance vertical heterogeneities in grain sizes due to sorting processes (Frey and Church, 2009), for which coarse particles are pushed towards the surface carried by a finer matrix (Figure 3.2b, and movie S3.1 and S3.2), drastically modifying the mean downstream surface particle velocity (Figure 3.2e). When the fines content is low ($C_{D<2\,mm}^{Phase\ II} < 10\,\%$), we estimate a mean downstream surface particle velocity of $u_x \approx 0.17$ m/s, whereas when the content is higher ($C_{D<2\,mm}^{Phase\ II} > 35\,\%$) we have $u_x \approx 0.39$ m/s, to be compared with the average downstream velocity of the underlying thick sediment flow $U_x \approx 0.10$ m/s. We also observe that the maximum values of ϕ are always reached when the fines content is maximum (Figure 3.3a and e). Phase III moves back to low values of solid concentration and typical bedload dynamics similar to phase I (see movie S3.1 and S3.2) with a mean downstream particle velocity $u_x \approx 0.30$ m/s.

3.5.2 Force fluctuations and seismic observations

The passage of the highly concentrated sediment flow (phase II, showed between vertical black dashed lines in Figure 3.2) is reflected by the sharp increase in mean basal force (Figure 3.2g and k). As observed previously by Piantini et al. (2021), phase II is associated with a strong decrease in seismic power compared to phase I and III (Figure 3.2f, h, j, and l). Here we confirm that such decrease in power also occurs in the force measurements, and we are able to precisely analyze its links with local changes in flow dynamics thanks to the local nature of our measurements (Figure 3.2g and k). The reduction of seismic and force power in fact occurs through two consecutive steps. A first decrease of about 5 dB occurs in the initial stages of phase II under a negligible amount of fines (Figure 3.2c, i and m), and a second and larger decrease of about 10 dB occurs when the maximum fines content passes through the sections closest to the respective seismic and force sensors (see red squares in Figure 3.2f, g, and h, Figure 3.2j, k, and l, and Figure 3.3a and e). We pick the times with maximum fines content using the cameras and confirm this observation by means of the sampling measurements made at the outlet, since the time delay between maximum sampled fines content and lowest levels of force power corresponds to the travel time of sediments from the force sensor to the outlet (using the estimated downstream velocity U_x).

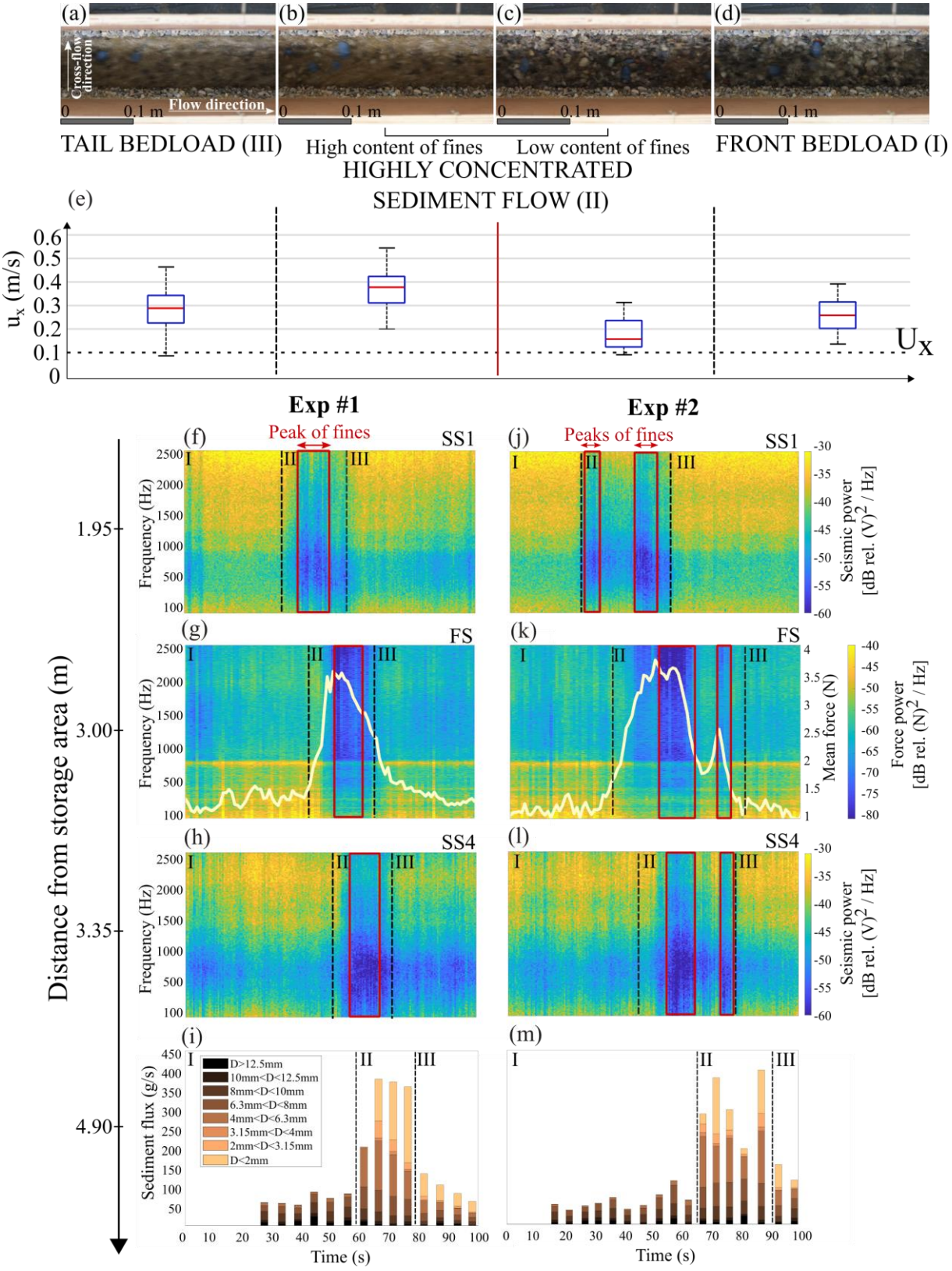

Figure 3.2 : General observations. (a to d) Photos from the upstream camera located close to SS1 showing the three different phases of a pulse. (e) Downstream particle velocity associated with each phase of a pulse. The red line in the middle represents the median, the bottom and top of each box the 25th and 75th percentiles, and the whiskers the minimum and maximum measurements. The macroscopic downstream velocity of the sediment flow U_x is shown with the horizontal dotted line. (f and h) and (j and l) Seismic power measured upstream and downstream, respectively, and (g and k) force power. The mean basal force is also

shown with the white curve in (g and k). The red squares delimit the time intervals exhibiting the maximum content of fines in phase II. (i and m) Outlet measurements of sediment flux and associated particle diameters (see legend). The vertical black dashed lines delimit the different phases.

3.5.3 Links between force power and bulk flow properties

In Figure 3.3 we evaluate the flow surface elevation (h), mean basal force ($\bar{F}$), and solid concentration (Φ) of phase II as a function of the measured force power. The first seconds of the highly concentrated sediment flows are characterized by weak positive relationships between force power and h, $\bar{F}$, and Φ (Figure 3.3b, c, d, f, g and h). However, past an inflexion point, the relationship between force power and flow properties becomes negative. In this range, we observe large counter-clockwise hysteresis in the relationships between force power and h and $\bar{F}$, that is, the same values of mean force and flow surface elevation are associated with significantly different force power (5 up to 10 dB differences) (Figure 3.3b, c, f and g). We observe sudden changes in the relationship between force power and h and $\bar{F}$ also at shorter time scales, materialized by the small loop around $t = 35$ s in Exp #2 (Figure 3.3f and g). These complexities arise when the fines content is maximum (Figure 3.3).

Interestingly, the hysteresis and loops described above are no longer significant when force power is evaluated versus Φ, in which case maximum Φ always corresponds to minimum force power (Figure 3.3d and h). Although a small clockwise hysteresis may be distinguished at high values of Φ for the present examples, we do not consider it as noteworthy because it is not systematically observed for other sediment flows (Supporting Information).

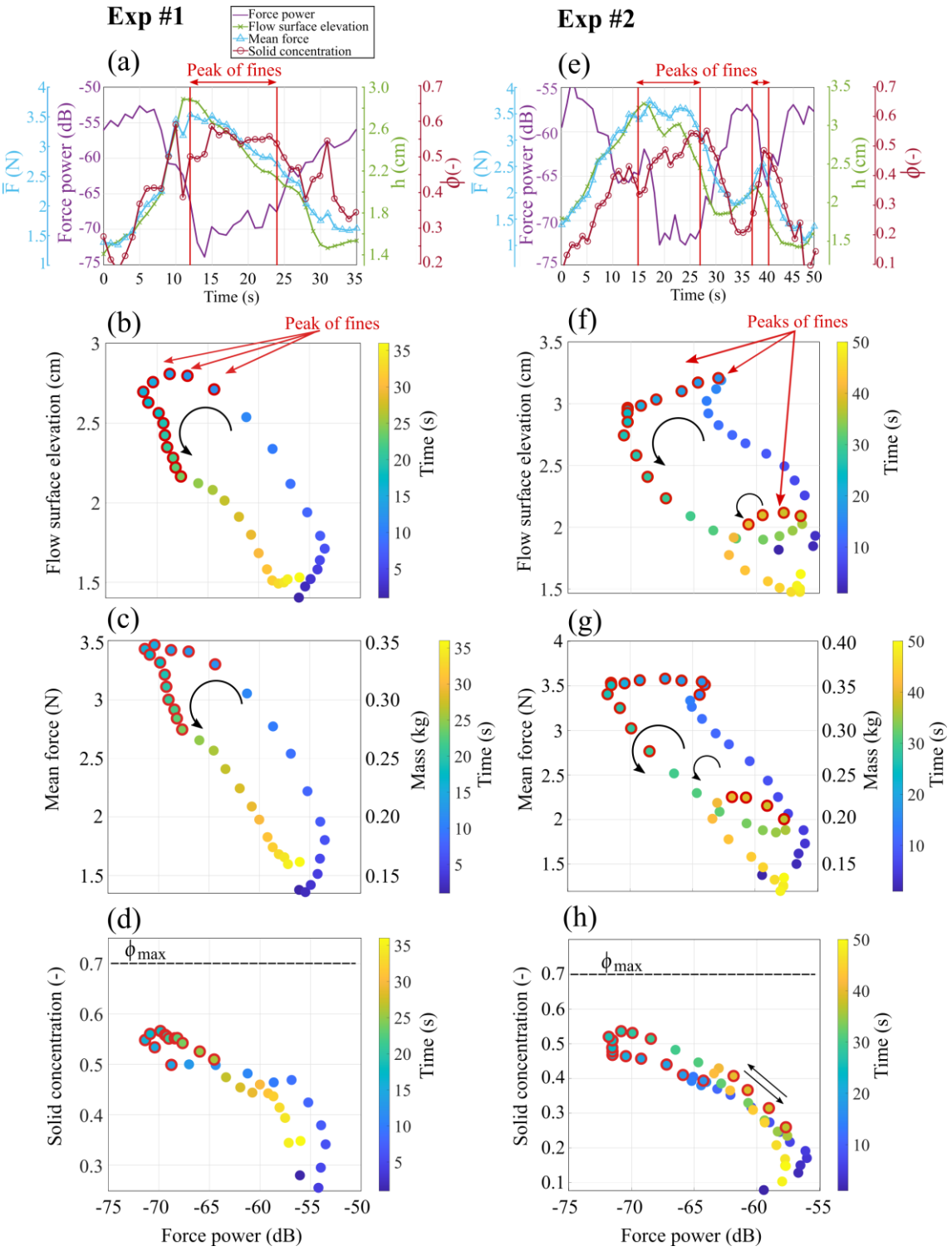

Figure 3.3 : Flow properties and force power of phase II. (a and e) Force power, h, $\bar{F}$, and Φ as a function of time. (b to d) and (f to h) Force power versus flow properties. Panels (c) and (g) also show the flow mass M in a secondary axis, computed through dividing the $\bar{F}$ by the acceleration due to gravity g. In panels (d) and (h) ϕ_{max} is shown with the horizontal dashed line. Time intervals with maximum fines content are marked in panels (a) and (e) with red vertical lines, and in the scatterplots with red circles. Hysteresis behaviors are highlighted with black curved arrows, while the vanishing of the small loop is highlighted in panel (h) with straight back and forth arrows.

3.6 Discussion and conclusions

3.6.1 Existing theories unlikely to explain our observations on phase II

In most current theories (Farin et al., 2019; Lai et al., 2018; Zhang et al., 2021b), force fluctuations are considered to be generated by impacts that are bed roughness-controlled, that is, particles impact the bed as they encounter bed roughness elements during their advection. Under this hypothesis, force fluctuations depend on the rate and amplitude of impacts that are mainly set by the average downstream velocity and size of particles, and by their number, which is considered proportional to solid concentration. Changes in these variables can be invoked to explain the 3 dB force power decrease between phase I and phase III (Supporting Information). However, the abrupt force power decrease by up to about 15 dB during phase II occurs under similar coarse grain fractions ($C_{D>8\,mm}^{Phase\ II} = 8\% \pm 2$ for Exp #1 and $C_{D>8\,mm}^{Phase\ II} = 14\% \pm 2$ for Exp #2), and similar average velocities, otherwise spatial disconnections within phase II would be expected, which is not observed. Furthermore, we observe a strong increase in solid concentration rather than a decrease as current theories would require to explain the reduction of force power.

One could hypothesize that the decrease in force power is due to the damping effect of a sediment layer forming at the base of the thick sediment flow, as observed in the presence of static sediment deposit (Kean et al., 2015; McCoy et al., 2013). However, we do not expect this process could primarily explain our observations as by means of a supplementary experiment we observe that a static sediment layer of almost half the total flow surface elevation covering the force plate (worst-case scenario) dampens the force power generated by a particle impact by only 6 dB, which is much smaller than the 15 dB observed in the experiments (Supporting Information). The observation that the minimum of force power always corresponds to the maximum fines content might indicate that fines control the reduction of force fluctuations, through carrying big particles in suspension, and thus reducing their impacts to the bed (Piantini et al., 2021) or avoiding their contribution in force chains generation (Zhang et al., 2021b). However, since force power significantly decreases even before the fines content becomes relevant, we believe such mechanism potentially occurs at a secondary level.

3.6.2 Solid concentration helps decipher the amplitude of force fluctuations

The key observation yielding further insight into the underlying source of reduced force fluctuations during phase II is the unique negative relationship and suppressed hysteresis and loops behaviors between force power and solid concentration (Figure 3.3d and h). We advance that solid concentration best describes force fluctuations amplitude as being a proxy for particle agitation. The link between solid concentration and particle agitation can be interpreted within the framework of the local $\mu(I)$ rheology of dense granular flows, for which solid concentration is a decreasing function of the dimensionless inertial number I (da Cruz et al., 2005; Forterre and Pouliquen, 2008; GDR Midi, 2004). This number compares the microscopic time scale of particles rearrangement due to confining pressure P and the macroscopic time scale linked to deformation due to shear rate $\dot{\gamma}$. Under the hypothesis of steady uniform state, and when the fluid has a negligible influence on the rheology, two-phase flows are controlled by the dry inertial number

(Cassar et al., 2005; Courrech du Pont et al., 2003; Maurin et al., 2016) expressed as $I_{dry} = \frac{\dot{\gamma} D}{\sqrt{P/\rho_s}}$, where D is the particle diameter. In order to position our experiments within the literature of granular flows, we estimate an average dry inertial number for phase II (the calculation of I is discussed in Supporting Information). We obtain $I_{dry} \sim 10^{-1}$, which is in the range of dense granular flows (da Cruz et al., 2005). In this range, a granular flow characterized by a higher I tends to dilate (i.e. relatively low solid concentration) as particles are agitated and inter-particle collisions are more likely to occur, while at a lower I particles are packed (i.e. relatively high solid concentration) and mainly interact with each other through long-lasting contacts. Our experimental setup does not allow us to estimate variations of I in time, but we suggest that solid concentration changes could reflect them. This would be consistent with the recent findings of a positive relationship between the amplitude of acoustic emissions and force fluctuations and the inertial number of dry granular flows (Arran et al., 2021; Bachelet et al., 2021)[3]. Macaulay & Rognon (2020) have shown that contact force fluctuations associated with micro-accelerations of the particles within a granular flow increase as the inertial number increase. Since these forces are expected to propagate towards the bed (Bachelet et al., 2021), we suggest that their study supports our hypothesis.

The central role played by solid concentration is further emphasized when comparing our findings with past studies. Allstadt et al. (2020) reported a negative relationship between bulk density and force fluctuations, as presented here, despite observing a positive relationship between flow surface elevation and mass and force fluctuations, which is opposed to our results. Similarly, Zhang et al. (2021b) observed a positive relationship between flow surface elevation and mass and force fluctuations, with the two flow properties being negatively correlated with bulk density. This reinforces our interpretation that solid concentration is the parameter controlling force fluctuations, and leads us to suggest that a positive relationship between flow surface elevation and/or mass and force fluctuations holds only when the former are negatively related with solid concentration. This is likely often the case for natural debris flows (Allstadt et al., 2020; Iverson, 1997), but the extent to which it applies to other sediment flows, such as sheetflows or highly concentrated sediment flows, remains to be investigated further. In this sense, we suggest that the $\mu(I)$ rheology may be an appropriate framework to unravel the links between different flow properties for a wide range of dense granular flows with various interstitial fluids (sheetflows, (Revil-Baudard and Chauchat, 2013); intense bedload, (Maurin et al., 206); debris flows, (Berzi and Jenkins, 2008)).

3.6.3 Implications for theoretical models

In existing theoretical models, in which force fluctuations are considered to be generated by roughness-controlled impacts, solid concentration is only weakly and positively related to the amplitude of force fluctuations, through its control on the number of particles impacting the bed or on the size of force chains (Farin et al., 2019; Zhang et al., 2021b). This approach likely holds for phase I, III and the first seconds of phase II. However, we advance that during phase II force fluctuations on the bed switch from being mainly generated by roughness-controlled impacts to

[3] During the defense, the examiner Anne Mangeney correctly pointed out that in the positive relationship found by Arran et al. (2021), the fluctuating forces are normalized by the mean basal force.

being mainly generated by agitation-controlled impacts as sediment flows become denser and reach solid concentrations above about half ϕ_{max}. A similar inflection point in the relationship between bulk density and force fluctuations was also observed by Allstadt et al. (2020) after the passage of the debris flow fronts. In the case of agitation-controlled impacts, the dependency of the amplitude of force fluctuations on solid concentration is negative and likely much stronger. In our experiments we show that relatively small variations of solid concentration ($\Delta\phi = 0.4 - 0.6$) are sufficient to modulate force power by nearly one to two orders of magnitude, which challenges the consideration that the expected range of variation of solid concentration ($\Delta\phi = 0.4 - 0.8$ for debris flows, following Iverson (1997)) is small enough for solid concentration to be approximated as constant (Farin et al., 2019; Zhang et al., 2021b). We therefore propose that theoretical models should incorporate a transition from roughness-controlled impacts to agitation-controlled impacts, where in the agitation-controlled regime the flow satisfies the $\mu(I)$ rheology and in particular the inverse relationship between the inertial number I and the solid concentration.

Acknowledgments

The authors declare no conflict of interest. This research has been supported by the Agence Nationale de la Recherche (grant no. 17-CE01-0008). We acknowledge the support of the INRAE Research Centre of Grenoble for the laboratory and instrumental equipment. We thank Jeroni Salens for helping in the installation of the force sensors, and Zavier Berti for the scientific discussions. We thank the associate editor Victor Tsai, Fabian Walter and anonymous reviewer for the fruitful comments on the manuscript.

Open Research

The data analyzed during the current study are available on the Zenodo platform via 10.5281/zenodo.7402495

3.7 Supporting Information

Introduction

In text S3.1 we give detailed information about the installation of the piezoelectric sensors and the installation and calibration of the force plate and sensor. In text S3.2 we provide specific information on how we estimate the bulk density, the sediment density, the maximum packing fraction and the downstream particle and sediment flow velocity. In text S3.3 we conduct impact experiments to investigate (i) the relative contribution to seismic vibrations of impacts on the sidewalls compared to impacts on the bed, (ii) the attenuation of the seismic waves generated by particle impacts to the bed with distance, and (iii) the dampening of impact force power due to the presence a static sediment layer. In text S3.4 we show results similar to in the main text but for additional sediment pulses not presented therein. In text S3.5 we discuss in which ways existing theories may explain differences in force power between phase I and III. Finally, in text S3.6 we explain how we calculate the inertial number I.

S3.1 Installation of the piezoelectric sensors and force plate and sensor

The piezoelectric sensors are mounted on the outside of one of the sidewalls of the channel, using mounting brackets and double-sided adhesive tape (Figure 3.4). The force plate and force sensor are installed to maximize its isolation from external flume vibrations. The force plate is supported by the force sensor (Figure 3.4a), which in turn rests on a steel support piece that is mechanically connected to the channel substructure (Figure 3.4a and b). The stiffness of the support piece is high in order to ensure that impacts on the force plate are efficiently transmitted to the force sensor. Shock absorbers are placed between the flume and the substructure to avoid the transmission of vibration to the force sensor from the substructure (Figure 3.4c). The force plate and the rest of the flume bed are connected by 5 mm-long seals (Figure 3.4d). To ensure continuity with the channel bed roughness, we cover with silicone and sediments the seals and the force plate like the rest of the channel bed (Figure 3.4e). The force sensor have been fitted under a preload of 25 kHz to ensure measurements stability and linearity between the applied load and the sensor output. This preload also allows avoiding changes in the response of the sensor as sediment deposits potentially accumulate on the force plate.

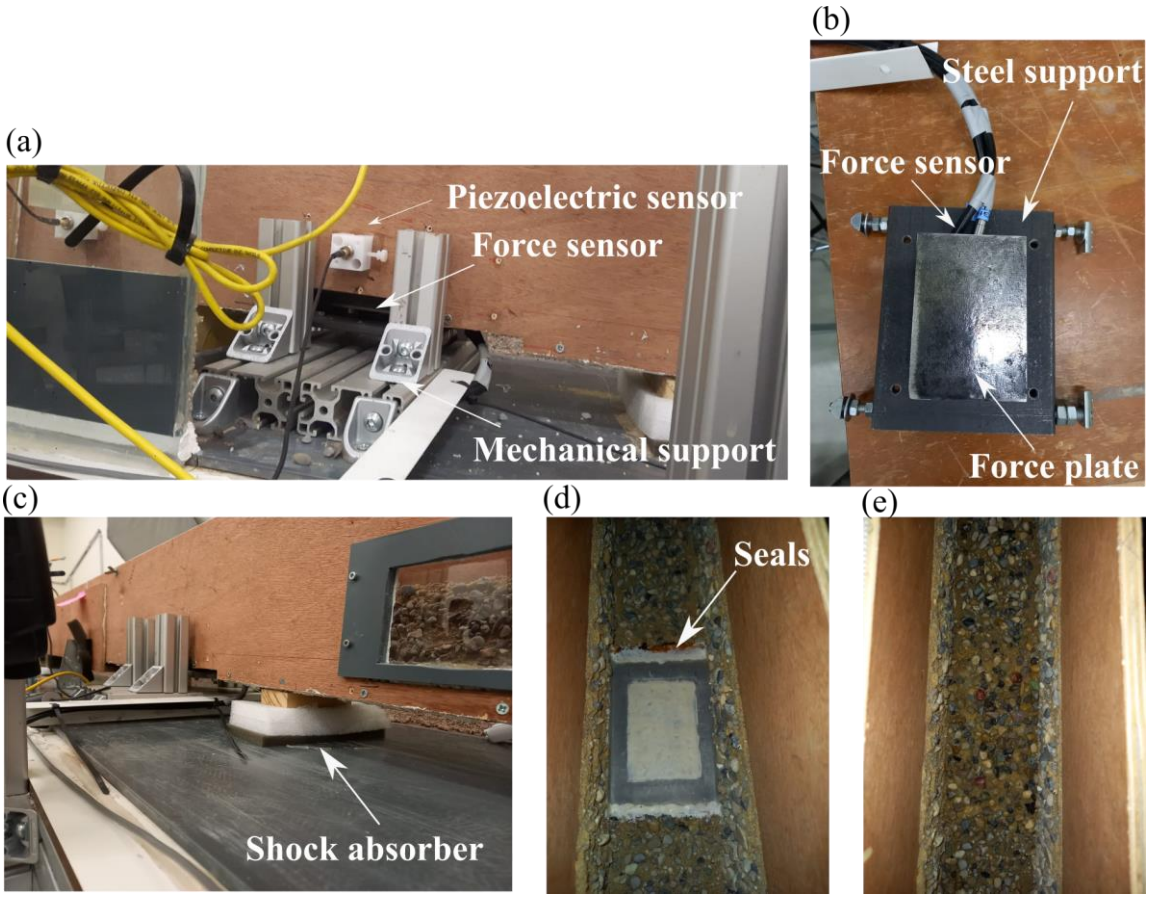

Figure 3.4 : Photos of the experimental setup and instruments. (a) Side view of the piezoelectric sensor mounted on the flume sidewall. Below are the different parts installed for the force measurements, i.e. the force sensor and its support. (b) Photo of the force sensor, force plate, and steel support before installation. (c) Side view of the flume with shock absorbers between the channel bed and substructure. (d) Top view

over the force plate. Lateral seals are visible. (e) Top view over the force plate after adding silicone and sediments.

S3.2 Estimations of bulk density, sediment density, maximum packing fraction, and particle and sediment flow velocity

Following equation 7 in the main text, in order to estimate the in-stream solid concentration, we need to estimate the bulk density $\rho(t)$ and the density of the sediment mixture ρ_s. We estimate the bulk density of the sediment flows following Iverson et al. (2010):

$$\rho(t) \approx \frac{\sigma_{bed}(t)}{gh(t)cos\theta} \tag{8}$$

where σ_{bed} is the mean basal normal stress, i.e. the mean basal normal force divided by the area of the force plate, g is acceleration due to gravity, $h(t)$ is the flow surface elevation, and θ is the channel slope. We assume that the mean basal normal stress balances the slope-normal static weight of the flow, which is totally supported by the force plate.

We estimate the sediment density ρ_s by means of a supplementary experiment in which we fill a cylinder of known volume V_{tot} with a mass M_s of sediments characterized by the grain size distribution of phase II (high content of fines). Then, we saturate the mass with water and we measure the volume of water V_w needed to fill all the voids between the grains. The sediment density is finally computed as $\rho_s = \frac{M_s}{(V_{tot}-V_w)}$.

This experiment also allows us to estimate the maximum packing fraction ϕ_{max} of the sediment mixture, computed as $\phi_{max} = \frac{(V_{tot}-V_w)}{V_{tot}}$.

We estimate the macroscopic velocity of the highly concentrated sediment flow (U_x) in three different ways: (i) by tracking the flow through the cameras installed along the channel; (ii) by evaluating time delays in the surface flow elevation measurements; (iii) by evaluating time delays in the seismic measurements. If one of the three estimations differ from the others by $\pm 50\%$, we consider it inaccurate and we compute the average of the remaining ones. We also estimate the local downstream velocity of surface particles (u_x) by manually tracking their displacement between consecutive frames taken by the upstream camera. We consider the biggest particles of the sediment mixture for practical reasons, as they are coloured in blue and therefore easy to identify, and because they play a major role in generating seismic vibrations through highly energetic impacts (Tsai et al., 2012).

S3.3 Impact experiments

We carry out supplementary experiments to investigate (i) the relative contribution to seismic vibrations of impacts on the sidewalls compared to impacts on the bed, (ii) the attenuation of the seismic waves generated by particle impacts to the bed with distance, and (iii) the dampening of impact force power due to the presence a static sediment layer. We evaluate the relative contribution of impacts on the sidewalls by using a hand-made pendulum that allows for the same force impact on the sidewall than that associated with the drop of a pebble of known mass ($m =$ 6.6 g) from a fixed height ($z = 5$ cm) to the bed. We produce three identical impacts at the same section and then we compute the power spectral density with the Welch's method (Welch, 1967). In Figure 3.5 we show the seismic power computed for the SS1 sensor by averaging over the three impacts. We observe that impacts on the sidewall dominate over impacts on the bed in the whole frequency range, but their contribution is relatively small in the frequency range of interest ($100 - 2500$ Hz).

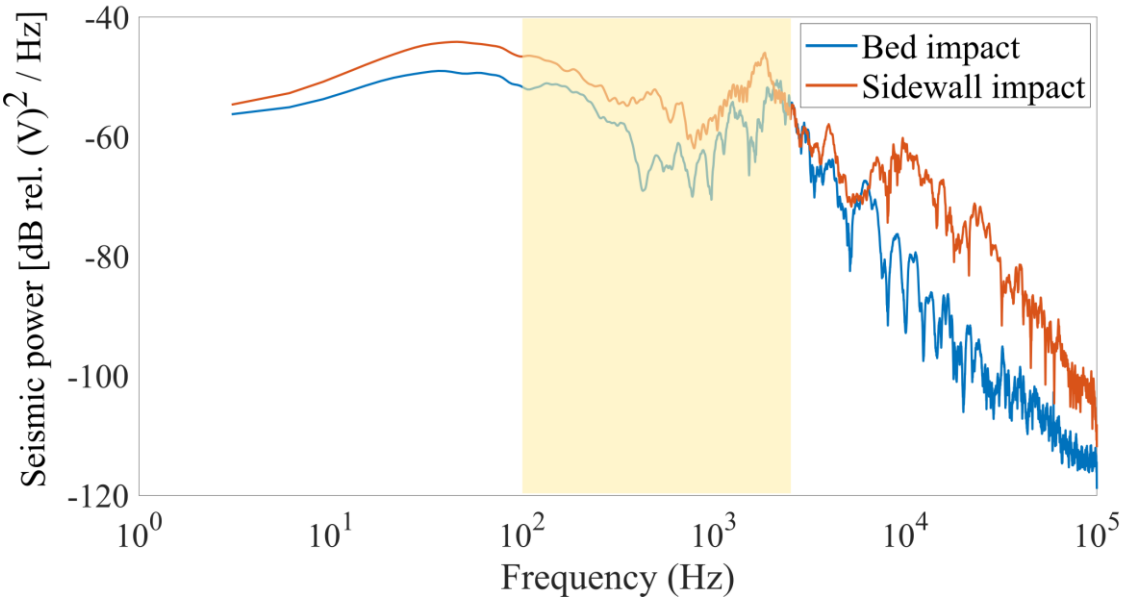

Figure 3.5 : Seismic power as a function of frequency for the impact to the bed (blue curve) and to the sidewall (orange curve). The highlighted area shows the frequency range of interest ($\Delta f = 100 - 2500$ Hz).

To investigate the attenuation of seismic waves with propagation distance along the channel we drop the pebble from the same fixed height in seven sections along the channel. We produce three identical impacts in each section and then we compute the power spectral density. In Figure 3.6 we show the average seismic power over the three impacts in the frequency range of interest ($\Delta f = 100 - 2500$ Hz) for all the seismic sensors and at the different sections. For most sensors, the peak seismic power occurs when the impact is located closest to the sensor (distance 0 m in the panels), and for most sensors the highest levels of seismic power are located within about 1 m around the sensor. The SS3 sensor exhibits a counter-intuitive behavior, as the impact occurring in the closest section is associated with the lowest seismic power (Figure 3.6b). We suggest this is due to the discontinuity between the force plate and the sidewall where the sensor SS3 is installed

interrupting the propagation of seismic waves. We can conclude that in the selected frequency range, seismic waves are strongly attenuated with distance, which ensures a local measure of seismic vibrations.

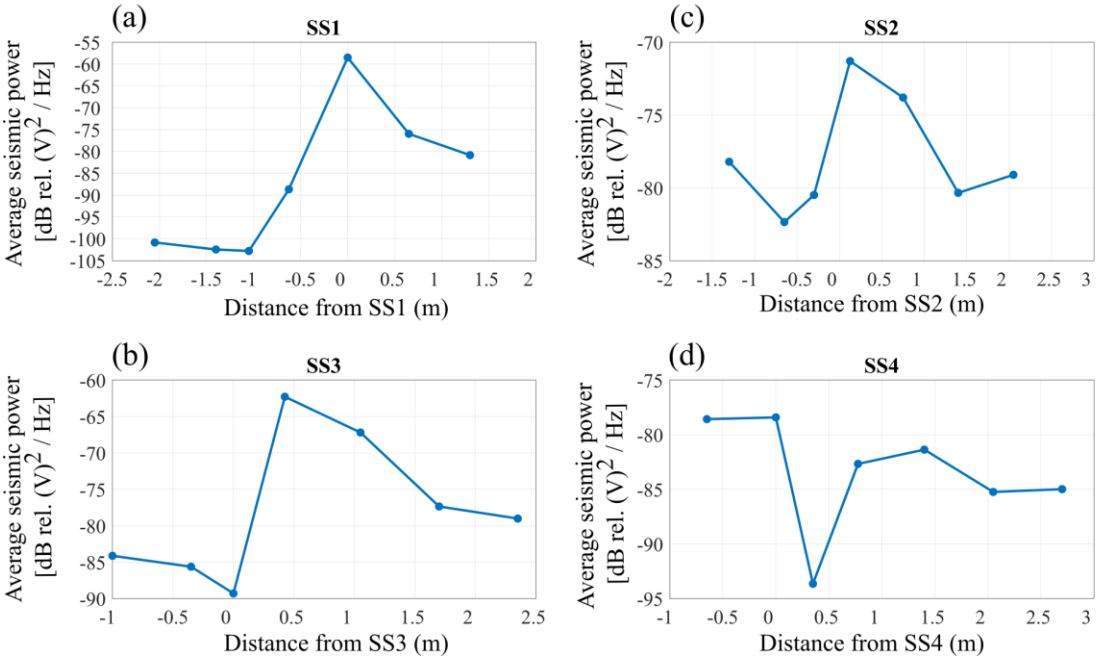

Figure 3.6 : Attenuation of seismic waves with distance for each seismic sensor. (a to d) The average seismic power is plotted as a function of the distance between the particle impact and the seismic sensor. A distance of zero corresponds to the section closest to the seismic sensor. Negative distances correspond to sections which are downstream of the seismic sensor.

In the main text we show that phase II is characterized by a strong decrease in force power compared to phase I and II. We test the hypothesis of the damping effect of a sediment layer potentially forming at the base of the thick sediment flow. We carry out a specific experiment in which we compare the force power associated with the impact of a pebble dropped from the fixed height ($z = 5$ cm) (i) on the rough bed and (ii) on a sediment layer covering the force plate. We investigate two different grain size distributions of the sediment layer with reference to phase II by varying the amount of fines ($C_{D<2\,mm}^{Phase\ II} < 10$ % and $C_{D<2\,mm}^{Phase\ II} > 35$ %). For each grain size distribution we test two different layer thicknesses (1 and 2 cm), we produce three identical impacts for each configuration (rough bed or sediment layer). In Figure 3.7 we show the average force power associated with particle impacts for each configuration and for the frequency range of interest ($\Delta f = 100 - 2500$ Hz). We observe that, regardless of the grain size distribution, the presence of a sediment layer dampens the force power associated with the particle impact with an average decrease of 6 dB, which is much smaller than the decrease of 15 dB observed during phase II in our experiments. Therefore, we do not find this process primarily explains the decrease in force power detected during the passage of phase II.

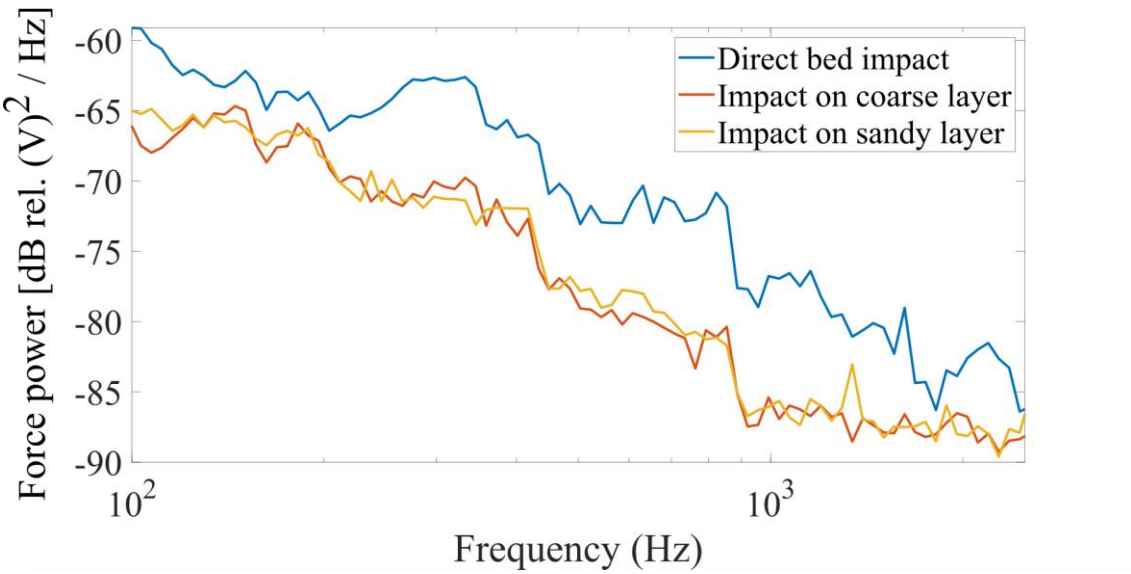

Figure 3.7 : Force power as a function of frequency for particle impacts in the three different configurations. For each grain size distribution of the sediment layer, the resulting spectrum is the average over the two layer thicknesses (1 and 2 cm).

S3.4 Additional sediment pulses

Two additional sediment pulses (Exp #3 and Exp #4) are shown in Figure 3.8 and 3.9. Similar to Exp #1 and Exp #2, phase I and phase III are characterized by the highest level of seismic and force power, while the passage of phase II is associated with a strong drop of these two quantities (Figure 3.8). The lowest levels of seismic and force power occur when the maximum fines content passes through the sections closest to the respective seismic and force sensors, as observed in the main text. Also the links between the flow properties and force power are consistent to those presented in the main text (Figure 3.9), with large counter-clockwise hysteresis in the relationships between force power and h and F (Figure 3.9b, c, f, and g), which are no longer significant when force power is evaluated versus Φ. Concerning the value of solid concentration of Exp #3, we observe that it attains the maximum packing fraction (Figure 3.9a). In Exp #4, the relationships between force power and Φ strongly flatten at high values of Φ (Figure 3.9h). It may indicate that in this experiment secondary mechanisms play a role in reducing force fluctuations regardless of Φ. As stated in the main text, this could be the effect of fines carrying in suspension big particles or affecting force chains (Piantini et al., 2021; Zhang et al., 2021).

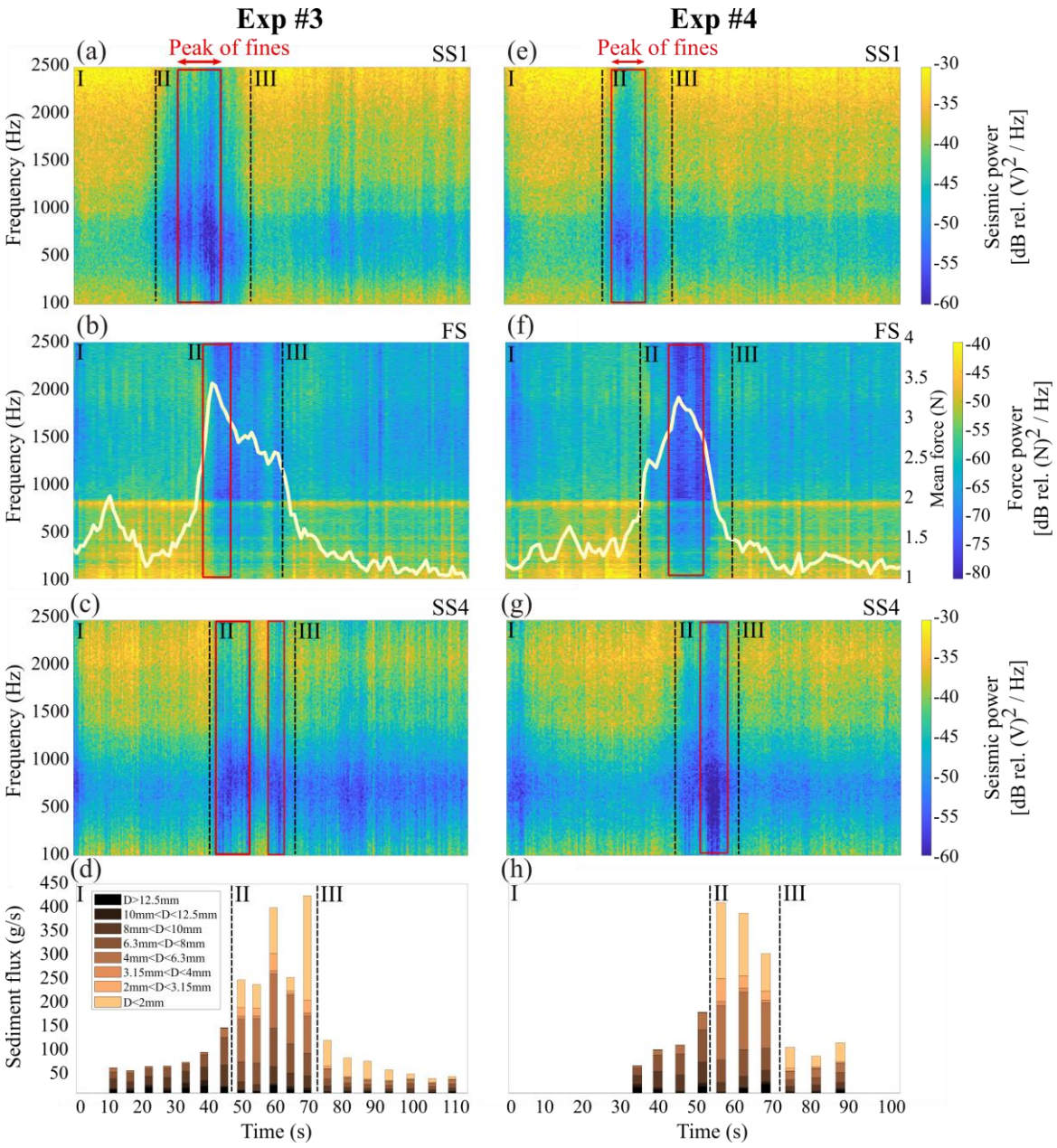

Figure 3.8 : Same figure as in the main text, but for additional sediment pulses. (a and c) and (e and g) Seismic power measured upstream and downstream, respectively, and (b and f) force power. The mean basal force is also shown with the white curve in (b and f). The red squares delimit the time intervals exhibiting the maximum content of fines in phase II. (d and h) Outlet measurements of sediment flux and associated particle diameters (see legend). The vertical black dashed lines delimit the different phases.

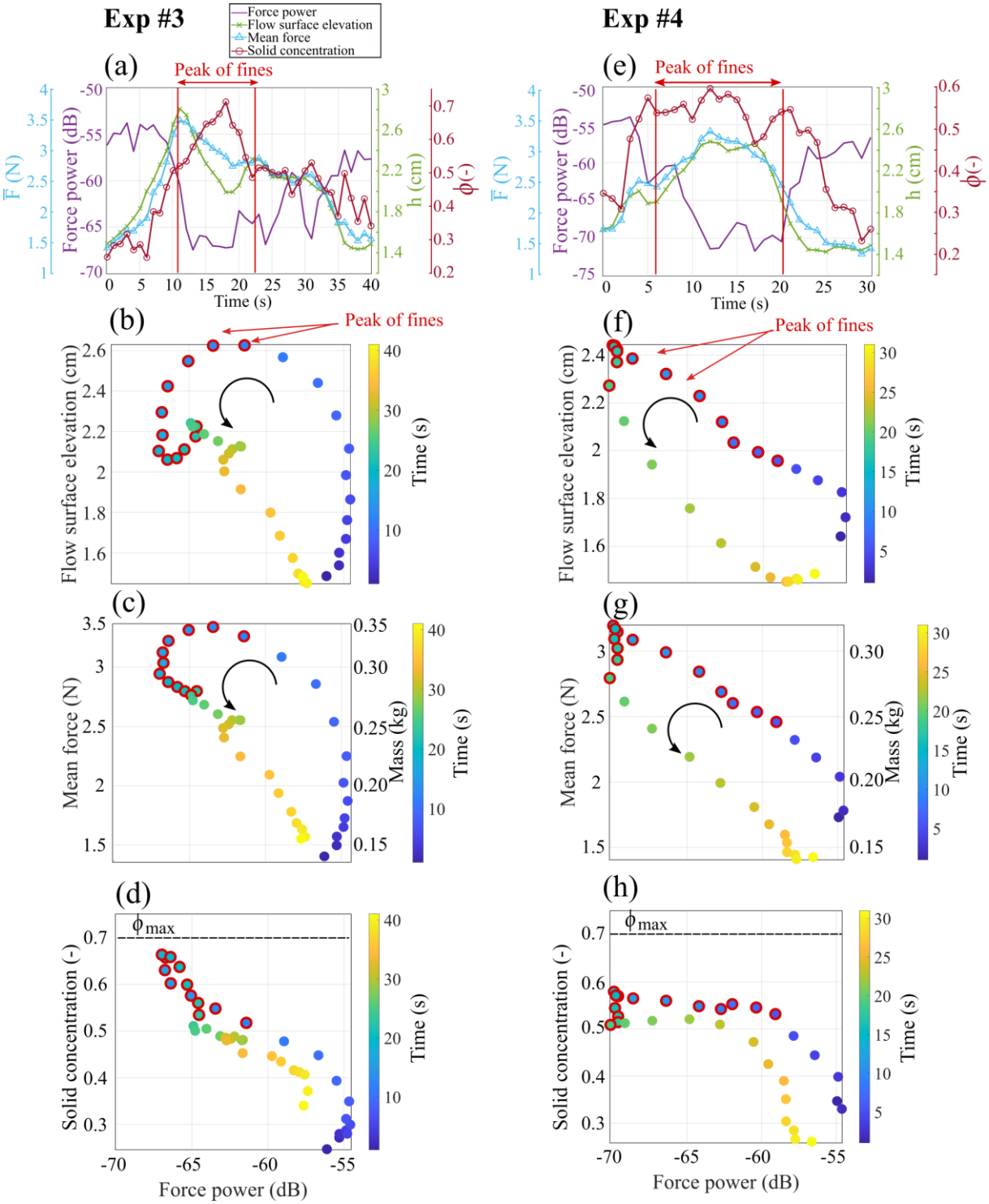

Figure 3.9 : Same figure as in the main text, but for additional sediment pulses. All panels refer to phase II. (a and e) Force power, h, $\bar{F}$, and Φ as a function of time. (b to d) and (f to h) Force power versus flow properties. Panels (c) and (g) also show the flow mass M in a secondary axis, computed through dividing the mean basal force by g. In panels (d) and (h) ϕ_{max} is shown with the horizontal dashed line. Time intervals with maximum fine content are marked in panels (a) and (e) with red vertical lines, and in the scatterplots with red circles. Hysteresis behaviors are highlighted with black curved arrows.

S3.5 Existing theory potentially explains differences in force power between phase I and phase III

We find that phase I is characterized by a slightly higher level of force power (+3 dB) than that of phase III. Here we investigate whether this difference may be explained by current theories (Farin et al., 2019; Lai et al., 2018; Zhang et al., 2021b) in which force fluctuations are considered to be generated by impacts that are bed-roughness controlled, that is, particles impact the bed as they encounter bed roughness elements. Under this consideration, force fluctuations depend on the rate and amplitude of impacts that are mainly set by the average downstream velocity and size of particles, and by their number, which is considered proportional to solid concentration. Following the model of Farin et al. (2019) for thin sediment flows ($D \sim h$), the seismic power P due to force fluctuations can be written as:

$$P = \frac{n}{t_i} I^2 \tag{9}$$

where $\frac{n}{t_i}$ is the total rate of impacts, in which n is the number of impacting particles and $\frac{1}{t_i}$ is the particle impact rate, and $I = mu_N$ is the basal impulse exerted on the bed by a particle of mass m impacting the bed with a bed-normal velocity u_N. The number of particles per meter square of the bed can be written as $\frac{\phi p(D)}{D^2}$, where $p(D)$ is the grain size distribution. Under the assumption that particle impacts are caused by velocity fluctuations controlled by the bed roughness, with these fluctuations being proportional to the average downstream velocity of the particles u_x, and the characteristic bed roughness length being similar to the particle diameter D, then the total rate of impacts can be written as $\frac{\bar{u}_x}{D^3} \phi p(D)$. Farin et al. (2019) further assume that $u_N \sim \bar{u}_x$. Approximating the particle mass with D^3, the seismic power of phase I and phase III can be finally written as:

$$P = {\bar{u}_x}^3 D^3 \phi p(D) \tag{10}$$

By using the flow properties presented in the main text, and assuming an average solid concentration $\phi = 0.2$ for both phase I and phase III of Exp #1 and Exp #3, we get a difference in seismic power $\Delta P^{Phase\ I - Phase\ III} = 2$ dB, which is close to the 3 dB observed. We conclude that existing theories may be able to explain the observations regarding phase I and phase III.

S3.6 Calculation of the inertial number I of phase II

In order to interpret our experiments in the context of granular flows rheology, we attempt at estimating an inertial number describing the dynamics of phase II. When dealing with two-phase

granular flows, three different regimes can be defined depending on the influence of the interstitial fluid on particle rearrangement (Cassar et al., 2005; Courrech du Pont et al., 2003). This distinction is based on the definition of two dimensionless numbers:

$$St = \frac{D\sqrt{\rho_s P}}{\eta_f} \tag{11}$$

$$r = \sqrt{\frac{\rho_s}{\rho_f C_D}} \tag{12}$$

where d is the particle diameter, η_f is the fluid viscosity, ρ_f is the fluid density, and C_D is the drag coefficient. If $St \gg 1$ and $r \gg 1$, the interstitial fluid has negligible influence on the rheology and the granular flow is described by the dry inertial number $I_{dry} = \frac{\dot{\gamma} D}{\sqrt{P/\rho_s}}$ (free-fall regime). If $St \ll 1$ and $r \gg St$, the viscous drag controls particle rearrangement and the granular flow is described by the viscous inertial number $I_{viscous} = \frac{\dot{\gamma}\eta_f}{P}$ (viscous regime). If $St \gg r$ and $r \ll 1$, the turbulent drag controls particle rearrangement and the granular flow is described by the turbulent inertial number $I_{turb} = \frac{\dot{\gamma} D}{\sqrt{P/\rho_f C_D}}$ (turbulent regime). In our experiments, we choose $D = D_{50}$ to characterize the grain size distribution of phase II. The interstitial fluid is water, then $\eta_f = 8.9 \times 10^{-4}$ Pa·s for water at 25°C and $\rho_f = 1000$ kg/m^3. Under the assumption that excess pore pressure is negligible, the granular pressure can be written as $P = (\rho_s - \rho_w)\phi g h cos\theta$ (Cassar et al., 2005). We estimate the drag coefficient as $C_D = (0.4 + \frac{24.4}{Re_P})(1-\phi)^{-3.1}$, following Chassagne et al.(2020), where Re_P is the particle Reynolds number (Piantini et al., 2021). Similarly to Maurin et al. (2016) who investigated bedload transport, we estimate $St \gg 1$ and $r \sim 1$, so that the phase II of our experiments can be considered at the boundary between the free-fall and turbulent regime. In this case, the dry inertial number can be considered as a good descriptor of the system (Maurin et al., 2016). By further assuming a Bagnold-like velocity profile we can compute the shear rate as $\dot{\gamma} = \frac{5U_x}{2h}$, and the dry inertial number becomes $I_{dry} = \frac{5U_x D_{50}}{2h\sqrt{\frac{(\rho_s-\rho_w)\phi g h cos\theta}{\rho_s}}}$. As stated in the main text, we find $I_{dry} \sim 10^{-1}$.

We acknowledge that these computations are based on strong assumptions that may not entirely hold in our experiments. At a first level, we do not know if in our experiments the rheology of phase II can be considered as local, and the unsteady flow conditions complicate the computations of an inertial number. Second, the computation itself contains several assumptions. We do not measure pore pressures, therefore the definition of granular pressure may be incomplete, and we assume a Bagnold-like velocity profile but we cannot verify the accuracy of this hypothesis. Despite these uncertainties, we believe that the $\mu(I)$ rheology can provide a valid framework to interpret the dynamics of our sediment flows, and that these assumptions allow us to estimate an indicative order of magnitude for the inertial number.

Additional Supporting Information (Files uploaded separately)[4]

Movie S3.1. Movie from the webcam installed above the force plate. It refers to Exp #2.

Movie S3.2. Movie from the camera installed close to the upstream piezoelectric sensor. It refers to Exp #2.

[4] To watch the videos please refer to the published article online

Chapter 4: The contribution of grain-to-grain interactions to the surging behavior of sediment pulses

4.1 Preface

When we designed the flume for the laboratory experiments, we decided to develop a flexible structure that would have allowed us to vary the slope of the channel. While the experiments carried out during this thesis have focussed on a single slope ($S = 18\%$), towards the end of the PhD a master thesis internship was set up with the aim to explore the seismic signature and mechanisms of the self-generated sediment pulses at very steep slope. The student Zavier Berti have spent 6 months in the laboratory of INRAE to carry out a novel set of experiments. His contribution is here acknowledged.

During the internship of Zavier, we interacted actively about the experimental protocol to follow and how to analyze the data, and we had fruitful discussions on the interpretation of the results by a physical and seismological point of view. In this chapter, I present the main findings of this new set of experiments which are in continuity with those of the previous chapters.

Préface

Lorsque nous avions conçu le canal pour les expériences, nous avions décidé de développer une structure flexible qui nous aurait permis de varier la pente du canal. Les expériences faites au cours de cette thèse se sont concentrées sur une seule pente ($S = 18\%$), mais vers la fin du doctorat un stage de master a été mis en place pour explorer la signature sismique et les mécanismes des bouffées sédimentaires à très forte pente. L'étudiant Zavier Berti a passé 6 mois au laboratoire de l'INRAE pour réaliser les expériences. Sa contribution est ici reconnue.

Pendant le stage de Zavier, nous avons interagi activement sur le protocole expérimental à suivre et la façon d'analyser les données, et nous avons eu des discussions fructueuses sur l'interprétation des résultats d'un point de vue physique et sismologique. Dans ce chapitre, je présente les principaux résultats de cette nouvelle série d'expériences qui sont en continuité avec ceux des chapitres précédents.

4.2 Methods

4.2.1 Experimental setup and measurements

We carry out laboratory experiments in the same flume used for the experiments presented in the previous chapter. However, compared to the original experimental setup here we increase the channel slope to 33%, and as the storage area is directly connected to the upstream part of the channel, its slope varies accordingly to 20%. We also modify the feeding system, whereby the input water and sediment fluxes are injected against a vertical plate before falling down on the storage area surface. In the original configuration the water and sediment fluxes were injected directly on the storage area through a pipe (Figure 2.3), but in this new setup it would have caused the fluxes to reach the channel without sediment accumulation.

We use the bimodal grain size distribution characterized by ~40% in weight of fine particles (0.5 mm < D < 2 mm) as in the previous experiments (Figure 2.4).We adapt the feeding conditions to the new experimental setup to respect similitude criteria with well-documented natural mountain rivers (Section 2.4.2). In addition to those considered in Section 2.4.2, we add the reach of the Riedbach stream which is characterized by a similar steep slope (38%) (Schneider et al., 2016), leading to an average geometric scaling parameter $\lambda = 54$. We prescribe a water discharge of 0.16 l/s and a sediment flux of 0.60 g/s. While recalling that the input sediment flux has not a direct impact on in-channel processes as being only functional to forming the upstream sediment deposit, the upscaled value of water discharge corresponds approximately to the maximum water flow due to glacial melt in the Riedbach stream (Schneider et al., 2016). However, the experiments are characterized by an in-channel transport stage ${\tau^*}/{\tau^*_{cr}}$ that is just above the threshold condition (${\tau^*}/{\tau^*_{cr}} = 1.25$), slightly higher compared to the experiments presented in the previous chapter.

With regard to the seismically relevant quantities, we focus our analysis on the force fluctuations measurements recorded by the force sensor (Figure 3.1). In addition to the normal forces, here we also explore the tangential forces. We analyze the force fluctuations following the routine presented in Section 3.4.2.

We use the video recordings to investigate the processes occurring in the storage area, and both the video recordings and flow surface elevation measurements (located in the same section of the force sensor) to investigate the in-channel processes.

In the following sections we present the results of three experiments that allowed us to investigate nine sediment pulses with their triggering, and propagation dynamics with their associated seismic signature.

4.3 Results

4.3.1 Dynamics of the storage area

The first phase of the processes occurring in the storage area is remarkably similar to those presented in Chapter II. In the first minutes of the run, the sediment pile starts developing with particles accumulating where they fall, with water both infiltrating the deposit and flowing over its surface. Thanks to the downward percolation of the fine particles, the surface of the deposit gets

coarsens (Figure 4.1a). Episodic local failures of the surface particles push the deposit on the sides and towards the connected channel, as evidenced by the emergence of the fine particles previously hidden in the subsurface (Figure 4.1b). The deposit grows in the vertical and horizontal direction, and a large part of the big grains reaches the inlet section of the channel (Figure 4.1c and d). At some point, a destabilisation occurs and the armour breaks (Figure 4.1e): the material slides forward from the top of the deposit, exposing a significant volume of fine particles to the flow, and then the coarse sediment layer on the surface starts sliding en masse and is transported towards the flume (Figure 4.1f). At this point, the dynamics of the storage area behaves differently compared to that observed in Chapter I. Instead of generating a sediment flux propagating in the downstream channel, the biggest particles accumulate at the front of the deposit, advancing slowly and momentarily blocking the mass behind (Figure 4.1f to h). However, as the erosion in the uspstream deposit escalates, a large amount of fine particles is released at high velocity. These particles destabilize the coarse "dam", and a widespread destabilization evacuates the material towards the downstream channel (Figure 4.1i). As observed in Chapter II, during a single run these processes repeat cyclically.

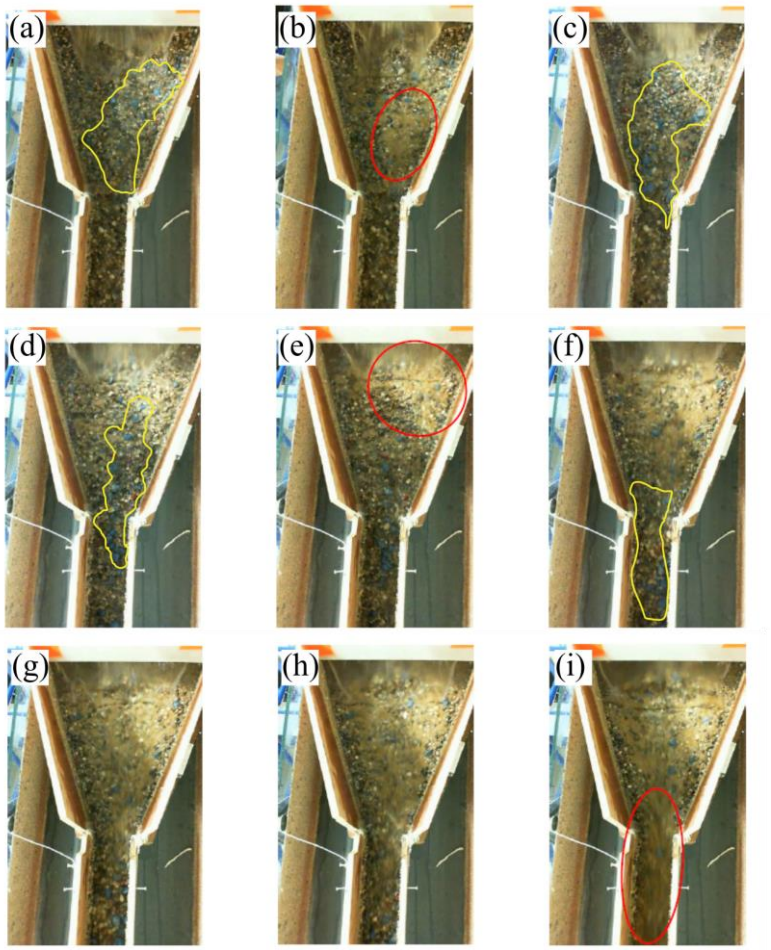

Figure 4.1 : The frames of the video recording above the upstream storage area show the processes occurring in the sediment deposit. Each panel represents a step of the cyclic behavior described in the text. In particular, the yellow-bordered portions of the deposit highlight the biggest particles of the sediment mixture and the surface armour, while the red circles indicate the major destabilizations with the release of fine particles evidenced by the brownish colors on the surface. Figure adapted from the report of Zavier Berti.

4.3.2 Propagation dynamics of the sediment pulse

At the beginning of the run, the channel is mostly free of sediments although a few small particles leaving the storage area during the formation of the deposit can be carried downstream as bedload. The arrival of the sediment pulse is materialized by the passage of a large amount of coarse particles rolling and sliding one above the other (Figure 4.2a, e, and f). Its transit is not continuous from top to bottom (i.e. from the storage area to the outlet section of the channel) but intermittent with various stops along the way. This cluster of coarse material acts like a moving dam, behind which a large volume of particles is restrained and grows in height (Figure 4.2b, g, and h). The motion of the sediment pulse is reactivated by the arrival of a trailing fast-moving flux of fine particles (Figure 4.2d, I, j, and movie S4.1). Indeed, when this flux meets the mass stuck along the channel, the fine particles fill the voids between the coarser ones, both downward (i.e. towards the channel bed) and in the flow direction (Figure 4.2g and h). This mechanism enhances the mobility of the deposited material, which starts to be eroded at the surface. The destabilized particles of the top layers slide and roll over a basal deposit (movie S4.1), and they move forward until they encounter the coarse front blocked along the channel. The sediment pulse is thus set in motion again as if it were pushed from behind (Figure 4.2c and movie S4.1). These dynamics repeat several times, until the sediment pulse reaches the outlet section.

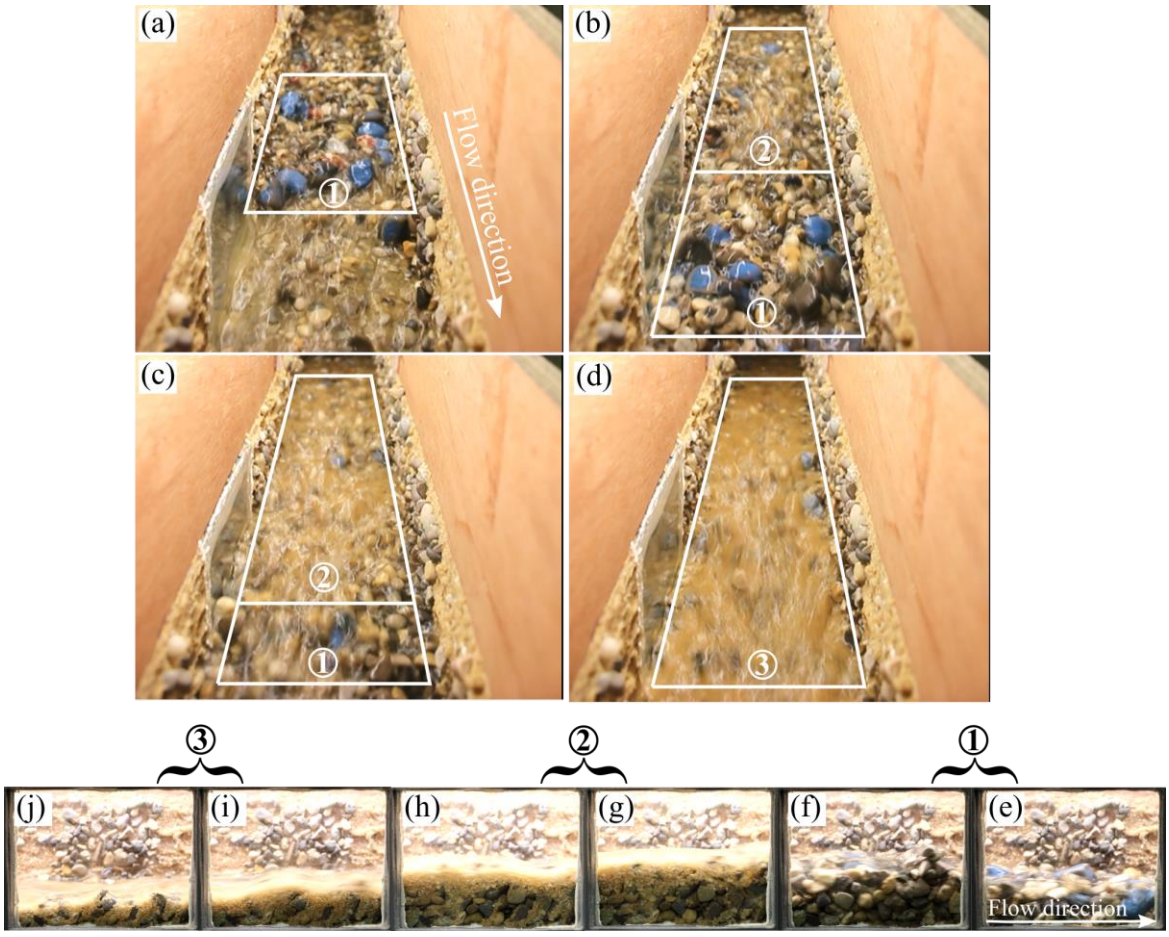

Figure 4.2 : Typical propagation dynamics of a sediment pulse. (a to d) Frames from the camera installed above the downstream part of the channel. The different components of the sediment pulses are highlighted

with the white squares. Note that compared to the experiments presented in the previous chapters, the camera has been moved downstream to include the lateral window on the sidewall. (e) to (j) Frames from the side camera installed close to the outlet section of the channel. The frames are consecutives in time and aligned next to each other to approximate the shape of a sediment pulse.

4.3.3 General observations on sediment pulse dynamics and its seismic signature

During the experiment presented in this section, we can observe four significant variations over time in the flow surface elevation and mean normal force measurements that correspond to the passage of sediment pulses (Figure 4.3a). Although the maximum values of these flow properties overlap, the mean normal force increases several seconds before the sharp increase of the flow surface elevation (see the orange bumps prior to the almost vertical cyan line, Figure 4.3a). This is particularly evident for the first sediment pulse, which is also the biggest in size, but can also be noticed for the other pulses. Thanks to the video recording, we realize that these increases of mean normal force are associated with the accumulation of coarse material above the force sensor (movie S4.1). These accumulations correspond to the blockages of the pulse front along the flume as described in the previous section. Since most of the time the accumulation of material occurs in the upstream section of the force plate, the flow surface elevation sensor does not detect significant variations (Figure 4.3a). Once the front destabilizes, the pulse advances and the flow surface elevation increases up to the maximum. In order to better visualize this mechanism, we estimate the bulk density of the flow following equation (8) from the previous chapter. In Figure 4.3b we can see that, in the time interval between 400 and 440 s, the bulk density increases up to unrealistic values, well above the density of the wet sediment mixture at rest ($\rho_{max} = 2235$ kg/m^3, orange horizontal dashed line in Figure 4.3b). This results from the gradual increase of mean normal force while the flow surface elevation remains constant (i.e. water flow level). However, at 440 s the bulk density drops and stagnate for ~ 20 s, highlighting the presence of the pulse body over the force sensor. The fact that the bulk density fluctuates around the maximum value of 2235 kg/m^3 (Figure 4.3b) suggests that a significant part of the pulse body is deposited, as observed in the previous section. After the passage of the body, the bulk density rises again to high values, which we verify is due to the presence of big particles resting over the force plate and not detected by the flow surface elevation sensor. Interestingly, we note that the mean tangential force behaves differently compared to the other flow properties during the passage of the pulse, with peaks occurring before the maximum levels of mean normal force and flow surface elevation (black arrows and yellow curve in Figure 4.3a). Thanks to the video recording, we observe that these peaks correspond to the destabilization of the front and its consequent passage over the force plate.

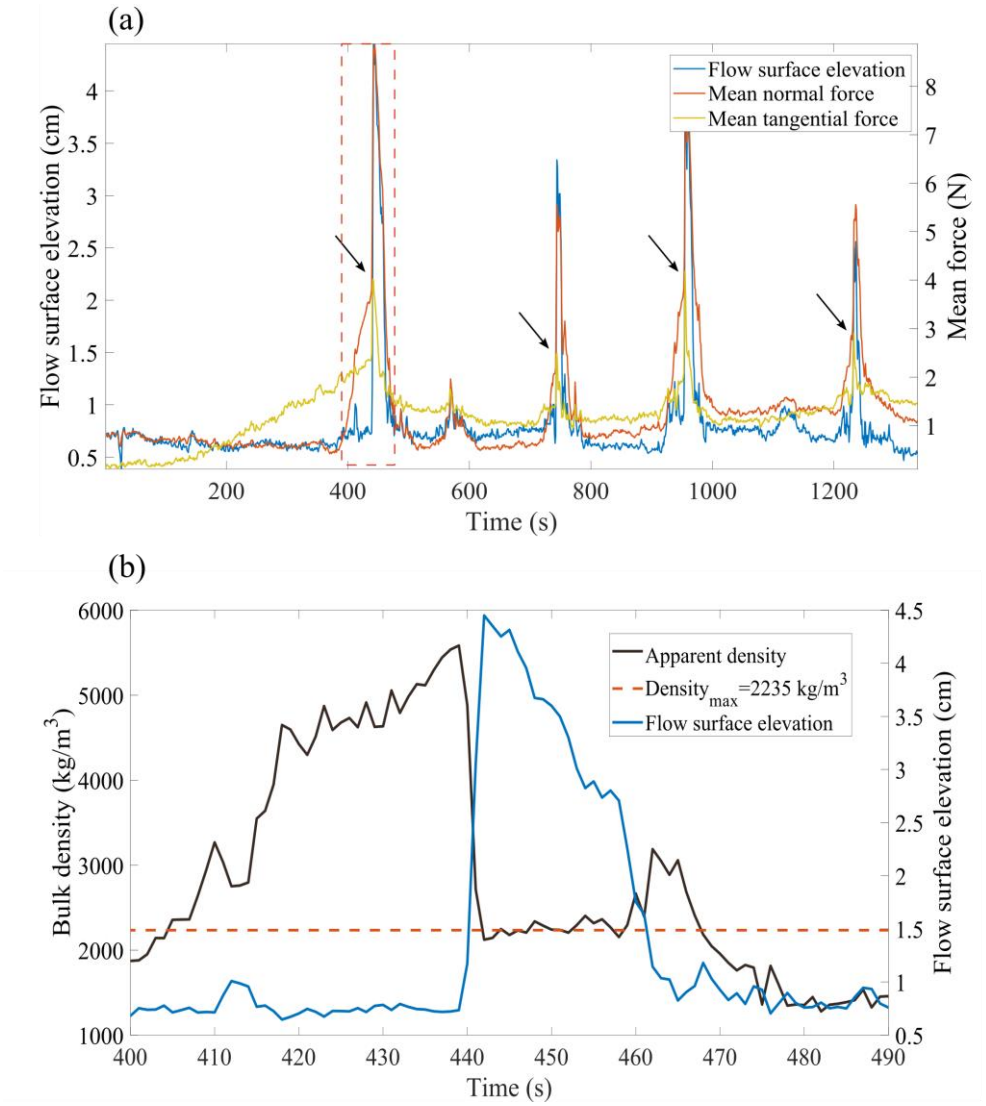

Figure 4.3 : Example of an experiment. (a) Comparison between flow surface elevation (cyan curve), mean normal (orange curve) and tangential (yellow curve) force. The black arrows indicate the peak of mean tangential force occurring during the passage of the pulse front. The dashed orange square highlights the pulse shown in (b). It's worth noting that the mean tangential force gradually increases at the beginning of the experiment, and we believe this is due to the stabilization of the force sensor. This effect is no more present after the first pulse. (b) Zoom on the first pulse of the experiment. Apparent bulk density (black curve), maximum density (orange horizontal dashed line), and flow surface elevation (cyan curve) are plotted as a function of time.

This is confirmed through Figure 4.4 in which we plot the seismic power and the mean tangential force detected by the force sensor. We can observe that the peaks of mean tangential force correspond to sharp increases in seismic power over all the frequency range (Figure 4.4), which are due to the passage of the pulse front. This is less evident in Figure 4.4d, because particles were transported as bedload (high seismic power in the first 10 s of Figure 4.4b and d). Note that bedload transport occurred especially when the sediment pulses were smaller (Figure 4.4b and d), while during bigger sediment pulses the blockage due to coarse material was strong enough to prevent particles from being transported downstream. The pulse body is characterized by a decrease in seismic power, while the trailing bedload makes the force power increasing again (Figure 4.4).

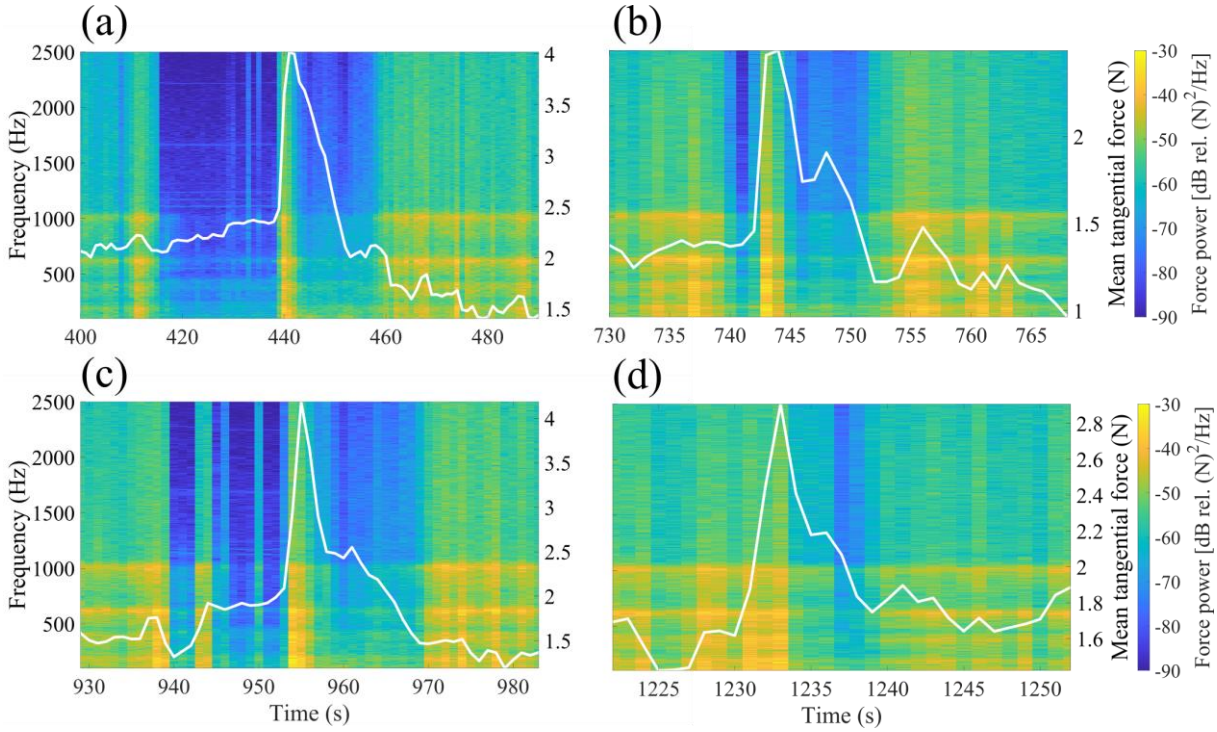

Figure 4.4 : (a) to (d) Spectrograms of the force power and mean tangential force (white curve) associated with the different sediment pulses of the experiment. Force power is a function of time and frequency.

4.3.4 Links between force power and flow properties

In Figure 4.5 we evaluate the relationships between flow properties (i.e. flow surface elevation and mean tangential and normal force) and force power for the pulse front and body. With regard to the pulse front, we do not observe significant trends, although a negative relationship between flow surface elevation and force power might be present if we exclude the lowest and higher values of flow surface elevation (Figure 4.5a and b). By contrast, the pulse body shows clearer links with negative relationships between force power and both flow surface elevation and mean normal force (Figure 4.5c and d). This is mainly due to three pulse bodies associated with significant size (flow surface elevation $>$ 5 cm). The relationships observed above for the pulse body result in a negative relationship between force power and bulk density (Figure 4.5e). However, data are scattered since variation in bulk density of ~300 kg/m^3 are associated with almost the same value of force power (see right side of Figure 4.5e). It's worth noting that two values of bulk density are higher than the maximum density of wet sediments at rest, which are probably due to errors in the measurements such as sediment deposition over the force plate not sensed by the flow surface elevation sensor.

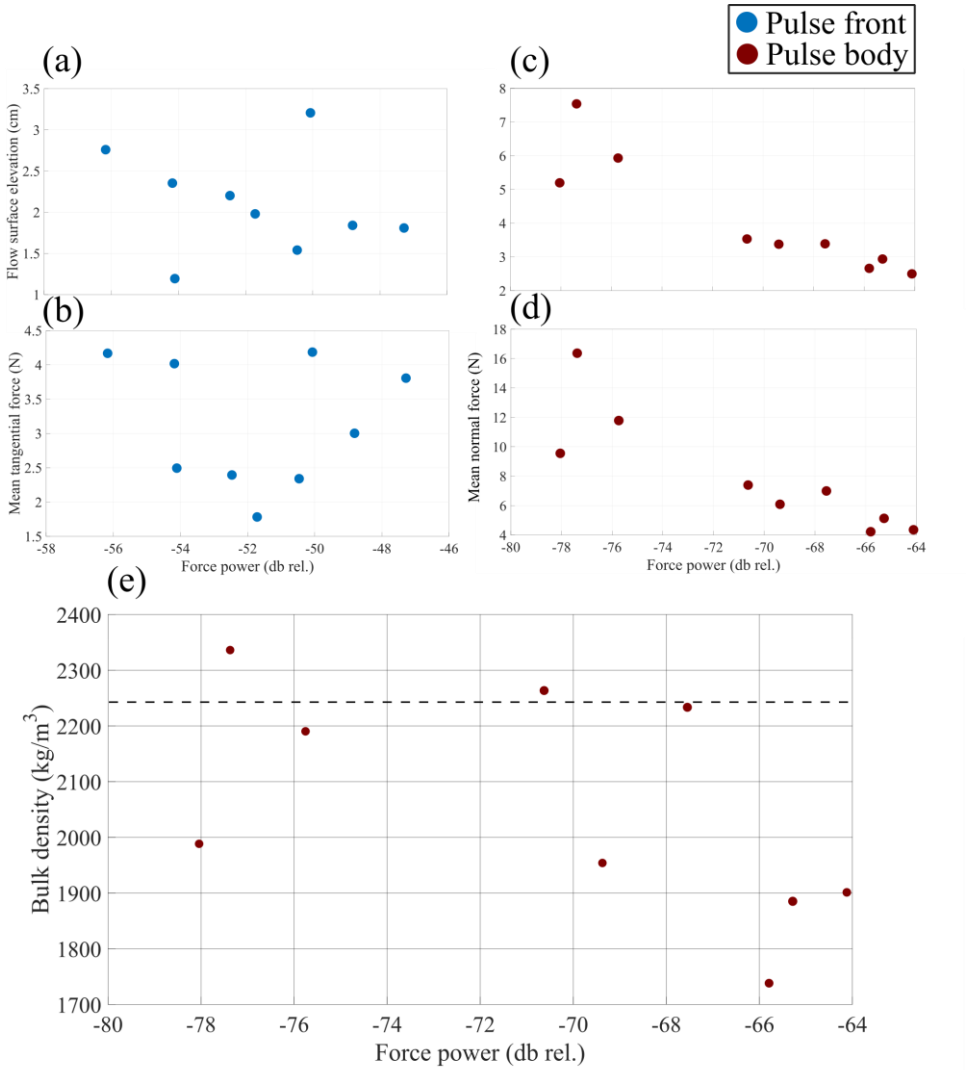

Figure 4.5 : Comparison between flow properties of the sediment pulse and generated force power. (a) and (b) with cyan dots refers to the pulse front, while (c) and (d) with the burgundy dots refers to the pulse body. The panels show force power against flow surface elevation and mean normal force. (e) Force power against bulk density of the pulse body. The black horizontal dashed line indicates the maximum density.

4.4 Discussion

4.4.1 The surging behavior of sediment pulses as set by grain sorting and force chains

In this chapter we present the results of experiments carried out in the same flume as the previous chapters, but with a significantly higher slope both in the storage area and in the channel (20% vs $0-1\%$, and 33% vs 18%, respectively). Under the same hydrological condition (around the threshold of motion), the experiments show similarities and differences. In the storage area, the destabilization of the sediment deposit develops one the armoured surface and particles move en

masse over finer particles, as observed in the previous chapters. However, in this case the destabilizations look less "energetic", that is, the coarse material does not enter the channel propagating downstream at high velocity, but rather it moves slower and it blocks at the foot of the deposit, clogging the inlet section of the channel. We advance that this might be due to the higher slope of the storage area, which reduces the stability of the deposit and therefore leads to smaller destabilizations.

The sediment transport dynamics along the channel is different in some respects. In the experiments on the 18% steep channel we observe significant bedload fluxes before the passage of the sediment pulse (the "front bedload" in Figure 3.2), which is likely due to the significant initial momentum exerted on the coarse material during destabilization. In this sense, Church et al. (2020) suggest that the critical shear stress for particle motion can be lowered by the momentum transferred by mass failure. By contrast, in the experiments at 33% this precursory bedload transport is less important and frequent. This happens because of the formation of the cluster of coarse material blocking the sediment supply from upstream, and leading to the formation of the sediment pulse. In the literature of debris flows, this temporary blockage of material is also called "moving dam" (Zanuttigh et al., 2007). The alternating dynamics of this natural dam (i.e. blockage and motion) have been associated with regressive instabilities, which are thought to be one of the mechanisms that drives the surging behavior of debris flows especially in confined channels. In Zanuttigh et al. (2007) the dam often breaks thanks to the input of fine material from slope erosion, which forms a slurry able to overtops the cluster of boulders or causes it to slide into motion. In our experiments we observe the same processes and we advance that the movement of the sediment pulse is driven by grain sorting which increases the flow transport capacity for the coarse particles, as observed in Chapter I, and in several past studies (Recking et al., 2009; Bacchi et al., 2014; Dudill et al., 2018; Chassagne et al., 2020). However, Zanuttigh et al. (2007) argue that the boulder dam is destabilized by the force exerted by the upstream sediment accumulation, which overcomes inter-particle and particle-boundary friction. In Figure 4.4 we observe that the destabilization and consequent passage of the front is characterized by a peak of mean tangential force. We suggest that this increase in tangential force could be an evidence of particles pushing from behind and transmitting forces in the form of force chains (Furbish et al., 2008; Estep & Dufek, 2012). Estep & Dufek (2012) suggest that the formation of network of force chains in granular flows can generate stresses exceeding the critical shear stress for motion. Similarly, Booth et al. (2014) show that force chains during mass failure have the capability to dislodge downhill "keystone" grains having large grain-pocket friction. We propose that both processes (i.e. grain sorting and the formation of force chains) could be the driving mechanisms of sediment pulse dynamics.

4.4.2 The seismic signature of the sediment pulse body as an end-member case of previous experiments

The analysis of the force power generated during the experiments confirm that the coarse front dominates the overall seismic signature of sediment pulses (Figure 4.4). Similar to the experiments presented in the previous chapter, the passage of the body is characterized by a reduction in force power, but in this case the reduction is stronger. As attested by the frames from the video recording (Figure 4.2e, f, g, h, i, and j), the pulse body is characterized by a thick basal deposition

that is eroded and moves downstream slowly. We suggest that this behavior can be seen as an end-member of the processes observed in the previous chapter. In these experiments, the bulk density reaches values that are close to the maximum bulk density of sediments at rest, meaning that particles are in a quasi-static regime with really slow deformation and particle agitation. The relationship between force power and bulk density is negative, which is consistent with the findings of the previous chapter. By contrast, the comparison between the flow properties (mean force and flow surface elevation) of the pulse front and the generated force power does not reveal significant trend. Further investigations are needed to understand if the generation of force chains could have an impact on the observations, leading to mechanisms that might influence the seismic signature of the pulse front. The model of Zhang et al. (2021) argues that force chains promote the generation of basal force fluctuations, but this argument still needs a thorough validation. In our experiments, under the hypothesis that the tangential mean force reflects force chains developing between the body and the front, we do not observe an increase in force power as expected by Zhang et al. (2021) (Figure 4.5b).

4.5 Conclusions

We carry out a novel set of experiments to investigate the triggering and propagation dynamics of sediment pulses at very high slope (33%), and to explore their seismic signature. Similar to the experiments at lower slope (18%), we observe a selective entrainment of the coarse material forming the armour of the sediment deposit due to the percolation of fine particles. The processes occurring in the storage area influences the propagation in the downstream channel, but in this case in-channel processes have a larger influence on the propagation dynamics of the sediment pulses. Sediment pulses are characterized by an intermittent movement that is dictated by the behavior of a frontal moving dam of coarse particles. We propose that the motion of the sediment pulse depend on grain sorting and on the formation of force chains, which are able to destabilize the front independently of the hydrological forcing. This finding highlights the importance of considering grain-to-grain interactions to understand the mobility of highly concentrated sediment flows around the threshold of motion. The force power measurements confirm that the front dominates the seismic signature of the sediment pulse, and that bulk density (i.e. solid concentration) is a good proxy for basal force fluctuations. Further investigations would be useful to explore the impact of force chains on the seismic signature of the pulse front.

4.6 Supporting Information

Additional Supporting Information (Files uploaded separately)

Movie S4.1: Movie of one sediment pulse from the experiment shown in the main text

Chapter 5: Using seismology to investigate the dynamics of a braided river reach under flood conditions

5.1 Preface

When my thesis directors proposed me to do this PhD, the project was already quite clear in their minds. In addition to laboratory experiments, the plan was to explore the potential of using seismic methods to study intense sediment transport in the field. In the laboratory we could focus on low-order confined channels and highly concentrated sediment flows, but what happens at the field scale for different river settings under flood conditions? In order to explore these questions, a field experiment was set up in the Séveraisse River (French Alps) in summer 2019. An array of 80 seismometers was installed around a braided reach of the river with the aim to capture a flood event and investigate its physics through a unique set of field observations. Unfortunately, at that time I was in Italy discussing my master thesis and I was not able to participate actively in the campaign. On the other hand, the experiment could not wait for the beginning of my PhD (a few months later), since summer is one of the most favorable periods for floods in Alpine regions, thanks to snow melt and thunderstorms. Despite the original plan to dedicate almost half of the PhD on this project and my sincere interest in analyzing these data, at the beginning of my third year I decided to still give priority to the laboratory experiments which were offering very interesting results, while demanding maintenance, instrumental improvements, and… workforce. The potential of this field experiment has been explored only partially in this manuscript, but I'm fully motivated in giving the credits it deserves in the near future.

This chapter presents and summarizes the preliminary results of the campaign on the Séveraisse River. I presented a part of these findings during the "Hydrométrie 2021: De la mesure à la prise de décision" Conference in Montpellier (France), which were then published as a paper on the LHB Hydroscience Journal: **Piantini, M.**[1,2], Gimbert, F.[1], Bakker, M.[1,2], Recking, A.[2], and Nanni, U.[3] (2022): Using a dense seismic array to study fluvial processes in a braided river reach under flood conditions, LHB. https://doi.org/10.1080/27678490.2022.2053314

[1] University Grenoble Alpes, CNRS, IRD, Institute for Geosciences and Environmental Research (IGE), Grenoble, France

[2] University Grenoble Alpes, INRAE, CNRS, IRD, Grenoble INP, IGE, 38000 Grenoble, France

[3] Department of Geosciences, University of Oslo, Oslo, Norway

Short note to the reader

The chapter contains supplementary analyses not included in the paper. In order to distinguish between them, I have highlighted the published work with the *italic font*.

Préface

Lorsque mes directeurs de thèse m'ont proposé de faire ce doctorat, le projet était déjà très clair dans leur esprit. En plus des expériences au laboratoire, j'aurais dû explorer le potentiel de l'utilisation des méthodes sismiques pour étudier le transport sédimentaire intense sur le terrain. Au laboratoire, nous pouvions nous concentrer sur des rivières de montagne confinées et stable, mais que se passe-t-il à l'échelle du terrain pour différents types de rivières en crue ? Afin d'explorer ces questions, une expérience de terrain a été mise en place dans la rivière Séveraisse (Alpes françaises) pendant l'été 2019. Un réseau de 80 sismomètres a été installé autour d'un tronçon en tresse de la rivière pour observer un événement de crue et étudier sa physique à travers un ensemble d'observations de terrain. Malheureusement, à cette époque, j'étais en Italie présenter ma thèse de master et je n'ai pas été en mesure de participer activement à la campagne. D'autre part, l'expérience ne pouvait pas attendre le début de mon doctorat (quelques mois plus tard), car l'été est l'une des périodes les plus favorables aux crues dans les régions alpines, grâce à la fonte des neiges et aux orages. Malgré le plan initial de consacrer presque la moitié du doctorat à ce projet et mon intérêt sincère pour analyser ces données, au début de ma troisième année, j'ai décidé de continuer à donner la priorité aux expériences au laboratoire qui offraient des résultats très intéressants, tout en exigeant de la maintenance, des améliorations instrumentales et... de la main-d'œuvre. Le potentiel de cette expérience de terrain n'a été que partiellement exploré dans ce manuscrit, mais je suis pleinement motivé pour lui donner les crédits qu'il mérite dans un futur proche.

Ce chapitre présente et résume les résultats préliminaires de la campagne sur la rivière Séveraisse. J'ai présenté une partie de ces résultats lors de la Conférence "Hydrométrie 2021 : De la mesure à la prise de décision" à Montpellier qui ont ensuite été publiés sous forme d'article sur le journal LHB Hydroscience : **Piantini, M.**[1,2], Gimbert, F.[1], Bakker, M.[1,2], Recking, A.[2], and Nanni, U.[3] (2022): Using a dense seismic array to study fluvial processes in a braided river reach under flood conditions, LHB. https://doi.org/10.1080/27678490.2022.2053314

[1] University Grenoble Alpes, CNRS, IRD, Institute for Geosciences and Environmental Research (IGE), Grenoble, France

[2] University Grenoble Alpes, INRAE, CNRS, IRD, Grenoble INP, IGE, 38000 Grenoble, France

[3] Department of Geosciences, University of Oslo, Oslo, Norway

Brève note au lecteur

Le chapitre contient des analyses supplémentaires qui ne figurent pas dans l'article. Afin de les distinguer, j'ai mis en évidence les travaux publiés en *italique*.

5.2 Introduction

Over the last decade, the unique capabilities of seismic techniques in investigating fluvial processes have been demonstrated (Burtin et al., 2008, 2016). As water turbulence and bedload transport generate seismic ground motions, the non-invasive and continuous detection of river-induced vibrations represents an alternative to traditional monitoring methods. Indeed, a large amount of information about the source of ground motion is embedded in a river-induced seismic signal. The velocity time series $u(t)$ of vertical ground motion can be expressed as:

$$u(t) = Ae^{iwt} \tag{13}$$

where t is time, A is the signal amplitude, i the unit imaginary number and the product ωt is the signal phase, with the angular frequency ω. Each of these variables carries different information on the river processes. On the one hand, the amplitude of the seismic signal has been studied and modelled to obtain the onset of bedload transport and estimation of sediment fluxes (Tsai et al., 2012; Bakker et al., 2020; Burtin et al., 2008; Roth et al., 2016; Schmandt et al., 2013), or the estimation of flow stage or water discharge (Gimbert et al., 2014). In particular, thanks to frequency-based scaling relationships between seismic power and water discharge, existing theories have been shown to be valid in the field under relatively low bedload transport rates (Bakker et al., 2020). However, theoretical predictions have not yet been tested in the case of flood events, when bedload fluxes are expected to be very intense. On the other hand, phase differences between seismic stations have allowed researchers to estimate the azimuth of in-channel sediment transport, i.e. its direction with respect to the receiver (Burtin et al., 2010; Chao et al., 2015). However, phase analysis has been shown to have a much greater potential for the identification of seismic sources. In particular, dense networks of seismometers (so-called dense seismic arrays) have been used to investigate the spatiotemporal dynamics of sources such as those associated with englacial fracturing (Gimbert et al., 2021), hydrothermal activity (Legaz et al., 2009) and geophysical extraction (Corciulo et al., 2012), with high temporal and spatial resolution. Since fluvial processes are highly variable in time and space, the use of dense seismic arrays could allow the detection and tracking of different sources of river-induced seismic ground motions (e.g. turbulence and bedload transport).

Here, we first test existing theories for a flood event that occurred at the end of the melt season in summer 2019 in a braided reach of the Séveraisse River (French Alps), which is the same field setting of Bakker et al. (2020). Second, we study the potential of dense seismic array monitoring to provide insight into river dynamics by analysing data from a field survey conducted on a 600 m-long reach of the river. In Sections 5.3 and 5.4 we present the study area and the methods used for the dense seismic array monitoring, respectively. Then, in Section 5.5, we show the results of our analysis. Finally, in Section 5.6 and 5.7 we discuss the capabilities and limitations of such seismic methods for studying fluvial processes, especially during flood events.

5.3 Study area and measurements

The Séveraisse River is a natural Alpine stream whose catchment is located in the Ecrins Massif, southeast French Alps. This study focuses on a 600 m long braided reach characterized by a maximum width of 90 m and a mean slope of 1% (Figure 5.1). The reach is easily accessible for field observations and is well equipped: water discharge and flow stage measurements are provided at a 10 −min resolution through an Électricité de France (EDF) stream gauge station at a bridge approximately 200 m downstream of the reach, while a camera installed on a rocky outcrop approximately 70 m above the channel covers the area of interest and provides time-lapse imagery. About 3 kilometres upstream of the studied reach, a monitoring station also provides rainfall measurements at a 6 −minutes pace.

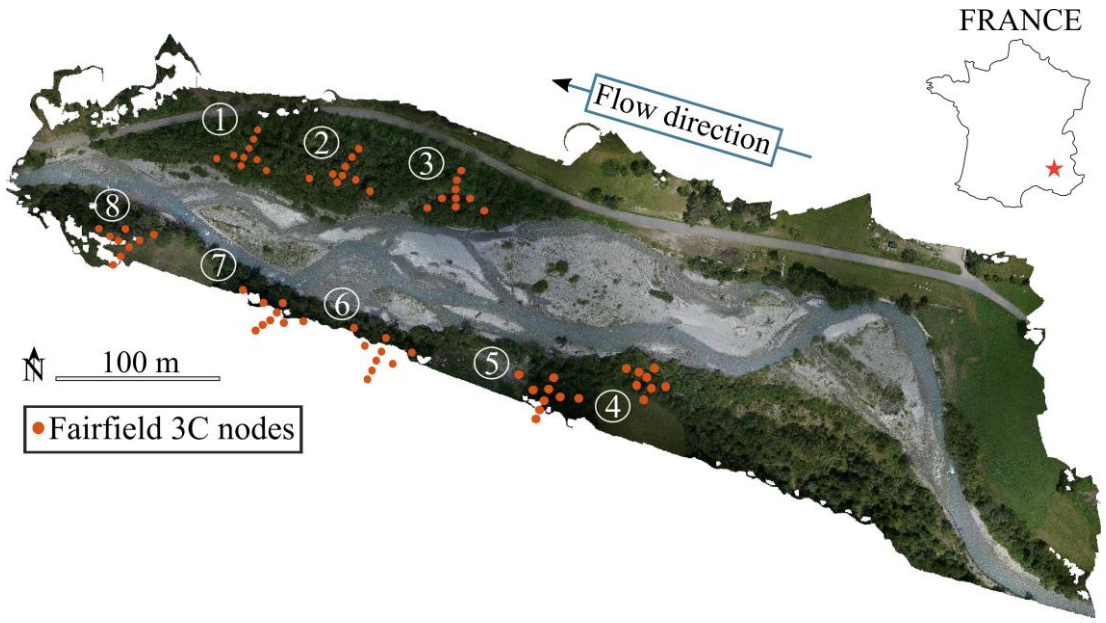

Figure 5.1 : Orthophoto of the studied braided reach of the Séveraisse River (courtesy of Laurent Borgniet, INRAE; used with permission), including the deployed seismometers. INRAE: Institut National de Recherche pour l'Agriculture, l'alimentation et l'Environnement.

In the first part of the seismic analysis, we take advantage of a geophone (3-component Sensor PE-6/B) installed next to the bridge where water discharge measurements are performed (distance of ~30 m from the channel). This section of the river is straight and laterally confined, and 12 m wide. The geophone is characterized by a sampling frequency f_s of 400 Hz, allowing the assessment of ground vibrations up to 200 Hz. We compute the power spectral density (PSD) of the signal recorded along the vertical by performing a fast Fourier transform with the Welch's averaging method (Welch, 1967). According to this method the time series is split into overlapping segments (here we chose an overlap of 50 %), and the final PSD results from the average of the PSDs of each segment. The temporal resolution over which the seismic power is determined is 3 s. For the comparison with the water discharge measurements we compute the median over 10 min, and we consider the $6 - 10$ Hz and $40 - 50$ Hz frequency bands as representative of water turbulence and

bedload transport, respectively. The lower limit of the investigated frequencies is set by the natural frequency of the sensor being 4.5 Hz.

For the second part of the seismic analysis, that is, the dense seismic array monitoring, we install 80 seismometers (Fairfield ZLand 3 components nodes) characterized by $f_s = 250$ Hz, allowing the assessment of ground vibrations up to 125 Hz. The experimental design of the array is presented in the following section.

5.4 Experimental design and methods for the dense seismic array

The capability to locate seismic events (i.e. the position of the source that generates them) depends on the extent to which they are detectable through the dense seismic array. Impulsive events are relatively straightforward to locate as long as they are well detected across the seismic network deployed around them, but the task is more challenging when events are only locally detectable and/or non-impulsive. Since the latter characteristics may be specific to river-induced ground motions, characterised by a varying nature that also depends on frequency (Gimbert et al., 2014), we deployed the seismic array following two main conditions typically used for systematically retrieving the spatial coordinates of seismic sources (Nanni et al., 2021):

$$\lambda = \frac{c}{f} > \Delta l \tag{14}$$

$$\Delta s \leq 2 \text{ or } 3d \tag{15}$$

where λ is the signal wavelength, defined as the ratio between phase velocity c and signal frequency f , Δl is the distance between seismometers, Δs is the maximum array aperture (i.e. the largest distance between seismometers of a subarray) and d is the source-to-array distance. The condition given by equation (14) is necessary to conduct sub- wavelength sampling of the seismic wave-field, which is required to extract coherent information at a small time scale while systematically processing the data. A seismic wave is said to be coherently detected within an array when a clear dominant signal is observed at each station. Ground motions detected over several seismometers can be reliably associated to a certain source only if the seismometer-to-seismometer distance is smaller than the signal wavelength (Nanni et al., 2021). The condition given by Equation (15) is necessary to obtain the spatial coordinates of the source, which is possible only when the source-to-array distance is small enough relative to the largest distance of seismometers of the array (Almendros et al., 1999). Given these needs, we installed a network of 80 seismometers mostly deployed in subarrays (Figure 5.1). We meet condition (14) at the subarray scale thanks to a mean distance between seismometers of 5 m, compared to an estimated wavelength varying from 10 to 100 m (with c varying from 200 to 400 m/s) in the frequency range of interest, while we overcome condition (15) by building several subarrays with $\Delta s \sim 20$ m covering the whole area of interest.

As previously stated, the seismometers record ground motions at a sampling frequency of 250 Hz. However, we apply a 5– 20 Hz band-pass filter to the data in order to focus on turbulence and bedload-induced ground motions (Bakker et al., 2020), thus removing all non- fluvial sources (e.g. rainfall-induced high-frequency ground vibrations (Roth et al., 2016)).

The method consists in measuring the differences in the arrival time (i.e. time delays) between each combination of seismometers of a given impulsive event observed across the array. Then, we build an

imaginary grid of points superimposed on the study area, and compute the time delays that would be generated by events located in the points of the grid (where each point is associated to its spatial coordinates (x, y)) and associated with a certain phase velocity (c). Finally, we search for the spatial coordinates and phase velocity for which the predicted time delays best match the observed ones. The final result is a spatial map defined as follows:

$$M(x, y, c) = \frac{1}{\frac{N!}{2!\,(N-2)!}} \sqrt{\sum_{i=1}^{N-1} \sum_{j>1}^{N} \left(\Delta t_{ij}^{observed} - \Delta t_{ij}^{predicted}\right)^2} \quad (16)$$

where M is the average mismatch between observed and predicted time delays, N is the number of seismometers, $\Delta t^{observed}$ are the observed time delays between each pair of seismometers and $\Delta t^{predicted}$ are the predicted time delays between each pair of seismometers. The x and y coordinates of the minimum of this map corresponds to the most likely location of the event.

5.5 Results

5.5.1 General seismic observations and seismic power scaling relationships

In the monitoring period presented in this study (1-4 July 2019) the Séveraisse experienced water discharges varying between ~12 m³/s and ~40 m³/s (Figure 5.2a), which are above the threshold associated with full particle mobility ($\tau^*/\tau_{cr}^* > 1$) estimated by Bakker et al. (2020) to be $Q_l > 11.9$ m³/s. As is often the case with Alpine rivers, in summer the Séveraisse is characterized by daily peak discharges due to snow-melt events occurring in the upper parts of the catchment. In this particular case, the magnitude and timing of these high-flow events are also affected by three rainfall events that anticipated and reinforced the peak in-stream water discharges (Figure 5.2a). The main flood event occurred on 2 and 3 July and was characterized by a return period of 2 to 5 years based on the available dataset. The seismometer installed next to the bridge depicts accurately what happened in the catchment (Figure 5.2b). Given the elevated water discharges and the proximity of the seismometer to the river, the background and relatively high seismic power at $f < 60$ Hz is attributed to river processes. The three peaks in water discharge are particularly evidenced by increases in seismic power in this frequency range, up to -120 dB. The three rainfall events are concomitant with sharp increases in seismic power at high frequencies ($f > 50$ Hz), which is consistent with previous works on rainfall-induced ground vibrations (Bakker et al., 2022).

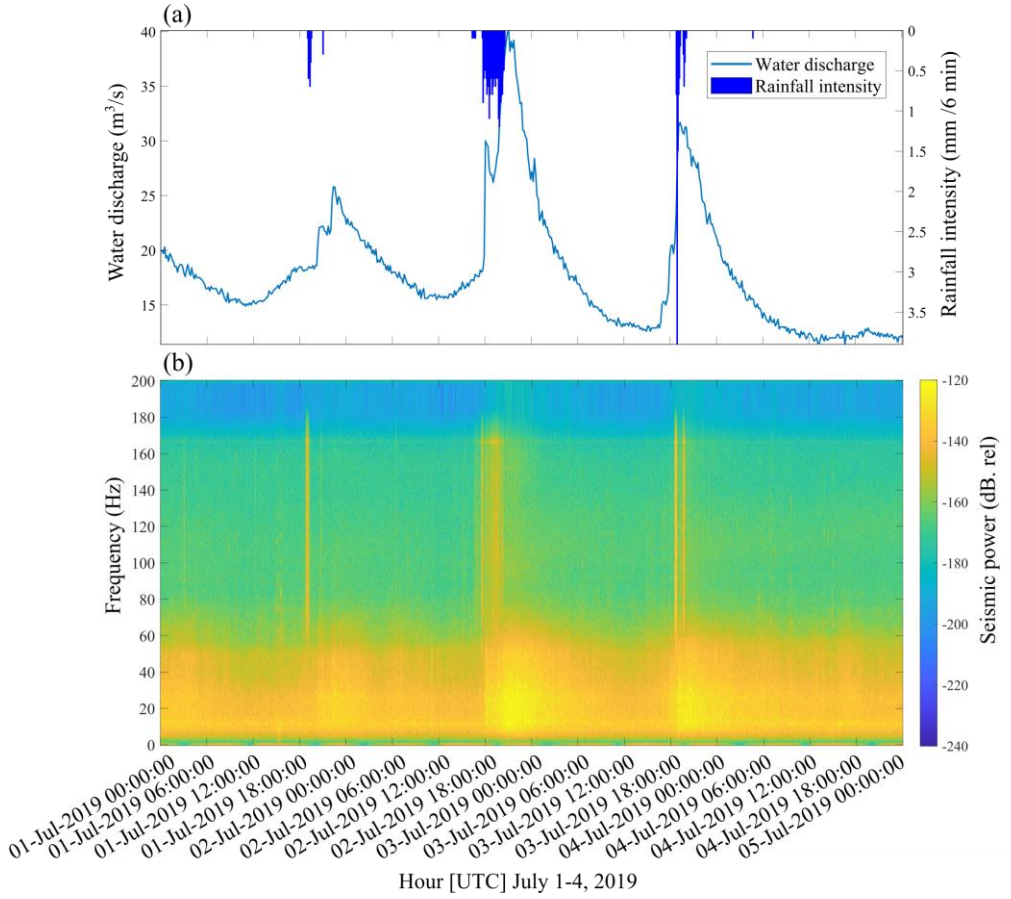

Figure 5.2 : (a) Water discharges (cyan curve) and rainfall intensity (blue bars) measured during the monitoring period. Water discharge measurements are made through a stream gauge station on a bridge which is 200 m downstream the study area, while rainfall data are provided by a monitoring station which is 3 km upstream of the study area. (b) Spectrogram of the observed seismic power as a function of time and frequency.

In order to get more insights into the dynamics of the river during the flood event and to test existing theories on river-induced ground vibrations, we explore the scaling relationships between seismic power and water discharge measurements, and for seismic power at the different frequency bands specified in Section 5.3 (Figure 5.3). At low frequencies ($6 - 10$ Hz), for water discharges $\sim < 25$ m³/s, the least square regression shows a power-law scaling having an exponent of 1.6. However, for water discharges $\sim > 25$ m³/s we observe a significant break in the slope, with a scaling power approaching an exponent of 3. Interestingly, after the main flood event (highlighted with the shaded area in Figure 5.3a), a hysteresis behaviour is present, that is, the same water discharge is associated with a higher seismic power compared to the pre-flood conditions ($\sim$3 dB higher). At higher frequencies ($40 - 50$ Hz) we observe a similar behaviour, though with different scaling relationships. For water discharges $\sim < 25$ m³/s, the exponent of the power-law scaling is 4.5, but for higher water discharges the scaling decreases to 3. This change in the scaling relationships appears to be influenced by the falling limb of the main flood event, which is characterized by a weaker slope (Figure 5.3b, red dashed line inside the shaded area). As for low frequency seismic power, we observe a hysteresis after the flood with the same water discharge being associated with a $\sim$5 dB higher level of seismic power (Figure 5.3b). If we compare low and high frequency seismic power for all the range of water discharges, we observe different scaling

relationships as well (Figure 5.3c). For water discharges ~ < 25 m³/s, the exponent of the power-law scaling is 2, while for higher water discharges it decreases towards 1.

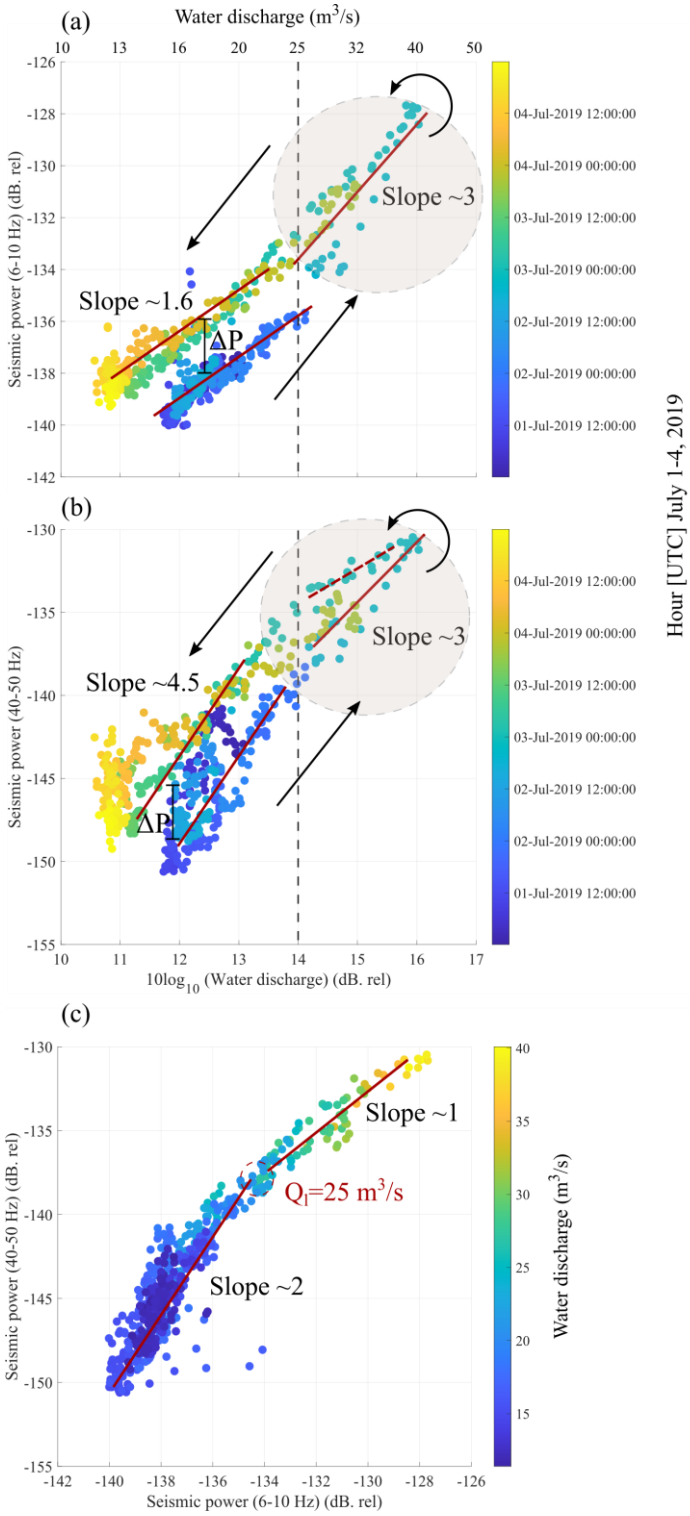

Figure 5.3 : (a) and (b) Seismic power in different frequency bands ($\Delta f = 6 - 10$ Hz and $\Delta f = 40 - 50$ Hz) plotted against water discharge measurements over time. Water discharge is shown as $10\log_{10}$ to match the dB scale of the seismic power (bottom x-label), and the equivalent values in m³/s are indicated in the top y-label. The black arrows show the evolution of the flood over time. The hysteresis behaviors are indicated with

vertical black lines. The shaded area indicates the main flood event. (c) Seismic power in the $6-10$ Hz frequency band against seismic power in the $40-50$ Hz frequency band. The colors in the scatter plots vary with the water discharge measurements. The threshold of $Q_1 = 25$ m^3/s is highlighted by the red dashed circle. Last square regressions are indicated with red lines. In panel (b) the red dashed line shows the apparent change in the exponent (last square regression is not computed in this case).

5.5.2 Localization of impulsive events

We perform event localization during *the main flood event that occurred on 2 and 3 July 2019. The middle section of the reach experienced morphological changes near the left bank during the event (Figure 5.5a and b). Following the steps presented in Section 5.4, we find that during the flood, impulsive events are detected across the dense array. As an example, Figure 5.4 shows three seconds of seismic recording for the five subarrays deployed in the middle section of the reach (subarrays 1, 2, 3, 6 and 7 in Figure 5.1). We can observe that two main impulsive events are detected with coherence across all five subarrays, meaning that these ground motions are very likely generated by the same dominant source. Indeed, the time delay between peaks within each subarray is on the order of 0.01 s. Moreover, time delays are visible between seismometers, so that an evaluation of phase coherence is possible for source localization.*

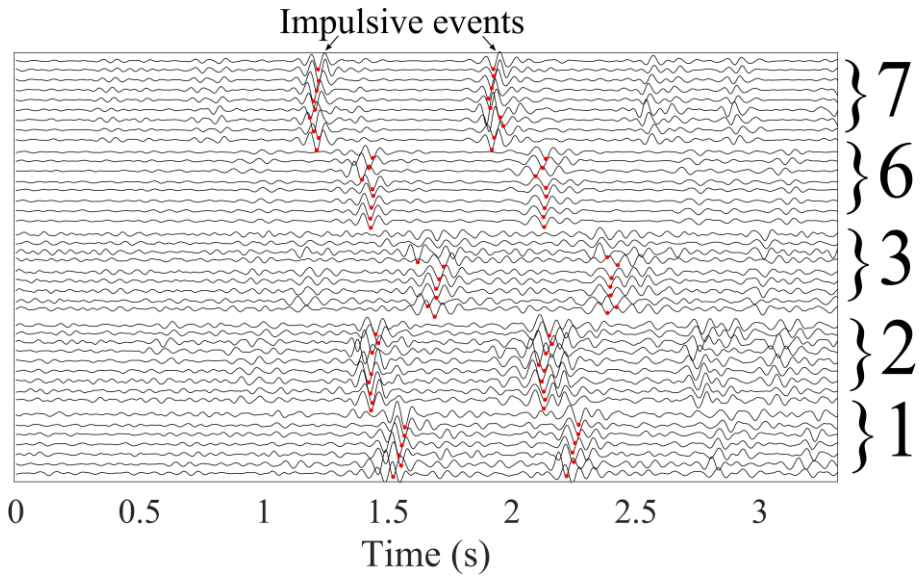

Figure 5.4 : Time recording of ground motion for the five subarrays located in the middle section of the channel. The two main impulsive events are highlighted with red dots on each recording. The amplitude of the seismic signal is normalized.

After measuring the existing time delays, and through the grid search, we find the location of the impulsive event (Figure 5.5c). The minimum average mismatch between observed and predicted time delays is obtained using a phase velocity $c = 200$ m/s, which is consistent with previous active seismic experiments at this field site (Bakker et al., 2020).

The minimum mismatch corresponds to the bend apex of an active channel within the reach. This area was almost inactive before the flood (Figure 5.5a), with water mainly flowing on the opposite bank,

while after the flood the same area shows evidence of a higher water flow (see flooded areas circled in yellow in Figure 5.5b). We identified the presence of boulders at the same location (Figure 5.5d), and we therefore interpret the investigated impulsive event as being associated with the motion of these boulders as a consequence of high stresses exerted on the bank during the flood.

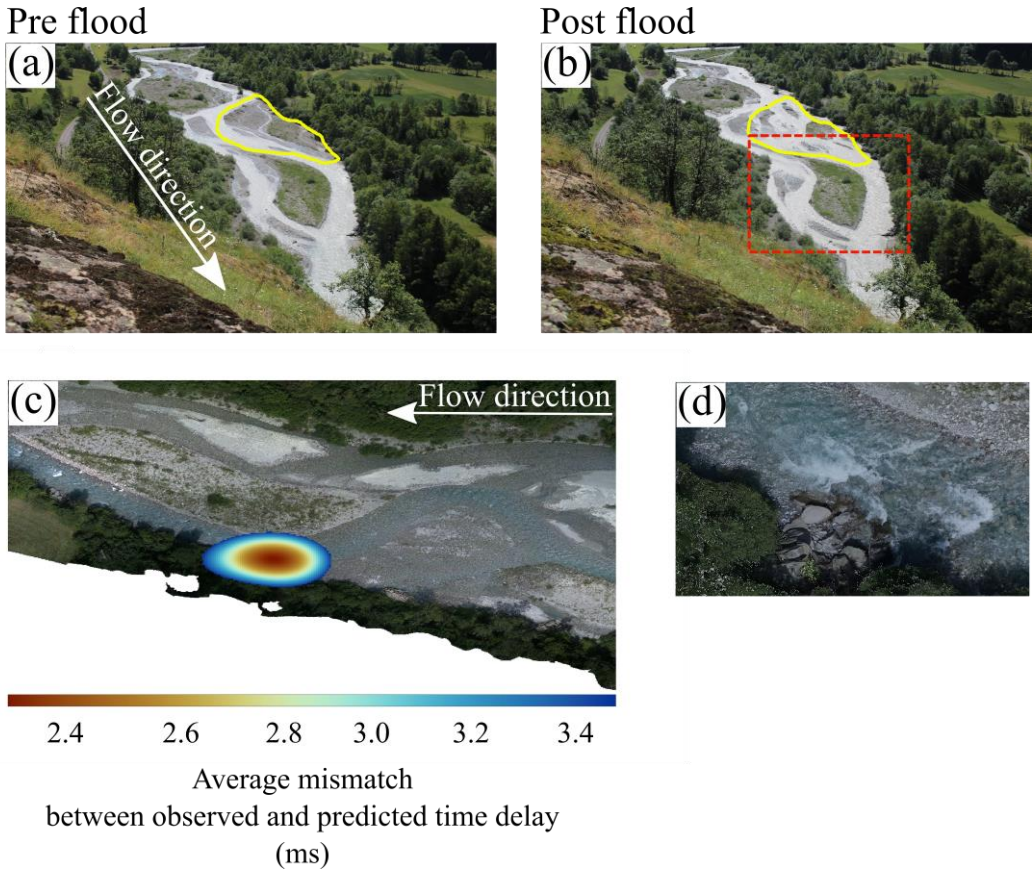

Figure 5.5 : (a) and (b) Time-lapse images of the braided reach before and after the event. The main morphological changes are highlighted in yellow; the red box indicates the active channel shown in (c). (c) Localization of the impulsive event on the orthophoto focusing on the area in the red box in (b). It is worth noting that the orthophoto was made two weeks after the flood. The map is derived for a phase velocity of 200 m/s. (d) Section of the active channel that corresponds to the location of the impulsive event in (c).

5.6 Discussion

5.6.1 Seismic power scaling relationships reveal river activity during the flood

We observe that the scaling relationships between the water discharge measurements and the low and high frequency seismic power are not constant but vary during the main high-flow event (Figure 5.3). For relatively low water discharge (i.e. $Q_l \sim < 25$ m³/s), the power-law scaling at low frequencies ($6 - 10$ Hz) is remarkably similar to that predicted by the physical modelling of turbulent flow ($P \sim {Q_w}^{1.4}$ in Gimbert et al., 2016), meaning that river-induced ground vibrations are dominated by water flow turbulence. This is consistent with the study of Bakker et al. (2020) that found a scaling of 1.5 for seismic power at $f = 10$ Hz (Figure 1.14 in the Introduction of the manuscript). However, the strong change of scaling up to 3 that we note for $Q_l \sim > 25$ m³/s suggest that water flow turbulence is no more the dominant source at these frequencies. Since the

analysis of Bakker et al. (2020) focussed on water discharges $\leq$ 25 m³/s, comparisons cannot be drawn at this regard.

We advance that the change of scaling could be due to sediment transport processes generating ground vibrations at frequencies lower than expected and covering a large part of the spectrum. This hypothesis is confirmed by the fact that at $\Delta f = 40 - 50$ Hz, in which bedload is predicted to dominate (Gimbert et al., 2014), the exponent of the power-law scaling between seismic power and water discharge is the same (Figure 5.3). This is also attested by the scaling of ~ 1 between low- and high-frequency seismic power for $Q_l \sim >$ 25 m³/s (Figure 5.3c). Low-frequency seismic power could be generated by the movement of big grains such as clasts or blocks, or by the transport of clusters of sediment in the form of concentrated sediment flows. These processes would generate low-frequency seismic signals thanks to the longer impact times on the riverbed, since the characteristic frequency of the generated seismic signal is inversely proportional to impact duration (Farin et al. (2015). At lower water discharge, the scaling of ~ 2 confirms that the different frequency bands are sensitive to distinct processes, i.e., water turbulence and bedload transport.

The power-law scaling at $\Delta f = 40 - 50$ Hz for $Q_l \sim <$ 25 m³/s is consistent with the range of values found by Bakker et al. (2020) for water discharges above the threshold of full particle mobility (i.e. 4.4 at $f = 30$ Hz and 5.3 at $f = 50$ Hz). The lower exponent for $Q_l \sim >$ 25 m³/s seems to be mainly due to the slow decline of high-frequency seismic power compared to water discharge during the falling limb of flood (red dashed line in Figure 5.3b). This behavior could be explained by a sustained bedload transport caused by pavement breakup after the flood peak as observed in this reach by Misset et al. (2019). It's worth mentioning that at high frequencies Bakker et al. (2020) as well observed a change in the power-law scaling, but in that case the slope got steeper and the inflection point corresponded to the threshold of full particle mobility, which is not our case.

5.6.2 Hysteresis behaviors between water discharge and seismic power after the flood

Through comparing the low- and high-frequency seismic power against the water discharge measurements, we observe hysteresis behavior between pre- and post-flood conditions. The difference of ~ 3 dB at low frequencies might be an indication of bed evolution caused by the flood (Roth et al., 2017). The model of Gimbert et al. (2014, 2016) predicts that water turbulence-induced seismic power depends strongly on the flow stage (i.e. water discharge), but also on bed roughness and river slope. Since seismic power is expected to scale inversely with grain-scale bed roughness (Gimbert et al., 2014), our observations of higher seismic power after the flood event might indicate the fining of the bed, consistent with pavement breakup (Misset et al., 2020). Similarly, the increased seismic power could be also associated with an increase of the bed slope, consistent with channel incision due to significant erosion during the flood. The study of Misset et al. (2020) in the same reach of the Séveraisse showed that the grain size distribution of the bed close to the bridge (i.e. close to where the seismometer is approximately installed) was significantly coarse, suggesting that bedload transport does not come from local bed mobilization but rather from material mobilized in the upstream braided section. However, their bedload measurements were done for maximum water discharge of 25.1 m³/s. As the flood considered here is associated with

much higher values ($Q_l = 40$ m³/s, return period of 2 to 5 years), we advance that geomorphological changes may have occurred.

We also observe hysteresis behavior for the high-frequency seismic power (~5 dB). Since this frequency band is expected to be associated with bedload-induced seismic power, as observed in past investigations (e.g. Burtin et al. 2008; Hsu et al. 2011; Schmandt et al. 2013) we suggest that the higher level of seismic power after the flood could be associated with sustained high bedload transport rates. Some studies have shown that high sediment transport after large flood can be related to the disruption of bed stability with a decrease of bed roughness or an enhanced sediment availability coming from the bed (Lenzi, 2001; Turowski et al., 2009). These hypotheses are plausible and consistent with the hysteresis observed at low frequencies.

5.6.3 The potential of using dense seismic array monitoring

The physics of flood events and their impact on river landscape are challenging to investigate with traditional monitoring techniques because of the highly dynamic nature of fluvial processes. Braided rivers are particularly challenging as morphological changes occur at various spatial and temporal scales *(Ashmore, 1991; Bertoldi et al., 2010). In this context, our work demonstrates the unique capability of dense seismic arrays in identifying different sources of river-induced seismic ground vibrations. During the 2–3 July 2019 flood on the Séveraisse River, we are able to locate seismic events on the bend apex of an active branch of the reach, and we interpret them as being associated to the bedload transport of clusters of large grains. Since boulders were placed as bank protection in the same location, our results could indicate either their destabilisation or high sediment transport activity in this channel section. It is worth noting that although this study focuses on a specific seismic event, a high number of impulsive events have been systematically detected during the flood. Therefore, further investigations should allow us to obtain a wide portrait of the river over long time scales. The short-term- average over long-term-average (STA/LTA) method can be used to build a catalogue of events having a certain amplitude* (Allen, 1978)*, as used by Gimbert et al.* (2021) *for events related to englacial fracturing. These preliminary results demonstrate the capability of the method to better understand the fluvial processes that play an important role in storing and transferring sediments in the braided river reach, which provides crucial information for geomorphological investigations and natural risk management. The use of our approach has several practical advantages compared to traditional monitoring techniques. Seismometers can autonomously monitor river processes for months at a time. Since the seismometers are installed next to the active channel, they cannot be damaged during high-flow events, which can thus be monitored with reliability. For now, this technique does not provide real-time monitoring, since data must be downloaded and analysed after the event, but in the future one could expect technological advances allowing direct transfer and automated analysis. Limitations for the implementation of dense seismic arrays include the following: (i) space is needed for the correct deployment of the seismic network (see Section 5.4), and (ii) anthropogenic sources of seismic noise might impact the analysis. These limitations are particularly pertinent in populated areas. Moreover, we underline the importance of targeted seismic field observations to identify the frequency band where impulsive events related to bedload dominate over other processes, and to investigate the characteristics of seismic wave propagation (e.g. phase velocity). This can help in defining the most appropriate frequency band for the detection routine and in interpreting the results. However, our study area is well suited for the presented method and*

particularly well documented, paving the way for a recursive phase-delay analysis that should enable us to trace the spatiotemporal dynamics of sediment transport processes at high resolution.

5.7 Conclusions

In this work we test the use of different seismic methods to study the fluvial processes occurring in a braided reach of the Séveraisse river during a flood occurred at the end of the melt season, in summer 2019. First, through investigating low-frequency seismic power against water discharge measurements, we show that at high flows the scaling relationship is not consistent with turbulent flow being the dominant source of ground vibrations. We suggest that bedload transport dominates over turbulence for a wide range of frequencies thanks to the transport of big particles or to the occurrence of concentrated sediment flows, which would generate low-frequency ground vibrations because of longer impact time on the riverbed. On the one hand, this indicates that inferring water discharge values from river-induced ground vibrations may be a difficult task for flood events, unless very low frequencies or seismometers installed at high distance from the river are used. On the other hand, the identification of changes in the power-law scaling can be used to identify critical water discharge above which significant bed morphological changes or pavement breakup are likely to happen. Hysteresis behaviors in the relationships between seismic power and water discharge at both low and high frequencies are a proxy for potential morphological changes and sustained high sediment transport rates caused by the event. Second, for the first time we study the potential of dense seismic array monitoring to locate sources of ground vibration in a river setting. During the flood, we observe impulsive signals that are coherently detected over the array, and which we interpret as being associated with the bedload transport of clusters of coarse grains (blocks). Through phase-delay analysis we are able to locate these seismic events on the bend apex of an active branch of the reach. These results demonstrate the capability of such a method to locate bedload activity at high spatiotemporal resolution, providing crucial information for geomorphological investigations and natural risk management.

Acknowledgements

The authors thank Adrien Gilbert and Benoit Urruty for assistance in the field during the installation of the dense seismic array, Sébastien Zanker for providing the water discharge measurements, and Laurent Borgniet for providing the orthophotos used in this study.

Funding

This work was supported by the Agence Nationale de la Recherche [17-CE01-0008].

Chapter 6: The physics and long-term impact of extreme floods through the lens of seismology: the case of the Storm Alex

6.1 Preface

This PhD thesis is part of a project of the French National Research Agency called SEISMORIV. Its title reads "Seismic monitoring of mountain rivers: an innovative way to quantify the control of extreme climatic events on river dynamics". When this proposal was submitted, I don't know if my thesis director Florent Gimbert would have imagined having the opportunity to study a so-called extreme climatic event. In October 2020, the Maritime Alps (southern France) were hit by the Storm Alex, which generated locally more than 600 mm of rain in less than 24 hours. This exceptional amount of rainfall triggered devastating floods in the mountain catchments of the region, causing several casualties and large infrastructure damages, and leaving an unprecedented footprint on the landscape. The catchments of the Vésubie and Roya rivers were particularly impacted and the scientific community started mobilizing its forces to study this extraordinary event. But how? The extreme flood destroyed regional rainfall and in-stream instrumentation, and the post-event field observations were still limited at that time. We decided to have a look on the signals recorded by the permanent seismic stations of the French Résif network, a research infrastructure that cover all the French territory to measure ground vibrations and the related natural hazards (e.g. earthquakes). The seismograms of the network deployed in the areas hit by the flood recorded extremely high levels of seismic power, indicating that it would have been possible to use these signals to investigate the event. In the days that followed, we contacted the colleagues of the University Côte d'Azur and we started a collaboration to analyze the physics of the flood. In this regard, I would like to thank Guillaume Piton for helping me in collecting all the information available on the event, especially thanks to his implication in the post-flood analyses.

This chapter presents and summarizes the results of the analysis carried out on the Vésubie and Roya catchments hit by the extreme flood event associated with the Storm Alex. A part of the findings has been published in a paper I co-authored. I include in this chapter the analyses presented in the paper I have been involved in. The paper is edited on the Natural Hazards and Earth System Sciences (NHESS) journal: Chmiel, M.[1,2,6], Godano, M.[1], **Piantini, M.[3]**, Brigode, P. [1,5], Gimbert, F.[3], Bakker, M.[3], Courboulex, F.[1], Ampuero, J.P.[1], Rivet, D.[1], Sladen, A.[1], Ambrois, D.[1], and Chapuis, M.[4] (2022): Brief communication: Seismological analysis of flood dynamics and hydrologically triggered earthquake swarms associated with Storm Alex, Nat. Hazards Earth Syst. Sci., 22, 1541–1558, https://doi.org/10.5194/nhess-22-1541-2022

[1] Géoazur, Observatoire de la Côte d'Azur, CNRS, IRD, Université Côte d'Azur, 06905 Sophia Antipolis, France

[2] Laboratory of Hydraulics, Hydrology and Glaciology, ETH Zürich, Zurich, Switzerland

[3] University Grenoble Alpes, CNRS, IRD, Institute for Geosciences and Environmental Research (IGE), Grenoble, France

[4] ESPACE, CNRS, Université Côte d'Azur, bd Edouard Herriot, 06204 Nice, France

[5] INRAE, UR HYCAR, Université Paris-Saclay, 1 Rue Pierre-Gilles de Gennes, 92160 Antony, France

[6] Swiss Federal Institute for Forest, Snow and Landscape Research WSL, Birmensdorf, Switzerland

Short note to the reader

The chapter contains supplementary analyses not included in the paper. In order to distinguish between them, I have highlighted the published work with the *italic font*.

Préface

Cette thèse de doctorat fait partie d'un projet de l'Agence Nationale de la Recherche française appelé SEISMORIV. Son titre est le suivant : "SEIsmic Monitoring of mountain Rivers: an innovative way to quantify the control of extreme climatic events on river dynamics". Lorsque ce projet a été soumise, je ne sais pas si mon directeur de thèse Florent aurait imaginé avoir l'opportunité d'étudier un événement climatique dit extrême. En octobre 2020, les Alpes maritimes (sud de la France) ont été frappées par la tempête Alex, qui a généré localement plus de 600 mm de pluie en moins de 24 heures. Cette quantité exceptionnelle de précipitations a déclenché des inondations dévastatrices dans les bassins versants des montagnes de la région, faisant plusieurs victimes et importants dégâts sur les infrastructures, et laissant une empreinte sans précédent sur le paysage. Les bassins versants de la Vésubie et de la Roya avaient été particulièrement touchés et la communauté scientifique avait commencé à mobiliser ses forces pour étudier cet événement extraordinaire. Mais comment ? La crue extrême avait détruit les instruments de mesure, et les observations de terrain après l'événement étaient encore limitées à l'époque. Nous avons décidé de jeter un coup d'œil aux signaux enregistrés par les stations sismiques permanentes du réseau français Résif, une infrastructure de recherche qui couvre tout le territoire français pour mesurer les vibrations du sol et les risques naturels qui y sont liés (par exemple les tremblements de terre). Les sismogrammes du réseau déployé dans les zones touchées par l'inondation avaient enregistré des niveaux de puissance sismique extrêmement élevés, indiquant qu'il aurait été possible d'utiliser ces signaux pour étudier l'événement. Dans les jours qui ont suivi, nous avons contacté les collègues de l'Université Côte d'Azur et nous avons commencé une collaboration pour analyser la physique de la crue. À ce regard, je voudrais remercier Guillaume Piton pour m'avoir aidé à récolter les informations disponibles sur l'événement, surtout grâce à son implication dans les analyses post-crue.

Ce chapitre présente et résume les résultats de l'analyse effectuée sur les bassins versants de la Vésubie et de la Roya touchés par l'événement de crue extrême associé à la tempête Alex. Une partie de ces résultats a été publiée dans un article où je suis co-auteur. J'inclus dans ce chapitre les analyses présentées dans l'article auxquelles j'ai participé. L'article est édité sur le journal Natural Hazards and Earth System Sciences (NHESS) : Chmiel, M.[1,2,6], Godano, M.[1], **Piantini, M.**[3], Brigode, P. [1,5], Gimbert, F.[3], Bakker, M.[3], Courboulex, F.[1], Ampuero, J.P.[1], Rivet, D.[1], Sladen, A.[1], Ambrois, D.[1], and Chapuis, M.[4] (2022): Brief communication: Seismological analysis of flood dynamics and hydrologically triggered earthquake swarms associated with Storm Alex, Nat. Hazards Earth Syst. Sci., 22, 1541–1558, https://doi.org/10.5194/nhess-22-1541-2022

[1] Géoazur, Observatoire de la Côte d'Azur, CNRS, IRD, Université Côte d'Azur, 06905 Sophia Antipolis, France

[2] Laboratory of Hydraulics, Hydrology and Glaciology, ETH Zürich, Zurich, Switzerland

[3] University Grenoble Alpes, CNRS, IRD, Institute for Geosciences and Environmental Research (IGE), Grenoble, France

[4] ESPACE, CNRS, Université Côte d'Azur, bd Edouard Herriot, 06204 Nice, France

Brève note au lecteur

Le chapitre contient des analyses supplémentaires qui ne figurent pas dans l'article. Afin de les distinguer, j'ai mis en évidence les travaux publiés en *italique*.

6.2 Introduction

How extreme floods events impact river morphology and landscape evolution has always been of great interest in the field of fluvial geomorphology and natural hazard management (Hooke, 2015). Many works have documented and described the morphological changes associated with such events, ranging from drastic channel widening and/or migration, variations in bed elevation, and formation of sediment bars and islands (Wolman and Miller, 1960; Magilligan et al., 1998; Marchi et al., 2010; Krapesch et al., 2011; Rinaldi et al., 2016). Several studies have also attempted at identifying the variables for predicting the channel response to extreme floods through considering the influence of hydraulic parameters (e.g. stream power, flow competence, and flood duration (Cenderelli and Wohl, 2003; Kale, 2007)). However, it has been shown that hydraulics is rarely sufficient to explain the geomorphic effects of extreme floods (Surian et al., 2016). A number of additional factors are thought to play a role, such as catchment morphometry, climate and lithology, river morphology, and sediment supply conditions (Harvey, 2001; Cenderelli and Wohl, 2003; Dean and Schmidt, 2013; Hooke, 2015; Scorpio et al., 2022). All these studies have provided material to the debate on what event magnitude and frequency are the most effective for the long-term evolution of landscape and channel stability, distinguishing between events with higher frequency but lower magnitude (from the concept of formative discharges (Wolman and Miller, 1960)), and flood events characterized by lower frequency but higher magnitude. Some authors reported relatively reduced modifications after large floods (Bryant and Gilvear, 1999), while others suggest that they might have major impacts in ephemeral streams in arid and semiarid regions (Harvey, 1984; Reid et al., 1985), bedrock channels (Jansen, 2006), or steep channels (Johnson and Warburton, 2002; Lenzi et al., 2006).

In the context of a warming climate, extreme climatic events are expected to increase in magnitude and frequency, and there is very high confidence that heavy rainfall events will become stronger as a consequence of higher temperatures (IPCC, 2022). This scenario has certainly played a role in the growing number of studies investigating the response of mountain rivers to floods generated by localized intense rainfall events, also called flash floods (Borga et al., 2014; Nelson and Dubé, 2016; Surian et al., 2016; Scorpio et al., 2018, 2022; Brenna et al., 2021). Compared to lowland, mountain catchments present all the ingredients to trigger extreme flood events associated with high water discharge and very intense sediment transport. Thanks to the steepness of the reliefs, rainfall and/or rain-on-snow events are easily transformed into surface runoff that moves rapidly through the catchment and towards channels (Wohl, 2010). Mountain rivers are also in close contact with the so-called sediment production zones (Wohl, 2010). The material produced can be stored for a variable amount of time in slope or terraces, but when destabilized by rainfall and/or surface runoff, it becomes a quasi-unlimited source of sediments for the coupled channels. Large amount of material can also be conveyed by landslides generated from the rainfall-induced failure of hillslopes. In forested catchments, these instabilities also supply large amount of wood, a factor that enhances the morphological impact of floods (Comiti et al., 2008; Lucia et al., 2015). During these events, mountain rivers transport sediments through a variety of processes for which the theoretical distinction between suspended and bedload transport valid for lowland rivers becomes incomplete. The literature usually refers to debris flows and debris floods (Iverson, 1997; Church & Jacob, 2020; Brenna et al., 2021). All these processes may also occur during the same event (Scheidl and Rickenmann, 2009).

As for lowland rivers, most studies on extreme floods in mountain rivers document pre- and post-states, aiming at quantifying the geomorphological impacts of such events within the channel and, more in general, in the landscape (e.g. Borga et al., 2014; Nelson & Dubé, 2015; Surian et al., 2015; Scorpio et al., 2018; Scorpio et al., 2022). By contrast, less is known about the physics of floods in terms of water discharge and sediment transport. This is mainly due to the lack of intra-event measurements and observations (Borga et al., 2014). Streamflow measurements of water discharge and depth are rarely documented for such events (Marchi et al., 2010). Moreover, floods often damage the instrumentation, and the morphological variations of the gauged sections (e.g. incision, sediment deposition, or widening) make the data difficult to interpret. Rainfall measurements are commonly used in order to fill this gap, and water discharges are estimated by means of rainfall-runoff models (Borga et al., 2007). Despite the usefulness of these methods, relying only on rainfall measurements without independent validations can be hazardous because the reduced spatial and temporal space associated with flash floods potentially enhance errors and uncertainties in the measurements (Zoccatelli et al., 2010). The picture gets worse for in-channel sediment transport processes, which are a difficult puzzle to solve in the case of extreme flood conditions although understanding how and when sediment moves is crucial to predict channel evolution and interpreting morphological changes (Brenna et al., 2021). This is particularly true when flash floods hit hitherto inactive streams, which therefore were not equipped with monitoring stations (Marchi et al., 2010). Some studies have shown higher sediment transport in the period following a large flood (Lenzi, 2001; Turowski et al., 2009). This is usually explained by the capability of such events to destroy bed stability, decreasing form roughness (therefore increasing transport capacity), and by an enhanced sediment availability coming from the bed and external sources. Although some works exist on the long-term evolution of sediment transport in rivers experiencing water discharge fluctuations, much less is known for extreme events during which the dramatic disruption of the bed morphology and/or the activation of bed-external sediment sources might play a role (Turowsky et al., 2009). These knowledge gaps highlight the need for an alternative way to monitor rivers to better understand the physics of extreme flood events.

Seismic methods have the potential to monitor surface and subsurface processes associated with extreme weather events. In particular, both turbulent flow and sediment transport generate ground motion in different frequency bands (Schmandt et al., 2013; Gimbert et al., 2014) that can be used to track the flood dynamics (e.g. Cook et al., 2018). Surface seismic waves are generated by impact forces exerted by mobile particles on the riverbed (e.g., Tsai et al., 2012; Gimbert et al., 2019), and ambient seismic measurements have recently been used to monitor bedload fluxes (Bakker et al., 2020; Lagarde et al., 2021). In the past decade, near-river seismic monitoring has been conducted during moderate-magnitude floods (e.g., Burtin et al., 2016; Roth et al., 2016) and controlled small-magnitude flow events (Schmandt et al., 2013, 2017). To date, extensive seismic investigations of large-magnitude flood events are rare and mostly associated with glacier lake outburst floods (Cook et al., 2018; Maurer et al., 2020) and natural hazard cascade (Cook et al., 2021).

Here, we present a set of seismological observations from 6 seismic stations from the permanent French Résif network and from the ESPACE laboratory of the Université Côte d'Azur, which captured the October 2020 extreme rainfall and flash floods caused by the Storm Alex in the southwestern Alps (Maritime Alps), southeast France (Carrega and Michelot, 2021). Three rivers

were strongly impacted: the Vésubie, the Roya, and the Tinée rivers. In this contribution we focus on the Vésubie and Roya catchments. We first present the peculiarities of this extreme event and describe the catchments of these two rivers. Then, we analyze the ground vibrations detected by the seismic stations during and after the flood, and we compare these observations with rainfall-runoff modelling (Brigode et al., 2022) and field surveys carried out after the event (RTM, 2022b, a) (Technic Reports on the Storm Alex). We show that seismic methods constitute an appealing tool to shed light on the dynamics of rivers under extreme flood conditions and on the long-term effect of the latter on sediment transport.

6.3 The Storm Alex

On 2 October 2020, the Maritime Alps were struck by a violent meteorological event called a "Mediterranean episode", caused by the Storm Alex (Carrega and Michelot, 2021). Although heavy rainfalls occur regularly in autumn in the Mediterranean region, the Storm Alex maximum daily rainfall was the highest that had occurred since the beginning of regional rainfall measurements in 1997. The rainfall started at 06:00 UTC on 2 October 2020, lasted for less than 24 h, and generated a cumulative intensity that locally exceeded three times the climatological October precipitation (at Saint-Martin-Vésubie following Météo-France, 2020), or the typical yearly average (> 600 mm, in the Roya catchment). These estimates have been obtained hourly with ANTILOPE rainfall estimation, produced by Météo-France and constrained by radar data and 40 rain gauges located in the region. The torrential rains triggered hazardous flash floods and landslides of an intensity and spatial extent that had never been documented previously in this area. The event had dramatic effects on the Vésubie and Roya catchments. After the storm, more than a thousand landslides have been identified on the hillslopes through satellite imaging (Prakash and Manconi, 2021). These soil failures damaged a number of houses and infrastructures, and conveyed large volumes of material (e.g. sediments and wood debris) to the rivers (Figure 6.1). In addition to this supply, the main channels received solid inputs by the low-order tributaries transporting all the material of the upstream sediment deposits destabilized by the heavy rains. The combination of unprecedented water discharges and massive sediment inputs affected particularly the Vésubie and Roya rivers, which experienced impressive in-channel sediment deposits of more than 4 m associated with widespread erosions of the banks with widening of the channels up to $\frac{W_{after}}{W_{before}} = 6$, where W_{after} and W_{before} are the channel width after and before the event (Technic Reports on the Storm Alex, 2022a, 2022b). As a consequence, the rivers flooded the inhabited valleys and swept away houses and infrastructure, cutting off entire communities and causing a number of casualties (Ginesta et al., 2022) (Figure 6.1).

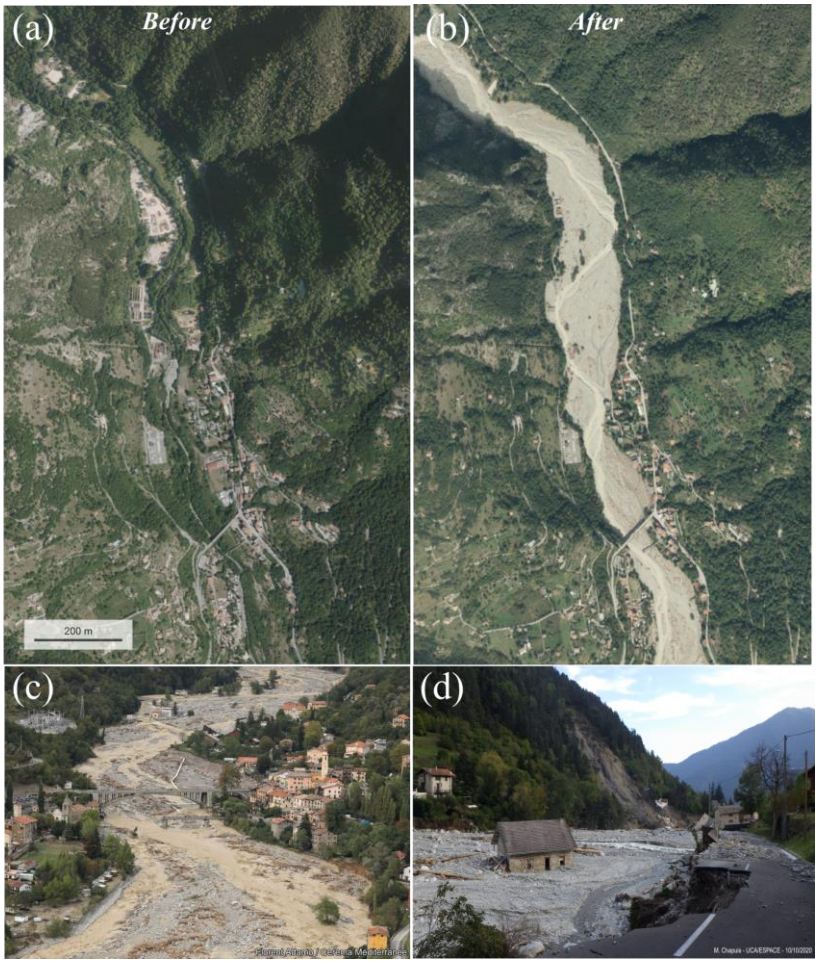

Figure 6.1 : The consequences of the Storm Alex in the Maritime Alps. (a) and (b) Aerial view showing the dramatic impact of the flood on a stretch of the Vésubie River. We can observe the extreme channel widening with large sediment accumulations on the valley. (c) Aerial view of the village of Roquebillière. (d) Partial bank collapse and deposited material next to the road in the commune of Roquebillière. Photo credits: © IGN France (https://www.geoportail.gouv.fr, 2022) for (a) and (b), and Florent Adamo/Cerema for (c) and (d).

6.4 Study area and methods

The Vésubie and Roya valleys are located at the south-eastern boundary of the French territory in the Alpes Maritimes department (Figure 6.2). The Vésubie valley is located at the end of the Alpine arc, on the southern edge of the Mercantour-Argentera massif. The source of the Vésubie river is the Lac Blanc (White Lake) at 2,665 m a.s.l, and it flows for about 45 km before joining the Var River. Its catchment area has a total surface of 392 km² and an average slope of 30%. The upper Vésubie catchment area is made up of two main sub-catchment areas: to the west, the Boréon, and to the east, the Vésubie, which flows into the Madone de Fenestre valley. The source of the Boréon is the Lac des Sagnes (Lake of Sagnes) under the south-eastern flank of the Guilié Peak (alt. 2,999 m a.s.l. – the highest point of the catchment). The Boréon receives contributions from numerous small tributaries. By crossing the Saint-Martin-Vésubie village, the water contributions come mainly from gullies on the right bank or directly from the slopes by surface runoff. After a course of 14 km, the Boréon reaches the Madone de Fenestre River. Numerous ravines covering a hundred hectares

contribute to the water and sediment contributions of the Vésubie. The Madone de Fenestre flows into the Boréon after a journey of about 14 km. The Boréon and Madone de Fenestre catchments drain the steepest reliefs with an average slope of around 60 %. From the Boréon - Madone de Fenestre confluence downstream of the village of Saint-Martin-Vésubie to the Var, the Vésubie receives water from numerous small tributaries whose catchment areas do not exceed 20 km². Among them we distinguish the Venanson River, a right-bank tributary characterized by a catchment area of 14.6 km² that flows into the Vésubie 1 km downstream of the Boréon and Madone de Fenestre, and the Gordolasque, a left-bank tributary with a catchment area of 59 km² joining the Vésubie immediately downstream of the urban crossing of Roquebillière (RTM, 2022b, 2022a).

The Roya River rises at the foot of the Col de Tende and flows into the Mediterranean Sea. Its catchment area has a total surface area of 671 km², with 89 % of the surface drained in France and 11 % in Italy. It is bordered to the west by the Vésubie catchment. The relief is steep with an average slope of 56 %. This is a characteristic feature of the Roya, with a narrow "V" shaped main valley, numerous gorges, and some wider areas corresponding to the main towns in the valley: Breil-sur-Roya, Fontan, Saint-Dalmas de Tende and Tende. The highest point of the Roya catchment, at 2935 m a.s.l, is the Grand Capelet mountain. Along its course, the Roya receives water from numerous tributaries. From upstream to downstream, among the main contributors we distinguish the Réfréi River, a left-bank tributary with a catchment area of 47 km² flowing into the Roya upstream of the town of Tende, the Levensa, a left-bank tributary of the Roya, having a catchment area of 68 km² and joining the Roya upstream of St-Dalmas de Tende, and the Cairos, right-bank tributary with a catchment area of 42 km² flowing into the Roya upstream of the village of Saorge (Figure 6.2) (RTM, 2022b, 2022a).

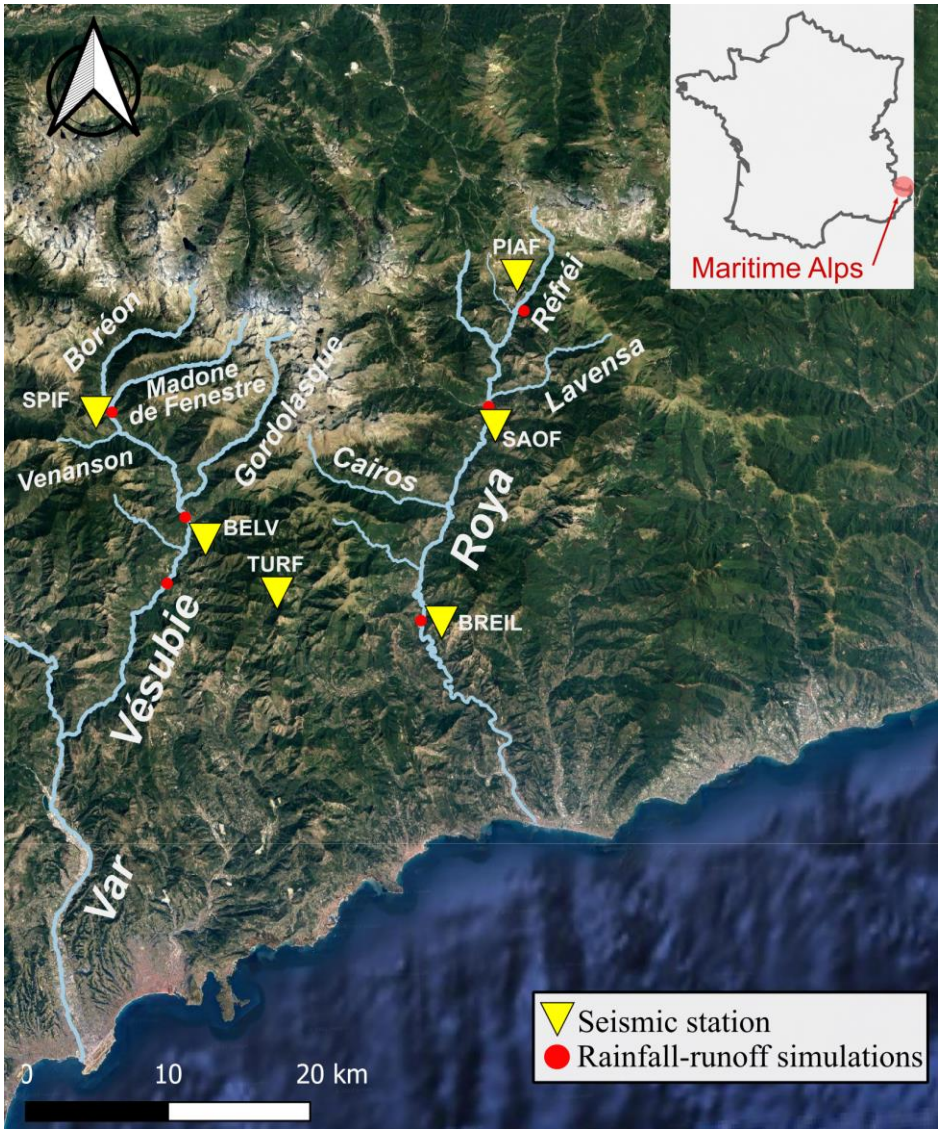

Figure 6.2 : Study area. The two catchments of the Vésubie and Roya rivers are shown with their main tributaries. The seismic stations used in this investigation are shown with yellow triangles, while the sections of the rainfall-runoff simulations are shown with red dots. The location of the site on the French territory is indicated on the top right of the figure. The background map is retrieved from © Google Maps, 2022.

We focus our analysis on the Vésubie and Roya catchments and their sub-catchments because, in addition to being two of the most strongly affected rivers in the region, the seismic station coverage is particularly suitable (Figure 6.2). We use 5 seismic stations (SPIF, BELV, TURF, PIAF, and SAOF) from the permanent French Résif network, and 1 additional geophone installed by the ESPACE laboratory of the Université Côte d'Azur (herein called BREIL, indicating the closest town). This monitoring system allows us to detect the seismic signal generated by the Storm Alex in different portions of the catchments, with the SPIF and PIAF stations being located in the upper parts of the catchments closer to headwater streams (Figure 6.2). All the information about the instruments and their locations is provided in Table 6.1

Table 6.1 : Specificities of the seismic stations used in this study. Within the second column, 3C stands for "three components".

Seismic station (ID)	Instrument type (-)	Sampling frequency (Hz)	Catchment location (-)	Closest river (-)	Distance (m)
SPIF	3C broad-band velocimeter	100	Vésubie catchment	Vésubie	1570
BELV	3C broad-band accelerometer	125	Vésubie catchment	Vésubie	630
TURF	3C broad-band velocimeter	100	Vésubie catchment	Vésubie	5970
PIAF	3C broad-band velocimeter	100	Roya catchment	Réfréi	76
SAOF	3C broad-band velocimeter	100	Roya catchment	Roya	234
BREIL	3C geophone	800	Roya catchment	Roya	20

To focus on river-generated seismic signals, we investigate high-frequency seismic signals between 2 and 45 Hz for all stations except BELV and TURF in which electronic noise does not allow us to analyze signals at frequencies higher than 20 Hz. We select this frequency band because seismic stations relatively close to the coast are sensitive to wind-waves around 1.5 Hz (Gimbert and Tsai, 2015), while at frequency $>$ 45 Hz seismic sensors are sensitive to rainfall (Bakker et al., 2021). After the removal of the instrumental response, we compute the power spectral density (PSD) of the signal recorded along the vertical by performing a fast Fourier transform with the Welch's averaging method (Welch, 1967). According to this method the time series is split into overlapping segments (here we chose an overlap of 50 %), and the final PSD results from the average of the PSDs of each segment. The temporal resolution over which the seismic power is determined depends on the goal of the analysis. We choose 5 s for investigating the seismic signal during the flood, and 10 min for long-term investigations. For these analyses we also average the data with a moving window of 5 min and 24 h in order to smooth the effects of episodic and short-lived energy signals linked to artefacts, e.g. electric signals caused by the thunderstorm, or the cyclic diurnal noise during workdays, respectively. In Section 6.5.1, which show the preliminary studies carried out in the framework of the published paper, we use slightly different input values for computing the seismic power in some of the analyses. In particular, by following previous work on debris flows (Lai et al., 2018) we investigate the signal's peak frequency in individual 200 s time windows between 2– 50 Hz. We also perform a frequency-dependent polarization analysis to determine the dominant back azimuth assuming that the seismic signature of the flood is dominated by surface waves at the SPIF station (Goodling et al., 2018). The horizontal azimuth and degree of polarization are determined based on the dominant eigenvector of the spectral covariance matrix of the three measured components (N, E, and Z), following the approach of Park et al. (1998) and its recent

application by Goodling et al. (2018). We determine these variables for 30 min intervals using 9 subwindows with 50% overlap. The dominant azimuth per frequency (θ) is obtained and given for a range $0 - 180°$ as there is a $180°$ ambiguity in this value.

Before the event, two stream gauges were installed along the Vésubie and Roya River at the Utelle and Tende stations, respectively. However, the instruments were destroyed by the flood, so that direct measures of water discharge are available only for the very first period of the flood which does not include the flood peaks. For these reasons, some studies and reports on the event have used the ANTIPOLE rainfall estimation (Brigode et al., 2022), which is produced by Météo-France, and the simple rainfall-runoff KLEM (Kinematic Local Excess Model; Borga et al., 2007) to simulate surface runoff. In this study we use the results of these simulations as estimations of water discharges for several sections along the rivers (courtesy of Pierre Brigode), which we thoroughly compare with our seismic observations. The method used for the simulations is based on the SCS-CN model that enables runoff estimations depending on the curve number (CN), an indicator of the runoff potential of a catchment. With a certain land use and specific soil properties, the CN value depends on the antecedent moisture condition. We use three different simulations which refer to different scenarios: CN70 (moderate saturation, with relatively high runoff), CN60, and CN50 (rather than dry conditions, with relatively low runoff and high infiltration) (see Supporting Information for specificities on the model).

6.5 Results

6.5.1 Preliminary observations on the Vésubie River

All three seismic stations installed in the Vésubie catchment (SPIF, BELV, and TURF) show elevated noise levels during the 24 h period starting at 07:00 UTC on 2 October 2020 that overlap with the duration of the Storm Alex (Carrega and Michelot, 2021) (Figure 6.3). The seismic power averaged in the 1–20 Hz frequency band for the SPIF and BELV stations (Figure 6.3a, b, and c) shows a rapid increase in recorded seismic power from 10:00 and 11:00 UTC, respectively. Three local seismic power maxima are visible at the SPIF and BELV stations. They are marked in color in Figure 6.3. We determine the thresholds manually; they delimit the values in seismic power when the seismic power strongly and rapidly increases. The maxima 1 and 2 are not marked in Figure 6.3c because we cannot identify them at the TURF station.

The first two seismic power maxima have pronounced high-amplitude peaks and arrive at 12:05 and 13:15 (SPIF), and 12:30 and 13:35 UTC (BELV). The third maximum has a distributed amplitude in time and occurs between ~16:00 and ~20:00 UTC at SPIF and ~16:00 and ~22:00 UTC at BELV. The seismic power recorded at the TURF station shows a progressive increase with a single broad peak between ~17:30 and ~22:00 UTC. The peak associated with the first maximum has the highest magnitude at the SPIF station, while all three maxima have similar magnitudes at the BELV station. The peak associated with the first maximum lasts for ~30 min, and that associated with the second maximum lasts for ~ 90 min. The peak associated with the third maximum is the broadest, lasting for 4 and 6 h at the SPIF and BELV stations, respectively.

For the sake of comparison with the runoff modelling, we use a linear scale for the seismic power representation in Figure 6.3a, b, and c. Runoff simulations show two runoff maxima at three analysed locations (Figure 6.3a, b, and c). The analyzed locations correspond to the river points with the shortest distance between the seismic stations and the Vésubie River and are shown in Figure 6.2.

Modelling predictions indicate that the runoff maxima occur at $14:00$, $14:25$, *and* $15:00$ *UTC (the first runoff maximum) and* $18:00$, $18:25$, *and* $19:00$ *UTC (the second runoff maximum), from upstream to downstream. The available stream gauge measurements at Utelle show a similar rapid increase in runoff to the seismic power and the rainfall–runoff model (Supporting Information). However, no maximum runoff measurements are available since the stream gauge was destroyed during the flood. To investigate potential changes in seismic noise sources, we calculate the peak frequency and the back azimuth (Figure 6.3d and e). In Figure 6.3d peak frequency values are color-coded by time, meaning that each color corresponds to the consecutive* 200 *s long time windows. The peak frequency corresponds to the frequency that has the maximum seismic power value in the analyzed time window. The peak frequency and back azimuth (*θ*, averaged in the* $3-8$ *Hz frequency band, Figure 6.3e) show a distinct value shift at the SPIF station before and during the flood. Starting from* $08:30$ *UTC multiple lightning strikes occurred at a distance of* 15 *km from the SPIF station (https://www.blitzortung.org/en/, last access: 3 November 2020, Supporting Information). At this time there are higher-amplitude arrivals visible at the SPIF station causing jumps in the peak frequency from* 2 *Hz to higher values of up to* $40-50$ *Hz at* $09:30$ *UTC (Supporting Information). These arrivals can be associated with lightning and/or thunder, rain, or anthropogenic activity. However, at* $11:00$ *UTC the peak frequency stabilizes at* 6 *Hz. Then, the peak frequency drops to* 4 *Hz at* $\sim 13:20$ *UTC and comes back to* 6 *Hz at* $\sim 15:00$ *UTC. This drop in the peak frequency coincides in time with the second seismic power maximum visible at the SPIF station. The back azimuth starts pointing along a* $100-120°$ *axis at* $10:00$ *UTC (Figure 6.3f) although the degree of polarization is relatively weak (*$\beta^2 \sim 0.5$*, Supporting Information). The dominant degree of polarization (*β^2 *in the range* $0-1$*), based on Koper and Hawley (2010), provides a measure for the confidence with which the horizontal azimuth can be interpreted, where* $\beta^2 > 0.5$ *is recommended by Goodling et al. (2018). Therefore, the back-azimuth observations should be taken with caution. The relative contributions of low-frequency (*$2-10$ *Hz) and high-frequency (*$10-45$ *Hz) seismic power are shown in Figure 6.3f. Different time periods characterized by a varying relationship between low-frequency and high-frequency seismic power can be identified: between* $08:30$ *and* $10:00$ *UTC the seismic power increases similarly in the two frequency range (slope* ~ 1*); between* $10:00$ *and* $16:00$ *UTC the high-frequency seismic power increases more strongly (slope* > 1*); and finally between* $16:00$ *UTC on 2 October and* $07:00$ *UTC on 3 October the seismic power decreases similarly. We discuss the significance of slope changes in the Discussion section.*

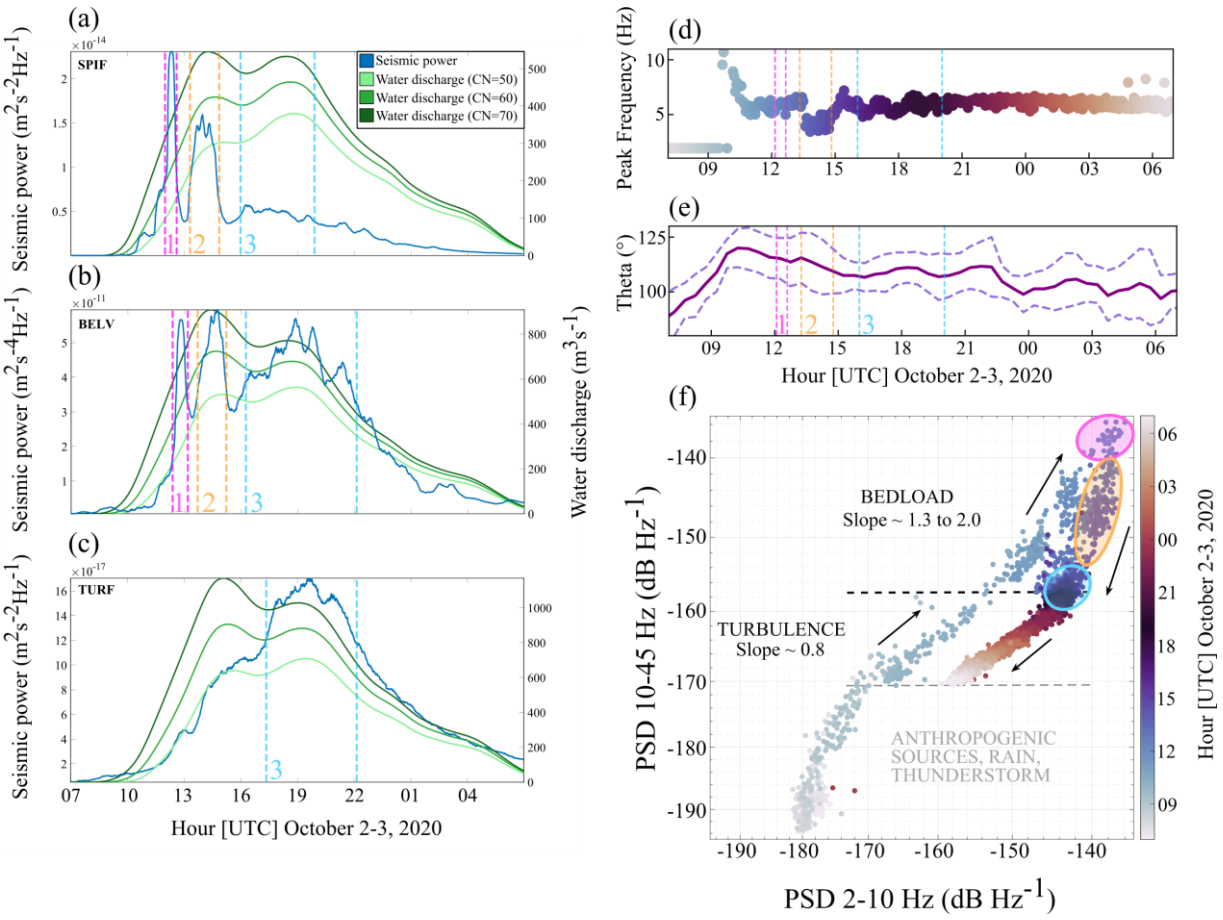

Figure 6.3 : Analysis of continuous seismic signals recorded during the Storm Alex. Seismic power (PSD) averaged between 1 and 20 Hz and recorded at stations (a) SPIF, (b) BELV, and (c) TURF. The results of the runoff simulation are marked in different shade of green (CN50, CN60, CN70), where CN denotes three different saturation scenarios of the catchment: CN70 (moderate saturation), CN60, and CN50 (rather dry conditions). Seismic power is smoothed with a moving time window of 30 min, and the runoff is calculated with a 5 min time step. (d) Peak frequency calculated for each 200 s segment. Peak frequency and the corresponding time segment are marked in the same color. (e) Back azimuth (smoothed over three consecutive 30 min time windows) calculated at the SPIF station averaged over 3– 8 Hz and its standard deviations (dashed lines). (f) Seismic power in the 2– 10 Hz frequency band versus seismic power in 10– 45 Hz at the SPIF station. All results are shown from 07: 00 UTC on 2 October to 07: 00 UTC on 3 October 2020.

6.5.2 General observations and seismic power scaling relationships with simulated water discharges

In the Vésubie catchment, the stations SPIF and BELV show elevated seismic power (PSD) from ~10: 00 UTC on 2 October to ~06: 00 UTC on 3 October in the frequency band 1– 20 Hz. The seismic power during Storm Alex is at least 20 dB and up to about 30 dB higher than the pre-flood background ambient seismic power levels. Since the decibel scale is a base-10 logarithmic scale, a 20 dB observed difference means 100-times higher seismic power. For the TURF station, the

seismic power increased by at least 100 times relative to the pre-flood conditions, especially at frequencies lower than 5 Hz (Figure 6.4a, b, c). Similar timing and values are observed in the Roya catchment, with the PIAF, SAOF, and BREIL stations being characterized by a strong increase in seismic power that starts during the morning of the 2 October, and with differences that reach 30 up to 40 dB compared to background ambient seismic noise (Figure 6.5a, b, c). Compared to the stations installed on the Vésubie, those in the Roya catchment are not limited in frequency for electric noise (see Methods), therefore we can observe that seismic power increases also at frequencies higher than 20 Hz, covering all the spectrum. It's worth mentioning that in the spectrograms of Figure 6.4 and 6.5 the background pre-flood conditions refer to night-time hours, therefore the difference in seismic power with respect to day-time hours would a bit lower, but still dramatic.

In Figure 6.4d, f, h, and 6.5d, f, and h we compare the seismic power with the water discharges simulated in the closest sections, of the closest river, to the seismic stations. With respect to the previous section in which we have done a similar exercise for the Vésubie River (Figure 6.3a, b, and c), here the analysis is characterized by two main differences. First, we now average the seismic power in the $2 - 4$ Hz frequency range because, within this range and for these distances between the seismic sensor and the channel, it is expected to be dominated by water flow turbulence (i.e. water level or discharge), rather than by other processes such as bedload transport (Gimbert et al., 2014). Second, both seismic power and water discharge are shown in the logarithmic unit (dB) in order to better visualize small variations of the two variables. We show three different simulations of water discharge referring to different saturation scenarios for the catchment (Supporting Information). We can observe that the low frequency seismic power detected by the stations follow quite closely the simulated variations in water discharge (Figure 6.4d, f, h, and Figure 6.4d, f, and h). The interpretation of the first phase of the investigated time period (between $07{:}00$ and $10{:}00$ UTC) is difficult due to several reasons. For some seismic stations, the background noise, which is calculated as the seismic noise of the day before at the same time, is elevated enough to cover the ground vibrations generated by the river (Figure 6.4d and h). Moreover, the direct comparison between water discharges and seismic power may be misleading in this phase because the simulations are performed with no initial base water flow, so that the logarithmic curve associated with water discharge begins at the first non-zero value due to the rainfall event. After the peak of the flood, the falling limb of the seismic power matches considerably the simulated decrease in water discharge for all stations (Figure 6.4 and 6.5). During the flood, several peaks are detected by both the seismic stations and the water discharge simulations (Figure 6.4e, g, i, and Figure 6.5e, g, and i). We comment on them distinguishing between the Vésubie (Figure 6.4) and Roya (Figure 6.5) catchments. The SPIF and BELV stations are characterized by three different increases in seismic power (Figure 6.4e and g). The first two peaks are relatively short-lived and more rapid, while the third one is materialized by a rather more distributed power. The first peak does not appear in the water discharge simulation, while the second and third match, albeit with a delay in the SPIF station, the peaks in the simulated water discharge for the Vésubie. Only two peaks are detected by the TURF station (Figure 6.4i), and they are concomitant with the peaks in the simulated water discharge.

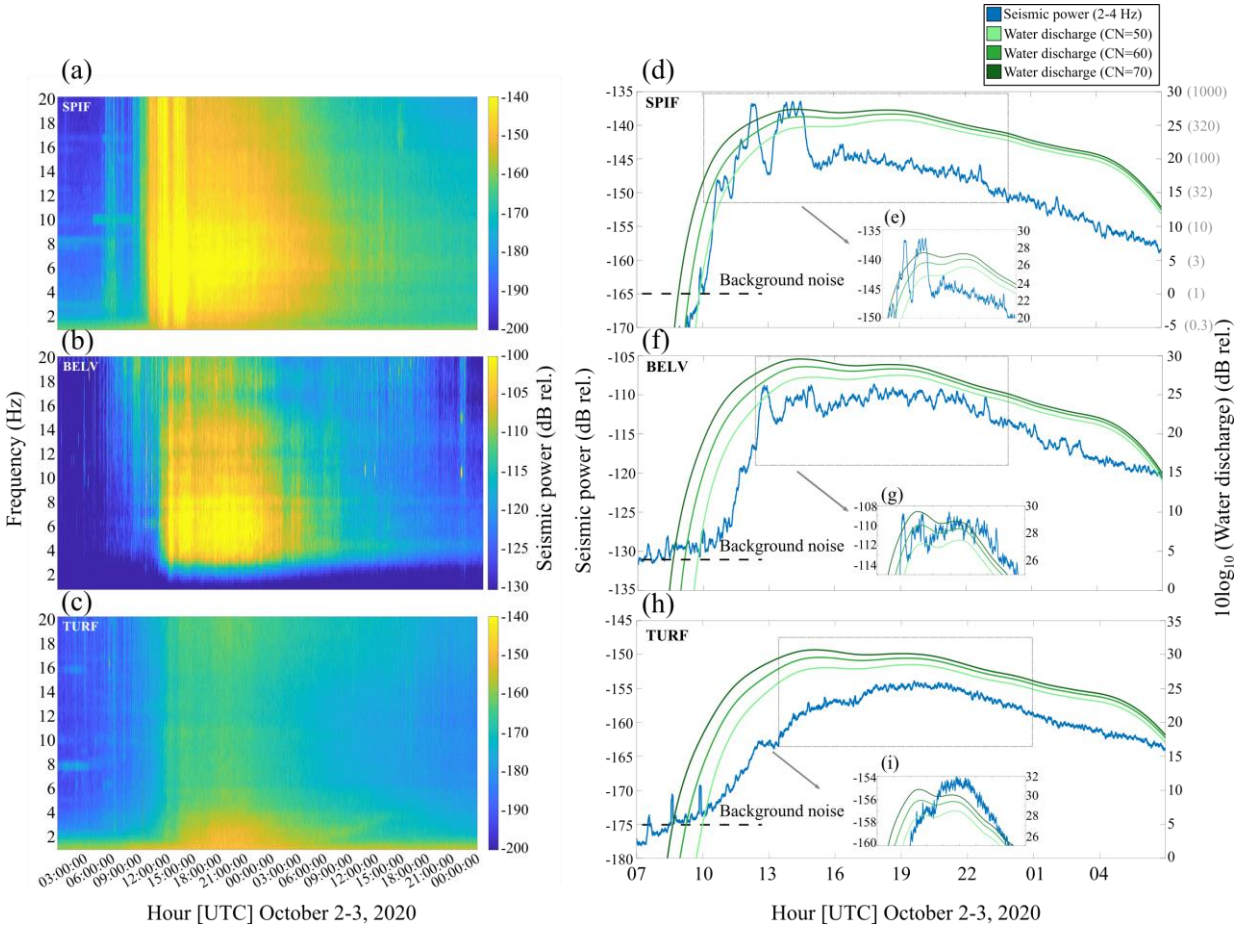

Figure 6.4 : (a) to (c) Seismic power detected by the SPIF, BELV, and TURF stations. Seismic power is shown as a function of time and frequency. Note that the BELV station is an accelerometer and not a velocimeter as the others (see table in the Methods section), and this explains why the level of seismic power is significantly higher compared to the SPIF and TURF stations. (d) to (i) Comparison between the water discharge estimations (different shades of green) and the seismic power averaged in the 2-4 Hz frequency range (cyan curve). The three simulations correspond to different CN values (see legend). Water discharges are shown as $10\log_{10}$ to match the logarithmic scale of the seismic power. The corresponding values in m^3/s are shown as an example on the right y-label of (d). The subpanels (e), (g), and (i) correspond to the zoomed time interval indicated by the dashed box in the main plots. The black horizontal dashed line indicates the level of background noise computed between 07:00 and 09:00 UTC of the day before.

At the PIAF station, which we recall being close to the Réfréi river, two main peaks in seismic power can be observed (Figure 6.5e). Although occurring later, two peaks also appear in the simulated water discharge. Interestingly, towards the end of the event (between 04: 00 and 05: 00 UTC), two small bumps are detected in both time-series and with the same delay as for the others. The comparison between the SAOF and BREIL stations and corresponding simulated water discharges show similar characteristics, with peaks visible in seismic power and water discharge simulations, in which seismic power peaks always occur earlier (Figure 6.5j and l). Interestingly, despite these time delays, the time interval between the peaks in seismic power is coherent with that of the simulated water discharges peaks.

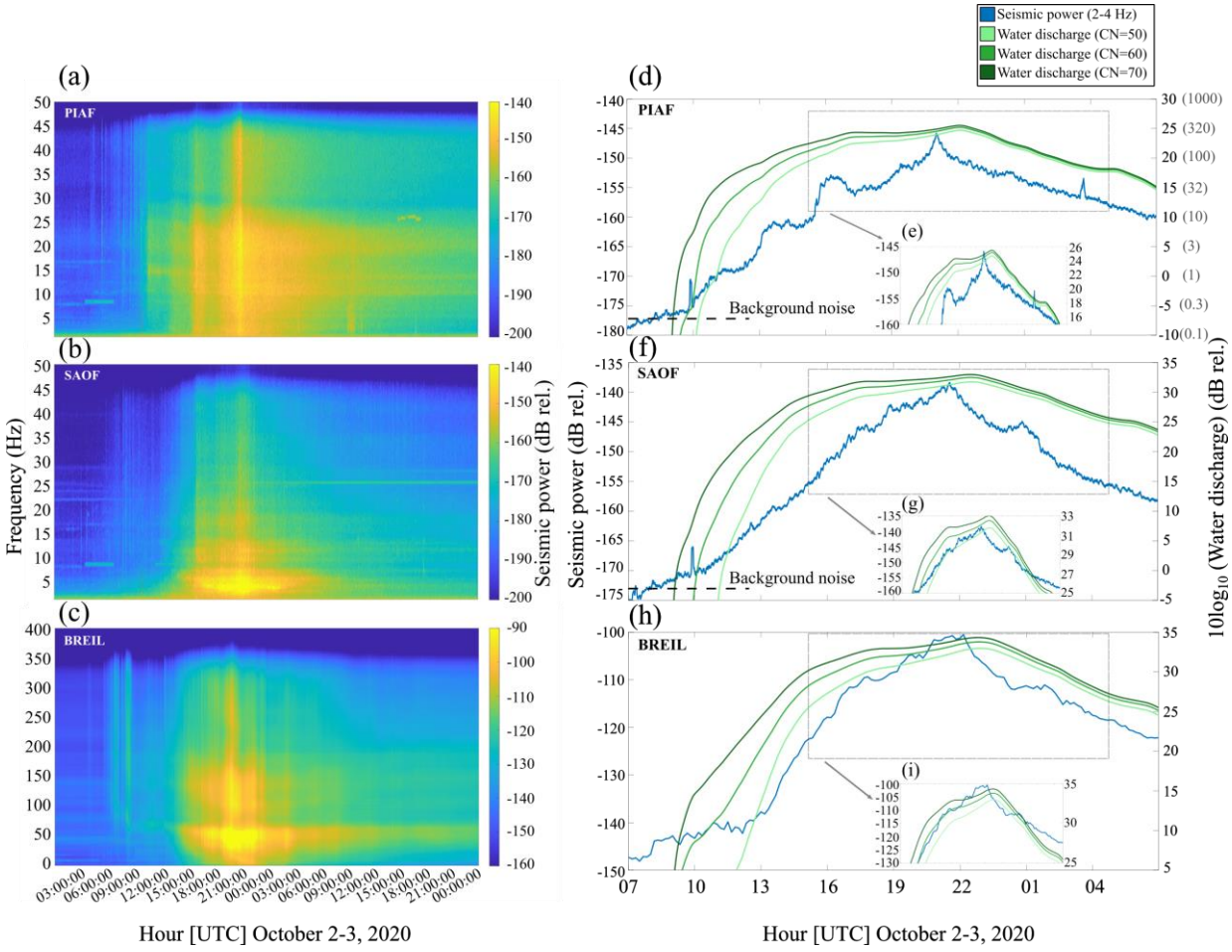

Figure 6.5 : (a) to (c) Seismic power detected by the PIAF, SAOF, and BREIL stations. Seismic power is shown as a function of time and frequency. Note the different frequency band of the BREIL station. (d) to (i) Comparison between the water discharge estimations (different shades of green) and the seismic power averaged in the 2-4 Hz frequency range (cyan curve). The three simulations correspond to different CN values (see legend). Water discharges are shown as $10\log_{10}$ to match the logarithmic scale of the seismic power. The corresponding values in m^3/s are shown as an example on the right y-label of (d). The subpanels (e), (g), and (i) correspond to the zoomed time interval indicated by the dashed box in the main plots. The black horizontal dashed line indicates the level of background noise computed between 07:00 and 09:00 UTC of the day before. Note that we do not have access to seismic data of the BREIL station before and the flood.

Until now we have compared the number and timing of these peaks, but also their amplitudes deserve comments. In particular, in almost all the stations we observe that in between the peaks, the seismic power varies in a range of 5 to 10 dB, while water discharge simulations vary between 1 to 3 dB in average (e.g. Figure 6.4e and g, and Figure 6.5e and g). This is in contrast with expectations from theories, in which seismic power scales with water discharge through a power-law of ~ 1.4 (Gimbert et al., 2016; Bakker et al., 2020). This observation makes us wonder if even at low frequencies ($2 - 4$ Hz) seismic power is sensitive to other sources than turbulence. In order to

investigate this aspect, in Figure 6.6 we plot low frequency seismic power ($2 - 4$ Hz), which we recall being considered as a proxy of water discharge, against high frequency seismic power ($20 - 40$ Hz) which is expected to be dominated by bedload transport (Gimbert et al., 2014; Bakker et al., 2020). Since the seismic signal recorded by the BELV station is affected by electric noise at frequency > 20 Hz, we choose a frequency range of $10 - 20$ Hz as characteristic of bedload transport. Following the theoretical model of Gimbert et al. (2014), within the selected frequency range bedload transport is expected to dominate over turbulence given the distance of 630 m between the BELV station and the river.[5]

As a first observation, the maximum seismic power at low frequencies always corresponds to the maximum seismic power at high frequency. For the SPIF and BELV stations we also observe a hysteretic behaviour between the rising and falling limb of the flood: same values of seismic power at low frequencies are associated with different levels of seismic power at high frequencies (from 5 to 10 dB). In general, the power-law scaling relationships are non-trivial. For the SPIF, PIAF, and BREIL stations the exponent slightly increase during the passage the flood peaks (Figure 6.6a, d, and f). By contrast, for the BELV and SAOF stations the exponent remains constant or decreases, respectively (Figure 6.6b and e). The TURF station, which is also the farthest, shows strong scatter and interpretations are difficult to be done (Figure 6.6c). Overall, it is worth emphasising that the power-law scaling relationships almost always have an exponent ~ 1, except for the first phase at the PIAF station (Figure 6.6d).

[5] The comparison between low frequency and high frequency seismic power for the SPIF station is already shown in section -- as a part of the published work. However, here we use different frequency bands which are better suited to the objective of this analysis.

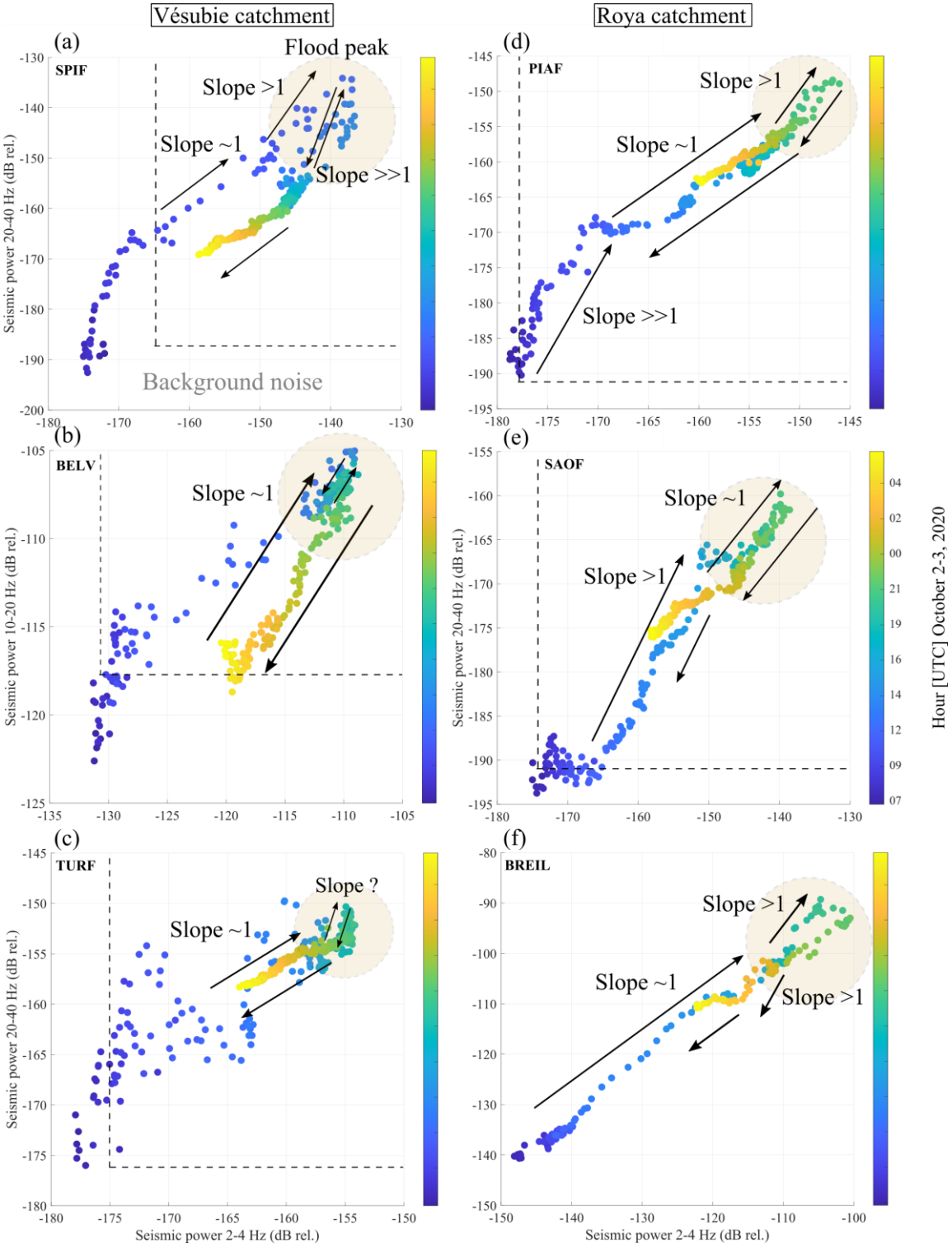

Figure 6.6 : (a) to (f) Scatterplots showing low-frequency ($2-4$ Hz) against high-frequency ($20-40$ Hz) seismic power at the different stations of the Vésubie and Roya catchments. Note that for the BELV station a frequency range of $10-20$ Hz has been used because of electric noise polluting the signal at higher frequencies. The black dashed lines highlight the seismic power associated with background noise. Note that we do not have access to seismic data of the BREIL station before and the flood. The black arrows show the evolution of the flood and the different slopes.

6.5.3 Long-term seismic signature of the rivers

After having investigated the dynamics of the river during the flood, we now explore the seismic signal detected by the seismic stations at a longer time scale, before and after the Alex Storm (September 2020 – February 2021). In Figure 6.7 we show the time series of seismic power averaged over two frequency ranges, $2-4$ Hz and $20-40$ Hz, for three seismic stations: the SPIF station close to the Vésubie (distance of 1570 m), the PIAF station close to the Réfréi (distance of 76 m), and the SAOF station close to the Roya (distance of 234 m). We do not have access to the long-term data of the other stations. For the SPIF station (Figure 6.7a) we observe that after the flooding of the Vésubie, the low frequency seismic power remained relatively high for ~ 2 months ($+3$ dB compared to the pre-flood noise), before reaching again the pre-flood noise level from November 2020. The high frequency seismic power behaves differently as ~ 10 days after the flood the seismic power returned to its previous level (Figure 6.7a). The PIAF station showed an opposite and noteworthy behaviour. Right after the flood, the low frequency seismic power returned to the pre-flood noise level, while the high frequency seismic power remained at a higher level for all the investigated time series, with an average power surplus of 8 dB. After the flood, in particular at the end of October 2020 and during winter 2020/2021 (from December 2020 to February 2021), we can observe increase in seismic power which we verify they correspond to high-flow events. Interestingly, the peaks in seismic power are much more pronounced in the high frequency signal compared to low frequencies. Concerning the SAOF station (Figure 6.7c), after the flood both the low and high frequency seismic power are characterized by an increase of ~ 3 dB for all the investigated time series. As for the PIAF station, flood events are visible at the end of October 2020 and during winter 2020/2021, but in this case the peak of seismic power are more pronounced at low frequencies.

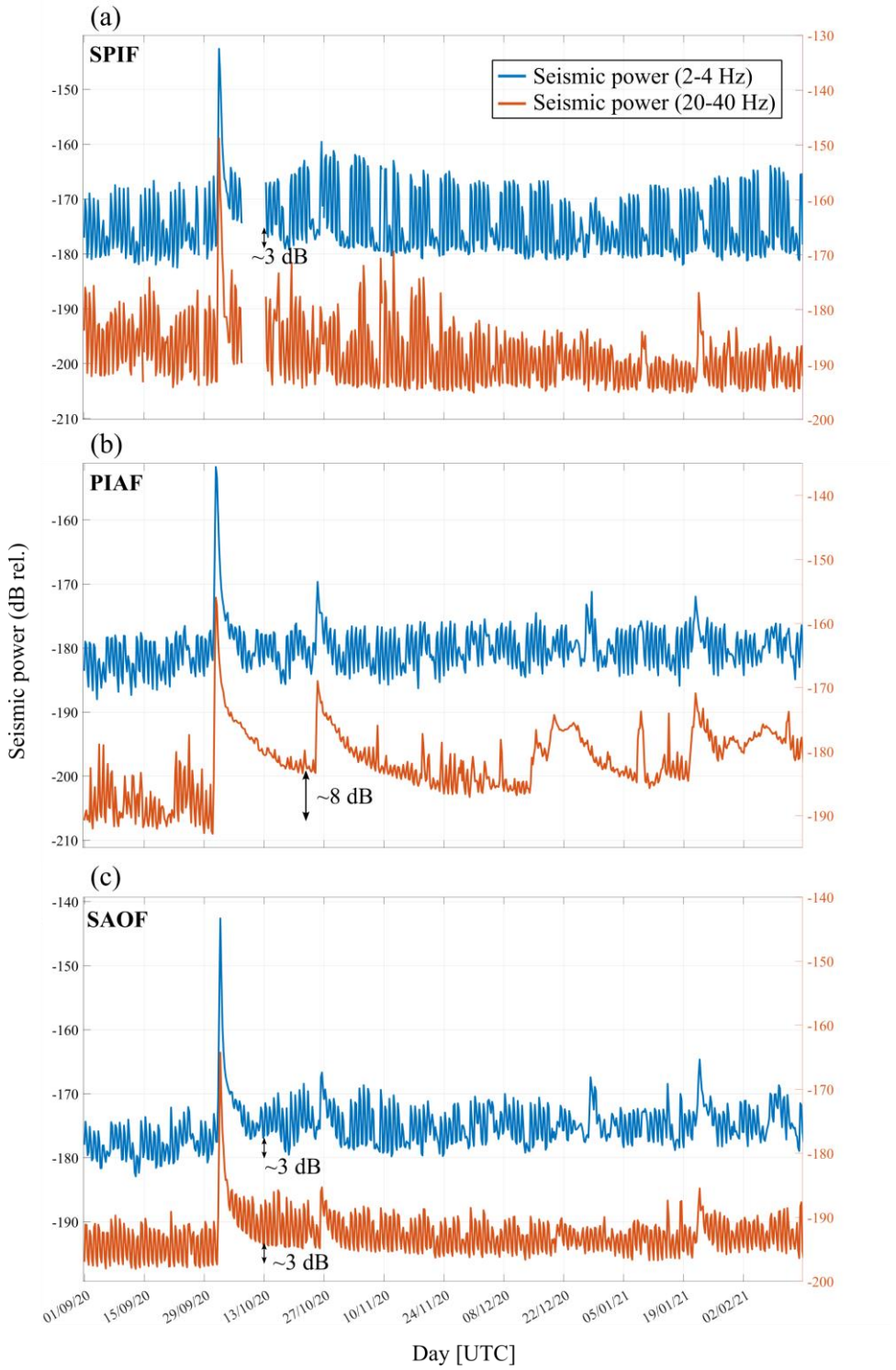

Figure 6.7 : (a) to (c) Comparison of the time-series of seismic power at low-frequency (2-4 Hz, cyan curve) and high-frequency (20-40 Hz, orange curve) for a period of 6 moths. We recall that the SPIF station refers to the Vésubie, the PIAF station to the Réfréi, and the SAOF station to the Roya River. Note that for the SPIF station in (a) there is a period of lacking data after the flood.

6.6 Discussion

6.6.1 The Vésubie River dynamics during the event

Comparison among the increased seismic power (at least 100 *and up to* 1000 *times larger than common noise levels), runoff modeling and runoff measurements indicates that the signals recorded by the SPIF, BELV, and TURF stations during Storm Alex are mostly generated by the flash flood on the Vésubie River. The rapid increase in seismic power, changes in peak frequencies, and dominant back azimuth suggest the flash flood on the Vésubie River started at about* $10:00$ *UTC. The back-azimuth values measured at the SPIF station point towards the* $110°$ *direction (Supporting Information), which does not point towards the closest river section (located at a back azimuth of* $66°$*). The back azimuth of* $\sim 110°$ *may be associated with a bending of the Vésubie River channel, a* ~ 2.5 *km long downstream reach of the Vésubie River that aligns with the estimated azimuth, or the confluence of the Venanson stream with the Vésubie River, which lies in the estimated direction (Supporting Information). This provides evidence that the commonly made assumption that the recorded seismic signals are associated with the river segments located closest to the station (e.g., Roth et al., 2016; Zhang et al., 2021) may not always be valid. Both seismic power and peak frequency are site-dependent seismic parameters; i.e., they depend on the seismic quality factor, the velocity of Rayleigh waves, and the source-station distance (Aki and Richards, 2002). However, according to a modified Tsai et al. (2012) model for hazardous flow monitoring from Lai et al. (2018), the seismic power is strongly sensitive to particle sediment size and flow speed, while the peak frequency mostly depends on the distance from the seismic source to the receiver. Also, previous observations reported no significant shift in peak frequency with varying runoff (Schmandt et al., 2013; Burtin et al., 2016). Therefore, the observed drop in the peak frequency (down to* 4 *Hz) that temporally correlates with the occurrence of the second seismic power maximum at the SPIF station can potentially be generated by a stronger, more distant source. Indeed, the flash flood impacted the adjacent hill slopes through undercutting and destabilization of the riverbanks, leading to bank, road, and bridge collapses and landslides distributed along the river network. Another possible explanation could be a tributary that becomes a dominant seismic source at this moment. However, the results of the rainfall–runoff modeling for large tributaries (the Boréon and Madone de Fenestre rivers) do not confirm this hypothesis. Also, the back-azimuth analysis does not show value changes during the second seismic power maximum. This can be due to (1) changes in the seismic source location that lie in the same general azimuthal direction; (2) the difference in timescale between back-azimuth estimates made over 30 min versus peak frequency calculations made over* 200 *s windows; or, perhaps most likely, (3) the low degree of polarization of the surface waves due to spatial spread of the source or to wave scattering.*

Since river flow turbulence is expected to preferentially generate ground motion at low frequencies compared to bedload transport (e.g., Burtin et al., 2011; Schmandt et al., 2013; Gimbert et al., 2014), the relationships between seismic power at low versus high frequencies can tell us whether our observations may be sensitive to bedload transport (Bakker et al., 2020). As the flood develops we observe a change in scaling between low- and high-frequency seismic power, materialized by a transition from a 0.8 *to a* 1.3 *scaling exponent as high-frequency seismic power becomes higher than* ~ 158 *dB (Figure 6.3f). We interpret this observation as an indication that high-frequency seismic power above the* 158 *dB threshold is mostly bedload induced. This is consistent with the expectation of enhanced bedload transport from this stage onwards due to increased bed shear stress and/or the activation of additional sediment supply sources from riverbed destabilization or bank erosion (Cook*

et al., 2018). Interestingly, after peak seismic energy has been reached, high-frequency seismic power drops drastically compared to low-frequency seismic power (with a scaling exponent of about 2), consistent with an abrupt decrease in sediment transport. Next, the low- versus high-frequency power scaling relation comes back to that observed during the early rising phase, consistent with higher frequencies over this time frame getting back to being mostly sensitive to water flow.
We also note that after the flood, the low-frequency seismic power is higher compared to before the flood ($\sim$*10 dB difference), which could be due to flood-induced changes in riverbed geometry and/or flow conditions (e.g., river roughness; Roth et al., 2017) that may preferentially affect low-frequency power. About 6 h passed between the beginning of the Storm Alex and the first flash-flood peak flow. The two seismic power maxima visible at the near-river stations (SPIF and BELV; the first maximum is marked in pink and the second one in orange in Figure 6.3) occurred in what we identified as the bedload transport phase in Figure 6.3f. Under the hypothesis that the two peaks associated with seismic power maxima represent the same moving source, we estimate their propagation velocity at* 5.8 ($\pm$1.2) *and* 4.8 ($\pm$1.5) *m/s, respectively. The details of the velocity and the error propagation calculation are given in Supporting Information. These peaks overlap in time with the first maximum of runoff simulations. Such elevated and short-lived peaks could be generated by flood waves. Similar peaks in seismic power generated by flood waves were observed during glacial lake outburst floods in the Himalayas by Cook et al. (2018) and Maurer et al. (2020). These peaks may also be associated with the passage of sediment pulses such as those experimentally investigated by Piantini et al. (2021) in a torrential river setting. Such pulses can be generated by external sediment inputs to the river, triggered by the sudden destabilization of debris deposits at the base of slopes and cliffs. The absence of the two main maxima on the TURF station can be related to a lack of sensitivity of this station to the bedload transport due to its large distance from the river (*$\sim$*6 km). Farther distance means stronger geometrical attenuation at higher frequencies versus lower frequencies and thus lower sensitivity to bedload compared to water flow (Gimbert et al., 2014). Also, this station samples a longer river segment because of its farther distance, which could smooth out moving peaks. Moreover, due to the location of the TURF station further to the east, this station can also be influenced by the flood on the Roya River that is located* $\sim$10 *km away from the station. The timing of the main seismic power maximum at the TURF station and the third seismic power maximum of the BELV station are well correlated with the runoff simulations and can be related to the maximum runoff. From maxima* 1 *to* 3*, there is a shift from short-lived peaks to a much more spread out distribution of power through time. That could be potentially related to different dynamics of the first two maxima (associated with two fast-propagating flood waves causing a sudden rise in seismic power) and a progressive increase in the seismic power associated with a progressive increase in the runoff. Finally, the differences between the observed seismic power and the runoff simulations indicate that the simple runoff simulation cannot fully explain the flash-flood dynamics. In future works, seismic observations can provide additional constraints for more accurate rainfall–runoff simulations needed to further investigate the spatio-temporal dynamics of flash floods.*

6.6.2 The relationships between seismic power and water discharge

In Section 6.5.2 we investigate the relationships between the seismic power detected by the seismic stations and the simulated water discharges. We show that the seismic power measurements follow quite well the variations of water discharges simulated for the closest

sections in the closest rivers (SPIF, BELV, and TURF for the Vésubie, SAOF and BREIL for the Roya, and PIAF for the Réfréi). As a first result, this confirm that during extreme climatic events river activity is able to generate ground vibrations that can be detected at relatively high distances (the TURF station being at ~ 6 km), as already shown in the literature also for much longer distances (Burtin et al., 2008; Cook et al., 2018; 2021). However, during the flood peaks the relationship between low frequency seismic power and water discharge is not trivial, since seismic power increases (and decreases) more strongly than the simulated water discharge. This might be due to several factors, concerning both the simulations and the seismic observations. One hypothesis is that the simulations underestimate the changes in water discharge. However, this would mean that in between the two flood peaks, the water discharge changed of 1 order of magnitude (given the increase of 10 dB in seismic power) in less than 30 minutes (e.g. Figure 6.4d and 6.5d) , which seems to be disproportioned even for an extreme flood like this one. Concerning the seismic observations, we must consider that channel geometry parameters (e.g. slope and roughness) and the relationship between water flow stage and discharge also affect the water turbulence-induced seismic signal. Given the morphological impact of the flood, we expect these factors to have changed during the event. We now comment on each of these factors. Bed roughness exerts a primary control on the seismic signature of flow turbulence at relatively low flow stage, i.e. when bed roughness and flow stage are of the same order of magnitude (Gimbert et al., 2014; Roth et al., 2017). As the flow stage attained several meters of depth, we suggest the influence of roughness elements to be negligible. Similarly, given the widespread evidences of channel widening and the massive in-channel sediment depositions (Figure 6.1), we exclude an increase in channel slope, which would have caused an increase in seismic power (Gimbert et al., 2014). Another hypothesis is a change in the relationship between flow stage and water discharge during the flood. According to Gimbert et al. (2014), the water discharge controls the low frequency seismic power because of its link with the water flow level. During flood events, strong incision in the riverbed can cause large increase in water flow level while the water discharge varies little, leading to stronger seismic signals. However, the post-flood observations of widening and in-channel depositions suggest that river incisions are unlikely to have occurred. More probably, we advance that the complex relationship between water discharge and low frequency seismic power during the flood peaks could be to the sensitivity of low frequency seismic power to sediment transport. Although bedload transport is expected to dominate over turbulence at higher frequencies (Gimbert et al., 2014; Bakker et al., 2020), it is possible that during such extreme events the massive transport of sediments and reworking of the bed generate low frequency seismic power. This could be confirmed by the first peak in seismic power (at $\Delta f = 2 - 4$ Hz) detected by the SPIF and BELV stations, which do not correspond to peak water discharges (Figure 6.4d and f).

As observed in the previous chapter, power-law scaling relationships between low- and high-frequency seismic power can be investigated to better understand fluvial processes. High values of the exponent are thought to be due to frequency bands being sensitive to different processes, while exponents ~ 1 most likely indicate a unique dominant source. Across the seismic network we observe a strong variability (Figure 6.6). For instance, during the rising limb of the flood, the exponent of the scaling relationship at the PIAF station is $>> 1$, suggesting that high sediment transport rates occurred thanks to an increased water discharge, with the two processes generating ground vibrations at different frequency bands (Figure 6.6d). During the falling limb of the flood, and for opposite reasons, this is also observed at the SPIF station (Figure 6.6a). Except

for the two specific time intervals, the power-scaling relationships are mostly characterized by an exponent ~1. We advance that this is due to high sediment transport activity being the dominant source of ground vibrations over the investigated frequency range, as observed during the flood in the Séveraisse River (see previous chapter). Sediment transport could generate low-frequency seismic power because of the transport of clasts and boulders, or the occurrence of highly concentrated sediment flows, which are likely associated with higher impact time on the riverbed producing seismic signals at lower frequency (Farin et al., 2015). This implies that the footprint of sediment transport could overlaps with that of turbulence during extreme flood events, and that this would be visible even at long distance.

6.6.3 The impact of extreme events on sediment transport

After having discussed the dynamics of the river during the flood, we explore the capability of seismic methods to explore the long-term impact of extreme floods on river dynamics. In Figure 6.7 we show that after the flood the seismic power remained in some cases high relative to the pre-flood depending. This is the case for the PIAF station, for which the post-flood high-frequency seismic power remained 8 dB higher than the pre-flood seismic level. We advance the hypothesis that this long-lasting high level of seismic power is due to high sediment transport rates in the Réfréi associated with not necessarily high water discharges occurring after the flood. The hypothesized increase of sediment transport rate following exceptional events is consistent with several findings from the literature regarding mountain rivers (Ashida et al., 1976; Lenzi et al., 1999; Turowski et al.,2009). For instance, Turowski et al. (2009) observed that ssediment transport rates in the Erlenbach increased significantly after two large events in 1995 and 2007 events over the entire range of discharges. First, the destruction or rearrangment of bed structures may had decreased form roughness. This led to an increase in total transport capacity. Second, the interlocking of grains was reduced. The 'jammed state' (Church and Zimmermann, 2007) may have been destroyed during the floods, and individual particles were thus more mobile afterwards. Third, erosion processes probably destabilized the banks and increased sediment supply from the hillslopes. We advance that all these processes may have occurred in the Réfréi. Due to the limited length of the time-series, we cannot estimate the recovery time of the river. It's worth mentioning that in some cases the high sediment transport activity has been observed for years (Turowski et al., 2009). The following floods observed at the end of October 2020 and in the winter 2020/2021 show that relatively low water discharge (inferred by seismic power at low frequencies) generated relatively high sediment transport (i.e. high seismic power at high frequencies). We advance that this is due to the perturbation exerted by the Storm Alex. This is also consistent with past observations that high magnitude flows reduced the threshold of particle motion (Masteller et al., 2019). These processes might have occurred also on the Roya close to the SAOF station, although with a lower magnitude (Figure 6.7c). We also analyze the seismic power detected by the PIAF station during a smaller flood event occurred in December 2019 (Figure 6.8). Compared to the Storm Alex, we observe that the high frequency seismic power returned to pre-flood noise level after only 2 weeks. This confirms the hypothesis that such long-term impact on sediment transport are possible only for really large flood events. It is important to note that such analyses are limited by the background noise characteristic of the site. In Figure 6.8a we can observe that the place

where the SPIF station is installed is characterized by significant daily fluctuations of seismic power. This suggest that before and after the flood, the seismic station was sensitive to other sources than the river, so that long-lasting levels of seismic power associated with river activity would be hidden by higher seismic power due to different sources. For this reason, we cannot use the SPIF station to investigate the impact of the flood on the Vésubie. Further investigations involving multiple seismic stations, at different distance and section along the rivers could be useful to better understand the overall impact of the Storm Alex on the catchments.

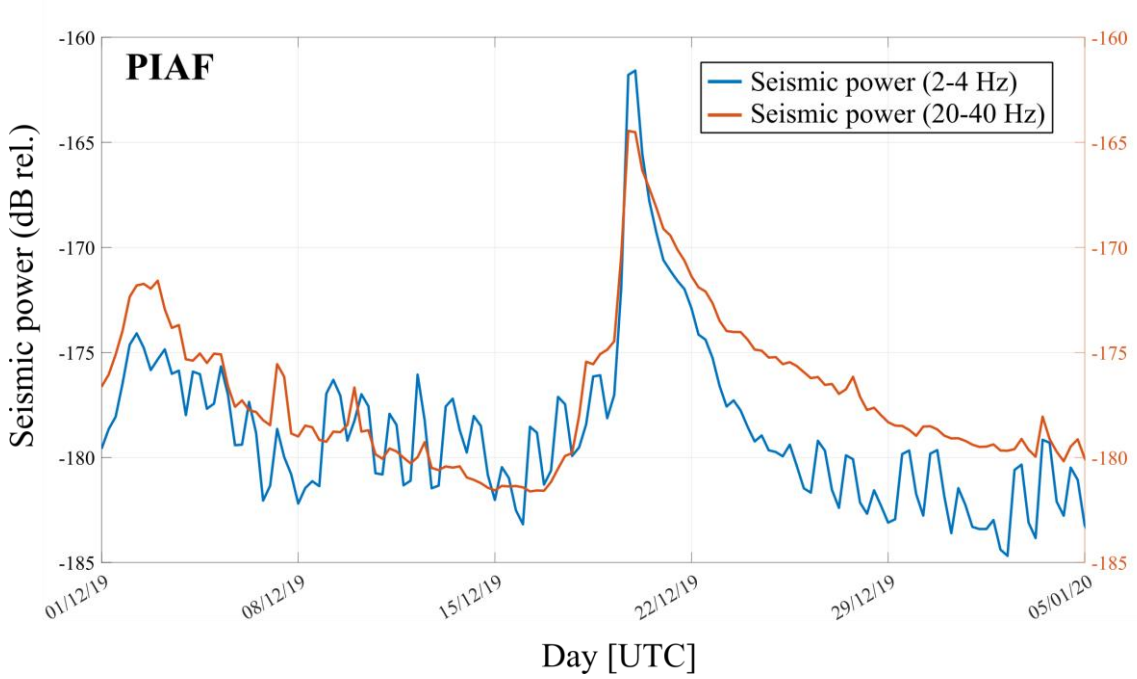

Figure 6.8 : Comparison of the time-series of seismic power at low-frequency (2-4 Hz, cyan curve) and high-frequency (20-40 Hz, orange curve) for a relatively small flood occurred in 2019.

6.7 Conclusions

On 2 October 2020, the Maritime Alps in southern France were struck by the devastating Storm Alex, which caused locally more than 600 mm of rain in less than 24 h. The extreme rainfall and flooding destroyed regional rain and stream gauges. That hindered our understanding of the spatial and temporal dynamics of rainfall–runoff processes during the storm. Here, we show that seismological observations from permanent seismic stations constrain these processes at a catchment scale. The analysis of seismic power, peak frequency, and the back azimuth provides us with the timing and velocity of the propagation of flash-flood waves associated with bedload-dominated phases of the flood on the Vésubie river. The comparison between water discharge simulations and seismic power at different stations for the Vésubie, Roya, and Réfréi rivers show a general agreement between the low frequency seismic power, considered as a proxy for water discharge, and the simulations. These promising observations suggest that seismic methods could be used to validate rainfall-runoff simulations, which are often the only way to estimate water discharges due to (i) the

paucity of stream-flow measurements and (ii) the difficulty to monitor floods. It remains to be investigated which method (i.e. seismic observations or rainfall-runoff simulations) best captures the timing of flood peaks. On the one hand, the simulations rely on rainfall measurements and estimations, which by themselves are uncertain, especially during extreme climatic events, and are built on physical assumptions that are difficult to validate (such as the velocity of water on the slopes and in the channels). On the other hand, seismic stations usually integrate the seismic vibrations over long stretches of the rivers, especially at high distance, and as discussed above they are potentially sensitive to sediment transport, which complicate the analysis of flood peaks. We suggest that these methods could be seen as complementary, providing the opportunity of better constraining the variations of water discharge during floods. Our results also show the capability of seismic methods to investigate the long-term impact of extreme flood events to sediment transport and river activity. In the case of the Réfréi river, the Alex Storm probably activated high sediment transport rates that lasted until (at least) six months after the event. In the future, installing seismic arrays at the catchment scale could help further investigate the dynamics of floods and quantify their long-term impact on sediment transport.

6.8 Supporting Information

Introduction

In text S6.1 we give detailed information about the rainfall-runoff simulations used in this study, and we show the comparison between the simulation and the stream gauge at Utelle. In text S6.2 we show through a figure the lightings and peak frequency estimations. In text S6.3 we give detailed information about the azimuth analysis and show the results of the polarization. Finally, in text S6.4 we discuss about the estimation of the propagation velocity of the peaks and its uncertainty.

S6.1 Rainfall-runoff simulations

Runoff is firstly estimated using the Soil Conservation Service curve number (SCS-CN) production function method. The SCS-CN function allows us to estimate the runoff from a rainfall event depending on the catchment saturation conditions (Figure 6.9). A simplified unit hydrograph routing function is then used to produce temporal runoff series. This analysis aims at estimating, for each studied catchment, the distances between each digital elevation model (DEM) grid cell and the considered outlet and uses the distance to root the runoff at the studied catchment outlets. A distinction is made between the distance travelled on the slopes and the distance travelled in the river (i.e., within the hydrographic network): the flow velocity on the slopes (fixed here at 0.2 *m/s) is assumed to be slower than that in the river (fixed here at* 5 *m/s). These distances are used to calculate, for each grid cell* x *belonging to a studied watershed, the transfer time* T[6] *(in seconds) between this grid cell* x *and the considered outlet:*

$$T(x) = \frac{L_h(x)}{v_h} + \frac{L_c(x)}{v_c} \tag{17}$$

[6] Note that in the published paper the transfer time is indicated with τ.

where $L_h(x)$ is the distance (on the slopes) between the grid cell x and the considered catchment outlet (m). v_h is the flow velocity on the slopes (m/s). $L_c(x)$ is the distance (in the river network) between the grid cell x and the considered catchment outlet [m]. v_c is the flow velocity in the river network (m/s). These transfer times are used to calculate the simulated flow, at time step t, at each studied outlet (denoted Q and expressed in m³/s) by the following expression (no initial base flow is considered in this study):

$$Q(t) = \int_A q(t - T(x), x)dx \tag{18}$$

where A is the catchment area upstream of the grid cell x (km²). q is the runoff estimated at time step t and at the grid cell x (m/s).

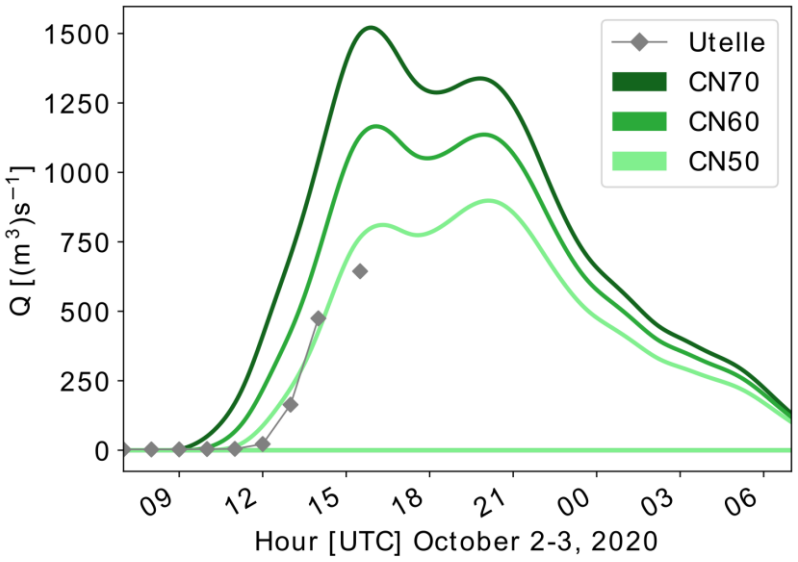

Figure 6.9 : *Runoff modelling for three different basin saturation scenarios: CN70 (moderate saturation), CN60, and CN50 (rather dry conditions). Available runoff measurements from the stream gauge at Utelle are presented in gray diamonds. The comparison between the stream gauge measurements and runoff modelling indicates rather dry basin conditions (CN50 scenario). However, there is an uncertainty in the runoff modelling related to the estimated flow velocities on the slope (0.2 m/s) and in the river (5.0 m/s). Moreover, the estimated runoff values are too low compared to the damage that occurred in the Vésubie catchment.*

S6.2 Lightning and peak frequency estimations

We report the figure following the comments made in the text. Additional information is in the caption.

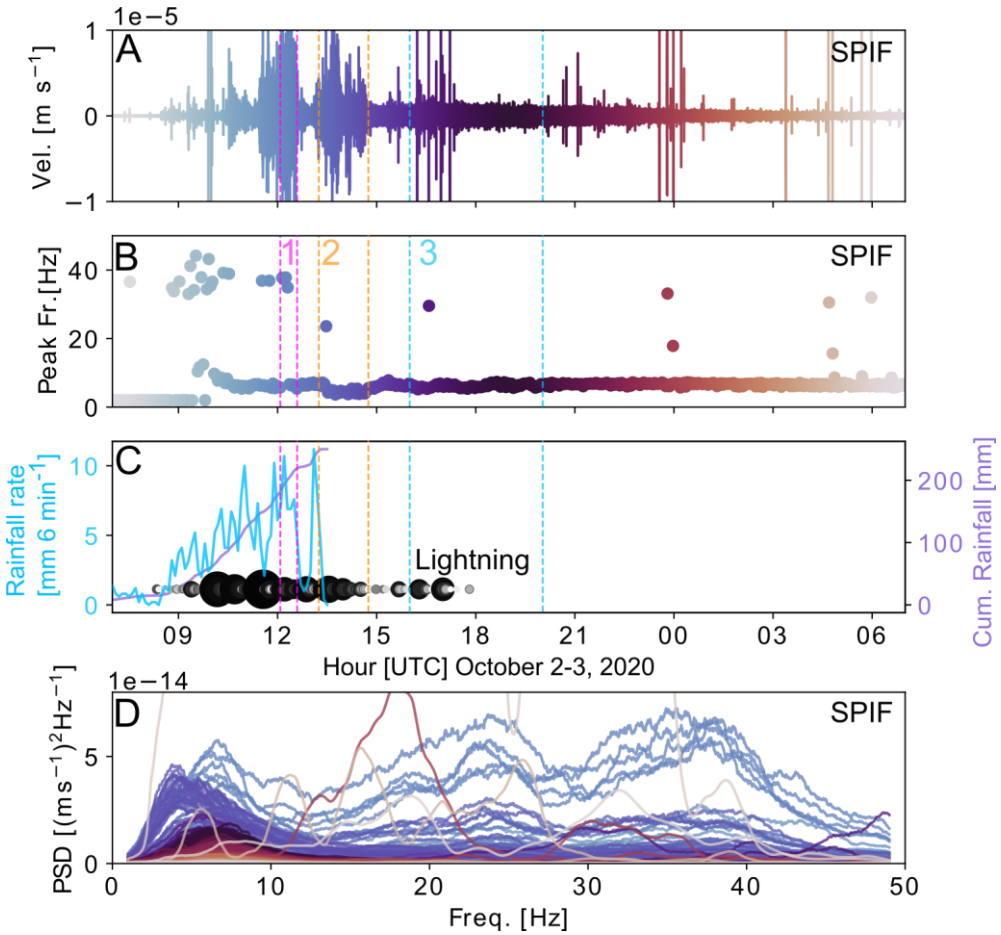

Figure 6.10 : *Analysis of seismic data recorded at the SPIF station and meteorological data. (a) Vertical ground velocity recorded filtered in* 1–50 *Hz. (b) Peak frequency calculated for each* 200 *s segment. (c) Rainfall measured by the rain gauge located at Saint-Martin-Vésubie. This is the closest rain gauge to the SPIF station located at a distance of* 1.9 *km. The measurement stopped when the instrument was destroyed. Lightning at a distance* < 15 *km from the SPIF station. Each circle represents a lightning strike; the larger and the darker the circle, the closer the lightning. (d) Seismic power calculated in windows of* 200 *s. The peak frequency, corresponding time segment, and seismic power (PSD) are marked in the same color.*

S6.3 Azimuth analysis

We perform a frequency-dependent polarization analysis to determine the dominant back azimuth assuming that the seismic signature of the flood is dominated by surface waves at the SPIF station (Goodling et al., 2018). The horizontal azimuth and degree of polarization are determined based on the dominant eigenvector of the spectral covariance matrix of the three measured components (N, E, and Z), following the approach of Park et al. (2005) and its recent application by Goodling et al. (2018). We determine these variables for 30 *min intervals using nine sub-windows with* 50% *overlap. The dominant azimuth per frequency (*θ*) is obtained and given for a range* 0–180° *as there is a* 180° *ambiguity in this value.*

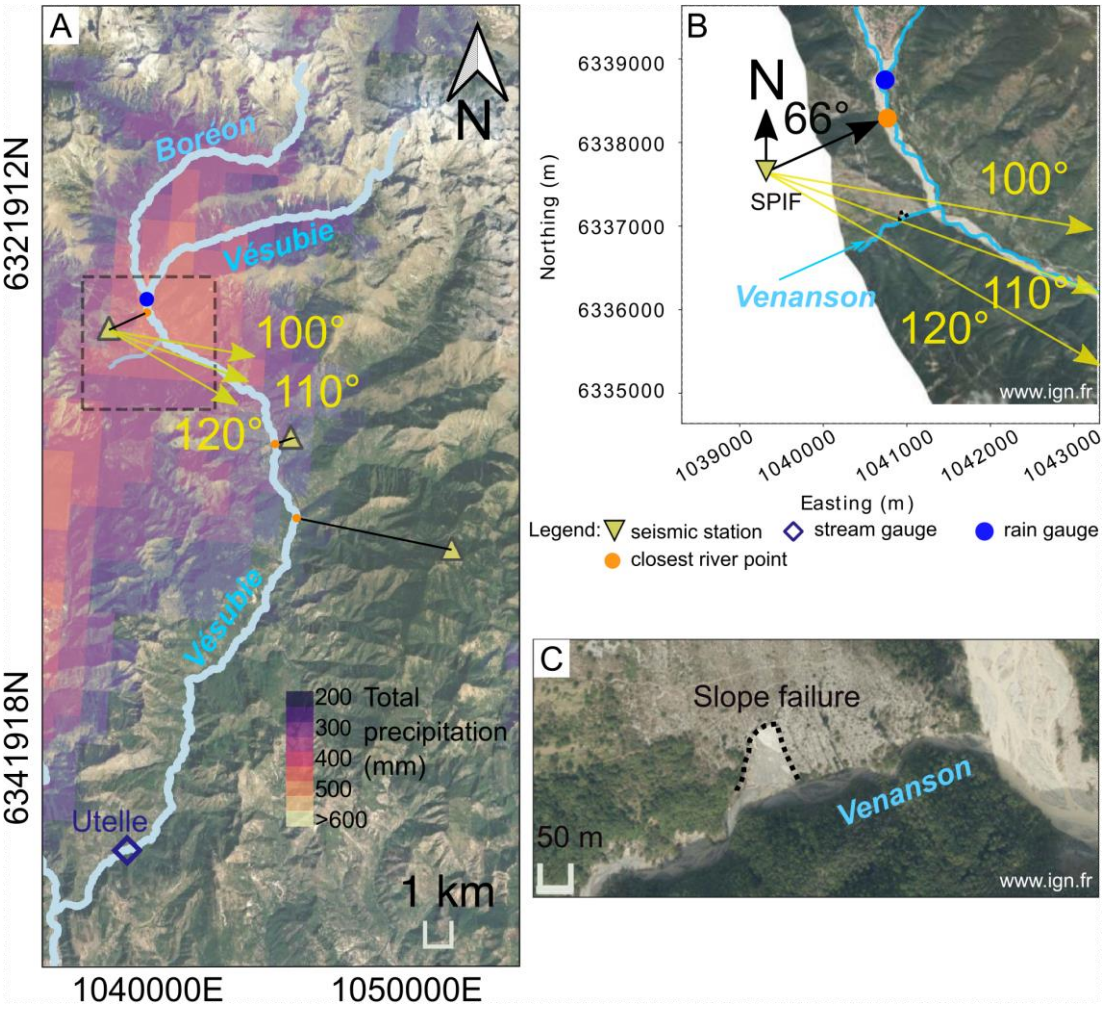

Figure 6.11 : *(a) Map section showing the Vésubie and the Boréon rivers. The 25 km² square used for the rainfall calculation is shown with dashed black lines. Background map source: © Google Maps 2021. (b) Zoomed-in view of the square marked in panel (a). Three dominant azimuths are indicated in yellow arrows, showing dominant noise directions of 100, 110, and 120° (source: IGN France, 2020). (c) Zoomed-in view of the intersection between the Venanson stream and the Vésubie River, with a slope failure indicated that is adjacent to the Venanson stream (source: IGN France, 2020).*

S6.4 Peak propagation velocity and uncertainty calculation

The peak arrival times are manually picked by taking the beginning of the maximum above fixed seismic power (PSD) thresholds (Figure 6.12). Also, we verify the time delay between the two PSDs using cross-correlation (Figure 6.13). We find two maxima of 0.30 and 0.15 at time lag values of 19 and 28 min, respectively. We calculate the peak propagation velocity as a ratio between the distance (d) of the two nearest river coordinates to the SPIF and BELV stations (8012 m) to manually pick the propagation time of the peaks (t). To calculate the distance, we use the nearest river coordinates to the stations, and we integrate the distance following the Vésubie River coordinates (8012 m). Then, we use error propagation to estimate the uncertainty in the estimated velocity propagation. For that, we use the variance formula assuming that the distance and time measurements are independent:

$$s_v = \sqrt{\left(-\frac{d}{t^2}\right)^2 s_t^2 + \left(\frac{1}{t}\right)^2 s_d^2} \qquad (19)$$

where d is the distance between the two nearest river coordinates to the SPIF and BELV stations (8012 m), t the manually picked propagation time of the peaks (s), s_t the standard deviation of the three propagation times (s) – (1) the manually picked propagation time of the peaks and (2) the two cross-correlation calculated propagation times – and s_d the standard deviation of the two distances (m) – (1) the distance between the nearest river coordinates to the SPIF and the BELV stations (8012 m) and (2) the distance of the closest river segment that aligns with the dominant back azimuth calculated at the SPIF station to the closest river coordinates to the BELV station (5512 m).

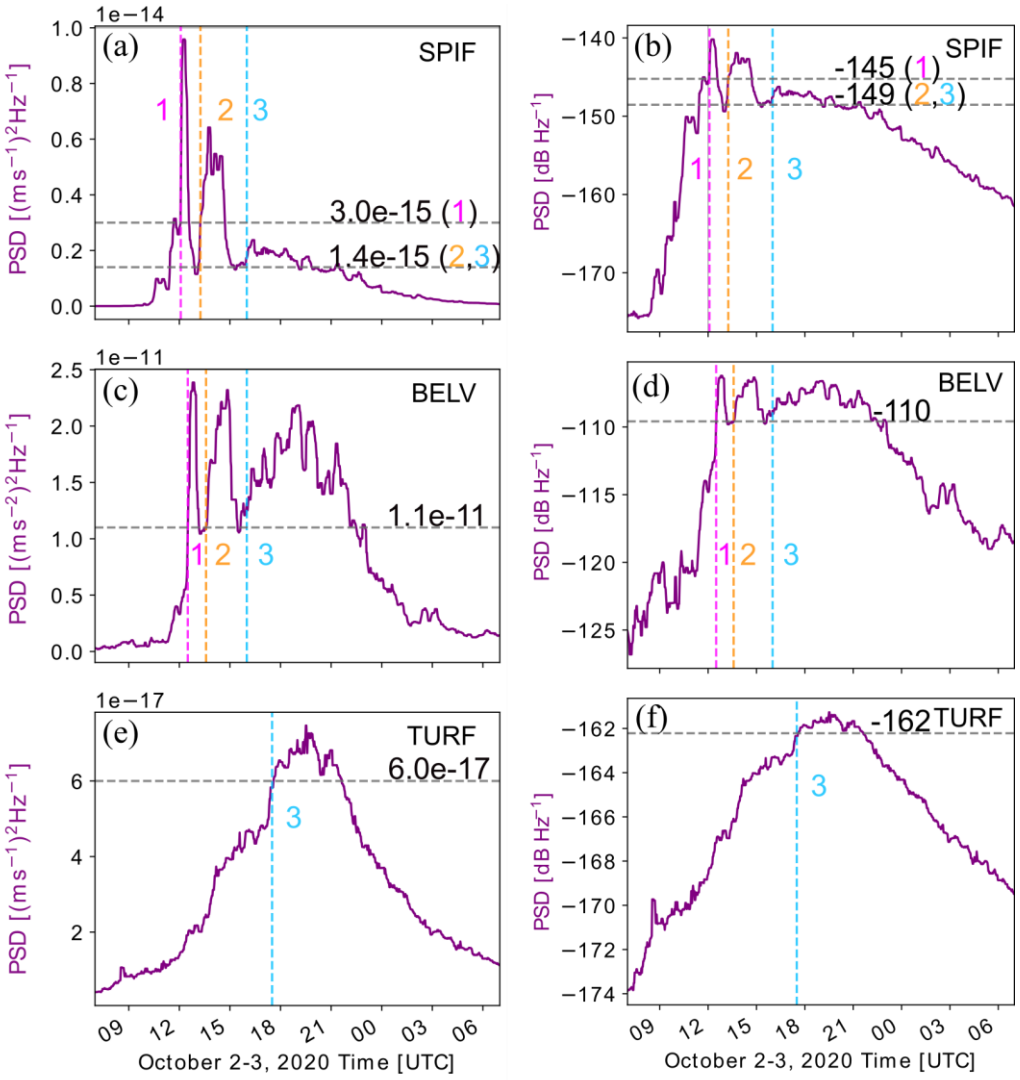

Figure 6.12 : *Seismic power (PSD) recorded at SPIF, BELV, and TURF seismic stations on a linear scale (a, c, e) and logarithmic scale (dB; b, d, f). The seismic power is averaged in the 1– 20 Hz frequency band, between 07: 00 UTC on 2 October and 07: 00 UTC on 3 October. Vertical lines show the starting hours of the three peaks, and the horizontal lines show the threshold used to define the peaks.*

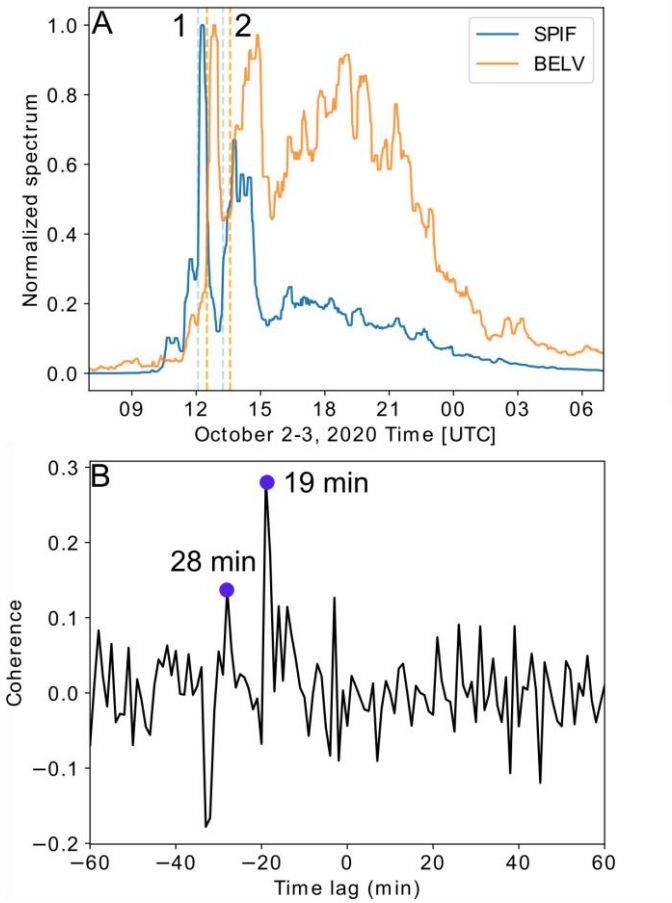

Figure 6.13 : *(a) Normalized seismic power recorded at the SPIF and the BELV stations smoothed over a 30 min moving time average. Arrivals times of peaks 1 and 2 are marked by dashed lines. (b) Normalized cross-correlation (coherence) between the normalized seismic power shown in (a).*

Chapter 7: Conclusions and perspectives

In this PhD we have tried to shed some light on the physics of intense sediment transport in mountain rivers. We have conducted a multidisciplinary study involving seismic observations that moved on two different but parallel tracks, that is, laboratory and field experiments. This diverse approach has allowed us to investigate the processes at different spatial scale and across a wide range of river settings.

Below, I summarize the specific findings and propose further developments of each thematic question we have addressed during this PhD.

Question 1 – What are the triggering and propagation dynamics associated with intense sediment transport in low-order mountain rivers, and what is their seismic signature?

1.1 The triggering and propagation dynamics of sediment pulses

In order to answer this question, we carried out downscaled laboratory experiments in the INRAE Research Centre of Grenoble. We built an original experimental setup wherein we supply liquid and solid discharge to a low-slope storage area connected to the upstream part of a 18% steep channel. Such an experimental configuration allowed us to investigate if a self-formed deposit could generate sediment pulses and how these later propagated in the downstream channel. We first focused on the processes that occurred in the storage area, that is, the triggering mechanisms. Under constant boundary conditions, when a bimodal grain size distribution with a high fraction of fine particles was used, the storage area was subject to alternating aggradation and erosion phases. We advance that the high morphological mobility of the deposit was mainly due to the presence of fine particles. In particular, if during the aggradation phase grain sorting enhanced the stability of the deposit in coarsening its surface, the infilling of the subsurface with fine particles contributed to the destabilization of the deposit by two means. First, it reduced the hydraulic conductivity of the deposit and causes the formation of a significant surface water flow that in turn increased the stresses over the armoured layer. Second, fine particles acted like a smooth carpet on which the coarser grains slide en masse. The experiments using the uniform coarse material and the bimodal mixture characterized by a low fraction of fine particles supported our hypotheses since for equal boundary conditions the deposit showed an inhibited mobility without any releases to the channel. These findings challenge the classical approach for which the sediment budget of mountain catchments is addressed in term of available volume, and the hydraulics is considered the main factor controlling the activation of external sediment supply. We advance that, in addition to hydrological conditions, the granulometric composition of sediment deposits should be carefully taken into account to assess their propensity to abruptly evacuate material to downstream channels.

With regard to the propagation mechanisms of the sediment pulses, we made the following observations. The evolution of the sediment deposit affected not only the magnitude of the sediment pulses, but also their rheology and dynamics. When major destabilizations of the upstream sediment deposit occurred, each sediment pulse can be divided into three different components: a front bedload characterized by a relatively low sediment flux made of the coarsest fraction of the mixture inherited by the destabilization of the deposit's surface; a body constituted

by the peak sediment flux and composed of a varying but significant concentration of fine particles coming from the deposit's subsurface; and a tail bedload characterized by a relatively low sediment flux and a wide grain size distribution. In particular, the body was characterized by a high solid concentration and exhibited a strong vertical rheological stratification, with surface particles being mainly driven by boundary shear stress and grain collisions, and deeper particles constituting a thick sediment flow characterized by frictional and enduring contacts. At higher slope and with similar hydraulic forcing, the sediment pulses showed intermittent dynamics dictated by the behavior of a frontal "moving dam" of coarse particles. The motion of the sediment pulse depended on the action of grain sorting processes and force chains able to destabilize the front and let the sediment pulse move forward. We found that some of all these features are remarkably similar to those of debris flows. We therefore advance that the typical anatomy of debris flows (i.e. being composed of a coarse front, a large body, and a finer tail) and dynamics (i.e. surging behavior) might result, in some case, not only from in-channel processes but also from a selective entrainments of grains occurring in the initiation zone as observed in these experiments.

1.2 The seismic signature of sediment pulses

The measurements of the seismic and force power generated during the experiments showed that the front and tail bedload dominated over highly concentrated sediment flows, which were instead associated with a strong decrease of the force fluctuations amplitude. During the passage of the highly concentrated sediment flow, we observed complex hysteresis behaviors between force fluctuations amplitude and flow surface elevation and mass that occurred during changes in the internal flow dynamics. By contrast, force fluctuations amplitude exhibited a unique negative relationship with solid concentration which suppressed the above-mentioned complexities. We advance that solid concentration best describes force fluctuations amplitude as being a proxy for particle agitation, and we propose to interpret this link within the framework of the local $\mu(I)$ rheology of dense granular flows. These findings have direct implications for existing theoretical models. Until now, force fluctuations are generally considered to be generated by roughness-controlled impacts, with solid concentration being only weakly and positively related to the amplitude of force fluctuations through its control on the number of particles impacting the bed. According to this approach, changes in solid concentration are usually neglected and its value is approximated as constant. These hypotheses hold for the front and tail bedload, consistent with this perspective being inherited from the theoretical framework of bedload transport (Tsai et al., 2012). However, we found that this approach is not suited to describe the seismic signature of our highly concentrated sediment flows. We advance that when sediment flows become denser, force fluctuations on the bed switch from being mainly generated by roughness-controlled impacts to being mainly generated by agitation-controlled impacts. In this case, the dependency of the amplitude of force fluctuations on solid concentration is negative and much stronger than expected. We therefore propose that theoretical models should incorporate a transition from roughness-controlled impacts to agitation-controlled impacts, where in the agitation-controlled regime the flow satisfies the $\mu(I)$ rheology and in particular the inverse relationship between the inertial number I and the solid concentration.

1.3 Future developments

As future developments, the experimental setup could be modified to investigate a wider range of configuration and boundary conditions. We have seen that the granulometric composition exerted

a major control on the processes that occurred in the storage area and along the channel. Our experimental equipment did not allow us to use silt and clay, but it could be interesting to test the influence of cohesive material on the processes. As the focus of our investigation was low-order mountain rivers, the bed and sidewalls were made of fixed rough elements. It could be interesting to explore the impact of (i) a different lateral confinement and (ii) a mobile bed on the propagation dynamics of the highly concentrated sediment flows. All these elements might affect (or not) the seismic signature of these sediment transport events (Haas et al., 2020), making the study of interest from a broader perspective. Finally, the seismic observations collected with these experiments could be used as a base to build a novel theoretical model for highly concentrated sediment flows taking into account our findings.

Question 2 – How can we use seismic observations to investigate intense sediment transport at the field scale and over a range of river settings?

2.1 The Séveraisse River

In summer 2019 a field experiment was set up in the Séveraisse River, a natural Alpine stream that flows from the Ecrins Massif in the French Alps. An array of 80 seismometers was installed on both river banks with the aim to investigate the physics of flood events in a 600 m long braided reach of the river. We also took advantage of a geophone installed next to a straight and laterally confined section of the river, and we complemented the seismic observations with water discharge measurements and time-lapse imagery. In this study we focused on four days (1-4 July 2019) of elevated water discharges (almost always above the modelled threshold of full particle mobility) during which we were able to capture a flood event associated with a return period of 2 to 5 years. In the first part of the study, we investigated the scaling relationships between the water discharge measurements and the seismic power recorded by the seismometer at low and high frequencies ($\Delta f = 6 - 10$ Hz and $\Delta f = 40 - 50$ Hz). Interestingly, we found that the scaling relationships varied during the flood event. For water discharges < 25 m^3/s, the power-law scaling relationships are consistent with existing theories and observations, indicating that water turbulence and bedload transport are the dominating sources of ground vibrations in the selected low and high frequency bands, respectively. However, for water discharges > 25 m^3/s the scaling relationships change and collapse over the same power-law for all the considered frequency range. We advance that this is due to sediment transport being the dominating source over the entire frequency range considered. This could be due to (i) the entrainment of relatively big grains or (ii) the passage of clusters of sediments in the form of concentrated sediment flows, which would generate ground vibrations at frequencies lower than expected because of longer particle impact times to the bed. The seismic observations also highlighted the impact of the flood on river activity, with counter-clockwise hysteresis behaviors between water discharge measurements and seismic power potentially indicating morphological changes and sustained high sediment transport rates after the event.

In the second part of the study, we explored the potential of using a dense seismic array to locate sources of ground vibrations at high spatial and temporal resolution along the braided reach of the Séveraisse River. This is the first time that such a method is applied to a river setting. During the main flood event, we observed impulsive signals that were coherently detected over the array of

seismometers. We interpreted these peaks of ground vibrations as being associated with the transport of coarse grains like clasts or blocks. Through a phase-delay analysis we were able to locate these seismic events, which were mainly distributed on the bend apex of an active branch of the reach. Since boulders were placed as bank protection in the same location, our results could indicate either their destabilisation or high sediment transport activity in this channel section. These results demonstrated the capability of a dense seismic array to locate sediment transport activity along the reach in a way that is not achievable by classic monitoring methods.

2.2 Future developments

The potential of this field experiment has yet to be entirely exploited. In this preliminary analysis the dense seismic array has been used to localize big impulsive signals. However, recent studies on an Alpine glacier have shown that a dense seismic array can be also used to track continuous and more spatially spread seismic signals, allowing in that case for the retrieval of a two-dimensional map of the subglacial drainage system (Nanni et al., 2021). These findings suggest that such a novel technique could be used in this river setting to track the displacement of landforms (e.g. islands or sediment bars) or the activation of different branches of the river during the flood, whose processes are expected to be associated with continuous seismic signals rather than impulsive signals. This would be particularly promising for the study of braided rivers, which are characterized by highly dynamic fluvial processes acting at various spatial and temporal scales.

2.3 The Vésubie and Roya catchments

In October 2020 the Maritime Alps were hit by the Storm Alex, which triggered devastating floods in the mountain catchments of the Vésubie and Roya rivers. The extreme rainfall and flooding destroyed most of the monitoring system, hindering the comprehension of the spatial and temporal dynamics of the processes occurred within the river system. We took advantage of the permanent seismic stations of the French Résif network installed in the region to investigate the physics of the event, and we complemented the seismic observations with rainfall-runoff modelling. The comparison between the estimated water discharges and seismic power at low frequencies revealed that the seismic stations were able to capture the evolution of the flood over time depicted by the simulations. However, we also observed that during the flood peaks the low frequency seismic power varied more strongly than the simulated water discharges. We advance that this is due to low frequencies being also sensitive to sediment transport, whose intensity during the flood peaks likely dominated over all the frequency range. The complementary use of seismic observations and rainfall-runoff modelling could be used to compensate the uncertainties associated with both techniques.

Through comparing the seismic signal recorded along different sections of the Vésubie and Roya rivers we gained insights on the in-channel processes associated with the flood. Along the Vésubie we observed significant peaks of seismic power occurring during the rising limb of the flood. Since these peaks do not coincide with the simulated peaks of water discharge, we suggest that they are due to the passage of either a flood wave disrupting the riverbed or a sediment pulse propagating

from the upper part of the catchment. These features were not found on the Roya and Refrei rivers, where the highest sediment transport rates likely corresponded with the peak water discharges.

Finally, we explored the capability of using seismic observations to explore the long-term impact of extreme flood on the river dynamics by analyzing the levels of seismic power after the Storm Alex. In the case of the seismic station located close to the Réfréi River, the high frequency seismic power was characterized by +8 dB compared to pre-flood conditions. Six months after the Storm Alex, the pre-flood level of seismic power wasn't yet recovered. We advance the hypothesis that this long-lasting high level of seismic power is associated with high sediment transport rates in the Réfréi which are not necessarily associated with high water discharges. We suggest that this high sediment transport activity might be due to an increased transport capacity due to a reduction of bed roughness, or increased sediment supply from the bed (e.g. due to pavement breakup) or from the hillslopes caused by landscape perturbation.

2.4 Future developments

We showed that seismic methods can be used to explore the physics of extreme floods. Networks of seismic sensors like the one used in this study cover large parts of the planet, and although being typically installed for other natural hazards (e.g. earthquakes), these seismic arrays have the potential to record a variety of geomorphic events (Cook et al., 2018; 2021). It could be interesting to build a catalogue of extreme floods occurred in different parts of the world, different river settings, and under different climatic forcing with the aim to quantify their short to long-term impacts on river activity through using seismic observations. The large dataset gathered at the multiple sites would allow extracting novel insights on the factors controlling the response of the landscape to such events and on the extent to which global climate change might play a role.

Finally, this multidisciplinary PhD has shown that intense sediment transport in mountain rivers is characterized by strong exchanges between hydraulic forcing, sediment supply conditions, and grain-to-grain interactions. These elements can be competitive or cooperative in the physics of intense sediment transport, as observed both in the laboratory and in the field. Although this complexity escapes from classical theories and monitoring techniques, we have shown that seismic methods constitute a valid tool to fill this lack of comprehension on the processes.

Bibliography

Abrahams, A. D. and Gao, P.: A bed-load transport model for rough turbulent open-channel flows on plane beds, Earth Surf. Process. Landforms, 31, 910–928, https://doi.org/10.1002/esp.1300, 2006.

Ackers, P. and White, W.: Sediment transport; new approach and analysis, Journal of the Hydraulics Division, 99, 2041–2060, 1973.

Adams, R. M.: Heartland of cities. Surveys of ancient settlement and land use on the central floodplain of the Euphrates, First Edition., University of Chicago Press, 384 pp., 1981.

Allen, R. V.: Automatic earthquake recognition and timing from single traces, Bulletin of the Seismological Society of America, 68, 1521–1532, https://doi.org/10.1785/BSSA0680051521, 1978.

Allstadt, K. E., Farin, M., Iverson, R. M., Obryk, M. K., Kean, J. W., Tsai, V. C., Rapstine, T. D., and Logan, M.: Measuring Basal Force Fluctuations of Debris Flows Using Seismic Recordings and Empirical Green's Functions, J. Geophys. Res. Earth Surf., 125, https://doi.org/10.1029/2020JF005590, 2020.

Almendros, J., Ibanez, J. M., Alguacil, G., and Del Pezzo, E.: Array analysis using circular-wave-front geometry:an application to locate the nearby seismo-volcanic source, Geophysical Journal International, 136, 159–170, https://doi.org/10.1046/j.1365-246X.1999.00699.x, 1999.

Ancey, C.: Bedload transport: a walk between randomness and determinism. Part 2. Challenges and prospects, Journal of Hydraulic Research, 58, 18–33, https://doi.org/10.1080/00221686.2019.1702595, 2020.

Ancey, C. and Heyman, J.: A microstructural approach to bed load transport: mean behaviour and fluctuations of particle transport rates, J. Fluid Mech., 744, 129–168, https://doi.org/10.1017/jfm.2014.74, 2014.

Ancey, C., Davison, A. C., Böhm, T., Jodeau, M., and Frey, P.: Entrainment and motion of coarse particles in a shallow water stream down a steep slope, J. Fluid Mech., 595, 83–114, https://doi.org/10.1017/S0022112007008774, 2008.

Arattano, M. and Moia, F.: Monitoring the propagation of a debris flow along a torrent, Hydrological Sciences Journal, 44, 811–823, https://doi.org/10.1080/02626669909492275, 1999.

Armanini, A. and Gregoretti, C.: Incipient sediment motion at high slopes in uniform flow condition: INCIPIENT MOTION, Water Resour. Res., 41, https://doi.org/10.1029/2005WR004001, 2005.

Armanini, A., Capart, H., Fraccarollo, L., and Larcher, M.: Rheological stratification in experimental free-surface flows of granular–liquid mixtures, J. Fluid Mech., 532, 269–319, https://doi.org/10.1017/S0022112005004283, 2005.

Arran, M. I., Mangeney, A., De Rosny, J., Farin, M., Toussaint, R., and Roche, O.: Laboratory Landquakes: Insights From Experiments Into the High-Frequency Seismic Signal Generated by Geophysical Granular Flows, J. Geophys. Res. Earth Surf., 126, https://doi.org/10.1029/2021JF006172, 2021.

Asano, Y. and Uchida, T.: Detailed documentation of dynamic changes in flow depth and surface velocity during a large flood in a steep mountain stream, Journal of Hydrology, 541, 127–135, https://doi.org/10.1016/j.jhydrol.2016.04.033, 2016.

Ashida, K. and Bayazit, M.: Initiation of motion and roughness of flows in steep channels, Proceedings of the 15th Congress of the International Association for Hydraulic Research, Delft, Netherlands, 475–484, 1973.

Ashmore, P. E.: How do gravel-bed rivers braid?, Can. J. Earth Sci., 28, 326–341, https://doi.org/10.1139/e91-030, 1991.

Bacchi, V., Recking, A., Eckert, N., Frey, P., Piton, G., and Naaim, M.: The effects of kinetic sorting on sediment mobility on steep slopes: GRAIN SORTING ON STEEP SLOPES, Earth Surf. Process. Landforms, 39, 1075–1086, https://doi.org/10.1002/esp.3564, 2014.

Bachelet, V., Mangeney, A., de Rosny, J., Toussaint, R., and Farin, M.: Elastic wave generated by granular impact on rough and erodible surfaces, Journal of Applied Physics, 123, 044901, https://doi.org/10.1063/1.5012979, 2018.

Bachelet, V., Mangeney, A., Toussaint, R., DeRosny, J., Farin, M., and Hibert, C.: Acoustic emissions of nearly steady and uniform granular flows: a proxy for flow dynamics and velocity fluctuations, https://doi.org/10.48550/ARXIV.2101.04161, 2021.

Badoux, A., Andres, N., and Turowski, J. M.: Damage costs due to bedload transport processes in Switzerland, Nat. Hazards Earth Syst. Sci., 14, 279–294, https://doi.org/10.5194/nhess-14-279-2014, 2014.

Baer, P., Huggel, C., McArdell, B. W., and Frank, F.: Changing debris flow activity after sudden sediment input: a case study from the Swiss Alps, Geology Today, 33, 216–223, https://doi.org/10.1111/gto.12211, 2017.

Bagnold, R. A.: An empirical correlation of bedload transport rates in flumes and natural rivers, Proc. R. Soc. Lond. A, 372, 453–473, https://doi.org/10.1098/rspa.1980.0122, 1980.

Bakker, M., Gimbert, F., Geay, T., Misset, C., Zanker, S., and Recking, A.: Field Application and Validation of a Seismic Bedload Transport Model, J. Geophys. Res. Earth Surf., 125, https://doi.org/10.1029/2019JF005416, 2020.

Basile, P., Testa, G., Moia, F., Peviani, M., and Saccardo, I.: Studio sperimentale sulla misura del trasporto solido di fondo mediante l'utilizzo di geofoni, Convegno di Idraulica e costruzioni idrauliche, Torino - Italia, 1996.

Bathurst, J. C.: Effect of Coarse Surface Layer on Bed-Load Transport, J. Hydraul. Eng., 133, 1192–1205, https://doi.org/10.1061/(ASCE)0733-9429(2007)133:11(1192), 2007.

Bathurst, J. C., Graf, W. H., and Cao, H. H.: Initiation of sediment transport in steep channels with coarse bed material, in: Mechanics of Sediment Transport, edited by: Sumer, B. M. and Müller, A., CRC Press, 207–213, https://doi.org/10.1201/9781003079019-27, 1983.

Benda, L. and Dunne, T.: Stochastic forcing of sediment supply to channel networks from landsliding and debris flow, Water Resour. Res., 33, 2849–2863, https://doi.org/10.1029/97WR02388, 1997.

Berti, M., Genevois, R., Simoni, A., and Tecca, P. R.: Field observations of a debris flow event in the Dolomites, Geomorphology, 29, 265–274, https://doi.org/10.1016/S0169-555X(99)00018-5, 1999.

Berti, M., Bernard, M., Gregoretti, C., and Simoni, A.: Physical Interpretation of Rainfall Thresholds for Runoff-Generated Debris Flows, J. Geophys. Res. Earth Surf., 125, https://doi.org/10.1029/2019JF005513, 2020.

Bertoldi, W., Zanoni, L., and Tubino, M.: Assessment of morphological changes induced by flow and flood pulses in a gravel bed braided river: The Tagliamento River (Italy), Geomorphology, 114, 348–360, https://doi.org/10.1016/j.geomorph.2009.07.017, 2010.

Bertrand, M., Liébault, F., and Piégay, H.: Debris-flow susceptibility of upland catchments, Nat Hazards, 67, 497–511, https://doi.org/10.1007/s11069-013-0575-4, 2013.

Booth, A. M., Hurley, R., Lamb, M. P., and Andrade, J. E.: Force chains as the link between particle and bulk friction angles in granular material: Granular force chains and friction angle, Geophys. Res. Lett., 41, 8862–8869, https://doi.org/10.1002/2014GL061981, 2014.

Borga, M., Boscolo, P., Zanon, F., and Sangati, M.: Hydrometeorological Analysis of the 29 August 2003 Flash Flood in the Eastern Italian Alps, Journal of Hydrometeorology, 8, 1049–1067, https://doi.org/10.1175/JHM593.1, 2007.

Borga, M., Stoffel, M., Marchi, L., Marra, F., and Jakob, M.: Hydrogeomorphic response to extreme rainfall in headwater systems: Flash floods and debris flows, Journal of Hydrology, 518, 194–205, https://doi.org/10.1016/j.jhydrol.2014.05.022, 2014.

Bovis, M. J. and Jakob, M.: The role of debris supply conditions in predicting debris flow activity, 16, 1999.

du Boys, P.: Le Rhône et les rivières à lit affouillable – Étude du régime du Rhône et de l'action exercée par les eaux sur un lit à fond de graviers indéfiniment affouillable, Annales des Ponts et Chaussées, 49, 141–195, 1879.

Brenna, A., Marchi, L., Borga, M., Ghinassi, M., Zaramella, M., and Surian, N.: Sediment–water flows in mountain catchments: Insights into transport mechanisms as responses to high-magnitude hydrological events, Journal of Hydrology, 602, 126716, https://doi.org/10.1016/j.jhydrol.2021.126716, 2021.

Brigode, P., Bourgin, F., Yassine, R., Delestre, O., and Lagrée, P.-Y.: Are Hydrologic-Hydraulic Coupling Approaches Able to Reproduce Alex Flash-Flood Dynamics and Impacts on Southeastern French Headwaters?, in: Advances in Hydroinformatics, edited by: Gourbesville, P. and Caignaert, G., Springer Nature Singapore, Singapore, 419–436, https://doi.org/10.1007/978-981-19-1600-7_27, 2022.

Brummer, C. J. and Montgomery, D. R.: Downstream coarsening in headwater channels: DOWNSTREAM COARSENING, Water Resour. Res., 39, https://doi.org/10.1029/2003WR001981, 2003.

Bryant, R. G. and Gilvear, D. J.: Quantifying geomorphic and riparian land cover changes either side of a large flood event using airborne remote sensing: River Tay, Scotland, Geomorphology, 29, 307–321, https://doi.org/10.1016/S0169-555X(99)00023-9, 1999.

Buffington, J. M. and Montgomery, D. R.: A systematic analysis of eight decades of incipient motion studies, with special reference to gravel-bedded rivers, Water Resour. Res., 33, 1993–2029, https://doi.org/10.1029/96WR03190, 1997.

Buffington, J. M., Montgomery, D. R., and Greenberg, H. M.: Basin-scale availability of salmonid spawning gravel as influenced by channel type and hydraulic roughness in mountain catchments, Can. J. Fish. Aquat. Sci., 61, 2085–2096, https://doi.org/10.1139/f04-141, 2004.

Bunte, K., Abt, S. R., Potyondy, J. P., and Ryan, S. E.: Measurement of Coarse Gravel and Cobble Transport Using Portable Bedload Traps, J. Hydraul. Eng., 130, 879–893, https://doi.org/10.1061/(ASCE)0733-9429(2004)130:9(879), 2004.

Burtin, A., Bollinger, L., Vergne, J., Cattin, R., and Nábělek, J. L.: Spectral analysis of seismic noise induced by rivers: A new tool to monitor spatiotemporal changes in stream hydrodynamics, J. Geophys. Res., 113, B05301, https://doi.org/10.1029/2007JB005034, 2008.

Burtin, A., Vergne, J., Rivera, L., and Dubernet, P.: Location of river-induced seismic signal from noise correlation functions: Location of river seismic signal, Geophysical Journal International, 182, 1161–1173, https://doi.org/10.1111/j.1365-246X.2010.04701.x, 2010.

Burtin, A., Cattin, R., Bollinger, L., Vergne, J., Steer, P., Robert, A., Findling, N., and Tiberi, C.: Towards the hydrologic and bed load monitoring from high-frequency seismic noise in a braided river: The "torrent de St Pierre", French Alps, Journal of Hydrology, 408, 43–53, https://doi.org/10.1016/j.jhydrol.2011.07.014, 2011.

Burtin, A., Hovius, N., and Turowski, J. M.: Seismic monitoring of torrential and fluvial processes, Earth Surf. Dynam., 4, 285–307, https://doi.org/10.5194/esurf-4-285-2016, 2016.

Butzer, K. W.: Long-term Nile flood variation and political discontinuities in Pharaonic Egypt, 1984.

Campbell, B.: Rivers and the Power of Ancient Rome, 608 pp., 2012.

Campbell, C. S.: Rapid Granular Flows, 36, 1990.

Campbell, C. S.: Granular shear flows at the elastic limit, J. Fluid Mech., 465, 261–291, https://doi.org/10.1017/S002211200200109X, 2002.

Carrega, P. and Michelot, N.: Une catastrophe hors norme d'origine météorologique le 2 octobre 2020 dans les montagnes des Alpes-Maritimes, physio-geo, 1–70, https://doi.org/10.4000/physio-geo.12370, 2021.

Casagli, N., Ermini, L., and Rosati, G.: Determining grain size distribution of the material composing landslide dams in the Northern Apennines: sampling and processing methods, Engineering Geology, 69, 83–97, https://doi.org/10.1016/S0013-7952(02)00249-1, 2003.

Cassar, C., Nicolas, M., and Pouliquen, O.: Submarine granular flows down inclined planes, Phys. Fluids, 17, 103301, https://doi.org/10.1063/1.2069864, 2005.

Cenderelli, D. A. and Wohl, E. E.: Flow hydraulics and geomorphic effects of glacial-lake outburst floods in the Mount Everest region, Nepal, Earth Surf. Process. Landforms, 28, 385–407, https://doi.org/10.1002/esp.448, 2003.

Chao, W.-A., Wu, Y.-M., Zhao, L., Tsai, V. C., and Chen, C.-H.: Seismologically determined bedload flux during the typhoon season, Sci Rep, 5, 8261, https://doi.org/10.1038/srep08261, 2015.

Chassagne, R., Maurin, R., Chauchat, J., and Frey, P.: Mobility of bidisperse mixtures during bedload transport, Phys. Rev. Fluids, 5, 114307, https://doi.org/10.1103/PhysRevFluids.5.114307, 2020.

Chiari, M. and Rickenmann, D.: Back-calculation of bedload transport in steep channels with a numerical model, Earth Surf. Process. Landforms, 36, 805–815, https://doi.org/10.1002/esp.2108, 2011.

Chmiel, M., Walter, F., Wenner, M., Zhang, Z., McArdell, B. W., and Hibert, C.: Machine Learning Improves Debris Flow Warning, Geophys Res Lett, 48, https://doi.org/10.1029/2020GL090874, 2021.

Church, M. and Jakob, M.: What Is a Debris Flood?, Water Resour. Res., 56, https://doi.org/10.1029/2020WR027144, 2020.

Coe, J. A., Cannon, S. H., and Santi, P. M.: Introduction to the special issue on debris flows initiated by runoff, erosion, and sediment entrainment in western North America, Geomorphology, 96, 247–249, https://doi.org/10.1016/j.geomorph.2007.05.001, 2008.

Cole, S. E., Cronin, S. J., Sherburn, S., and Manville, V.: Seismic signals of snow-slurry lahars in motion: 25 September 2007, Mt Ruapehu, New Zealand, Geophys. Res. Lett., 36, L09405, https://doi.org/10.1029/2009GL038030, 2009.

Comiti, F., Andreoli, A., Mao, L., and Lenzi, M. A.: Wood storage in three mountain streams of the Southern Andes and its hydro-morphological effects, Earth Surf. Process. Landforms, 33, 244–262, https://doi.org/10.1002/esp.1541, 2008.

Comiti, F., Cadol, D., and Wohl, E.: Flow regimes, bed morphology, and flow resistance in self-formed step-pool channels: FLOW RESISTANCE IN STEP-POOL CHANNELS, Water Resour. Res., 45, https://doi.org/10.1029/2008WR007259, 2009.

Comiti, F., Marchi, L., Macconi, P., Arattano, M., Bertoldi, G., Borga, M., Brardinoni, F., Cavalli, M., D'Agostino, V., Penna, D., and Theule, J.: A new monitoring station for debris flows in the European Alps: first observations in the Gadria basin, Nat Hazards, 73, 1175–1198, https://doi.org/10.1007/s11069-014-1088-5, 2014.

Comiti, F., Mao, L., Penna, D., Dell'Agnese, A., Engel, M., Rathburn, S., and Cavalli, M.: Glacier melt runoff controls bedload transport in Alpine catchments, Earth and Planetary Science Letters, 520, 77–86, https://doi.org/10.1016/j.epsl.2019.05.031, 2019.

Cook, K. L. and Dietze, M.: Seismic Advances in Process Geomorphology, Annu. Rev. Earth Planet. Sci., 50, 183–204, https://doi.org/10.1146/annurev-earth-032320-085133, 2022.

Cook, K. L., Andermann, C., Gimbert, F., Adhikari, B. R., and Hovius, N.: Glacial lake outburst floods as drivers of fluvial erosion in the Himalaya, Science, 362, 53–57, https://doi.org/10.1126/science.aat4981, 2018.

Cook, K. L., Rekapalli, R., Dietze, M., Pilz, M., Cesca, S., Rao, N. P., Srinagesh, D., Paul, H., Metz, M., Mandal, P., Suresh, G., Cotton, F., Tiwari, V. M., and Hovius, N.: Detection and potential early warning of catastrophic flow events with regional seismic networks, Science, 374, 87–92, https://doi.org/10.1126/science.abj1227, 2021.

Corciulo, M., Roux, P., Campillo, M., Dubucq, D., and Kuperman, W. A.: Multiscale matched-field processing for noise-source localization in exploration geophysics, GEOPHYSICS, 77, KS33–KS41, https://doi.org/10.1190/geo2011-0438.1, 2012.

Courrech du Pont, S., Gondret, P., Perrin, B., and Rabaud, M.: Granular Avalanches in Fluids, Phys. Rev. Lett., 90, 044301, https://doi.org/10.1103/PhysRevLett.90.044301, 2003.

Coviello, V., Arattano, M., and Turconi, L.: Detecting torrential processes from a distance with a seismic monitoring network, Nat Hazards, 78, 2055–2080, https://doi.org/10.1007/s11069-015-1819-2, 2015.

Coviello, V., Capra, L., Vázquez, R., and Márquez-Ramírez, V. H.: Seismic characterization of hyperconcentrated flows in a volcanic environment: Seismic characterization of hyperconcentrated flows, Earth Surf. Process. Landforms, 43, 2219–2231, https://doi.org/10.1002/esp.4387, 2018.

Coviello, V., Arattano, M., Comiti, F., Macconi, P., and Marchi, L.: Seismic Characterization of Debris Flows: Insights into Energy Radiation and Implications for Warning, J. Geophys. Res. Earth Surf., 124, 1440–1463, https://doi.org/10.1029/2018JF004683, 2019.

da Cruz, F., Emam, S., Prochnow, M., Roux, J.-N., and Chevoir, F.: Rheophysics of dense granular materials: Discrete simulation of plane shear flows, Phys. Rev. E, 72, 021309, https://doi.org/10.1103/PhysRevE.72.021309, 2005.

Cui, Y. and Parker, G.: Numerical Model of Sediment Pulses and Sediment-Supply Disturbances in Mountain Rivers, J. Hydraul. Eng., 131, 646–656, https://doi.org/10.1061/(ASCE)0733-9429(2005)131:8(646), 2005.

Cui, Y., Parker, G., Lisle, T. E., Gott, J., Hansler-Ball, M. E., Pizzuto, J. E., Allmendinger, N. E., and Reed, J. M.: Sediment pulses in mountain rivers: 1. Experiments, Water Resour. Res., 39, https://doi.org/10.1029/2002WR001803, 2003.

Curran, J. C. and Wilcock, P. R.: Effect of Sand Supply on Transport Rates in a Gravel-Bed Channel, J. Hydraul. Eng., 131, 961–967, https://doi.org/10.1061/(ASCE)0733-9429(2005)131:11(961), 2005.

Davies, T. R. and McSaveney, M. J.: The role of rock fragmentation in the motion of large landslides, Engineering Geology, 109, 67–79, https://doi.org/10.1016/j.enggeo.2008.11.004, 2009.

Dean, D. J. and Schmidt, J. C.: The geomorphic effectiveness of a large flood on the Rio Grande in the Big Bend region: Insights on geomorphic controls and post-flood geomorphic response, Geomorphology, 201, 183–198, https://doi.org/10.1016/j.geomorph.2013.06.020, 2013.

Dudill, A., Lafaye de Micheaux, H., Frey, P., and Church, M.: Introducing Finer Grains Into Bedload: The Transition to a New Equilibrium, J. Geophys. Res. Earth Surf., 123, 2602–2619, https://doi.org/10.1029/2018JF004847, 2018.

Einstein, H.: The bed-load function for sediment transportation in open channel flows, United States Department of Agriculture, 1950.

Ekström, G., Nettles, M., and Abers, G. A.: Glacial Earthquakes, Science, 302, 622–624, https://doi.org/10.1126/science.1088057, 2003.

Estep, J. and Dufek, J.: Substrate effects from force chain dynamics in dense granular flows, J. Geophys. Res., 117, 2011JF002125, https://doi.org/10.1029/2011JF002125, 2012.

Farin, M., Tsai, V. C., Lamb, M. P., and Allstadt, K. E.: A physical model of the high-frequency seismic signal generated by debris flows, Earth Surf. Process. Landforms, 44, 2529–2543, https://doi.org/10.1002/esp.4677, 2019.

Ferguson, R. I.: Channel forms and channel changes, in: British Rivers, Lewin J, 90–125, 1981.

Ferguson, R. I.: The missing dimension: effects of lateral variation on 1-D calculations of fluvial bedload transport, Geomorphology, 56, 1–14, https://doi.org/10.1016/S0169-555X(03)00042-4, 2003.

Fontana, G. D. and Marchi, L.: Slope-area relationships and sediment dynamics in two alpine streams, Hydrol. Process., 17, 73–87, https://doi.org/10.1002/hyp.1115, 2003.

Forterre, Y. and Pouliquen, O.: Flows of Dense Granular Media, Annu. Rev. Fluid Mech., 40, 1–24, https://doi.org/10.1146/annurev.fluid.40.111406.102142, 2008.

Francalanci, S., Solari, L., Toffolon, M., and Parker, G.: Do alternate bars affect sediment transport and flow resistance in gravel-bed rivers?: DO ALTERNATE BARS AFFECT SEDIMENT TRANSPORT AND FLOW RESISTANCE?, Earth Surf. Process. Landforms, 37, 866–875, https://doi.org/10.1002/esp.3217, 2012.

Frantti, G. E.: The nature of high-frequency Earth noise spectra, GEOPHYSICS, 28, 547–562, https://doi.org/10.1190/1.1439228, 1963.

Frey, P. and Church, M.: How River Beds Move, Science, 325, 1509–1510, https://doi.org/10.1126/science.1178516, 2009.

Frey, P. and Church, M.: Bedload: a granular phenomenon, Earth Surf. Process. Landforms, 36, 58–69, https://doi.org/10.1002/esp.2103, 2011.

Fryirs, K.: (Dis)Connectivity in catchment sediment cascades: a fresh look at the sediment delivery problem: (DIS)CONNECTIVITY IN CATCHMENT SEDIMENT CASCADES, Earth Surf. Process. Landforms, 38, 30–46, https://doi.org/10.1002/esp.3242, 2013.

Furbish, D. J., Schmeeckle, M. W., and Roering, J. J.: Thermal and force-chain effects in an experimental, sloping granular shear flow, Earth Surf. Process. Landforms, 33, 2108–2117, https://doi.org/10.1002/esp.1655, 2008.

GDR MiDi: On dense granular flows, Eur. Phys. J. E, 14, 341–365, https://doi.org/10.1140/epje/i2003-10153-0, 2004.

Geay, T., Belleudy, P., Gervaise, C., Habersack, H., Aigner, J., Kreisler, A., Seitz, H., and Laronne, J. B.: Passive acoustic monitoring of bed load discharge in a large gravel bed river, J. Geophys. Res. Earth Surf., 122, 528–545, https://doi.org/10.1002/2016JF004112, 2017.

Gilbert, G. K.: The transportation of debris by running water, US Geologial Survey, Washington, DC, 1914.

Gilmore, M. H.: Tracking Ocean Storms with the Seismograph, Bulletin of the American Meteorological Society, 28, 73–86, https://doi.org/10.1175/1520-0477-28.2.73, 1947.

Gimbert, F. and Tsai, V. C.: Predicting short-period, wind-wave-generated seismic noise in coastal regions, Earth and Planetary Science Letters, 426, 280–292, https://doi.org/10.1016/j.epsl.2015.06.017, 2015.

Gimbert, F., Tsai, V. C., and Lamb, M. P.: A physical model for seismic noise generation by turbulent flow in rivers, J. Geophys. Res. Earth Surf., 119, 2209–2238, https://doi.org/10.1002/2014JF003201, 2014.

Gimbert, F., Tsai, V. C., Amundson, J. M., Bartholomaus, T. C., and Walter, J. I.: Subseasonal changes observed in subglacial channel pressure, size, and sediment transport, Geophys. Res. Lett., 43, 3786–3794, https://doi.org/10.1002/2016GL068337, 2016.

Gimbert, F., Fuller, B. M., Lamb, M. P., Tsai, V. C., and Johnson, J. P. L.: Particle transport mechanics and induced seismic noise in steep flume experiments with accelerometer-embedded tracers: Experimental Testing of Seismic Noise Generated by Sediment Transport, Earth Surf. Process. Landforms, 44, 219–241, https://doi.org/10.1002/esp.4495, 2019.

Gimbert, F., Nanni, U., Roux, P., Helmstetter, A., Garambois, S., Lecointre, A., Walpersdorf, A., Jourdain, B., Langlais, M., Laarman, O., Lindner, F., Sergeant, A., Vincent, C., and Walter, F.: A Multi-Physics Experiment with a Temporary Dense Seismic Array on the Argentière Glacier, French Alps: The RESOLVE Project, Seismological Research Letters, 92, 1185–1201, https://doi.org/10.1785/0220200280, 2021.

Ginesta, M., Yiou, P., Messori, G., and Faranda, D.: A methodology for attributing severe extratropical cyclones to climate change based on reanalysis data: the case study of storm Alex 2020, Clim Dyn, https://doi.org/10.1007/s00382-022-06565-x, 2022.

Goldhirsch, I.: Rapid Granular Flows, Annu. Rev. Fluid Mech., 35, 267–293, https://doi.org/10.1146/annurev.fluid.35.101101.161114, 2003.

Gomez, B., Naff, R. L., and Hubbell, D. W.: Temporal variations in bedload transport rates associated with the migration of bedforms, Earth Surf. Process. Landforms, 14, 135–156, https://doi.org/10.1002/esp.3290140205, 1989.

Goodling, P. J., Lekic, V., and Prestegaard, K.: Seismic signature of turbulence during the 2017 Oroville Dam spillway erosion crisis, Earth Surf. Dynam., 6, 351–367, https://doi.org/10.5194/esurf-6-351-2018, 2018.

Govi, M., Maraga, F., and Moia, F.: Seismic detectors for continuous bed load monitoring in a gravel stream, Hydrological Sciences Journal, 38, 123–132, https://doi.org/10.1080/02626669309492650, 1993.

Gray, J. M. N. T.: Particle Segregation in Dense Granular Flows, Annu. Rev. Fluid Mech., 50, 407–433, https://doi.org/10.1146/annurev-fluid-122316-045201, 2018.

Gray, J. R., Laronne, J. B., and Marr, J. D. G.: Bedload-surrogate monitoring technologies: U.S. Geological Survey Scientific Investigations Report, 2010.

Gregoretti, C.: The initiation of debris flow at high slopes: experimental results, Journal of Hydraulic Research, 38, 83–88, https://doi.org/10.1080/00221680009498343, 2000.

Gregoretti, C. and Fontana, G. D.: The triggering of debris flow due to channel-bed failure in some alpine headwater basins of the Dolomites: analyses of critical runoff, Hydrol. Process., 22, 2248–2263, https://doi.org/10.1002/hyp.6821, 2008.

Gregoretti, C., Degetto, M., Bernard, M., Crucil, G., Pimazzoni, A., De Vido, G., Berti, M., Simoni, A., and Lanzoni, S.: Runoff of small rocky headwater catchments: Field observations and hydrological modeling: RUNOFF OF SMALL ROCKY HEADWATER CATCHMENTS, Water Resour. Res., 52, 8138–8158, https://doi.org/10.1002/2016WR018675, 2016.

Haas, T., Åberg, A. S., Walter, F., and Zhang, Z.: Deciphering seismic and normal-force fluctuation signatures of debris flows: An experimental assessment of effects of flow composition and dynamics, Earth Surf. Process. Landforms, esp.5168, https://doi.org/10.1002/esp.5168, 2021.

Harvey, A. M.: Geomorphological response to an extreme flood: A case from southeast Spain, Earth Surf. Process. Landforms, 9, 267–279, https://doi.org/10.1002/esp.3290090306, 1984.

Harvey, A. M.: Coupling between hillslopes and channels in upland fluvial systems: implications for landscape sensitivity, illustrated from the Howgill Fells, northwest England, CATENA, 42, 225–250, https://doi.org/10.1016/S0341-8162(00)00139-9, 2001.

Heckmann, T. and Schwanghart, W.: Geomorphic coupling and sediment connectivity in an alpine catchment — Exploring sediment cascades using graph theory, Geomorphology, 182, 89–103, https://doi.org/10.1016/j.geomorph.2012.10.033, 2013.

Heyman, J., Mettra, F., Ma, H. B., and Ancey, C.: Statistics of bedload transport over steep slopes: Separation of time scales and collective motion: BEDLOAD, TIME SCALES, AND COLLECTIVE MOTION, Geophys. Res. Lett., 40, 128–133, https://doi.org/10.1029/2012GL054280, 2013.

Hoey, T.: Temporal variations in bedload transport rates and sediment storage in gravel-bed rivers, Progress in Physical Geography: Earth and Environment, 16, 319–338, https://doi.org/10.1177/030913339201600303, 1992.

Hooke, J. M.: Variations in flood magnitude–effect relations and the implications for flood risk assessment and river management, Geomorphology, 251, 91–107, https://doi.org/10.1016/j.geomorph.2015.05.014, 2015.

Houssais, M., Ortiz, C. P., Durian, D. J., and Jerolmack, D. J.: Onset of sediment transport is a continuous transition driven by fluid shear and granular creep, Nat Commun, 6, 6527, https://doi.org/10.1038/ncomms7527, 2015.

Hsu, L., Finnegan, N. J., and Brodsky, E. E.: A seismic signature of river bedload transport during storm events: SEISMIC SIGNATURE OF RIVER BEDLOAD, Geophys. Res. Lett., 38, n/a-n/a, https://doi.org/10.1029/2011GL047759, 2011.

Hsu, L., Dietrich, W. E., and Sklar, L. S.: Mean and fluctuating basal forces generated by granular flows: Laboratory observations in a large vertically rotating drum, J. Geophys. Res. Earth Surf., 119, 1283–1309, https://doi.org/10.1002/2013JF003078, 2014.

Hu, W., Scaringi, G., Xu, Q., Pei, Z., Van Asch, T. W. J., and Hicher, P.-Y.: Sensitivity of the initiation and runout of flowslides in loose granular deposits to the content of small particles: An insight from flume tests, Engineering Geology, 231, 34–44, https://doi.org/10.1016/j.enggeo.2017.10.001, 2017.

Hu, W., Scaringi, G., Xu, Q., and Huang, R.: Internal Erosion Controls Failure and Runout of Loose Granular Deposits: Evidence From Flume Tests and Implications for Postseismic Slope Healing, Geophys. Res. Lett., 45, 5518–5527, https://doi.org/10.1029/2018GL078030, 2018.

Huang, C.-J., Yin, H.-Y., Chen, C.-Y., Yeh, C.-H., and Wang, C.-L.: Ground vibrations produced by rock motions and debris flows, J. Geophys. Res., 112, F02014, https://doi.org/10.1029/2005JF000437, 2007.

Hubbell, D. W.: Bedload sampling and analysis, Sediment Transport in Gravel-Beds Rivers, 89–106, 1987.

Hungr, O.: Analysis of debris flow surges using the theory of uniformly progressive flow, Earth Surf. Process. Landforms, 25, 483–495, https://doi.org/10.1002/(SICI)1096-9837(200005)25:5<483::AID-ESP76>3.0.CO;2-Z, 2000.

Hungr, O., Leroueil, S., and Picarelli, L.: The Varnes classification of landslide types, an update, Landslides, 11, 167–194, https://doi.org/10.1007/s10346-013-0436-y, 2014.

Imaizumi, F., Sidle, R. C., Tsuchiya, S., and Ohsaka, O.: Hydrogeomorphic processes in a steep debris flow initiation zone: Hydrogeomorphology of debris flow sites, Geophys. Res. Lett., 33, n/a-n/a, https://doi.org/10.1029/2006GL026250, 2006.

Iseya, F. and Ikeda, H.: Pulsations in Bedload Transport Rates Induced by a Longitudinal Sediment Sorting: A Flume Study using Sand and Gravel Mixtures, Geografiska Annaler: Series A, Physical Geography, 69, 15–27, https://doi.org/10.1080/04353676.1987.11880193, 1987.

Iverson, R. M.: The physics of debris flows, Rev. Geophys., 35, 245–296, https://doi.org/10.1029/97RG00426, 1997.

Iverson, R. M., Reid, M. E., and LaHusen, R. G.: Debris-flow mobilization from landslides, Annu. Rev. Earth Planet. Sci., 25, 85–138, https://doi.org/10.1146/annurev.earth.25.1.85, 1997.

Iverson, R. M., Logan, M., LaHusen, R. G., and Berti, M.: The perfect debris flow? Aggregated results from 28 large-scale experiments, J. Geophys. Res., 115, F03005, https://doi.org/10.1029/2009JF001514, 2010.

Jakob, M., Hungr, O., and Jakob, D. M.: Debris-flow hazards and related phenomena, Berlin: Springer, 2005.

Jansen, J. D.: Flood magnitude–frequency and lithologic control on bedrock river incision in post-orogenic terrain, Geomorphology, 82, 39–57, https://doi.org/10.1016/j.geomorph.2005.08.018, 2006.

John Wolcott: Nonfluvial Control of Bimodal Grain-Size Distributions in River-Bed Gravels, SEPM JSR, Vol. 58, https://doi.org/10.1306/212F8ED6-2B24-11D7-8648000102C1865D, 1988.

Johnson, R. M. and Warburton, J.: Flooding and geomorphic impacts in a mountain torrent: Raise Beck, central Lake District, England, Earth Surf. Process. Landforms, 27, 945–969, https://doi.org/10.1002/esp.386, 2002.

Kale, V. S.: Geomorphic effectiveness of extraordinary floods on three large rivers of the Indian Peninsula, Geomorphology, 85, 306–316, https://doi.org/10.1016/j.geomorph.2006.03.026, 2007.

Kanamori, H. and Given, J. W.: Analysis of long-period seismic waves excited by the May 18, 1980, eruption of Mount St. Helens-A terrestrial monopole?, J. Geophys. Res., 87, 5422–5432, https://doi.org/10.1029/JB087iB07p05422, 1982.

Kean, J. W., McCoy, S. W., Tucker, G. E., Staley, D. M., and Coe, J. A.: Runoff generated debris flows: Observations and modeling of surge initiation, magnitude, and frequency, Journal of Geophysical Research: Earth Surface, 118, 2190–2207, 2013.

Kean, J. W., Coe, J. A., Coviello, V., Smith, J. B., McCoy, S. W., and Arattano, M.: Estimating rates of debris flow entrainment from ground vibrations, Geophys. Res. Lett., 42, 6365–6372, https://doi.org/10.1002/2015GL064811, 2015.

Kishimura, K. and Izumi, K.: Seismic Signals Induced by Snow Avalnche Flow, Natural Hazards, 15, 89–100, https://doi.org/10.1023/A:1007934815584, 1997.

Krapesch, G., Hauer, C., and Habersack, H.: Scale orientated analysis of river width changes due to extreme flood hazards, Nat. Hazards Earth Syst. Sci., 11, 2137–2147, https://doi.org/10.5194/nhess-11-2137-2011, 2011.

Lagarde, S., Dietze, M., Gimbert, F., Laronne, J. B., Turowski, J. M., and Halfi, E.: Grain-Size Distribution and Propagation Effects on Seismic Signals Generated by Bedload Transport, Water Res, 57, https://doi.org/10.1029/2020WR028700, 2021.

Lai, V. H., Tsai, V. C., Lamb, M. P., Ulizio, T. P., and Beer, A. R.: The Seismic Signature of Debris Flows: Flow Mechanics and Early Warning at Montecito, California, Geophys. Res. Lett., 45, 5528–5535, https://doi.org/10.1029/2018GL077683, 2018.

Lai, Z., Vallejo, L. E., Zhou, W., Ma, G., Espitia, J. M., Caicedo, B., and Chang, X.: Collapse of Granular Columns With Fractal Particle Size Distribution: Implications for Understanding the Role of Small Particles in Granular Flows, Geophys. Res. Lett., 44, https://doi.org/10.1002/2017GL075689, 2017.

Lamand, E., Piton, G., and Recking, A.: Hydrologie et hydraulique torrentielle, étude d'un cas pratique: la Roize, 90, 2017.

Lamb, M. P., Dietrich, W. E., and Venditti, J. G.: Is the critical Shields stress for incipient sediment motion dependent on channel-bed slope?, J. Geophys. Res., 113, F02008, https://doi.org/10.1029/2007JF000831, 2008.

Lane, E.: Design of stable channels, Transactions of the American Society of Civil Engineers, 120, 1234– 1260, 1955.

Larose, E., Carrière, S., Voisin, C., Bottelin, P., Baillet, L., Guéguen, P., Walter, F., Jongmans, D., Guillier, B., Garambois, S., Gimbert, F., and Massey, C.: Environmental seismology: What can we learn on earth surface processes with ambient noise?, Journal of Applied Geophysics, 116, 62–74, https://doi.org/10.1016/j.jappgeo.2015.02.001, 2015.

Lee, A. J. and Ferguson, R. I.: Velocity and flow resistance in step-pool streams, Geomorphology, 46, 59–71, https://doi.org/10.1016/S0169-555X(02)00054-5, 2002.

Lee, D. B. and Jerolmack, D.: Determining the scales of collective entrainment in collision-driven bed load, Earth Surf. Dynam., 6, 1089–1099, https://doi.org/10.5194/esurf-6-1089-2018, 2018.

Legaz, A., Revil, A., Roux, P., Vandemeulebrouck, J., Gouédard, P., Hurst, T., and Bolève, A.: Self-potential and passive seismic monitoring of hydrothermal activity: A case study at Iodine Pool, Waimangu geothermal valley, New Zealand, Journal of Volcanology and Geothermal Research, 179, 11–18, https://doi.org/10.1016/j.jvolgeores.2008.09.015, 2009.

Lenzi, M. A.: Step-pool evolution in the Rio Cordon, northeastern Italy, Earth Surf. Process. Landforms, 26, 991–1008, https://doi.org/10.1002/esp.239, 2001.

Lenzi, M. A., D'Agostino, V., and Billi, P.: Bedload transport in the instrumented catchment of the Rio Cordon, CATENA, 36, 171–190, https://doi.org/10.1016/S0341-8162(99)00016-8, 1999.

Lenzi, M. A., Mao, L., and Comiti, F.: Magnitude-frequency analysis of bed load data in an Alpine boulder bed stream, Water Resour. Res., 40, https://doi.org/10.1029/2003WR002961, 2004.

Lenzi, M. A., Mao, L., and Comiti, F.: Effective discharge for sediment transport in a mountain river: Computational approaches and geomorphic effectiveness, Journal of Hydrology, 326, 257–276, https://doi.org/10.1016/j.jhydrol.2005.10.031, 2006.

Liébault, F., Laronne, J. B., Klotz, S., and Bel, C.: Seasonal bedload pulses in a small alpine catchment, Geomorphology, 398, 108055, https://doi.org/10.1016/j.geomorph.2021.108055, 2022.

Linares-Guerrero, E., Goujon, C., and Zenit, R.: Increased mobility of bidisperse granular avalanches, J. Fluid Mech., 593, 475–504, https://doi.org/10.1017/S0022112007008932, 2007.

Lisle, T. E., Pizzuto, J. E., Ikeda, H., Iseya, F., and Kodama, Y.: Evolution of a sediment wave in an experimental channel, Water Resour. Res., 33, 1971–1981, https://doi.org/10.1029/97WR01180, 1997.

Loye, A., Jaboyedoff, M., Theule, J. I., and Liébault, F.: Headwater sediment dynamics in a debris flow catchment constrained by high-resolution topographic surveys, Earth Surf. Dynam., 4, 489–513, https://doi.org/10.5194/esurf-4-489-2016, 2016.

Lucía, A., Comiti, F., Borga, M., Cavalli, M., and Marchi, L.: Dynamics of large wood during a flash flood in two mountain catchments, Nat. Hazards Earth Syst. Sci., 15, 1741–1755, https://doi.org/10.5194/nhess-15-1741-2015, 2015.

Macaulay, M. and Rognon, P.: Two mechanisms of momentum transfer in granular flows, Phys. Rev. E, 101, 050901, https://doi.org/10.1103/PhysRevE.101.050901, 2020.

Magilligan, F. J., Phillips, J. D., James, L. A., and Gomez, B.: Geomorphic and Sedimentological Controls on the Effectiveness of an Extreme Flood, The Journal of Geology, 106, 87–96, https://doi.org/10.1086/516009, 1998.

Manville, V. and White, J. D. L.: Incipient granular mass flows at the base of sediment-laden floods, and the roles of flow competence and flow capacity in the deposition of stratified bouldery sands, Sedimentary Geology, 155, 157–173, https://doi.org/10.1016/S0037-0738(02)00294-4, 2003.

Mao, L. and Lenzi, M. A.: Sediment mobility and bedload transport conditions in an alpine stream, Hydrol. Process., 21, 1882–1891, https://doi.org/10.1002/hyp.6372, 2007.

Mao, L., Cavalli, M., Comiti, F., Marchi, L., Lenzi, M. A., and Arattano, M.: Sediment transfer processes in two Alpine catchments of contrasting morphological settings, Journal of Hydrology, 364, 88–98, https://doi.org/10.1016/j.jhydrol.2008.10.021, 2009.

Marchi, L., Arattano, M., and Deganutti, A. M.: Ten years of debris-flow monitoring in the Moscardo Torrent (Italian Alps), Geomorphology, 46, 1–17, https://doi.org/10.1016/S0169-555X(01)00162-3, 2002.

Marchi, L., Borga, M., Preciso, E., and Gaume, E.: Characterisation of selected extreme flash floods in Europe and implications for flood risk management, Journal of Hydrology, 394, 118–133, https://doi.org/10.1016/j.jhydrol.2010.07.017, 2010.

Masteller, C. C., Finnegan, N. J., Turowski, J. M., Yager, E. M., and Rickenmann, D.: History-Dependent Threshold for Motion Revealed by Continuous Bedload Transport Measurements in a Steep Mountain Stream, Geophys. Res. Lett., 46, 2583–2591, https://doi.org/10.1029/2018GL081325, 2019.

Maurer, J. M., Schaefer, J. M., Russell, J. B., Rupper, S., Wangdi, N., Putnam, A. E., and Young, N.: Seismic observations, numerical modeling, and geomorphic analysis of a glacier lake outburst flood in the Himalayas, Sci. Adv., 6, eaba3645, https://doi.org/10.1126/sciadv.aba3645, 2020.

Maurin, R., Chauchat, J., and Frey, P.: Dense granular flow rheology in turbulent bedload transport, J. Fluid Mech., 804, 490–512, https://doi.org/10.1017/jfm.2016.520, 2016.

McCoy, S. W., Kean, J. W., Coe, J. A., Tucker, G. E., Staley, D. M., and Wasklewicz, T. A.: Sediment entrainment by debris flows: In situ measurements from the headwaters of a steep catchment: SEDIMENT ENTRAINMENT BY DEBRIS FLOWS, J. Geophys. Res., 117, n/a-n/a, https://doi.org/10.1029/2011JF002278, 2012.

McCoy, S. W., Tucker, G. E., Kean, J. W., and Coe, J. A.: Field measurement of basal forces generated by erosive debris flows: DEBRIS FLOW BASAL FORCE, J. Geophys. Res. Earth Surf., 118, 589–602, https://doi.org/10.1002/jgrf.20041, 2013.

Meyer-Peter, E. and Mueller, R.: Formulas for bed-load transport, IAHSR 2nd meeting, Stockholm, 1948.

Misset, C., Recking, A., Legout, C., Bakker, M., Bodereau, N., Borgniet, L., Cassel, M., Geay, T., Gimbert, F., Navratil, O., Piegay, H., Valsangkar, N., Cazilhac, M., Poirel, A., and Zanker, S.: Combining multi-physical measurements to quantify bedload transport and morphodynamics interactions in an Alpine braiding river reach, Geomorphology, 351, 106877, https://doi.org/10.1016/j.geomorph.2019.106877, 2020.

Mizuyama, T., Oda, A., Laronne, J. B., Nonaka, M., and Matsuoka, M.: Laboratory tests of a Japanese pipe hydrophone for continuousmonitoring of coarse bedload, Bedload-Surrogate Monitoring Technologies, 319–335, 2010.

Montgomery, D. R., Schmidt, K. M., Dietrich, W. E., and McKean, J.: Instrumental record of debris flow initiation during natural rainfall: Implications for modeling slope stability, J. Geophys. Res., 114, F01031, https://doi.org/10.1029/2008JF001078, 2009.

Morozova, G. S.: A review of Holocene avulsions of the Tigris and Euphrates rivers and possible effects on the evolution of civilizations in lower Mesopotamia, Geoarchaeology, 20, 401–423, https://doi.org/10.1002/gea.20057, 2005.

Nanni, U., Gimbert, F., Roux, P., and Lecointre, A.: Observing the subglacial hydrology network and its dynamics with a dense seismic array, Proc Natl Acad Sci USA, 118, e2023757118, https://doi.org/10.1073/pnas.2023757118, 2021.

Nelson, A. and Dubé, K.: Channel response to an extreme flood and sediment pulse in a mixed bedrock and gravel-bed river: Channel Response to an Extreme Flood and Sediment Pulse, Earth Surf. Process. Landforms, 41, 178–195, https://doi.org/10.1002/esp.3843, 2016.

Palucis, M. C., Ulizio, T., Fuller, B., and Lamb, M. P.: Intense Granular Sheetflow in Steep Streams, Geophys. Res. Lett., 45, 5509–5517, https://doi.org/10.1029/2018GL077526, 2018.

Park, C. B., Miller, R. D., and Xia, J.: Imaging dispersion curves of surface waves on multi-channel record, in: SEG Technical Program Expanded Abstracts 1998, SEG Technical Program Expanded Abstracts 1998, 1377–1380, https://doi.org/10.1190/1.1820161, 1998.

Parker, G., Paola, C., Whipple, K. X., and Mohrig, D.: Alluvial Fans Formed by Channelized Fluvial and Sheet Flow. I: Theory, Journal of Hydraulic Engineering, 124, 985–995, https://doi.org/10.1061/(ASCE)0733-9429(1998)124:10(985), 1998.

Parker, G., Seminara, G., and Solari, L.: Bed load at low Shields stress on arbitrarily sloping beds: Alternative entrainment formulation: ENTRAINMENT FORMULATION BEDLOAD ON ARBITRARY SLOPE, Water Resour. Res., 39, https://doi.org/10.1029/2001WR001253, 2003.

Peakall, J., Ashworth, P., and Best, J.: Physical modelling in fluvial geomorphology: principles, applications and unresolved issues, in: The scientific nature of geomorphology: proceedings of the 27th Binghamton Symposium in Geomorphology, John Wiley and Sons, Chichester, 221–253, 1996.

Phillips, J., Hogg, A., Kerswell, R., and Thomas, N.: Enhanced mobility of granular mixtures of fine and coarse particles, Earth and Planetary Science Letters, 246, 466–480, https://doi.org/10.1016/j.epsl.2006.04.007, 2006.

Phillips, J. D.: The job of the river, Earth Surf. Process. Landforms, 35, 305–313, https://doi.org/10.1002/esp.1915, 2010.

Piantini, M., Gimbert, F., Bellot, H., and Recking, A.: Triggering and propagation of exogenous sediment pulses in mountain channels: insights from flume experiments with seismic monitoring, Earth Surf. Dynam., 9, 1423–1439, https://doi.org/10.5194/esurf-9-1423-2021, 2021.

Piton, G.: Sediment transport control by check dams and open check dams in Alpine torrents, Doctoral dissertation, Univ. Grenoble Alpes, IRSTEA, Centre de Grenoble, 2016.

Piton, G. and Recking, A.: The concept of travelling bedload and its consequences for bedload computation in mountain streams: HOW TO ACCOUNT FOR ALLOGENIC SUPPLY IN BEDLOAD TRANSPORT EQUATIONS?, Earth Surf. Process. Landforms, 42, 1505–1519, https://doi.org/10.1002/esp.4105, 2017.

Prakash, N. and Manconi, A.: Rapid Mapping of Landslides Triggered by the Storm Alex, October 2020, in: 2021 IEEE International Geoscience and Remote Sensing Symposium IGARSS, IGARSS 2021 - 2021 IEEE International Geoscience and Remote Sensing Symposium, Brussels, Belgium, 1808–1811, https://doi.org/10.1109/IGARSS47720.2021.9553321, 2021.

Prancevic, J. P. and Lamb, M. P.: Unraveling bed slope from relative roughness in initial sediment motion: Relative roughness and incipient motion, J. Geophys. Res. Earth Surf., 120, 474–489, https://doi.org/10.1002/2014JF003323, 2015.

Prancevic, J. P., Lamb, M. P., and Fuller, B. M.: Incipient sediment motion across the river to debris-flow transition, Geology, 42, 191–194, https://doi.org/10.1130/G34927.1, 2014.

Recking, A.: Theoretical development on the effects of changing flow hydraulics on incipient bed load motion: INCIPIENT MOTION CONDITIONS, Water Resour. Res., 45, https://doi.org/10.1029/2008WR006826, 2009.

Recking, A.: A comparison between flume and field bed load transport data and consequences for surface-based bed load transport prediction: FLUME AND FIELD BED LOAD TRANSPORT, Water Resour. Res., 46, https://doi.org/10.1029/2009WR008007, 2010.

Recking, A.: Influence of sediment supply on mountain streams bedload transport, Geomorphology, 175–176, 139–150, https://doi.org/10.1016/j.geomorph.2012.07.005, 2012.

Recking, A.: Relations between bed recharge and magnitude of mountain streams erosions, Journal of Hydro-environment Research, 8, 143–152, https://doi.org/10.1016/j.jher.2013.08.005, 2014.

Recking, A., Frey, P., Paquier, A., Belleudy, P., and Champagne, J. Y.: Feedback between bed load transport and flow resistance in gravel and cobble bed rivers: FEEDBACK BETWEEN BED LOAD AND FLOW RESISTANCE, Water Resour. Res., 44, https://doi.org/10.1029/2007WR006219, 2008.

Recking, A., Frey, P., Paquier, A., and Belleudy, P.: An experimental investigation of mechanisms involved in bed load sheet production and migration, J. Geophys. Res., 114, F03010, https://doi.org/10.1029/2008JF000990, 2009.

Recking, A., Liébault, F., Peteuil, C., and Jolimet, T.: Testing bedload transport equations with consideration of time scales, Earth Surf. Process. Landforms, 37, 774–789, https://doi.org/10.1002/esp.3213, 2012.

Recking, A., Piton, G., Vazquez-Tarrio, D., and Parker, G.: Quantifying the Morphological Print of Bedload Transport: Morphological Print, Earth Surf. Process. Landforms, 41, 809–822, https://doi.org/10.1002/esp.3869, 2016.

Reid, I., Frostick, L. E., and Layman, J. T.: The incidence and nature of bedload transport during flood flows in coarse-grained alluvial channels, Earth Surf. Process. Landforms, 10, 33–44, https://doi.org/10.1002/esp.3290100107, 1985.

Rennie, C. D.: Site specificity of bed load measurement using an acoustic Doppler current profiler, J. Geophys. Res., 109, F03003, https://doi.org/10.1029/2003JF000106, 2004.

Rickenmann, D.: Comparison of bed load transport in torrents and gravel bed streams, Water Resour. Res., 37, 3295–3305, https://doi.org/10.1029/2001WR000319, 2001.

Rickenmann, D. and Recking, A.: Evaluation of flow resistance in gravel-bed rivers through a large field data set, Water Resour. Res., 47, https://doi.org/10.1029/2010WR009793, 2011.

Rickenmann, D., Turowski, J. M., Fritschi, B., Klaiber, A., and Ludwig, A.: Bedload transport measurements at the Erlenbach stream with geophones and automated basket samplers: BEDLOAD TRANSPORT MEASUREMENTS IN THE ERLENBACH, Earth Surf. Process. Landforms, 37, 1000–1011, https://doi.org/10.1002/esp.3225, 2012.

Rickenmann, D., Turowski, J. M., Fritschi, B., Wyss, C., Laronne, J., Barzilai, R., Reid, I., Kreisler, A., Aigner, J., Seitz, H., and Habersack, H.: Bedload transport measurements with impact plate geophones: comparison of sensor calibration in different gravel-bed streams: IMPACT PLATE GEOPHONE CALIBRATION, Earth Surf. Process. Landforms, 39, 928–942, https://doi.org/10.1002/esp.3499, 2014.

Rinaldi, M., Amponsah, W., Benvenuti, M., Borga, M., Comiti, F., Lucía, A., Marchi, L., Nardi, L., Righini, M., and Surian, N.: An integrated approach for investigating geomorphic response to extreme events: methodological framework and application to the October 2011 flood in the Magra River catchment, Italy: Integrated Approach for Investigating Geomorphic Response to Floods, Earth Surf. Process. Landforms, 41, 835–846, https://doi.org/10.1002/esp.3902, 2016.

Roth, D. L., Finnegan, N. J., Brodsky, E. E., Cook, K. L., Stark, C. P., and Wang, H. W.: Migration of a coarse fluvial sediment pulse detected by hysteresis in bedload generated seismic waves, Earth and Planetary Science Letters, 404, 144–153, https://doi.org/10.1016/j.epsl.2014.07.019, 2014.

Roth, D. L., Brodsky, E. E., Finnegan, N. J., Rickenmann, Dieter., Turowski, J. M., and Badoux, A.: Bed load sediment transport inferred from seismic signals near a river, J. Geophys. Res. Earth Surf., 121, 725–747, https://doi.org/10.1002/2015JF003782, 2016.

Roth, D. L., Finnegan, N. J., Brodsky, E. E., Rickenmann, D., Turowski, J. M., Badoux, A., and Gimbert, F.: Bed load transport and boundary roughness changes as competing causes of hysteresis in the relationship between river discharge and seismic amplitude recorded near a steep mountain stream, J. Geophys. Res. Earth Surf., 122, 1182–1200, https://doi.org/10.1002/2016JF004062, 2017.

RTM, (ONF): Retour d'expérience technique de la crue du 2 octobre 2020 dans la vallée de la Roya, 2022a.

RTM, (ONF): Retour d'expérience technique de la crue du 2 octobre 2020 dans la vallée de la Vésubie, 2022b.

Ryan, S. E., Porth, L. S., and Troendle, C. A.: Coarse sediment transport in mountain streams in Colorado and Wyoming, USA, Earth Surf. Process. Landforms, 30, 269–288, https://doi.org/10.1002/esp.1128, 2005.

Savage, S. B. and Lun, C. K. K.: Particle size segregation in inclined chute flow of dry cohesionless granular solids, J. Fluid Mech., 189, 311–335, https://doi.org/10.1017/S002211208800103X, 1988.

Scheidl, C. and Rickenmann, D.: Empirical prediction of debris-flow mobility and deposition on fans, Earth Surf. Process. Landforms, n/a-n/a, https://doi.org/10.1002/esp.1897, 2009.

Schmandt, B., Aster, R. C., Scherler, D., Tsai, V. C., and Karlstrom, K.: Multiple fluvial processes detected by riverside seismic and infrasound monitoring of a controlled flood in the Grand Canyon, Geophys. Res. Lett., 40, 4858–4863, https://doi.org/10.1002/grl.50953, 2013.

Schmandt, B., Gaeuman, D., Stewart, R., Hansen, S. M., Tsai, V. C., and Smith, J.: Seismic array constraints on reach-scale bedload transport, Geology, 45, 299–302, https://doi.org/10.1130/G38639.1, 2017.

Schneider, J. M., Turowski, J. M., Rickenmann, D., Hegglin, R., Arrigo, S., Mao, L., and Kirchner, J. W.: Scaling relationships between bed load volumes, transport distances, and stream power in steep mountain channels: Tracer Erlenbach, J. Geophys. Res. Earth Surf., 119, 533–549, https://doi.org/10.1002/2013JF002874, 2014.

Schneider, J. M., Rickenmann, D., Turowski, J. M., Schmid, B., and Kirchner, J. W.: Bed load transport in a very steep mountain stream (Riedbach, Switzerland): Measurement and prediction: BED LOAD TRANSPORT RIEDBACH, Water Resour. Res., 52, 9522–9541, https://doi.org/10.1002/2016WR019308, 2016.

Schoklitsch, A.: Handbuch des Wasserbaus, Springer Verlag, 1962.

Schumm, S. A.: The Fluvial System, John Wiley, Chichester and New York, 338 pp., 1977.

Scorpio, V., Crema, S., Marra, F., Righini, M., Ciccarese, G., Borga, M., Cavalli, M., Corsini, A., Marchi, L., Surian, N., and Comiti, F.: Basin-scale analysis of the geomorphic effectiveness of flash floods: A study in the northern Apennines (Italy), Science of The Total Environment, 640–641, 337–351, https://doi.org/10.1016/j.scitotenv.2018.05.252, 2018.

Scorpio, V., Cavalli, M., Steger, S., Crema, S., Marra, F., Zaramella, M., Borga, M., Marchi, L., and Comiti, F.: Storm characteristics dictate sediment dynamics and geomorphic changes in mountain channels: A case study in the Italian Alps, Geomorphology, 403, 108173, https://doi.org/10.1016/j.geomorph.2022.108173, 2022.

Shields, A.: Application of similarity principles and turbulence research to bed load movement, US Dept of Agr. , Soil Conservation Service Cooperative Laboratory, 1936.

Sklar, L. S., Fadde, J., Venditti, J. G., Nelson, P., Wydzga, M. A., Cui, Y., and Dietrich, W. E.: Translation and dispersion of sediment pulses in flume experiments simulating gravel augmentation below dams: TRANSLATION AND DISPERSION OF SEDIMENT PULSES, Water Resour. Res., 45, https://doi.org/10.1029/2008WR007346, 2009.

Sklar, L. S., Riebe, C. S., Marshall, J. A., Genetti, J., Leclere, S., Lukens, C. L., and Merces, V.: The problem of predicting the size distribution of sediment supplied by hillslopes to rivers, Geomorphology, 277, 31–49, https://doi.org/10.1016/j.geomorph.2016.05.005, 2017.

Solari, L. and Parker, G.: The Curious Case of Mobility Reversal in Sediment Mixtures, J. Hydraul. Eng., 126, 185–197, https://doi.org/10.1061/(ASCE)0733-9429(2000)126:3(185), 2000.

Stock, J. D. and Dietrich, W. E.: Erosion of steepland valleys by debris flows, Geological Society of America Bulletin, 118, 1125–1148, https://doi.org/10.1130/B25902.1, 2006.

Surian, N., Righini, M., Lucía, A., Nardi, L., Amponsah, W., Benvenuti, M., Borga, M., Cavalli, M., Comiti, F., Marchi, L., Rinaldi, M., and Viero, A.: Channel response to extreme floods: Insights on controlling factors from six mountain rivers in northern Apennines, Italy, Geomorphology, 272, 78–91, https://doi.org/10.1016/j.geomorph.2016.02.002, 2016.

Sutherland, D. G., Ball, M. H., Hilton, S. J., and Lisle, T. E.: Evolution of a landslide-induced sediment wave in the Navarro River, California, Geological Society of America Bulletin, 13, 2002.

Takahashi, T.: Debris flow: mechanics, prediction and countermeasures, 2. ed., CRC Press/Balkema, Boca Raton, Fla., 551 pp., 2014.

Tsai, V. C., Minchew, B., Lamb, M. P., and Ampuero, J.-P.: A physical model for seismic noise generation from sediment transport in rivers: SEISMIC NOISE FROM SEDIMENT TRANSPORT, Geophys. Res. Lett., 39, n/a-n/a, https://doi.org/10.1029/2011GL050255, 2012.

Turowski, J. M., Yager, E. M., Badoux, A., Rickenmann, D., and Molnar, P.: The impact of exceptional events on erosion, bedload transport and channel stability in a step-pool channel, Earth Surf. Process. Landforms, 34, 1661–1673, https://doi.org/10.1002/esp.1855, 2009.

Van Rijn, L. C.: Sediment Transport, Part I: Bed Load Transport, J. Hydraul. Eng., 110, 1431–1456, https://doi.org/10.1061/(ASCE)0733-9429(1984)110:10(1431), 1984.

Walter, F., Burtin, A., McArdell, B. W., Hovius, N., Weder, B., and Turowski, J. M.: Testing seismic amplitude source location for fast debris-flow detection at Illgraben, Switzerland, Nat. Hazards Earth Syst. Sci., 17, 939–955, https://doi.org/10.5194/nhess-17-939-2017, 2017.

Welch, P.: The use of fast Fourier transform for the estimation of power spectra: A method based on time averaging over short, modified periodograms, IEEE Trans. Audio Electroacoust., 15, 70–73, https://doi.org/10.1109/TAU.1967.1161901, 1967.

Wilcock, P. R. and Crowe, J. C.: Surface-based Transport Model for Mixed-Size Sediment, J. Hydraul. Eng., 129, 120–128, https://doi.org/10.1061/(ASCE)0733-9429(2003)129:2(120), 2003.

Wilcock, P. R. and Southard, J. B.: Experimental study of incipient motion in mixed-size sediment, Water Resour. Res., 24, 1137–1151, https://doi.org/10.1029/WR024i007p01137, 1988.

Wilcock, P. R., Kenworthy, S. T., and Crowe, J. C.: Experimental study of the transport of mixed sand and gravel, Water Resour. Res., 37, 3349–3358, https://doi.org/10.1029/2001WR000683, 2001.

Wohl, E. E.: Mountain rivers revisited, American Geophysical Union, Washington, DC, 573 pp., 2010.

Wolman, M. G. and Miller, J. P.: Magnitude and Frequency of Forces in Geomorphic Processes, The Journal of Geology, 68, 54–74, https://doi.org/10.1086/626637, 1960.

Y. K. Sohn: On Traction-Carpet Sedimentation, SEPM JSR, Vol. 67, https://doi.org/10.1306/D42685AE-2B26-11D7-8648000102C1865D, 1997.

Zanuttigh, B. and Lamberti, A.: Instability and surge development in debris flows, Rev. Geophys., 45, n/a-n/a, https://doi.org/10.1029/2005RG000175, 2007.

Zhang, M. and McSaveney, M. J.: Rock avalanche deposits store quantitative evidence on internal shear during runout: Avalanche Deposits Store Shear Evidence, Geophys. Res. Lett., 44, 8814–8821, https://doi.org/10.1002/2017GL073774, 2017.

Zhang, Z., Walter, F., McArdell, B. W., Haas, T., Wenner, M., Chmiel, M., and He, S.: Analyzing Bulk Flow Characteristics of Debris Flows Using Their High Frequency Seismic Signature, JGR Solid Earth, 126, https://doi.org/10.1029/2021JB022755, 2021a.

Zhang, Z., Walter, F., McArdell, B. W., Wenner, M., Chmiel, M., de Haas, T., and He, S.: Insights From the Particle Impact Model Into the High-Frequency Seismic Signature of Debris Flows, Geophys. Res. Lett., 48, https://doi.org/10.1029/2020GL088994, 2021b.

Zimmermann, A., Church, M., and Hassan, M. A.: Step-pool stability: Testing the jammed state hypothesis: STEP-POOL STABILITY, J. Geophys. Res., 115, https://doi.org/10.1029/2009JF001365, 2010.

Zoccatelli, D., Borga, M., Zanon, F., Antonescu, B., and Stancalie, G.: Which rainfall spatial information for flash flood response modelling? A numerical investigation based on data from the Carpathian range, Romania, Journal of Hydrology, 394, 148–161, https://doi.org/10.1016/j.jhydrol.2010.07.019, 2010.